DYNAMIC STABILITY OF MAGNETORHEOLOGICAL ELASTOMER BASED SANDWICH BEAMS

A Thesis Submitted in Partial Fulfillment of the Requirements

for the Degree of

DOCTOR OF PHILOSOPHY

by

Biswajit Nayak

(Roll No. 07610307)

Department of Mechanical Engineering

Indian Institute of Technology Guwahati

Guwahati-781039

INDIA

January, 2013

Department of Mechanical Engineering
Indian Institute of Technology Guwahati
Guwahati-781039
INDIA

CERTIFICATE

It is certified that the work contained in the thesis entitled "**DYNAMIC STABILITY OF MAGNETORHEOLOGICAL ELASTOMER BASED SANDWICH BEAMS**" submitted by **Mr. Biswajit Nayak** to the Indian Institute of Technology Guwahati for the award of the degree of Doctor of Philosophy has been carried out under our supervision in the Department of Mechanical Engineering, Indian Institute of Technology Guwahati. This work has not been submitted elsewhere for the award of any other degree or diploma.

The thesis, in our opinion, has reached the standard fulfilling the requirements for the award of degree of Doctor of Philosophy in accordance with the regulations of the institute.

Dr. Santosha Kumar Dwivedy
Professor
Department of Mechanical Engineering
Indian Institute of Technology Guwahati
Guwahati - 781039
India

Dr. K. S. R. Krishna Murthy
Associate Professor
Department of Mechanical Engineering
Indian Institute of Technology Guwahati
Guwahati - 781039
India

Dedicated to……

Mr. Brahmananda Nayak

Mrs. Bimala Nayak

My parents for their blessing and guidance

Mrs. Smrutismitadebadarshini

My wife for her great understanding and encouragement

Master Sai Biswasmruti Nayak

My son for his love and affection

Mr. Bibekananda Nayak

Mrs. Mamata Nayak

Mrs. Manoja Manjari Nayak

My brother and sisters for their love, affection and inspiration

Acknowledgement

I wish to express my deep gratitude to all those who have helped me in various ways during the tenure of my PhD work at IIT Guwahati. I have been supported and accompanied by many people and each one has played an indispensable role during my work. I am greatful to all of them.

I am greatly indebted to my supervisor Professor Santosha Kumar Dwivedy and Dr. K. S. R. Krishna Murthy who inspired me to pursue research in the field of design. I am highly grateful to them for their guidance and encouragement during the research work. Without their support, advice and motivation, it would have just been an impossible task for me to carry over this research work. I am always gratitude to both of my supervisors for their endless freedom, encouragement, and motivation which they have provided to achieve this goal.

I would like to thank my doctoral committee chairman, Professor D. Chakraborty for his valuable suggestions and encouragement during the period of my research work. Also, I would like to extend my appreciation to my doctoral committee members Professor S. K. Kakoty and Professor S. Talukdar for their constructive criticisms and helpful suggestions which make thesis improvement. I am also grateful to the past and present heads of the Mechanical Engineering Department, Professor U. S. Dixit, Professor D. Chakraborty and Professor P. Mahanta for extending various facilities during the tenure of my doctoral programme.

I wish to express my sincere thanks to Mr. Dhruba Jyoti Bordoloi, Mr. Sanjib Sarma, Mr. Rituraj Saikia, Mr. Jiten Basumatary and Mr. Saiffuddin Ahmed, for their assistance whenever needed during experimentation. I am very much thankful to the workshop staff Mr. Nandan Kanan Das, Mr, Dilip Chetri, Mr. Dipak Kr. Deka, Mr**.** Minesh C. Medhi, Mr. Bijoy K. Choudhury and Mr. Upen Gohain for their efficiency and cheerful readiness to help me in fabricating the experimental setup precisely and accurately.

My sincere thanks go to my friends Mr. Ratnakar Das, Mr. Dillip K. Biswal, Sreekanth P. S. Rama**,** Mrs. N. Shanmuga Priya, Mr. Purnendu Kumar Mandal, Mr. V. Satheesh kumar, Mr. Mohit Lal, Mr. C. Shravankumar, Mr. Amitava Ghatak, and Mr. Naresh Kumar Nitture for their help, support and advice in different occasions of my PhD work.

I shall always be grateful to my parents Mr. Brahmananda Nayak and Mrs. Bimala Nayak for their great encouragement, love and warm wishes. The mental support I got from

my brother (Mr. Bibekananda Nayak), brother-in-law (Mr. Santosh K. Rout and Mr. Nagen Rout), father in law (Mr. Tikam Jena) and mother in law (Mrs. Majulata Jena) is very effective and highly appreciable. Most deeply, I thank my wife Smrutismitadebabarshini for her constant encouragement, support, patience and motivation for the completion of this work. Love and affection of my son (OM) and nephews (Gudu and Suman) are source of inspiration during my entire PhD programme. I may have missed out a few names in the following list; my sincere apologies are due for any such inadvertent oversight.

Finally, I bow my head to the God Almighty in deepest gratitude and ask for his blessings.

15th January 2013

Biswajit Nayak
IIT Guwahati

Abstract

The work presented in this thesis is concerned with the theoretical and experimental investigation of the dynamic characteristics and stability of the magnetorheological elastomer (MRE) based sandwich beams subjected to periodic axial load and magnetic field. An extensive literature review has been presented which covers the use of various types of MREs for sandwich beam construction, free and forced vibration and stability analysis of sandwich beams. It is observed that a few works are available on dynamic characteristics and stability of MRE embedded sandwich beam and hence an attempt has been made to study theoretically and experimentally the above mentioned system.

Initially, using classical sandwich beam theory, extended Hamilton's principle along with generalized Galerkin's method the governing equation of motion of a sandwich beam with MRE embedded viscoelastic core and conductive skins has been derived when it is subjected to static magnetic field. The effects of magnetic field, core thickness, percentage of iron particles and carbon blacks on the free vibration responses and regions of parametric instability have been studied for various end conditions of the sandwich beam.

The same system is studied by applying time varying magnetic field and periodic axial load. The system is reduced to that of a parametrically excited system with two frequency excitation. Method of multiple scales is used to study the stability boundaries for various resonance conditions with simply supported and clamped free boundary conditions.

As the classical methods can only be used for systems with simple geometry and classical boundary conditions, finite element method (FEM) has been employed to study the vibration problems in general purpose MRE embedded sandwich beam with static magnetic field. Using FEM the dynamic characteristics and stability of

different configurations of the sandwich beam based on number, length and location of MRE patches in a viscoelastic core has been investigated. An investigation has also been carried out for a rotating sandwich beam. Harmonic balance method has been used to obtain the instability regions.

In addition to the systems described above where stiff MRE core with metallic skins have been used, the study has been extended by considering a sandwich beam with non-conductive composite skins and flexible MRE core. Finite element formulation is carried out using higher order theory where independent transverse displacements of skins have been assumed considering a transverse flexible MRE core. This assumption has been verified experimentally by taking sandwich beam with foam core. Natural frequency and loss factors of this sandwich beam have been determined for different system parameters such as magnetic field, fiber angle and static load. Then the frequency response of this system has been studied under transverse harmonic force acting on the top skin. The studies further extended by applying periodic axial load and by determining the instability regions for the principal parametric resonance for first mode considering the above mentioned system parameters. The material properties of the MRE core used in the above numerical analysis have been obtained by characterising the fabricated MRE.

To experimentally verify the developed theories, isotropic MREs are fabricated by adding carbonyl iron particles in the silicon rubber matrix. To further improve the mechanical properties of the elastomer nano sized carbon blacks have been used. Various tests such as microscopic and morphological analysis, thermo-gravimetric analysis (TGA), MH measurement, dynamic-mechanical analysis (DMA), thermo-mechanical analysis (TMA), tensile test and magneto-rheological test are conducted to characterize the fabricated MREs.

Finally, an experimental study has been performed to illustrate the dynamic characteristics of the sandwich beams with MRE core. The sandwich beams are prepared using the fabricated MREs embedded in between two elastic aluminum skins. Six different sandwich beams are fabricated by varying the skin thickness, core thickness and MRE with and without carbon black. An experimental set up has been fabricated to investigate the dynamic properties of the MRE embedded

sandwich beam under the magnetic field. The modal frequencies obtained experimentally are compared with the frequencies obtained from the analytical model considering anti-plane core, finite element model based on classical sandwich beam theory and finite element model considering flexible core based on higher order theory. The numerically obtained theoretical results are found to be in good agreement with the experimental results.

Due to controllable shear properties of the MRE embedded viscoelastic core and the magnetoelastic loads on the conductive skins, the stiffness and hence the dynamic characteristics such as modal frequencies and loss factors of the sandwich beam are enhanced by application of magnetic field. It is also found that the MRE based sandwich beam is influenced by the parameters such as number, length and location of the MRE segment in a viscoelastic core under the applied magnetic field.

The instability regions of the sandwich beam subjected to periodic axial load are found to change with various system parameters and boundary conditions. The values of critical dynamic load and the critical dynamic magnetic field below which the system can operate for any excitation frequency without any vibration are influenced by the boundary conditions, dimension and material properties of the system, damping and applied magnetic field. It is observed that the vibration of the sandwich beam can be actively or passively attenuated by using MRE patch in the viscoelastic core and by applying magnetic field. As these results depend on several system parameters the developed formulations and closed form expressions for instability regions can be effectively used for designing a vibration free sandwich beam subjected to periodic axial load. This research work on sandwich configurations can be utilized for developing smart devices with controllable stiffness which can find many industrial applications.

Contents

List of Figures

List of Tables

Nomenclature

$A_j\ (j = \mathrm{t,b,c})$	Cross sectional area of top (t) and bottom (b) skins and the core (c) respectively
B_d	Time varying magnetic field
B_s	Static magnetic field
B_{dcr}	Critical dynamic magnetic field
b	Width of the sandwich beam
$E_j\ (j = \mathrm{t,b})$	Young's modulus of top (t) and bottom skins (b) respectively
$E_j\ (j = 1,2)$	Young's modulus of composite skin in directions 1 and 2.
$E_c^{'}$	Storage Young's modulus of core
$E_c^{''}$	Loss Young's modulus of core
$\left[F_f\right]$	Geometric stiffness matrix of the system
G_{12}	In plane shear modulus of the skin material
$G_c^{'}$	Shear storage modulus
$G_c^{''}$	Shear loss modulus
$G_c^{*}\ (c = \mathrm{v,e})$	Complex shear modulus of the non-MRE (v) and MRE (e) part of the core respectively
H	Heaviside function
$h_j\ (j = \mathrm{t,b,c})$	Thickness of top (t) and bottom (b) skins and the core (c) respectively
$I_j\ (j = \mathrm{t,b,c})$	Moment of inertia of top (t) and bottom (b) skins and the core (c) respectively
$[K]$	Stiffness matrix of the system
L	Length of the beam
l_e	Elemental length
$[M]$	Mass matrix of the system
m	Mass per unit length of the system

$m_j \ (j=t,b,c)$	Mass per unit length of top (t) and bottom (b) skins and the core (c) respectively
$m_j^m \ (j=t,b)$	Distributed moment in top (t) and bottom (b) skins due to magnetic field
N	North pole of the magnet
N	Total number of elements of the sandwich beam
N_h	Rotational speed
n	Number of elements before and not including the element under consideration
$n_j \ (j=t,b)$	Horizontal force induced in top (t) and bottom (b) skins due to magnetic field
P	Axial load
P_s	Static axial load
P_d	Time varying axial load
P_{dcr}	Critical dynamic axial load
$\bar{Q}_{ij}\big)_k \ (k=t,b)$	Reduced stiffness coefficients of top (t) and bottom (t) skins respectively
$\hat{Q}_{ij}\big)_k \ (k=t,b)$	modified reduced stiffness constant of top (t) and bottom (t) skins respectively
$Q_{ij}\big)_c$	Stiffness coefficients of core
$q(t)$	Time modulation
R	Hub radius to length of beam ratio
r	Hub radius
S	South pole of the magnet
T	Kinetic energy
t	Time
U	Potential energy of the system
$U_j \ (j=\mathrm{t,b,c})$	Potential energy of top (t) and bottom skins and the core (c) respectively
$u_j \ (j=t,b,c)$	Axial displacement of top (t) and bottom (b) skins and the core (c) respectively
w	Transverse displacement
$w_j \ (j=t,b,c)$	Transverse displacement of top (t) and bottom (b) skins and the core (c) respectively
W	Work done
Ω_1	Frequency of the dynamic magnetic field

Ω_2	Frequency of the dynamic axial load
Ω_e	Frequency of excitation of harmonic force
α	Static load factor
β	Dynamic load factor
γ_c	Shear strain of the core
δ	Logarithmic decrement
ϕ	Fiber angle of composite skin
θ	Setting angle
ε	Book keeping parameter
μ_0	Permeability of air
μ_e	Permeability of skin material
ν_{12}	Poisson's ratio of skin materials
η	Loss factor of the system
η_c	Loss factor of the core material
ζ	Damping ratio

1

Introduction and Literature Review

1.1 Introduction

Layered materials and sandwich structures are often used in structural systems to utilise the advantages of the different materials. The inclusion of different materials offers the possibility to combine specific material properties, and to improve mechanical properties while reducing the component weight. These have been received a great deal of attention because of their technologically interesting applications in many areas of engineering. Sandwich construction offers the structural designer many attractive features such as high specific stiffness, good buckling resistance, easy reparability, high corrosion resistance, good energy absorption capability, high fatigue life, buoyancy and lower maintenance cost, when compared to traditional complete metallic structures. Thus, the analysis of such structural systems has been investigated for long time due to these advantages. Sandwich structures are increasingly being used in the design of high performance load carrying structures when high specific strength and stiffness to weight ratios are desired. The most important applications are found in the transport industry such as in aerospaces, aircraft, automobiles, railroad, robot and marine industries where a high stiffness/weight and strength/weight ratio provides increased payload capacity, improved preference and lower energy consumption. Sandwich panels are also available today for a wide variety of applications in building structures.

Fig. 1.1 shows a typical configuration of a sandwich panel model for use in general construction. According to the American Society for Testing and Materials (ASTM C 274-99), "*a structural sandwich construction can be defined as a special form of a laminated composite, comprising of a combination of different materials*

that are bonded together to each other so as to utilise the properties of each separate element to the structural advantage of the whole assembly".

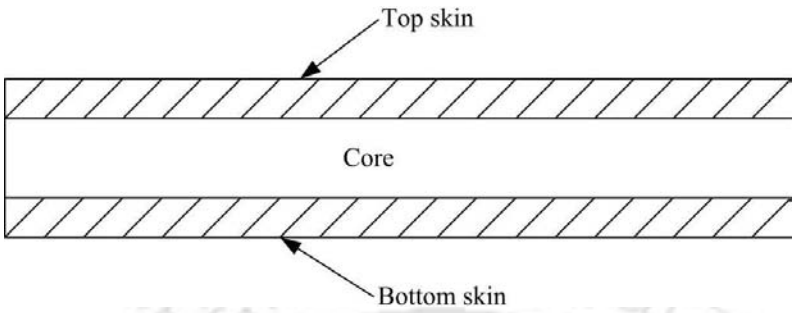

Figure 1.1 Sandwich panel model

An ordinary sandwich structure usually consists of two stiff skins attached on either side of a light thick core. It may also be configured as multiple cores with multiple skins. The light core reduces the overall density of the structure and the skins of the sandwich structure provide the strength. Integral bonding between skins and core give a material of superior bending stiffness and specific strength. Also optimal designs can be obtained for different applications by choosing different materials and geometric configurations of the skins and cores. Generally metallic skins and viscoelastic core materials are used in sandwich structures. Now a days metallic skins have been replaced by composite materials due to light weight, high strength, greater resistance to corrosion and wear, thermal-acoustical insulation, low thermal expansion and low thermal conductivity, etc. The sandwich beams with composite skins are widely used in structures, especially in aircraft, spacecraft and other applications due to their high strength-to-weight and stiffness-to-weight ratios. A wide varity of core materials such as thermocol, PVC, foam and magnetorheological elastomer etc are used in sandwich structures. The most important advantage of sandwich structures is its adaptiveness.

Sandwich structures are often subjected to various kinds of static and dynamic loading which give rise to severe vibration problems that not only affect the operation but also cause damage to components. The vibration can be controlled passively by structural modification or by actively by modifying the structural property with an external agency without changing the structure itself. However, it is

difficult to use the passive control scheme when the frequency of vibration of the structures varies in a wide range. Therefore, it is essential to adopt smart materials to attenuate vibration by means of bonding or embedding them and creating composite or sandwich structures.

Various smart materials such as piezoelectric materials, shape memory alloys, magnetostrictive materials, optical fibers, controllable fluids and elastomers are being used for vibration damping, shape control, noise reduction, vibration/damage sensing, heat sensing and for many other applications in engineering. Smart materials can respond to changes in their environment and actively alter some physical or chemical properties according to the change. One of such material to improve the design of high stiffness and high strength sandwich structures is the use of magnetorheological elastomer (MRE) as core. Magnetorheological elastomers comprise of a class of smart materials whose rheological properties can be controlled rapidly and reversibly by the application of an external magnetic field. Sandwich beams with MRE cores possess field-controllable flexural rigidities due to the field-dependant shear modulus of the MRE core (Zhou and Wang, 2005, 2006a and 2006b).

Sometimes these sandwich structures are subjected to axial periodic load and vibrate in transverse direction for some amplitude and frequency of external excitation. Such systems are generally called as parametrically excited systems as their governing equation of motion contains the periodic excitation as coefficient of the response of the system. The general description about parametrically excited system is given by Nayfeh and Mook, (1979), Cartmell, (1990) and Nayfeh and Balachandran, (2004). These systems are different from the system subjected to forced vibration in which the forcing terms appear as an inhomogeneous term in the governing equations of motion of the system. While in case of forced vibration the excitation force and response takes place in same direction, in case of parametrically excited system the response takes place in the direction orthogonal to the direction of forcing. Further in forced vibration a small excitation cannot produce a large response unless the frequency of the excitation is close to one of the natural frequencies of the system which is known as *primary resonance*, however a small

parametric excitation can produce a large response when the frequency of the excitation is close to twice of the natural frequencies of the system. Such a response is termed as *principal parametric resonance*. Also resonance can occur at a frequency which is combination of sum or difference of different modal frequencies. In parametrically excited systems one may obtain the regions in the systems states space for which the systems become unstable. These regions are known as instability regions and there are many studies to find out these regions by using different techniques.

In the present work a detailed dynamic analysis of magnetorheological elastomer embedded sandwich beam has been carried out. Both classical and higher order theories have been used to formulate the governing equation of motion of the systems. Finite element formulation has also been carried out to study the dynamics of both non-rotating and rotating sandwich beams. Several combinations of skin and core materials are taken and the systems are studied for free and forced vibration. Applying periodic axial load and time varying magnetic field the sandwich structure has been modelled as parametrically excited system and the parametric instability regions have been obtained for various system parameters. To actively reduce the vibration of the system both static and time varying magnetic fields have been used.

In this chapter a detailed literature review has been carried out in section 1.2 and it is summarised in section 1.3. The motivation of the present work has been highlighted in section 1.4 and the objective of present work is given in section 1.5. Finally, the thesis organisation is given in section 1.6.

1.2 Literature Review

In this section, comprehensive reviews of literatures are carried out on sandwich beams considering materials and material properties used in sandwich beam, applications of magnetorheological elastomers, sandwich beam theories, free and forced vibration of sandwich beam.

1.2.1 Materials and Material Properties of Sandwich Beam

Due to the development of new materials, there is vast choice of materials with different properties for skin and core of sandwich beams. Choice of skin and core

materials in a sandwich beam depends on the material requirements such as high strength, light weight, environmental resistance, surface finish, etc.

1.2.1.1 Skin Materials

The skins are the most important part of a sandwich beam. Choice of skin material is important from the point of view of environmental considerations as this part of the structure comes in direct contact with the environment. In most of the cases the top and bottom skins are of same materials, but depending upon requirements, they may be different also.

Now-a-days a wide variety of materials are available to use as skins, such as sheets of metals like aluminum, titanium, steel etc., and fiber reinforced composites. Fiber reinforced composites have many advantages such as tailorable material properties, low density and high specific strength. Polymers can be used both for skin and core material (Gupta, 2003, Langdon *et al.*, 2012).

In case of metallic components, welding or brazing is used as a means to bind the core and skins together. Use of adhesives is also possible for such cases but they are more widely used for bonding when the core and skins are of polymeric materials. A detailed description of fiber reinforced composite materials is outlined in (Vinson and Chou, 1975) and some of commonly used skin materials can be found in (Allen, 1969, Tsai and Hahn, 1980).

1.2.1.2 Core Materials

When a sandwich beam is subjected to bending the skins are put into compression/tension, and the core is subjected into shear. It therefore follows that the global deformations and core shear stresses are produced by the shear strains in the core. The most important properties of a core are its shear strength and stiffness. The core must be capable to withstand compressive loads in order to prevent failure due to wrinkling or buckling, especially in lightweight applications with thin laminate skins. Another important failure mechanism is the delamination of the core and the skins. For polymer matrix composite skins bonded to foam cores, the epoxy used to make the bond is usually stronger than the foam and failure will generally

occur in the foam. The reduction of vibration and noise of sandwich structures depend on the core material used.

A variety of materials are used as core in sandwich structures and these are (a) polymeric foam cores (PET, PMI, PS, PU, PVC etc.) (b) synthetic cores (c) wood cores (balsa and cedar) (d) magnetostrictive material core (magnetorheological fluids and magnetorheological elastomers etc.). The core may be of plane structure or it may be honeycomb and corrugated type. The description of numbers of core materials based on the preference requirements are outlined in (Vinson, 1999, Herbeck, *et al*., 2003, Li, 2006). Typical mechanical and thermal properties of some core materials can be found in (Jansson *et al.*, 1979).

For last few decades the magnetostrictive materials such as magnetorheological fluids (MRFs) and magnetorheological elastomers (MREs) are used as core materials in sandwich beams for vibration reduction. Since the shear modulus of above materials change with magnetic field the stiffness of the sandwich beams can be changed by external magnetic forces (Yeh *et al*., 2004, Zhou and Wang, 2006a, Rajamohan *et al*., 2010).

Magnetorheological fluids (MRF) are smart materials whose properties (viscosity) can be changed by external magnetic field. MR fluids are made of micron sized magnetically permeable particles suspended in a non-magnetic medium. Under a magnetic field, MR fluids change from a liquid to a semi-solid sate which change the rheological properties such as viscosity and yield stress of the fluids. The advantages of MR fluids include fast response times, high dynamic yield stress, low plastic viscosity and broad operational temperature range. They are less affected by contaminant and can be adapted to structures in saline environments. Due to the above properties, the MRFs find many applications such as semi-active dampers for vehicles, buildings and bridges etc. (Jolly *et al.*, 1999, Carlson and Jolly, 2000, Ginder *et al.*, 2000, Ribakov and Gluck, 2002, Sahasrabudhe and Nagarajaiah, 2005, Gratzer *et al.*, 2008). In the present work, magnetorheological elastomers (MREs) are used as core material. A detailed literature review on MRE is given in the following subsections.

1.2.2 Magnetorheological elastomers

Magnetorheological elastomers typically consist of magnetically polarisable particles in a non-magnetic elastomer such as synthetic or natural rubber. Particles inside the elastomer can be homogeneously distributed or they can be grouped to form chain-like columnar structures under a steady magnetic field as shown in Fig. 1.2. In order to produce an aligned structure, magnetic field is applied to the polymer composite during cross linking so that columnar particle structures form and become locked in their place upon the final cure.

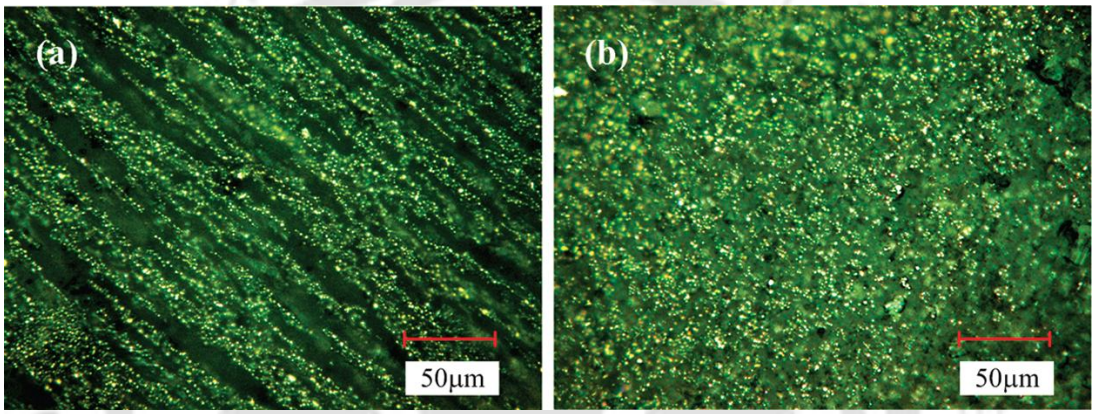

Figure 1.2 (a) Aligned MRE particles under the magnetic field and (b) randomly dispersed MRE particles without magnetic filed (Liao *et al.*, 2012).

In behaviour, the MR elastomers are quite analogous to MR fluids. The main difference is the chain-like structures of MRE are developed during curing process, while the chain like structures of MRF is formed during application. While MRE is solid and it operates in pre-yield regime, MRF is liquid and it operates in post-yield regime (Jolly *et al.*, 1996a). MRF is used to develop viscosity controllable devices; however MRE is used for developing stiffness-controllable devices (Zhou and Wang, 2005). Since, in MRF the chain-like structures are formed during application and those chains depend upon many factors such as jump rate of applied magnetic fields and the motion of magnetic poles, MRF is not suitable in applications. However MRE is stable in applications since the chain-like structures are formed during curing process. From this point of view, MRE is more promising smart material.

1.2.2.1 Applications of MRE

The studies of Bergstrom, (1999) and Von Lockette et al., (2006) revels that MREs offer enormous flexibility as the base elastomers are easily moulded, provide good durability, exhibit hyperelastic behaviour, and can be tailored to provide desired mechanical and thermal characteristics. Combining the magnetostrictive and elastomer properties they are capable of highly responsive sensing and controlled actuation in real-time.

Magnetorheological (MR) materials with tunable elastic properties may find many applications in elastomer bearings and vibration absorbers. Ford motor company patented an automotive bushing that used magnetorheological elastomer (Watson, 1997, Stewart *et al.*, 1998). The MREs are suitable for the applications where, stiffness or resonance frequency change is required (Jolly *et al.*, 1999, Carlson and Jolly, 2000). Toyota Central Research and Development Laboratory has also developed tunable engine mounts containing silicone gels with iron particles (Shiga *et al.*, 2003). Kallio, (2005) notated that many suspension applications involve relatively large deflections at low frequencies (below 100 Hz). He investigated the possibility of using magnetorheological elastomers as field dependant tunable spring elements for active vibration control. Deng *et al.*, (2006), Deng and Gong, (2008) developed an adaptive tuned vibration absorber (ATVA) using magnetorheological elastomer as shown in Fig. 1.3.

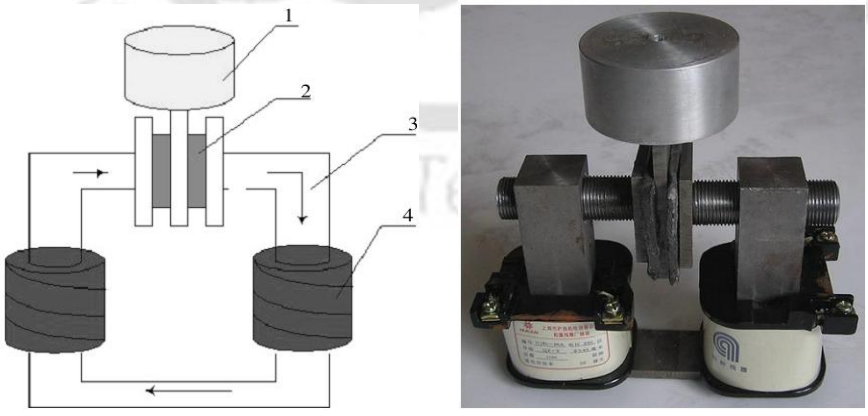

(a) (b)

Figure 1.3 (a) Schematic diagram of the ATVA developed 1: Oscillator; 2: MREs; 3: Magnetic conductor; 4: Coils. (b) Photograph of the ATVA developed. (Deng *et al.*, 2006).

As shear modulus of MRE depends on the field strength, the equivalent stiffness of the ATVA changes with the field strength as well as the coil current. Consequently, the natural frequency of the ATVA can be controlled by the coil current. Thus, the ATVA natural frequency can be changed by tuning the coil current to trace the external excitation frequency. When the tuned ATVA frequency matches the excitation frequency, the vibration can be attenuated significantly.

1.2.2.2 Experimental Study on MRE Behavior

For the past few decades various MREs are being developed using different combinations of materials or various kinds of experimental schemes for improving the MR effect and mechanical properties. The properties of the MRE depend on the volume percentage of magnetic particles in the elastomer matrix and the different size and the structural alignment of the particles after curing the MRE under a magnetic field. Jolly *et al.*, (1999) experimentally investigated that the maximum percentage of change in modulus is being observed at a strain range of 1-2%. Blom and Kari, (2005) reported that under a magnetic field, the maximum increase in stiffness is 115% at an audible frequency range of 100-1000 Hz. Davis, (1999) and Lokander and Stenberg, (2003) have shown that maximum magnetorheological effect on elastomers has been reported to be achieved when the iron particle fill rate is about 30% of the total volume. Lokander and Stenberg, (2003) showed that changing the matrix material does not influence the absolute MR effect of the composite, when the same kind of filler particles is used. Lokander and Stenberg, (2003) and Jolly *et al.*, (1996b) have reported that the maximal increase of the elastic modulus due to MR effect to be 0.7 MPa in magnetic fields of about 0.8 T. Davis, (1999) has shown that the alignment of the particles does not affect the zero-field modulus compare to the particles with homogenous distribution.

Lokander and Stenberg, (2003) shown that the MREs with large irregular particles have a large MR effect compare to the MREs with spherical carbonyl iron particles although the particles are not aligned within the material. Abramchuk *et al.*, (2007) observed that the MRE can behave as an anisotropic material by varying the direction of the applied magnetic field and the columnar structure of the particles.

Varga *et al.,* (2006) reported that the most significant effect was found in case of structured MREs if the applied field is parallel to the particle alignment and to the mechanical stress. Kallio, (2005), Stepanov *et al.,* (2007) studied the mechanical and damping properties (shear modulus and loss factor values) by applying compressive loading with and without applied magnetic field. Liao *et al.*, 2012 shows that MREs are a durable material which can be operated in severe temperatures condition with low voltage supplies.

Wang, *et al.,* (2006) observed the effects of rubber/magnetic particle interactions on the performance of magnetorheological elastomers containing carbonyl iron particles based on silicon rubber matrix without using a magnetic field during curing by γ-ray radiation. Zhang *et al.*, (2007) proposed a novel structure MREs have the much larger field-dependant modulus than that of conventional ones. Chen *et al.,* (2007) fabricated high modulus MREs based on natural rubber by considering the influences of various fabrication conditions and reported that the iron particle weight fraction plays an important role in the enhancement of shear modulus. It has been observed that the relative MR effect is reduced from 133% to 107% when iron particles content changed from 80% to 90% even though the zero field shear modulus increases to 4.2 MPa. Later, Chen *et al.,* (2008) developed new MREs with different weight percentages of carbon black in addition to iron particles which further improves the mechanical performance of MR elastomers. Choi, (2009) has fabricated the MREs taking room temperature vulcanized silicone. Kaleta *et al.,* (2011) presented a method to fabricate the magnetorheological elastomers (MRE) with thermoplastic elastomer matrix.

1.2.3 Sandwich Beam Theories

In past number of theories have been developed and the available expertise is summerised in Stamm and Witte, (1974), Allen, (1969), Plantema, (1996) and Noor (1996). According to Frostig and Thomsen, for three layer sandwich beam three main categories of sandwich beam theories can be distinguished, viz., classical theory, superposition theory and higher-order theory. Each theory makes assumptions in modeling the behavior of the core, faces and the interaction between

them which results into different sets of differential equations. Literature related to classical and higher order theories along with finite element method is discussed in the following sections.

1.2.3.1 Classical Theory

According to Zenkert, (1995) and Allen, (1998) on sandwich construction, the classical theories make use of the following two basic assumptions:

- No transverse flexibility of the core material occurs, which means that the deflections of the upper and lower faces are equal to each other. This is also known as the "antiplane" concept.
- The longitudinal displacement distribution throughout the height of the core is linear.

Gordaninejad and Bert, (1989) used thick skins and improved the classical theory. Reissner, (1998) included the shear strain effect on the bending, but considered the average bending behaviour of the composite beam only. Thus the total displacement of the sandwich panel is split into two parts, as indicated in the Fig. 1.4. In the primary deformation, the sandwich panel behaves like a normal beam without shear while in the secondary deformation the faces bend about their own neutral axis and the core deforms under shear. This approach is useful if no local loading and peeling

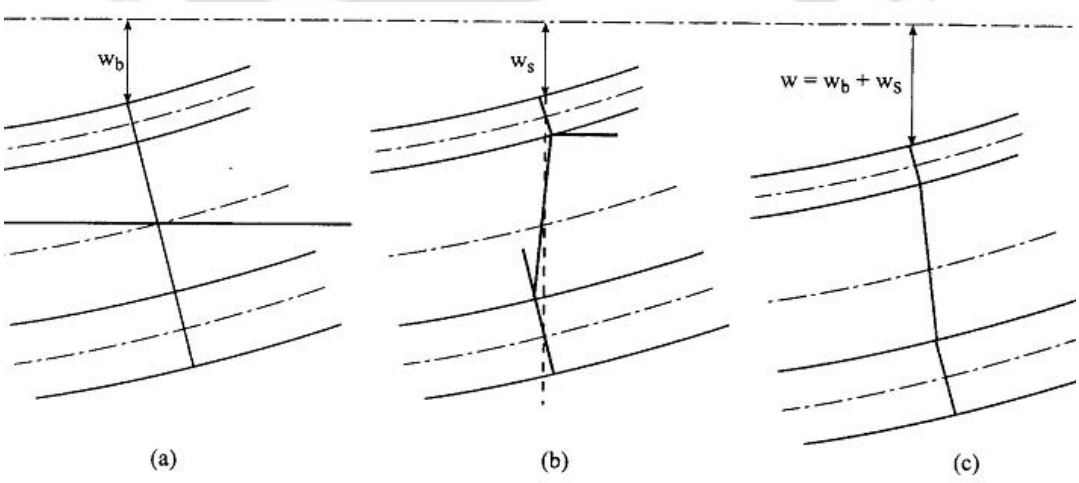

Figure 1.4 Displacement according to classical theories. (a) Primary deformation as a beam, (b) Secondary deformation due to shear and (c) Total displacement. (Straalen, 2000)

exist and anti-plane core is used. Ditaranto, (1965), Mead and Markus, (1970) and Rao, (1978) used the classical theory to study the vibration analysis of sandwich structures. Later many works has been reported using classical sandwich beam theories (Ganesan and Pradeep, 2002, Sun *et al.*, 2003, Rajamohan *et al.*, 2010 etc.).

1.2.3.2 Higher-Order Theory

In case of sandwich panel with a transversely flexible core the assumptions of classical theories are no longer valid. To take both the non-linear displacement fields of the core material and realistic supports into account, higher-order theories have been developed during the end of eighties and nineties (Piening, 1989). A higher-order approach was used by Reddy, (1990) and Kapania and Raciti, (1989) for laminated composite plates. Krishnamurthy and Vellaichamy, (1987) showed that analytical results based on higher-order theories of laminated composite plates were in agreement with experimental results. Frostig *et al*., (1991), Frostig and Baruch, (1994) and Frostig and Thomsen, (2004) studied the behaviour of sandwich beam with a flexible core, using a higher order approach to define the effects of the core flexibility on the stresses and deflections. Zhou and Wang, (2005, 2006a and 2006b), have studied the dynamic properties of a three layered MRE based sandwich beam using higher order theory. Mantari *et al*., (2011) developed a new higher higher order theory for composite/sandwich plates and shells. They presented the static and dynamic results for cylindrical and spherical shells and plates.

In Fig. 1.5 one can clearly observe that the assumption made in classical theory i.e. the deflections of the top and bottom layers are equal to each other which are no longer valid when a transversely flexible core is used. So one can use higher order theory in place of classical theory to obtain accurate result when a flexible core is used.

1.2.3.3 Finite element methods

In most of the work analytical techniques are applied to simple structures with classical boundary conditions. But these works cannot be directly applied to design structures with complicated geometry. In such cases, numerical methods such as

finite element method (FEM) are very useful. Most of the finite-element methods for sandwich panels are based on two-dimensional plate and shell models. Burton and Noor, (1995) and Noor *et al.*, (1996) reviewed different computational models based on two-dimensional finite-element approaches for sandwich panels. Many researchers have studied the dynamic behaviour of sandwich beams with different skins and core materials using finite element methods (Baber *et al.*, 1997, Amichi and Atalla, 2009, Arvin et al., 2010, Chalak *et al.*, 2011 etc). More literatures on finite element methods used for analysis of sandwich beams are given in the following subsections.

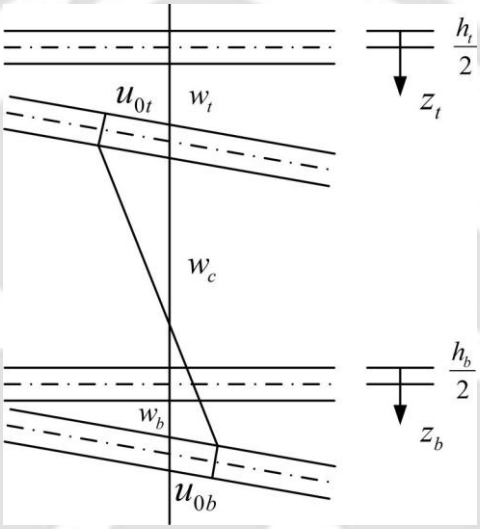

Figure 1.5 Higher-order approach.

1.2.4 Free and Forced Vibration of Sandwich Beams

An extensive study on the free and forced vibration analysis of sandwich beams with viscoelastic core has been carried out by a number of investigators. Kerwin, (1959) was the first to develop an expression for a measure of damping of a beam with a constrained viscoelastic layer. Ditaranto, (1965), Mead and Sivakumaran, (1966), Mead and Markus, (1970) and Asnani and Nakra, (1970) studied the free vibration problem of sandwich beams using the classical approach. They derived the governing differential equations of motion of a sandwich beam and imposed boundary conditions to obtain the natural frequencies and mode shapes. Jones *et al.*, (1967), evaluated the damping capacity of a sandwich beam with viscoelastic core

theoretically and experimentally. Chatterjee and Baumgarten, (1971) obtained the fundamental frequencies and loss factor for a simply supported sandwich beam using classical approach and validated with the experimental results. Ahmed, (1972) presented a finite element technique and investigated the natural frequencies of free vibration of a honeycomb sandwich beam for different end conditions.

Rao, (1978) derived the sixth order differential equation of motion by using energy method and determined the natural frequencies and loss factors of sandwich beams with viscoelastic core for various boundary conditions using classical sandwich beam theory. Lall *et al.*, (1988) used three different methods to analyse the partially covered sandwich beams. He observed that method by Markus, (1974) only gives modal loss factor, whereas Rayleigh-Ritz method gives both loss factor and resonant frequencies. Dewa *et al*., (1991) theoretically and experimentally studied the damping effectiveness of partially covered sandwich beams. They noted that the damping capacity of partially covered beams have better than fully covered beams.

Frostig *et al*., (1991), Frostig and Baruch, (1994) studied the free vibration characteristics of symmetric and non-symmetric sandwich beam with a flexible core, using a higher order theory. Frostig and Thomsen, (2004) studied the free vibration of sandwich panels with a flexible core by considering two types of computational models. The first model uses the vertical shear stresses in the core in addition to the displacements of the upper and the lower face sheets as its unknowns. The second model assumes a polynomial description of the displacement fields in the core that is based on the displacement fields of the first model.

Banerjee, (2003) studied the free vibration of sandwich beams using the dynamic stiffness method. Later Banerjee and Sobey, (2005) modified the model by idealising the top and bottom layers as Rayleigh beams whereas the central core as a Timoshenko beam to investigate the free vibration characteristics of the sandwich beams. Howson and Zare, (2005) developed an exact dynamic member stiffness matrix (exact finite element), which defines the flexural motion of a three-layered sandwich beam with unequal faceplates from the closed form solution of the governing equation. Banerjee *et al*., (2007) investigated the free vibration characteristics using an accurate dynamic stiffness model for a three-layered

sandwich beam of unequal thicknesses. Each layer of the beam is idealised by the Timoshenko beam theory. They derived a tenth-order differential equation of motion. Experimentally they also determined the natural frequencies and compared their results with the published result by Howson and Zare, (2005).

Mead and Markus, (1969) derived a sixth order differential equation to study the force vibration of a sandwich beam with viscoelastic core for various boundary conditions. Rao, (1977) studied the forced vibration of a sandwich beam with viscoelastic core subjected to moving forces. He observed that the increase in the shear stiffness of the core materials the dynamic magnification of the central deflection of the beam reduces. Kapur *et al.*, (1977) made the analysis to study the dynamic response of two and three-layered viscoelastically damped beams subjected to half sine shock excitation considered both rotary and longitudinal inertia.

Qian and Demao, (1990) carried out modal analysis as well as response calculation of sandwich beam with viscoelastic core in time domain using finite element technique. Salet and Hamelink, (1991) developed a numerical model based on finite difference method, for nonlinear analysis of sandwich beams with simply supported boundary conditions. Baber *et al*., (1997) presented a finite element model for the harmonic response of three-layered sandwich beams assuming nonlinear vibration of displacements through the thickness of the core.

Barbosa and Farage, (2008) presented a Golla-Hughes Method based finite element model to study the vibration of sandwich beam with viscoelastic core. Amichi and Atalla, (2009), introduced a sandwich finite element for laminated steels which is based on discrete displacement approach. It allows for both symmetrical and unsymmetrical configurations of the sandwich beam with viscoelastic core. Chalak *et al*., (2011) investigated the free vibration response of laminated sandwich beams with a soft core using C_0 finite element beam model. Galucio *et al.*, (2007) presented a co-rotational finite element formulation of an adaptive sandwich beam composed of a viscoelastic core constrained by laminated elastic/piezoelectric faces.

The study of dynamic characteristics of rotating beams is very important in design of rotating structural elements. Many works have been reported on free and forced vibration of rotating beams using various approaches and different methods

(Putter and Manor, 1978, Bhat, 1986, Lee, 1994). Hoa, (1979) investigated the free vibration of a rotating beam with tip mass considering different system parameters. Abbas (1986) determined the instability regions of a rotating Timoshenko beam by finite element method. Wei *et al*., (2006) studied the vibration control of a flexible rotating sandwich beam with electrorheological (ER) core.

The sandwich beams with composite skins are widely used in structures, especially in aircraft, spacecraft and other applications due to their high strength-to-weight and stiffness-to-weight ratios. Many researchers have studied the behaviour of sandwich structures with composite faces. Various global and other higher order theories have been developed to analyze vibration and stability of composite and sandwich structures (Kant *et al.*, 1998, Matsunaga, 2001, Matsunaga, 2007, Zhen and Chen, 2008). Pradeep and Ganesan, (2007) analysed the buckling and vibration behaviour of a sandwich beam having viscoelastic core under thermal environments, using the finite element method. They have investigated the variation of natural frequencies and loss factors with respect to temperature and core thickness. Cetkovic and Vuksanovic, (2009) used the generalized layerwise theory for bending, free vibrations and buckling analysis of laminated composite and sandwich plate. Over the past decades efforts have been spend to study the transient dynamic analysis of composite plate and beam under various loading (Mallikarjuna and Kant, 1993, Marur and Kant, 1997, Nayak *et al* ., 2004). Tagarielli *et al*., (2007) experimentally studied the dynamic strength of composite sandwich beams with the different core composition and sandwich beam geometry under impact loading. Sastri, (2012) presented a FE formulation using classical sandwich beam theory to study the free and forced vibration of a sandwich beam with composite skins. Also, numerous researchers have investigated the damping property of laminated sandwich composite beams embedded with a viscoelastic core in terms of the modal loss factor for the corresponding vibration mode (Yim *et al*., 2003, Manconi and Mac, 2010). Ghinet and Atalla, (2011) described the modeling of the dynamic response of thick composite laminate plates and beams with linear viscoelastic damping under unit force or displacement excitation. They have solved the problem by analytical discrete laminate method. Hwu *et al.*, (2004) studied the vibration suppression of a

sandwich beam with composite skins and viscoelastic core. Kim and Hwang, (2002) studied the natural frequencies of sandwich beams with honeycomb core and carbon/epoxy laminated composite faces. Vibration analysis also has been done.

A number of FE modelings have been proposed for the analysis of composite laminates and sandwich structures (Goyal and Kapania, 2007, Reddy, 1984, Murthy *et al*., 2005, Subramanian 2006). Subramanian, (2006) developed a two-node C^1 finite element of eight degrees of freedom per node to determine the natural frequencies of laminated composite beams with various boundary conditions. Arvin *et al*., (2010) used the finite element analysis to study the free and forced vibration of composite sandwich beams with viscoelastic core. Mantari *et al*., (2011) presented a new higher order shear deformation theory for analyzing the static and dynamic behaviour of multilayered sandwich and composite plates and shells. They proposed a new displacement field depends on a parameter ‘‘m’’, whose value is determined so as to give results closest to the 3D elasticity bending solutions. Vidal and Polit, (2011) presented a sine model including zig-zag function for the study of statics and vibration of laminated composite beams. Degiovanni *et al*., (2010) proposed a finite element approach based on the Hermitian zig-zag theory and on the sub-laminates concept to determine the accurate global and local responses of sandwich beams.

1.2.5 Stability Study of parametrically Excited Sandwich Beams

For determining the stability and boundaries separating stability from instability there are a number of analytical techniques available which can be divided broadly into three classes. The first class uses Hill’s method of infinite determinants. This technique is used extensively for single-degree-of- freedom system, and can also be applied to multi-degrees-of-freedom system. The second class consists of perturbation methods that are based on the assumption that the variable-coefficient terms are small. The third class uses Liapunov’s theory but it is limited by the ability to find a suitable Liapunov function.

Bolotin, (1964) developed a method which is based on harmonic balance method and studied the dynamic stability of a rod subjected to periodic longitudinal

compressive forces for parametric resonance case. Steven (1966) modified the Bolotin's method to study the stability of viscoelastic columns. Saito and Otomi, (1979) investigated the stability of viscoelastic beams and viscoelastic end supports under axial and tangential periodic loads. He obtained the regions of instability for simple and combination resonances by modifying Hsu, (1963) procedure.

Bauld, (1967) considered the dynamic stability of sandwich columns with pinned ends under pulsating axial loads. Chonan, (1982a) studied the stability of two- layered sandwich beams with elastic bonding subjected to constant horizontal and tangential compressive forces. The effect of the stiffness of the interface bond on the divergence and flutter type instability loads, as well as natural frequency is investigated. Also Chonan, (1982b) investigated vibration and stability of a two-layered beam with imperfect bonding. The normal and shear bond stresses at the interface of the layers are taken to depend on the respective relative vertical and horizontal displacements of the layers.

Kar and Sujata, (1991) studied the dynamic stability of a tapered symmetric sandwich beam. Ray and Kar, (1995a and 1995b) investigated the parametric instability regions of the sandwich beam for various boundary conditions. Later, Ray and Kar, (1996a, 1996b and1996c) determined the parametric instability regions of partially covered and multilayed sandwich beams subjected to periodic axial loading. Ray and Kar, (1996d) analyzed the parametric instability of a pinned-pinned, three-layered sandwich beam with viscoelastic core by including the extensional and rotary inertias as well as bending and shear in all the layers. Dwivedy *et al*., (2007) obtained parametric instability regions of a three-layered soft-cored symmetric sandwich beam subjected to a periodic axial load using higher order theory for various boundary conditions using modified Hsu's method.

Lin and Chen, (2002) investigated the instability regions of a rotating composite beam with a constrained damping layer subjected to periodic axial load. Later Lin and Chen, (2003) studied the dynamic behaviour and dynamic instability of a rotating beam with a constrained damping layer by finite element method.

Fereidooni *et al.*, (2008) developed a new beam model with optimum degrees of freedom to descritize the equation of motion of a laminated prismatic composite four

layer beam. They investigated the instability regions of the beam subjected to periodic axial load for the simple resonance case.

1.2.6 Magnetorheological Material Based Adaptive Sandwich Structures

For last few decades the MR materials have been used as core materials to achieve controllable properties of sandwich beams under magnetic field (Sun *et al*., 2003, Yalcintas and Dai, 2004, Prieto *et al.*, 2010). Sun *et al*., (2003) presented a detailed analysis of dynamic characteristics of adaptive beam based on MR materials. Using oscillatory rheometry techniques, the relationship between the magnetic field and the complex shear modulus of MR materials in the pre-yield regime has been developed. Yalcintas and Dai, (2004) used magnetorheological materials to observe the vibration suppression capabilities in real time for three layered MR adaptive sandwich beam structures. Prieto *et al.*, (2010) investigated the controllability of vibration characteristics of magnetorheological cantilever sandwich beams in the form of vibrations in vibration amplitudes and shifts in magnitudes of the resontant natural frequency. Rajamohan *et al.*, (2010) studied the dynamic properties of a partially treated multi-layer beam with magnetorheological fluids.

In recent years, the development of MRE embedded sandwich beams was initiated. The flexural rigidities of the MRE cored sandwich beams are controlled with magnetic field due to field dependant shear modulus of the MRE core (Zhou *et al.*, 2006, Zhou and Wang, 2005, Zhou and Wang, 2006). Zhou and Wang, (2005) carried out theoretical study on MRE embedded smart sandwich beams with non-conductive skins based on higher order sandwich beam theory. Later Zhou and Wang, (2006a and 2006b) developed dynamic equations of motion of a vibrating MRE embedded soft cored sandwich beam with conductive skins subjected to magnetic field. The magnetoelastic forces induced in the system due to the application of magnetic fields (Yabuno *et al*., 1988, Yabuno *et al*. 1989, Zhou and Wang, 2006b). Due to application of magnetic field Ying and Ni, (2009) derived a sixth order partial differential equation of motion of a MRE cored clamped free sandwich beam and studied the micro-vibration response considering a supplemental mass under stochastic support micro-motion excitation. Wei *et al*., (2008)

experimentally obtained the natural frequencies and responses of the MRE cored sandwich beam with magnetic field and excitation frequencies. Choi, (2010) investigated the dynamic behaviour of smart sandwich structures with MRE core and steel skins. Hu *et al.,* (2011) experimentally presented the vibration characteristics of a MRE cored sandwich beam subjected to non-homogeneous magnetic field. It was shown that the sandwich beam has the capability to left shift the first natural frequency when the magnetic field is increased in the activated regions.

Recently, the stability of sandwich beams with MR material core subjected to periodic axial load was initiated. Yeh *et al.,* **(**2004) investigated the dynamic stability problems of a sandwich beam with a constrained layer and an ER fluid core. Dwivedy *et al*., (2009) modelled a sandwich beam with soft core using higher order theory. They studied the parametric instability regions of the sandwich beam subjected to periodic axial load.

1.3 Summary of Literature Review

In the previous section a critical review of the dynamic characteristics and stability analysis of sandwich beams has been presented. Different features and behaviors of MRE have also been presented. From the literature survey it has been observed that magnetorheological elastomer can be effectively used in sandwich structures for vibration attenuation. The conclusions drawn from this literature review could be outlined as follows:

- Most of literatures on dynamic analysis of sandwich structures are mainly on free and forced vibration of the sandwich structures with viscoelastic core. The variation of natural frequencies and loss factor of the structure are studied for different system parameters. The viscoelastic layers constrained between elastic layers are used for effective damping of flexural vibrations of structures over a wide range of frequencies. Since the viscoelastic core does not respond to any environmental stimuli, it cannot be used for active vibration control of sandwich structures.

- To actively reduce the vibration of the system magnetorheological elastomer core can be used whose stiffness and damping properties can be externally controlled by changing the complex shear modulus with application of suitable magnetic field.
- MREs operate in the pre-yield regime and suppress force for large vibration amplitude with small amount of energy. Therefore, MRE can be used by means of bonding or embedding to composite or sandwich structures for active vibration and noise isolation.
- Most of the studies on sandwich beams are based on metallic skins. But due to development of many composite materials which are of light weight and have tailorable properties composite sandwich beams find many industrial applications. It may be noted that no study is available on sandwich beams with composite skins and MRE core.
- It may be noted that some studies have been carried out on rotating beams with constrained viscoelastic layer. The vibration analysis of a rotating sandwich beam with MRE core and conductive skins however, has not yet been explored.
- When the sandwich beams are subjected to axial periodic load the governing equation can be written by the well known Mathieu-Hill's equation which is a form of equation describing the parametrically excited system. In case of sandwich beam with viscoelastic or MRE core, the coefficients of different terms in these equations are complex. This makes the analysis complicated and hence very few studies are available on parametrically excited sandwich beams.
- Many researchers studied the parametric instability of sandwich structures with viscoelastic core subjected to periodic axial load. Both classical and finite element modeling have been carried out. This study of parametric instability is very important in design point of view as one obtains critical dynamic load to avoid vibration in the system.
- Only very a few studies are available on dynamic studies of MRE as a core in sandwich beams.

- It has been observed that no study has been carried out on MRE embedded sandwich beam with time varying magnetic field. Static magnetic field has been considered in all the previous studies on MRE embedded sandwich beam.
- Along with periodic axial load and time varying magnetic field the system is subjected to multi frequency parametric excitation. Though these types of systems are studied for general parametrically excited system it is very much required to study the specific sandwich beam systems as superposition theory cannot be applicable to nonlinear systems.
- The experimental studies of sandwich beams are limited to the systems with viscoelastic core. Recently few researchers have tried to study the free and forced vibration of MRE embedded sandwich beam. However, it is observed that the research on the experimental work of the effect of various system parameters of sandwich beam such as skin thickness, core thickness and isotropic MREs with and without carbon black on dynamic characteristics is still lacking.

1.4 Motivation of the Present Work

From the summery, it is felt that more investigation is required on MRE embedded sandwich beams before engaging them for industrial applications and design and developing semi-active devices for vibration control. Following are some key limitations in the current literature which motivates for further investigation.

- In MRE based sandwich structures, one may use full MRE core or it may be in the form of MRE patches embedded in viscoelastic core. The effects of number, length and location of MRE segments in a viscoelastic core for improving damping and stiffness of the structure have yet to be investigated. As a result, different configurations of sandwich beams with the variation of length and location of MRE segments in the viscoelastic core needs to be considered for dynamic analysis.
- Application of classical and higher order sandwich beam theories which are previously applied to viscoelastic cored sandwich beam may be extended for MRE embedded viscoelastic cored sandwich beam. The applicability of these

theories for MRE embedded sandwich beam is required to be investigated experimentally.

- Many structures are vibrated due to excitation forces with variation of frequency which makes the system to a parametrically excited system. Therefore, the dynamic stability of a parametrically excited sandwich beams with MRE embedded viscoelastic core needs to be studied for different resonance cases.
- Since the skins of the sandwich beam strengthen the bulk flexural rigidity, it is necessary to study the dynamic behaviour of MRE embedded sandwich beams with different skin materials such as metallic and composite skins.
- Most of the literatures on performance of isotropic MREs mainly considered the combinations of different synthetic and natural rubbers and iron particles. However, the effects of nano-sized carbon blacks on the characteristics and properties of isotropic MREs has not been considered, which could also enhance the performance of MRE materials. Therefore, addition of carbon blacks in the matrix for the fabrication of isotropic MREs needs to be considered.
- The characterization and properties of isotropic MREs without and with carbon black needs to be understood to enhance the performance of MRE.
- Dynamic characteristics of the MRE cored sandwich beam are influenced by various system parameters such as skin and core thickness and external magnetic field etc. So an experimental study of free and forced vibration of MRE cored sandwich beam with variation of these parameters should be investigated.

1.5 Objectives of the Present Work

The aim of this thesis is to study theoretically and experimentally the dynamic behavior and stability of partially and fully treated MRE embedded sandwich beams under magnetic field for various system parameters and boundary conditions. The objectives of the present work are as follows.

- To theoretically investigate the free vibration response and parametric instability regions of MRE embedded viscoelastic cored smart sandwich beams with conductive skins and static magnetic field for various boundary conditions using classical sandwich beam theory.

- To theoretically study the dynamic stability of MRE embedded viscoelastic cored smart sandwich structure with conductive skins subjected to periodic axial load and time varying magnetic field.
- To investigate the effect of number, length and location of MRE segments in the viscoelastic core on the dynamic behavior and stability of MRE-based adaptive sandwich beam with conductive skins using finite element method.
- To study the dynamic characteristics and stability of MRE cored rotating sandwich beam using finite element method.
- To study the dynamic behavior and stability of sandwich beam with flexible MRE core and non-conductive composite skins.
- To develop silicon rubber based isotropic MREs with and without addition of nano sized carbon black to experimentally validate the developed theoretical models.
- To characterize the developed MREs to obtain the elastic, magnetic, thermal and rheological properties.
- To develop experimental set up to study the vibration characteristics of MRE embedded sandwich beams.
- To conduct an experimental study of MRE cored sandwich beams for different system parameters to validate the analytical and finite element approaches.

1.6 Organisation of the Thesis

This thesis consists of six major chapters and is organised in the following ways:

In chapter 2, the analytical modelling of the sandwich beam with MRE embedded viscoelastic core with conductive skins has been carried out based on classical sandwich beam theory. The instability regions of the sandwich beam are investigated for various system parameters and boundary conditions. Chapter 3 deals with the stability of the MRE embedded viscoelastic cored sandwich beams subjected to time varying magnetic field and periodic axial load. Chapter 4 analyses the effect of number, length and location of the MRE segments in a viscoelastic core on the dynamic characteristics and stability of the sandwich beam. Here finite

element method is used to model the sandwich beam. Apart from these, dynamic characteristics and stability of a rotating sandwich beam with MRE core has also been investigated in this chapter. Chapter 5 is devoted to the study of dynamic characteristics and stability of a sandwich beam with flexible MRE core and graphite epoxy skins using finite element method.

Chapter 6 presents the fabrication and characterisation of isotropic soft MREs with and without addition of nano-sized carbon black. Also experimental studies have been presented to study the free and forced vibration of sandwich beam with the different MRE cores. The analytical and finite element models are validated using the experimental results. Finally, the conclusions and the scope for future work are given in chapter 7.

2

Dynamic Analysis of MRE-based Sandwich Beam with Conductive Skins under Various Boundary Conditions

2.1 Introduction

Dynamic analysis of sandwich beams can be done by modeling them as uniform beams with different boundary conditions. These structures quite often are subjected to time varying parametric excitation, which may lead to their instability. In section 2.2, the modeling of a three layered symmetric sandwich beam is carried out using the classical sandwich beam theory and extended Hamilton's principle. In section 2.3, the generalized Galarkin's method is used to derive the temporal equation of motion. In section 2.4, the modified Hsu method (Ray and Kar, 1995b) is discussed to investigate the stability boundary. Numerical results and discussions have been carried out in section 2.5. The results have been validated using experiments and previously published results. Many parametric studies have been carried out to demonstrate the usefulness of the MRE embedded sandwich beam for vibration reduction.

2.2 Mathematical Modeling

Figure 2.1 shows a three layered symmetric sandwich beam of length *L*, width *b*, with two conductive skins and a core which is composed of an MRE part and two non-MRE viscoelastic parts. The chain-like structures of iron particles inside the MRE part are perpendicular to the skins. The applied magnetic field with flux density B_s is parallel to such chain-like structures and is perpendicular to the skins. The top, core and bottom layer thickness are $2h_t$, $2h_c$ and $2h_b$, respectively. An axial periodic load $P(t) = P_s + P_d \cos\Omega_2 t$ has been applied to the sandwich beam

where, Ω_2 being the frequency of the applied load, t being the time, P_s and P_d are the amplitude of static and dynamic loads, respectively. In this analysis $E_j\,(j=t,b)$ and G_c^* $(c=v,e)$ are the Young's modulus of skin materials and complex shear modulus of the core, respectively. Subscripts t,b,v and e represent top, bottom, viscoelastic and MRE, respectively.

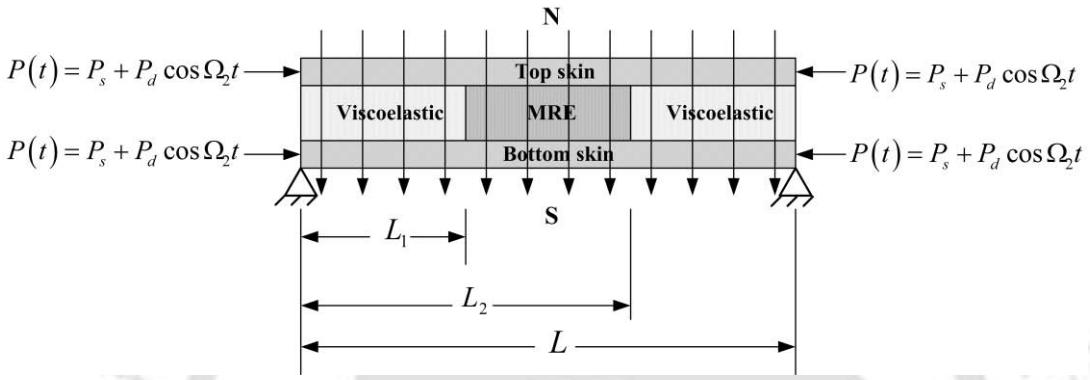

Figure 2.1 Schematic diagram of a three layered sandwich beam with MRE embedded viscoelastic core subjected to periodic axial load and static magnetic field.

The following assumptions are considered for developing the governing differential equations of motion of a three layer symmetric sandwich beam.

The skins are made of homogeneous and isotropic materials and bend as per Euler-Bernoulli beam theory. The MRE and non-MRE core materials are only subjected to shear deformation associated with axial displacements and the longitudinal direct stresses are negligible. The shear modulus of the core is assumed to be a distributing function along the longitudinal direction since the MRE part of the core is affected by the magnetic field while the non-MRE parts are not affected by the magnetic field. Transverse normal strains in both core and skins are neglected so that the transverse displacements 'w' of all points on a cross section are equal. There is perfect bonding between layers of the sandwich beam and hence there is no slippage or delamination between the layers during deformation.

In the present work the assumption of the transverse displacement 'w' of the upper and lower skins are equal as an anti-plane core is considered. Unlike the work of Frostig and Baruch, (1994) where the core is assumed to be flexible in transverse

direction, here the MRE embedded viscoelastic core is assumed to be incompressible in transverse direction.

Total strain energy (U) of the sandwich beam which is given by the following expression, is due to the bending and axial loading in the top and bottom skins and shearing of the core layer which consist of both MRE and non-MRE parts.

$$U = (U_t)_{\text{bending}} + (U_t)_{\text{extension}} + (U_c)_{\text{shearing}} + (U_b)_{\text{bending}} + (U_b)_{\text{extension}}, \tag{2.1}$$

where, $(U_t)_{\text{bending}} = \frac{1}{2}\int_0^L E_t I_t w_{,xx}^2 dx,$ $(U_t)_{\text{extension}} = \frac{1}{2}\int_0^L E_t A_t u_{t,x}^2 dx,$

$(U_b)_{\text{bending}} = \frac{1}{2}\int_0^L E_b I_b w_{,xx}^2 dx,$ $(U_b)_{\text{extension}} = \frac{1}{2}\int_0^L E_b A_b u_{b,x}^2 dx,$

and $(U_c)_{\text{shearing}} = \frac{1}{2}\int_0^L G_c^* A_c \gamma_c^2 dx$ (2.2)

Here, $()_{,x}$ represents the differentiation with respect to x. U_t, U_c and U_b are the strain energy of top, core and bottom layers, respectively. A_t, A_c and A_b are the cross sectional areas of top, core and bottom layers, respectively. I_t and I_b are moment of inertia of the top and bottom skins, respectively. γ_c denotes the shear strain in the core. u_{0t} and u_{0b} denote axial displacement of the centre-line of the top and bottom skins, respectively. The complex shear modulus, $G_c^* = G_c^{'}(1 + j\eta_c)$, where $G_c^{'}$ is the shear storage modulus, $j = \sqrt{-1}$ and η_c is the core loss factor. It may be noted that while the complex shear modulus and core loss factor of the viscoelastic part of the core remain constant, these parameters for the MRE part changes with the application of magnetic field. The experimentally obtained core loss factor and shear modulus of two different types of magnetorheological elastomer have been considered in this work.

From Fig. 2.2, the axial displacements and shear strain are related by

$$u_t - u_b = cw_{,x} - 2h_c\gamma_c. \tag{2.3}$$

Taking Kerwin's (1959) assumption of a weak core one can write

$$E_t A_t u_{t,x} + E_b A_b u_{b,x} = 0 \tag{2.4}$$

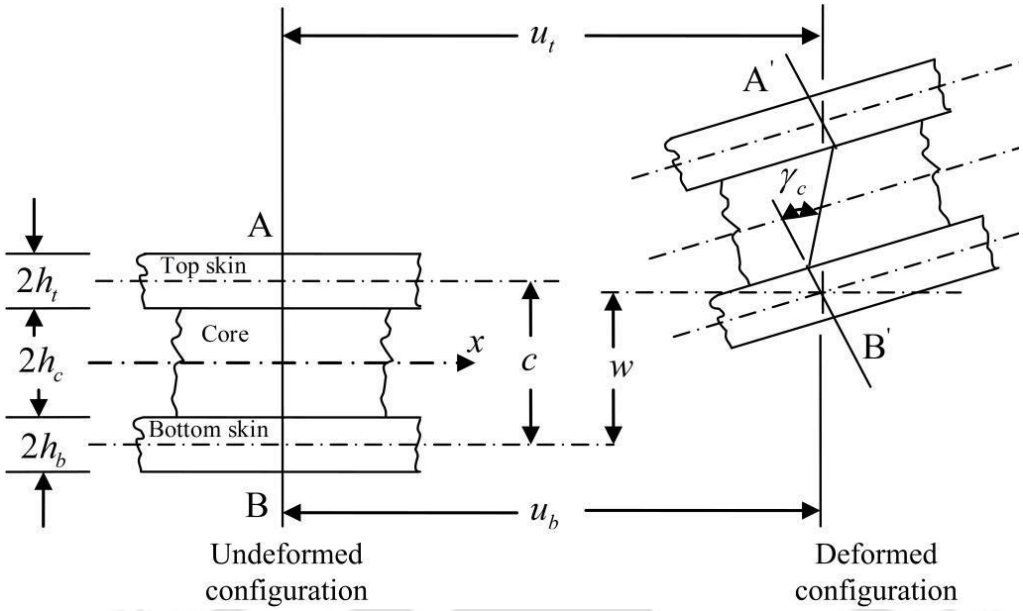

Figure 2.2 Sandwich beam before and after deformation

Solving the equations (2.3) and (2.4), the expressions for axial displacement of the top and bottom skins can be given by

$$u_t = \left(\frac{E_b A_b}{E_t A_t + E_b A_b} \right) \frac{c}{L} \left(L \frac{\partial w}{\partial x} - u \right) \tag{2.5}$$

and

$$u_b = \left(\frac{-E_t A_t}{E_t A_t + E_b A_b} \right) \frac{c}{L} \left(L \frac{\partial w}{\partial x} - u \right) \tag{2.6}$$

Here, the expression for u which is a function of shear strain γ_c in the core layer is given by

$$u = \frac{2h_c L}{c} \gamma_c . \tag{2.7}$$

The kinetic energy T of the beam can be given as follows:

$$T = \frac{1}{2} \int_0^L m w_{,t}^2 dx , \tag{2.8}$$

where, m is the mass of the beam per unit length and $(\ )_{,t}$ represents the differentiation with respect to time t.

When the skins of the sandwich beam vibrate in a magnetic field the eddy current is induced in the skins. Due to motion-induced eddy current the Lorenz body force is developed which causes the tensile deformation of the beam. Also, the surface stress is developed due to Maxwell's stress jumps which induce shear deformation of the beam and generate flexural moment distribution on the beam. Thus, the magnetoelastic loads applied to the conductive skins is equivalent to the horizontal force distribution n_j and the distributed moments m_j^m which are expressed in terms of the longitudinal displacement, u_j and transverse displacement, w_j as (Zhou and Wang, 2006b)

$$n_j = \frac{B_s{}^2 b h_j}{\mu_{ej}} u_{j,xx} \tag{2.9}$$

and

$$m_j^m = \frac{B_s{}^2 b h_j}{\mu_0}\left(\frac{\pi}{2\ln\dfrac{x}{L-x}}u_{j,x} - \frac{h_j}{2\pi}w_{j,xx}\ln\frac{x}{L-x} + w_{j,x}\right) - \frac{B_s{}^2 b h_j{}^3}{12\mu_{ej}}w_{j,xxx}. \tag{2.10}$$

Here, subscript $j = t$ and b for top and bottom skins, respectively, μ_0 and μ_e are, respectively the permeability of the free space and the skin materials.

The non-conservative work done due to the applied axial periodic load and the above mentioned magnetoelastic loads and moments can be given by

$$W = \frac{1}{2}\int_0^L P w_{,x}^2 dx + \int_0^L \left[n_t u_t + n_b u_b + m_t^m w_{,x} + m_b^m w_{,x} \right] dx, \tag{2.11}$$

where, n_t, and n_b are the horizontal forces and m_t^m and m_b^m are the distributed moments in top and bottom skins respectively due to the application of magnetic field. P is the axial periodic load.

The following non-dimensional parameters are used in this analysis. $t_0 = (mL^4/D)^{1/2}$, $\bar{t} = t/t_0$, $\bar{x} = x/L$, $\bar{u} = u/L$, $\bar{w} = w/L$, $\bar{\omega} = \omega t_0$, $\bar{P}_s = P_s L^2/D$, $\bar{P}_d = P_d L^2/D$, $\ddot{\bar{w}} = (mL^3/D)\ddot{w}$, $\bar{w}_{\bar{x}\bar{x}} = L w_{xx}$, $\bar{u}_{\bar{x}\bar{x}} = L u_{xx}$, $\bar{w}_{\bar{x}\bar{x}\bar{x}} = L^2 w_{xxx}$, $\bar{u}_{\bar{x}\bar{x}\bar{x}} = L^2 u_{xxx}$ and

$$\bar{w}_{\bar{x}\bar{x}\bar{x}\bar{x}} = L^3 w_{xxxx} \tag{2.12}$$

Here, $\bar{P}_s$ and $\bar{P}_d$ are respectively, the amplitude of non-dimensional static and dynamic load; $\bar{t}$ is the non-dimensional time and $D=\left(E_{\mathrm{t}}I_t+E_{\mathrm{b}}I_b\right)$.

Using Eqs. (2.1)-(2.12), the governing equations of motion are derived by applying the extended Hamilton's principle. The resulting non-dimensional equations of motion for coupled transverse and axial vibrations are

$$\ddot{\bar{w}}+\left(1+Y\right)w_{\bar{x}\bar{x}\bar{x}\bar{x}}+Y\frac{B_s^{\,2}}{\mu_e E_{\mathrm{t}}}\bar{w}_{\bar{x}\bar{x}\bar{x}\bar{x}}-\frac{B_s^{\,2}}{\mu_e E_{\mathrm{t}}}\bar{w}_{\bar{x}\bar{x}\bar{x}\bar{x}}-\frac{6}{\pi}\left(\frac{B_s^{\,2}}{\mu_0 E_{\mathrm{t}}}\right)\left(\frac{L}{h_t}\right)\ln\left(\frac{\bar{x}}{1-\bar{x}}\right)\bar{w}_{\bar{x}\bar{x}\bar{x}}$$

$$-Y\bar{u}_{\bar{x}\bar{x}\bar{x}}-Y\frac{B_s^{\,2}}{\mu_e E_{\mathrm{t}}}\bar{u}_{\bar{x}\bar{x}\bar{x}}+3\left(\frac{B_s^{\,2}}{\mu_0 E_{\mathrm{t}}}\right)\left(\frac{L}{h_t}\right)^2\bar{w}_{\bar{x}\bar{x}}+\left(\bar{P}_s+\bar{P}_d\cos\bar{\Omega}_2\bar{t}\right)\bar{w}_{\bar{x}\bar{x}}=0, \quad (2.13)$$

$$\bar{w}_{\bar{x}\bar{x}\bar{x}}-\bar{u}_{\bar{x}\bar{x}}+g_c^{\,*}\left(\frac{h_t}{h_c}\right)^2\bar{u}+\frac{B_s^{\,2}}{\mu_e E_{\mathrm{t}}}\bar{w}_{\bar{x}\bar{x}\bar{x}}-\frac{B_s^{\,2}}{\mu_e E_{\mathrm{t}}}\bar{u}_{\bar{x}\bar{x}}=0. \quad (2.14)$$

Here, $g_{\mathrm{c}}^{\,*}=g_{\mathrm{c}}\left(1+j\eta_{\mathrm{c}}\right)$, $g_{\mathrm{c}}=\left(\frac{G_c^{'}}{2E_t}\right)\left(\frac{h_c}{h_t}\right)\left(\frac{L}{h_t}\right)^2$ is the shear parameter, subscript $c=v$ or e depending upon non-MRE or MRE parts in the core, respectively. $Y=3\left(1+\frac{h_c}{h_t}\right)^2$. Equations (2.13) and (2.14) will reduce to that of Ray and Kar, (1995b) in the absence of magnetic field and MRE patch in the core of the sandwich beam.

2.3 Approximate Solutions

Solutions of Eqs. (2.13) and (2.14) are assumed in the form, $\bar{w}\left(\bar{x},\bar{t}\right)=\sum_{m=1}^{r}q_m\left(\bar{t}\right)w_m\left(\bar{x}\right)$, $\bar{u}\left(\bar{x},\bar{t}\right)=\sum_{k=r+1}^{s}q_k\left(\bar{t}\right)u_k\left(\bar{x}\right)$, where q_m and q_k are the time modulation and $w_m\left(\bar{x}\right)$ and $u_k\left(\bar{x}\right)$ are the shape functions. Using generalized Galerkin's method Eqs. (2.13) and (2.14) can be written as follows.

$$\left[M\right]\ddot{\mathrm{Q}}_1+\left[K_{11}\right]\mathrm{Q}_1+\left[K_{12}\right]\mathrm{Q}_2-\bar{P}\left[F_f\right]\mathrm{Q}_1=0 \quad (2.15)$$

$$\left[K_{21}\right]\mathrm{Q}_1+\left[K_{22}\right]\mathrm{Q}_2=0 \quad (2.16)$$

where, $\left[K_{21}\right]=\left[K_{12}\right]^{\mathrm{T}}$, $\mathrm{Q}_1=\left\{q_1,q_2,.....q_r\right\}^{\mathrm{T}}$ and $\mathrm{Q}_2=\left\{q_{r+1},q_{r+2},.....q_s\right\}^{\mathrm{T}}$

Substituting Eq. (2.16) in Eq. (2.15) leads to the following equation of motion.

$$[M]\ddot{Q}_1+[K]Q_1-\left(\bar{P}_d\cos\bar{\Omega}_2\bar{t}\right)\left[F_f\right]Q_1=0 \tag{2.17}$$

where, $[K]=[K_{11}]-\bar{P}_s\left[F_f\right]-[K_{12}][K_{22}]^{-1}[K_{12}]^{\mathrm{T}}$

Here $[M]$ and $[K]$ are mass and stiffness matrices respectively and $\left[F_f\right]$ is the geometric stiffness matrix.

The elements of various matrices are given as follows:

$$M_{ij}=\int_0^1 w_i w_j d\bar{x},$$

$$(K_{11})_{ij}=\int_0^1(1+Y)w_{i,\bar{x}\bar{x}}w_{j,\bar{x}\bar{x}}d\bar{x}+\int_0^1 Y\frac{B_s^{\,2}}{\mu_e E_{\mathrm{t}}}w_{i,\bar{x}\bar{x}}w_{j,\bar{x}\bar{x}}d\bar{x}-\int_0^1\frac{B_s^{\,2}}{\mu_e E_{\mathrm{t}}}w_{i,\bar{x}\bar{x}}w_{j,\bar{x}\bar{x}}d\bar{x}$$

$$-\int_0^1\frac{6}{\pi}\frac{B_s^{\,2}}{\mu_0 E_{\mathrm{t}}}\left(\frac{L}{h_t}\right)\ln\left(\frac{\bar{x}}{1-\bar{x}}\right)w_{i,\bar{x}}w_{j,\bar{x}\bar{x}}d\bar{x}-\int_0^1 3\frac{B_s^{\,2}}{\mu_0 E_{\mathrm{t}}}\left(\frac{L}{h_t}\right)^2 w_{i,\bar{x}}w_{j,\bar{x}}d\bar{x},$$

$$(K_{12})_{ik}=-\int_0^1 Y w_{i,\bar{x}\bar{x}}u_{k,\bar{x}}d\bar{x}-\int_0^1 Y\frac{B_s^{\,2}}{\mu_e E_{\mathrm{t}}}w_{i,\bar{x}\bar{x}}u_{k,\bar{x}}d\bar{x},$$

$$(K_{22})_{kl}=\int_0^1 Y u_{k,\bar{x}}u_{l,\bar{x}}d\bar{x}+\int_0^1 Y\frac{B_s^{\,2}}{\mu_e E_{\mathrm{t}}}u_{k,\bar{x}}u_{l,\bar{x}}d\bar{x}+\int_0^1 Y g_v^*\left(\frac{h_1}{h_2}\right)^2 u_{k,\bar{x}}u_{l,\bar{x}}H_1 d\bar{x}$$

$$+\int_0^1 Y g_e^*\left(\frac{h_1}{h_2}\right)^2 u_{k,\bar{x}}u_{l,\bar{x}}H_2 d\bar{x},$$

$$F_{fij}=\int_0^1 w_{i,\bar{x}}w_{j,\bar{x}}d\bar{x}.$$

where, $i, j = 1, 2, 3,\ldots\ldots\ldots\ldots$, r; $k, l = (r+1),\ldots\ldots\ldots\ldots$, s

$$H_1=1-H\left(\bar{x}-\bar{L}_1\right)+H\left(\bar{x}-\bar{L}_2\right),\quad H_2=H\left(\bar{x}-\bar{L}_1\right)+H\left(\bar{x}-\bar{L}_2\right). \tag{2.18}$$

Here, H is the Heaviside function, $\bar{L}_1=L_1/L$ and $\bar{L}_2=L_2/L$. Lengths L_1 and L_2 are shown in Fig. 2.1. Here it may be noted that the Heaviside function is used to take care the location of the MRE patch in the core of the sandwich beam. Taking $[R]$ as the normalized modal matrix of $[M]^{-1}[K]$ and using linear transformation $Q_1=[R]q$ in Eq. (2.17), one may obtain

$$\ddot{q}_m + (\omega_m^*)^2 q_m + 2\varepsilon \cos\bar{\Omega}_2 \bar{t} \sum_{n=1}^{S} b_{mn}^* q_n = 0. \tag{2.19}$$

where, $m = 1,2,.....r$

Here $\left(\omega_m^*\right)^2$ are the distinct eigenvalues of $[M]^{-1}[K]$ and b_{mn}^* are the elements of the complex matrix $[B] = -[R]^{-1}[M]^{-1}[F][R]$, and $\varepsilon = \bar{P}_d/2 < 1$. The complex frequency and forcing parameters in terms of real and imaginary parts are given by $\omega_m^* = \omega_{m,R} + j\omega_{m,I}$ and $b_{mn}^* = b_{mn,R} + jb_{mn,I}$.

In this work the sandwich beam with five different boundary conditions viz. (a) simply supported, (b) guided-pinned, (c) clamped-free (d) clamped-pinned and (e) clamped-clamped unrestrained have been considered. The shape functions taken for the numerical calculations are same as those in the work of Ray and Kar, (1995b). For the completeness of the work, these shape functions as follows:

For simply supported beam:

$$w_m(\bar{x}) = \sin(m\pi\bar{x}), \quad u_k(\bar{x}) = \cos(\bar{k}\pi\bar{x}) \tag{2.20}$$

where, $\bar{k} = k - r$

For guided-pinned:

$$w_m(\bar{x}) = \cos\left((2m-1)\pi\bar{x}/2\right), \quad u_k(\bar{x}) = -\left(\left(2\bar{k}-1\right)\pi/2\right)\sin\left(\left(2\bar{k}-1\right)\pi\bar{x}/2\right) \tag{2.21}$$

For cantilevered:

$$w_m(\bar{x}) = (m+3)(m+2)\left((m+2)(m+1)-\mu_2\right)\bar{x}^{(m+1)} + \left[2(m+3)(m+1)\right.$$
$$\left.\left(\mu_2 - m(m+2)\right) + \mu_1 m(m+1)/\left((m+2)(m+1)-\mu_2\right)\right]\bar{x}^{(m+2)} + \left[(m+2)\right.$$
$$\left.(m+1)\left(m(m+1)-\mu_2\right) - \mu_1 m(m+1)^2/\left((m+3)(m+2)(m+1) - (m+3)\mu_2\right)\right]\bar{x}^{(m+3)},$$

$$u_k(\bar{x}) = \left(\bar{k}+1\right)\bar{x}^{\bar{k}} - \bar{k}\bar{x}^{(\bar{k}+1)} \tag{2.22}$$

For clamped-pinned:

$$w_m(\bar{x}) = 2(m+2)\bar{x}^{(m+1)} - (4m+6)\bar{x}^{(m+2)} + 2(m+1)\bar{x}^{(m+3)}, \; u_k(\bar{x}) = \left(\bar{k}+1\right)\bar{x}^{\bar{k}} - \bar{k}\bar{x}^{(\bar{k}+1)} \tag{2.23}$$

For clamped-clamped unrestrained:

$$w_m(\bar{x}) = (m+3)(m+2)^2(m+1)\left(\bar{x}^{(m+1)} - 2\bar{x}^{(m+2)} + \bar{x}^{(m+3)}\right),$$

$$u_k(\bar{x}) = \left(\bar{k}+1\right)\bar{x}^{\bar{k}} + \left[2/\left(\bar{k}+1\right) - \bar{k}\right] - \bar{x}^{(\bar{k}+1)} \tag{2.24}$$

For free vibration analysis of the system one may substitute $P(t) = 0$ (i.e., $P_s = P_d = 0$) in equation (2.17). The natural frequencies can be obtained by finding the eigenvalues of the resulting $[M]^{-1}[K]$ matrix. Also the free vibration response can be obtained by numerically solving equation (2.17) after substituting $P_s = P_d = 0$. In contrast to the analysis of sandwich beam using higher order theory (Dwivedy *et al.*, 2009), one needs to solve four times less no of equations for finding the response of the system using the proposed approach. Unlike the work of Howson and Zare, (2005), where a sixth order differential equation has been solved, or the work of Banerjee *et al*., (2007), where a tenth order differential equation has been solved to obtained the natural frequencies of the system, in the present work a fourth order differential equation has been solved for the dynamic analysis of the system.

To obtain the principal parametric instability region following expressions derived by using the modified Hsu method (Ray and Kar, 1995b), has been used.

$$\left|(\bar{\Omega}_2/2) - \omega_{\alpha,R}\right| < \frac{1}{4}\chi_\alpha \text{, where, } \chi_\alpha = \left[\frac{4\varepsilon^2\left(b^2{}_{\alpha\alpha,R} + b^2{}_{\alpha\alpha,I}\right)}{\omega^2{}_{\alpha,R}} - 16\omega^2{}_{\alpha,I}\right]^{1/2}, \tag{2.25}$$

where, $\alpha = 1, 2, 3, \ldots\ldots\ldots\ldots\ldots, r$.

A code has been developed using MATLAB to determine the system response and instability regions of the sandwich beam with different boundary conditions.

2.4 Results and Discussions

Initially experiment has been carried out to validate the assumption of equal transverse displacements in the top and bottom skins of a transversely stiff viscoelastic cored sandwich beam. Then the free vibration analysis of the MRE embedded sandwich beam has been carried out and the natural frequencies obtained in the present analysis are compared with those analytically and experimentally

obtained published results. After validating the free vibration characteristics of the system, the parametric instability regions of the sandwich beam for five different boundary conditions viz., (a) simply supported, (b) guided-pinned, (c) clamped-free (d) clamped-pinned and (e) clamped-clamped unrestrained end conditions have been determined for the first three modes of transverse vibration.

2.4.1 Validation of the Assumption

Experimental measurements of transverse displacements of the skins of two sandwich beam samples under free vibration have been carried out using an impulse hammer kit with its associated software for data capturing and analysis. The beam samples are fabricated from commercial grade aluminum sheets as skins and commercial grade rubber sheets as core. The fabricated beam has a span, $L = 500$ mm; width, $b = 30$ mm; the top and bottom skins thickness, $2h_t = 2h_b = 2$ mm, the core thickness, $2h_c = 6$ mm. The experimental set up using the impact hammer kit consisting of a PC driven ACE dynamic signal analyser and two accelerometers are shown in Fig. 2.3. Brüel and Kjaer made PULSE analyzer (type 3560 D, software version 13.1.0) and accelerometers (type 4396, sensitivity-9.88 and 9.9 mv/ms^{-2}) are used for analysis purpose. Both the test specimens were cantilevered with one end fully built-in in order to prevent all displacements. The accelerometers are set one below another at fixed positions on the top and bottom skins of the test specimen. The response signals recorded by the accelerometers attached to the test specimen. The frequency and time responses are shown in the Fig. 2.4 and Fig. 2.5 respectively when the accelerometers are placed at the free end of the test specimen. It is found that, the transverse displacements of the top and bottom skins have same amplitude and frequency having some phase difference between them. Hence, the assumption of having same transverse displacement in the top and bottom skin in a viscoelastic cored sandwich beam is validated. The Young's modulus and density of aluminum obtained from the experiment are 69.53 GPa and 2618.03 kg/m^3 and for rubber, the shear modulus and density are 1.886 MPa, 1800 kg/m^3, respectively, the theoretical fundamental frequency is found to be 16.06 Hz, which is in good agreement with the experimental result, 17 Hz (Fig. 2.4).

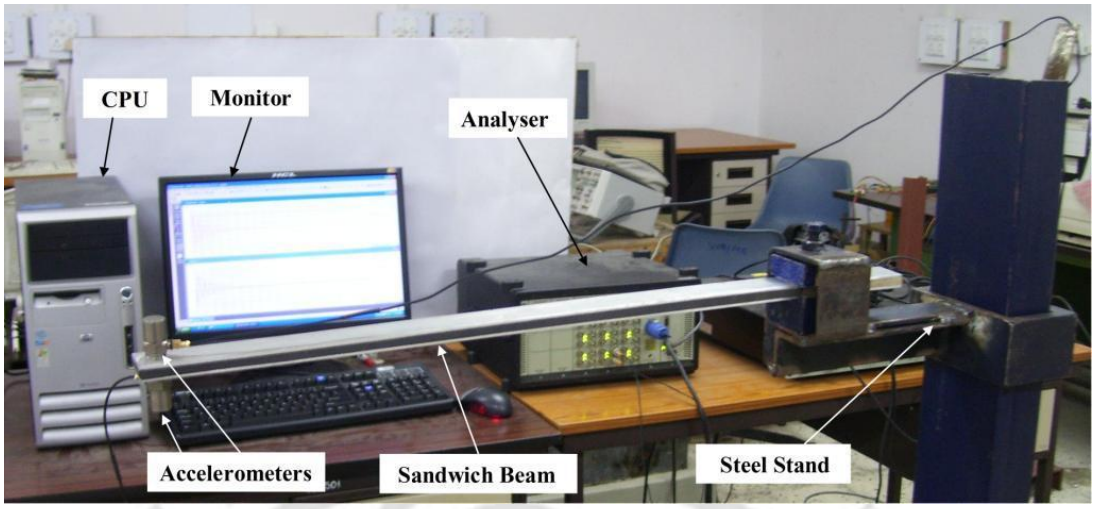

Figure 2.3 Experimental set up for determination of response of top and bottom skins.

2.4.2 Comparison of Natural Frequencies

Taking the axially applied periodic load to be zero, the governing equation of motion (2.17) reduces to that of the free transverse vibration of an MRE embedded sandwich beam with magnetic field. As mentioned in section 2.3, the natural frequencies of the systems are obtained by finding the eigenvalues of the resulting dynamic matrix $\left([A]=[M]^{-1}[K]\right)$. Also, the free vibration responses for sandwich beam with and without the MRE patch have been plotted using Runge-Kutta method. Following five different case studies have been considered.

Case 1: Taking the following nondimensional parameters of the sandwich beam as given in Ray and Kar, (1995b) the natural frequencies of the sandwich beam without magnetic field and MRE patch have been determined. The ratio of core thickness to skin thickness, h_c/h_t =1, shear parameter g = 0.05, core loss factor η_c = 0.18 and the ratio of shear modulus of core to Young's modulus of skin G_c/E_t = 0.0002 have been considered here. The natural frequencies for simply supported, guided-pinned, clamped-free, clamped-pinned and clamped-clamped unrestrained end conditions have been determined for the first three modes as given in Table 2.1. It may be observed that these results are in good agreement with those obtained by Ray and Kar, (1995b).

This was expected as the equation of motion reduces to that of Ray and Kar [13] in the absence of MRE patch and magnetic field. This validates the code developed in the present work using MATLAB.

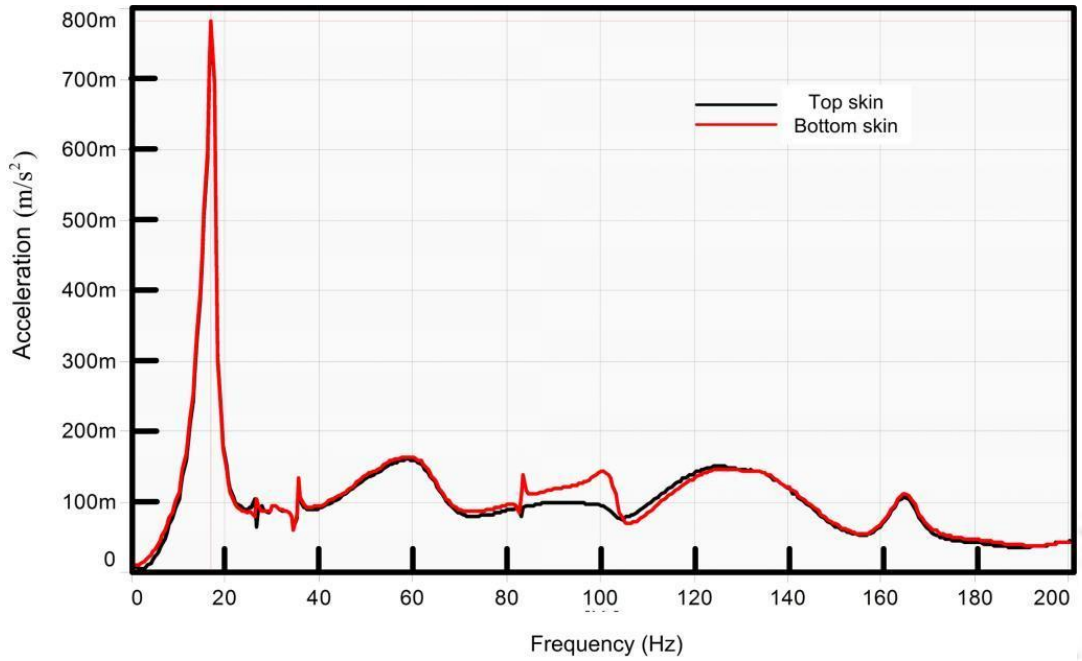

Figure 2.4 Frequency response of both the skins of the sandwich beam subjected to free vibration

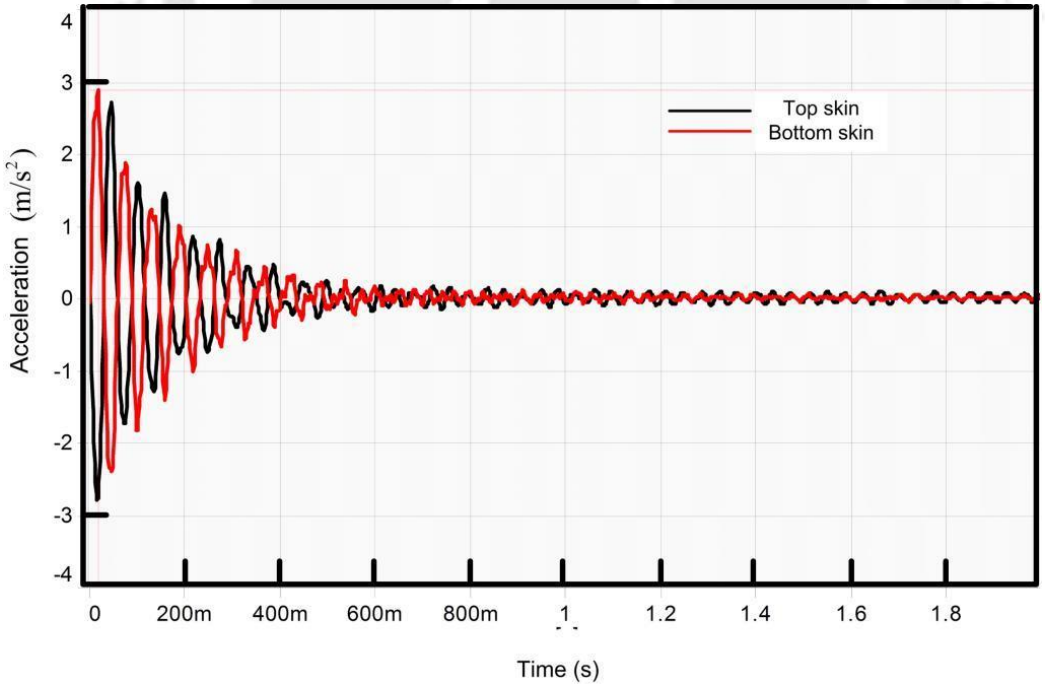

Figure 2.5 Time response of both the skins of the sandwich beam subjected to free vibration

Table 2.1 Comparison of the first three mode non-dimensional modal frequencies of the sandwich beam without magnetic field and MRE patch for five different boundary conditions.

End arrangements of the sandwich beam	Non-dimensional modal frequencies		
	Mode	Present Analysis	Ray and Kar, (1995b) (From Figures (5,7,8,9and 13))
Simply Supported	1	10.16	10.00
	2	39.77	39.50
	3	89.12	89.00
Guided Pinned	1	2.74	2.50
	2	22.50	22.48
	3	61.98	61.75
Clamped-free	1	3.88	3.75
	2	22.46	22.35
	3	62.14	62.00
Clamped Pinned	1	15.64	15.50
	2	50.23	50.00
	3	104.66	104.50
Clamped-Clamped Unrestrained	1	22.89	22.50
	2	64.42	64.02
	3	123.17	122.50

Case 2: In this case the natural frequencies of a simply supported beam have been compared with those of Howson and Zare, (2005). Here the system parameters are length, $L = 0.9144$ m, width, $b = 25.4$ mm, core thickness, h_c =12.7 mm, skin thickness, $h_t = h_b = 0.4572$ mm, $E_t = E_b = 68.9$ GPa, $G_c = 82.68$ MPa, $\rho_t = \rho_b = 2680$ kg/m^3 and $\rho_c = 32.8$ kg/m^3 which are same as that in (Howson and Zare, 2005). The frequencies are shown in Table 2.2 and are found to be very close to the frequencies reported by Howson and Zare, (2005) which are obtained by using finite element method. It may be noted that Howson and Zare, (2005) used a sixth

order differential equation of motion and here a fourth order differential equation of motion is used in the analysis. This shows the usefulness of this work where a lower order differential equation is solved to get similar results.

Table 2.2 Comparison of the modal frequencies (Hz) of a simply supported sandwich beam.

End arrangement of the sandwich beam	Modal frequencies (Hz)		
	Mode	Present Analysis	Howson and Zare, (2005)
Simply Supported	1	57.136	57.136
	2	219.585	219.585
	3	465.173	465.172
	4	768.178	768.177
	5	1106.686	1106.68
	6	1465.109	1465.10

Case 3: Here the modal frequencies of a cantilever sandwich beam have been obtained by taking the system parameters $E_t = E_b = 72$ GPa, $G_c = 0.5$ MPa, $\rho_t = \rho_b = 2700$ kg/m^3, $\rho_c = 950$ kg/m^3, skins thickness, $h_t = h_b = 2$ mm, core thickness, $h_c = 18$ mm, width, $b = 25$ mm and length, $L = 500$ mm which are similar to those taken by the experimental work of Banerjee *et al*., (2007). Table 2.3 shows the theoretically and experimentally obtained natural frequencies in work of Banerjee *et al*., (2007) and those in the present work. It may be noted that Banerjee *et al*., (2007) used a tenth order differential equation of motion in their theoretical work and here a fourth order differential equation of motion is used in the analysis. From Table 2.3 it is noted that while there is a wide mismatch between the theoretical and experimental work of Banerjee *et al*., (2007), the first and third mode frequencies obtained in the present work are in very good agreement with those of the experimental work of Banerjee *et al*., (2007). This shows the applicability of the present simpler model.

Table 2.3 Comparison of the present modal frequencies (Hz) with the experimentally obtained modal frequencies (Banerjee *et al*., 2007) of a cantilevered sandwich beam.

End arrangement	Mode	Modal frequencies (Hz)		
		Present Analysis	Banerjee *et al*., (2007) Experimental	Banerjee *et al*, (2007) Theoretical
Cantilever	1	12.308	11.25	10.46
	2	43.204	33.75	36.31
	3	94.427	93.75	75.94

Case 4: In this example, a simply supported fully MRE cored sandwich beam used in the theoretical and experimental work of Sun *et al.*, (2003) has been considered. Table 2.4 shows the fundamental frequencies which are obtained for the system without and with the applied magnetic field of 900 Oe. The system parameters considered are $E_t = E_b = 70$ GPa, $G_t = G_b = 65.6$ MPa, $\rho_t = \rho_b = 2700$ kg/m^3, $G_c = 0.621$ MPa (at 0 T) and $G_c = 1.167$ MPa (at 0.09 T), $\rho_c = 3.5$ kg/m^3, skins thickness $h_t = h_b = 1$ mm, core thickness, $h_c = 1$ mm, width, $b = 25$ mm and length, $L = 400$ mm.

It may be observed that though the theoretical results of Sun *et al.*, (2003) are not in good agreement with their experimental results, the present results are in very good agreement with the experimental results of Sun *et al.*, (2003).

Table 2.4 Comparison of the present fundamental frequencies with the theoretically and experimentally obtained fundamental frequencies of Sun *et al.*, (2003).

Magnetic Field	Fundamental frequency (Hz)		
	Present Analysis	Sun *et al.*, (2003) Theoretical	Sun *et al.*, (2003) Experimental
0 T	34.016	22.23	31.373
0.09 T (900Oe)	40.499	23.24	41.176

Case 5: In this case, considering a magnetic field of 1Tesla, the natural frequencies of the MRE embedded foam cored simply supported sandwich beam used in the work of Zhou and Wang, (2006b) has been compared with those obtained in the present analysis. The natural frequencies are shown in Table 2.5 taking system parameters $E_t = E_b = 72$ GPa, $\rho_t = \rho_b = 2700$ kg/m^3,

$G_c = 0.6208$ MPa and $\rho_c = 1100$ kg/m^3; and physical parameters, top and bottom skins thickness $h_t = h_b = 0.1$ mm, core thickness, $h_c = 2$ mm, width, $b = 0.1L$ mm and length, $L = 150$ mm. It has been found that a maximum of 5% of difference obtained between these two works. It may be noted that higher order theory is used in the work of Zhou and Wang, (2006b).

Table 2.5 Comparison of the modal frequencies (Hz) obtained in the present analysis with those obtained by Zhou and Wang, (2006b).

Magnetic field	Modal frequencies (Hz)			Percentage of difference
	Mode	Present Analysis	Zhou and Wang, (2006b)	
1 T	1	67.338	68.816	2.14
	2	144.923	152.441	4.91
	3	222.145	225.08	1.30

As the natural frequencies obtained using the present analysis are in good agreement with the experimentally and analytically obtained natural frequencies by several researchers, the principal parametric resonances which occur near twice the natural frequencies may be considered to be in consistent with the experimental findings. The time response of MRE embedded simply supported sandwich beam has been discussed in the following subsection.

2.4.3 Free Vibration Response of MRE Embedded Sandwich Beam

In this subsection the time response of the MRE embedded sandwich beam with and without magnetic field has been plotted to show the advantage of using magnetic field to reduce the vibration. This has also been compared with a similar sandwich beam without considering MRE patch. Following physical parameters have been taken for the numerical analysis. The span of the beam, $L = 230$ mm; width, $b = 23$ mm; the top and bottom skins thickness, $2h_t = 2h_b = 4$ mm, the core thickness, $2h_c = 8$ mm. The top and bottom aluminum skins have Young's modulus 72 GPa and density 2700 kg/m^3. The zero field shear modulus and young's modulus of both MRE (Chen *et al.*, 2007 and *Chen et al.*, 2008) and non-MRE parts are same. The

length of the MRE patch is one third of the length of the core and is symmetrically placed at the middle. MRE containing 80% of iron particles has been considered in this work and its properties are taken from the experimental work of Chen *et al.*, (2007) which is given in Table 2.6.

Table 2.6 Variations of shear modulus and core loss factor with magnetic field for two different natural rubber based MREs.

Magnetic field B_s (T)	Shear modulus, G (MPa)		Core loss factor, η_c	
	80% of iron particles (Chen *et al.*, 2007)	33% of iron particles and 7% carbon black (Chen *et al.*, 2008)	80% of iron particles (Chen *et al.*, 2007)	33% of iron particles and 7% carbon black (Chen *et al.*, 2008)
0.2	4.143	4.100	0.283	0.18
0.4	5.571	6.000	0.292	0.18
0.6	6.143	8.000	0.275	0.18
0.8	6.143	8.000	0.263	0.18

Figure 2.6 shows the first three modes free vibration response of the simply supported sandwich beam without and with MRE patch in the core. The solid line shows the response for the system without MRE patch. For the system with MRE patch, the dotted line and dashed lines show the response of the system with magnetic fields of 0.2 T and 0.6 T, respectively. With the insertion of MRE patch the response peak decreases with the application of magnetic field. It has been observed that with the increase in magnetic field to 0.6 T for the MRE embedded viscoelastic core the response peak decreases by 6%, 36% and 28% as compared to the viscoelastic cored sandwich beam for the fast, second and third modes, respectively.

Now by considering a clamped-free sandwich beam with MRE embedded viscoelastic core the free vibration responses have been obtained for a magnetic field of 0.2 T and 0.6 T (Fig. 2.7). The physical dimensions and material properties are

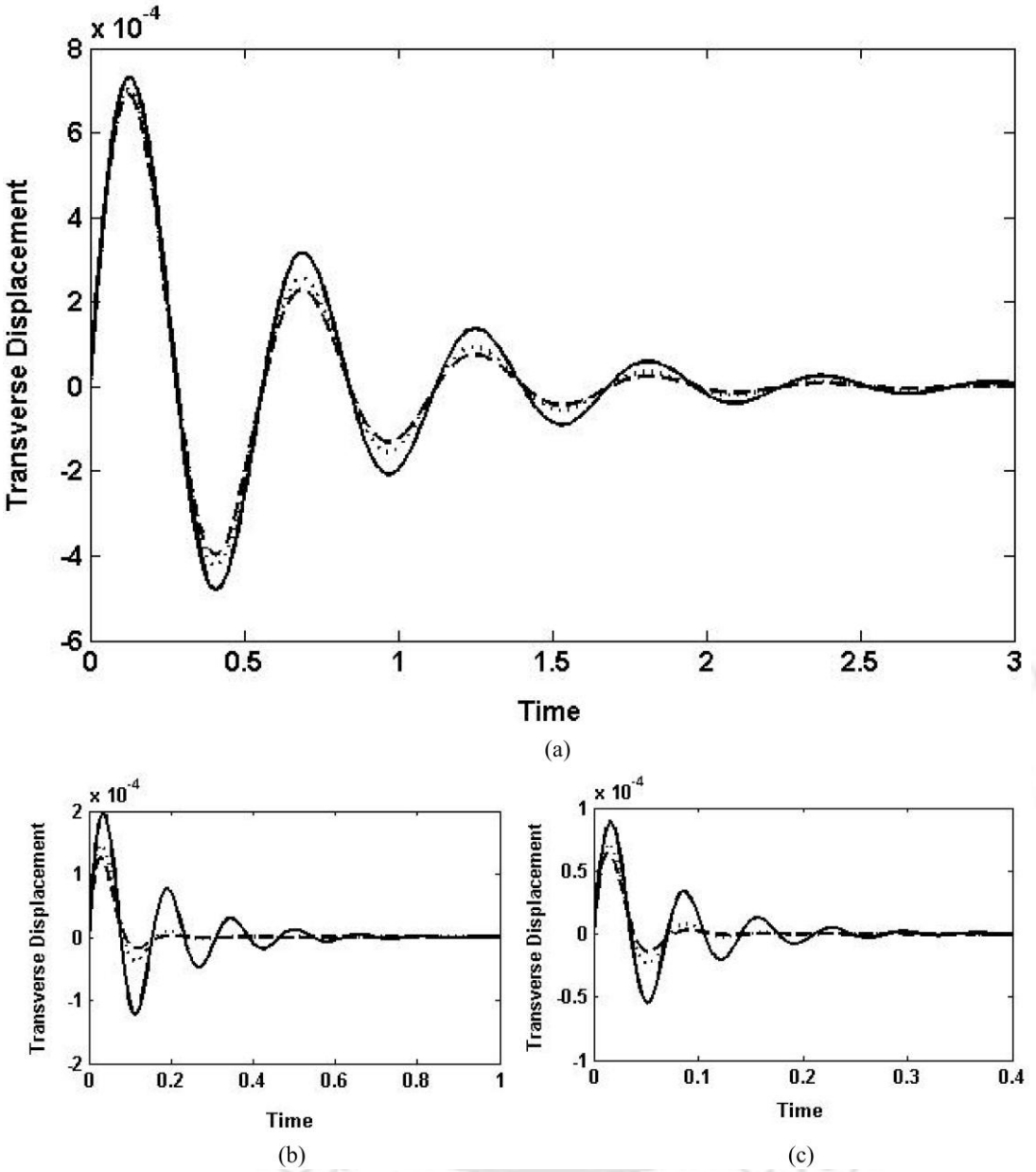

Figure 2.6 Free vibration response of a simply supported sandwich beam with and without MRE patch in the core for (a) first mode, (b) second mode and (c) third mode —— viscoelastic core, ····· $B_s = 0.2\,\mathrm{T}$ and – – – $B_s = 0.6\,\mathrm{T}$.

same as those of the simply supported beam considered before. These responses have been compared with that of a viscoelastic cored clamped-free sandwich beam. It has been observed that with the increase in magnetic field the response amplitude decreases. For example, as shown in Fig. 2.6, with a magnetic field of 0.6 T, for the MRE embedded viscoelastic core the response amplitude decreases by 30.63% for

the first mode, 12.7% for the second mode and 30.4% for the third mode in comparison to the viscoelastic cored sandwich beam.

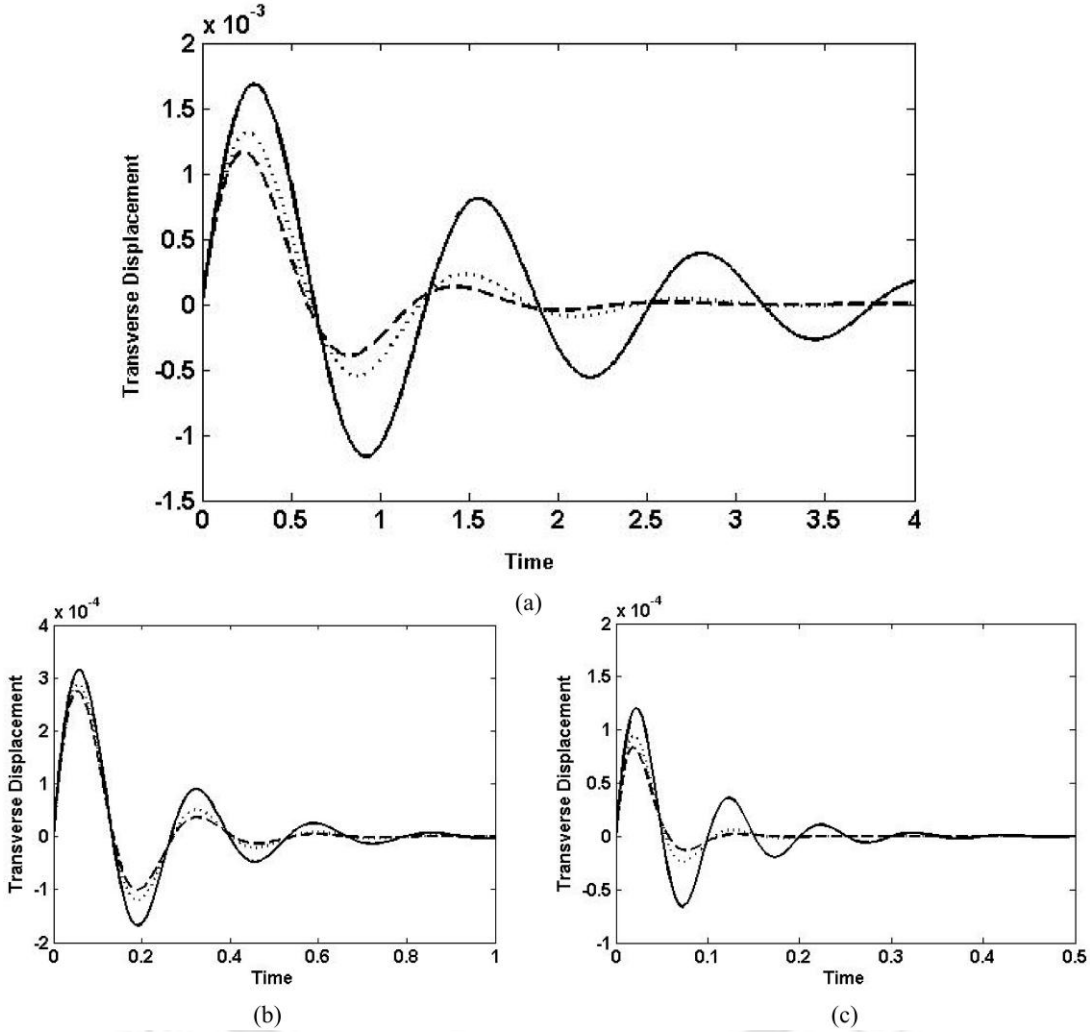

Figure 2.7 Free vibration response of a clamped-free sandwich beam with and without MRE patch in the core for (a) first mode, (b) second mode and (c) third mode. ——— viscoelastic core, ····· $B_s = 0.2\,\mathrm{T}$ and – – – $B_s = 0.6\,\mathrm{T}$.

Figure 2.8 shows the first three mode free vibration responses of a simply supported sandwich beam with four different cores, viz., core 1: fully viscoelastic, core 2: MRE embedded viscoelastic core with MRE patch length $L/3$, core 3: MRE embedded viscoelastic core with MRE patch length $2L/3$, and core 4: fully MRE core. Figure 2.9 shows similar plots for a clamped-free sandwich beam. From these two figures one may clearly observe that by increasing the length of the MRE patch, the response amplitude decreases.

Hence, these two examples illustrate that it is possible to control the free vibration of MRE embedded viscoelastic core sandwich beam with the application of magnetic field. For a clamped-free sandwich beam the vibration reduction is found to be more in comparison to that of a simply supported sandwich beam.

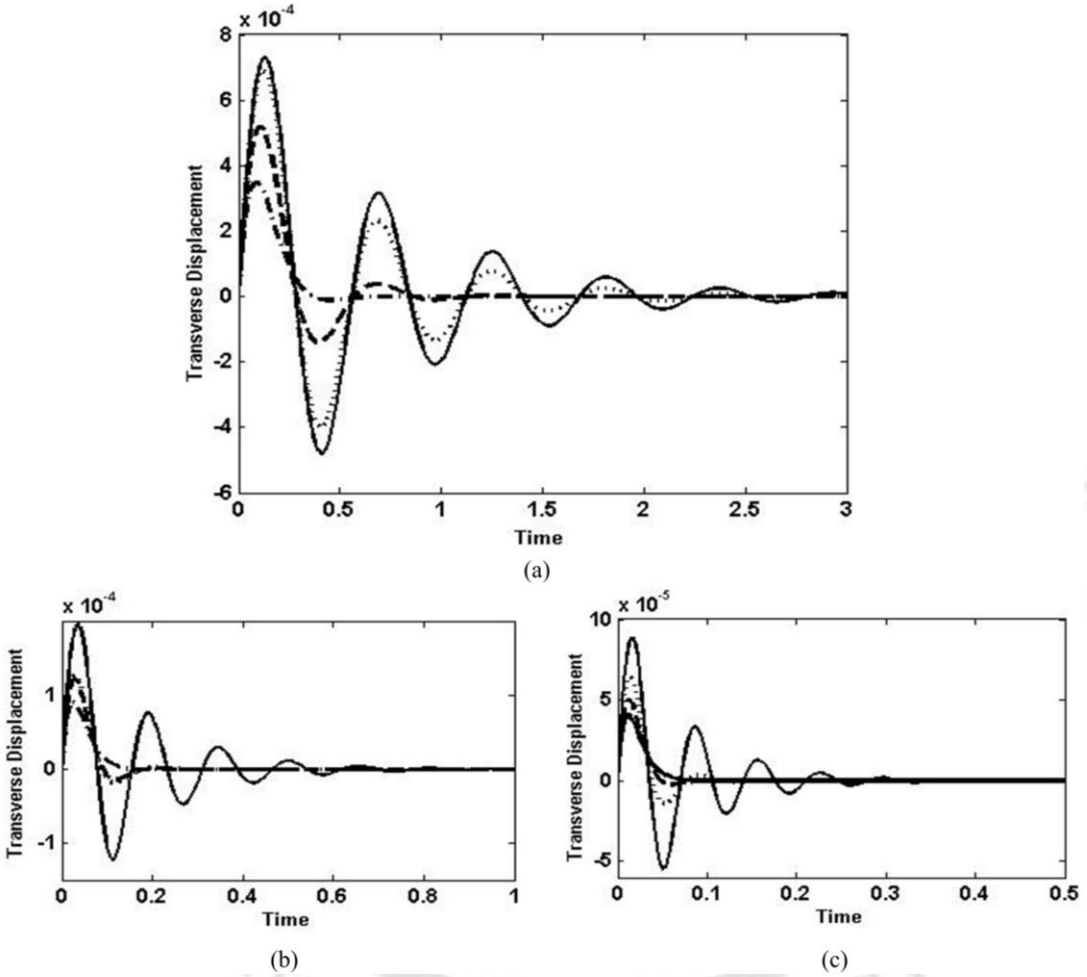

Figure 2.8 Free vibration response of a simply supported sandwich beam with variation of length of MRE patch for (a) first mode (b) second mode and (c) third mode at a magnetic field of 0.4T. ——— core 1, ····· core 2, – – – core 3 and — · — core 4.

2.4.4 Instability Regions of MRE embedded Sandwich Beam with Periodic Axial Load

In this section the sandwich beam considered in section 2.4.3 is taken for finding the parametric instability regions. For numerical analysis purpose, the developed natural rubber based MRE with iron particles and carbon blacks have been considered.

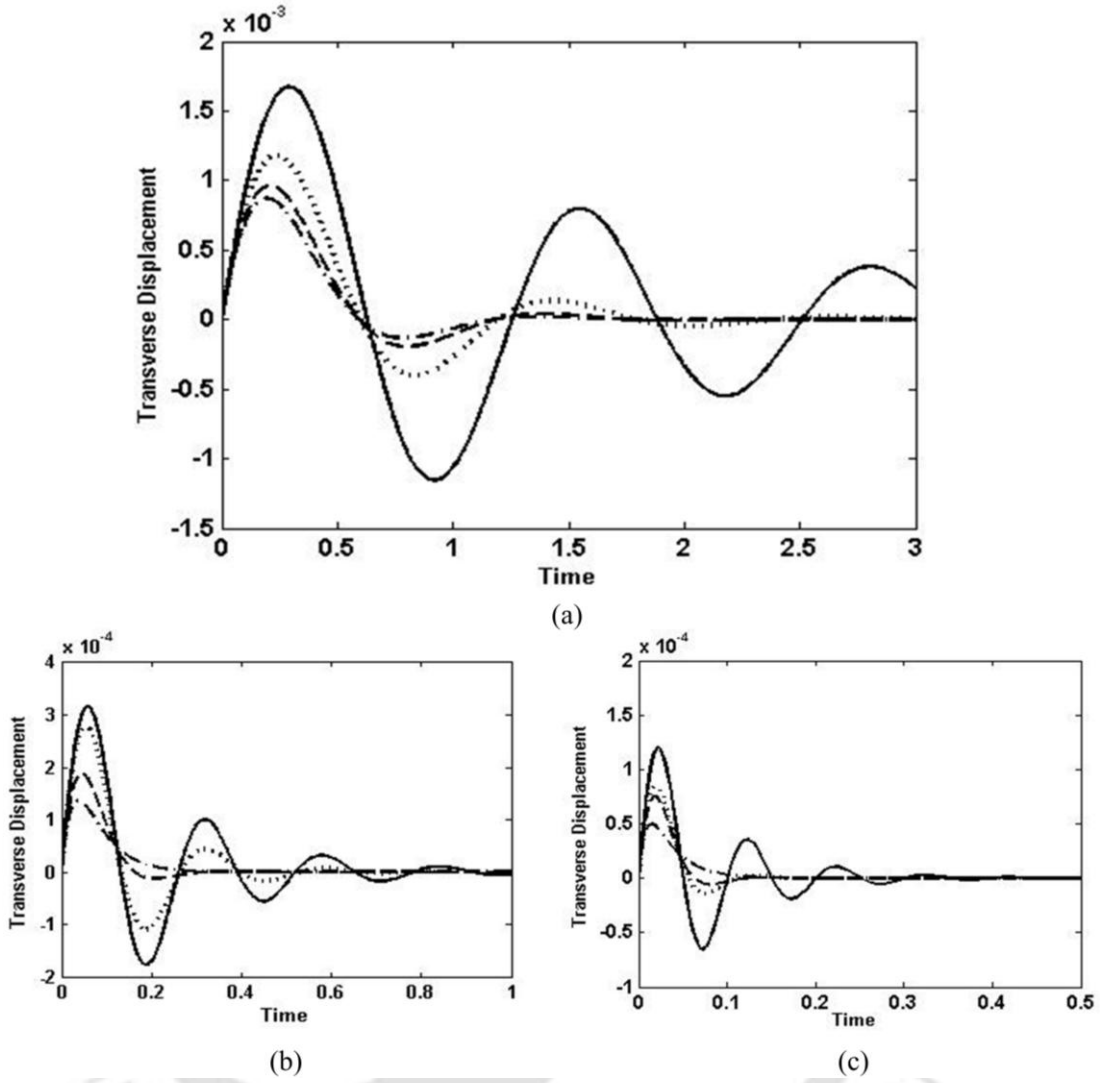

Figure 2.9 Free vibration response of a clamped-free sandwich beam with variation of length of MRE patch for (a) first mode (b) second mode and (c) third mode at a magnetic field of 0.4T. ——— core 1, ····· core 2, – – – core 3 and — · — core 4.

Table 2.6 shows the variation of material properties with magnetic field obtained experimentally for two different natural rubber based MRE, viz., MRE containing 80% iron particles (Chen *et al.*, 2007), and MRE containing 33% of iron particles with 7% of carbon black (Chen *et al.*, 2008). The MRE with 80% of iron particles has the ratio of plasticizer to natural rubber equal to 1. Similarly the MRE with 33% of iron particles and 7% of carbon black has the ratio of plasticizer to natural rubber equal to 1.03 (Chen *et al.*, 2008). It may be observed that for 7% carbon black, the variation in core loss factor is negligible. It may be noted that the percentage of plasticizers used in both

cases are different. It may also be observed that for a particular percentage of iron particles, with increase in magnetic field, the shear modulus increases and the core loss factor initially increases and then decreases. By reducing the iron particle to 33% and adding 7% carbon black one may observe that the shear modulus is more than that of MRE with 80% iron particle. But the core loss factor which is a measure of damping has a lower value in this case and is unaffected by using magnetic field.

The variations of shear modulus and core loss factor for MRE with different percentage of iron particles and carbon black have been shown in Table 2.7. It is observed from the experiment (Chen *et al.*, 2007) that for same magnetic field strength, with increase in percentage of iron particles, the shear modulus and core loss factor increases. Use of higher percentage of plasticizer also increases the shear modulus and core loss factor. For example in case of 60 percentage iron particle where the weight fraction of plasticizer is 20%, the shear modulus and core loss factor are respectively 1.857 MPa and 0.163, but for MRE with 33% iron and 7% carbon black the weight fraction of plasticizer is 30.9 % and here the shear modulus and core loss factor are respectively, 2.2 MPa and 0.25 (Chen *et al.*, 2008). For same percentage of iron particle, with increase in percentage of carbon black, though the shear modulus increases, the core loss factor decreases. The non-dimensional static load parameter $\bar{P}_0$ has been taken as 0.1.

Table 2.7 Variation of shear modulus and core loss factor for natural rubber based MREs with percentage of iron particles (ratio of plasticizers to natural rubber =1) (Chen *et al.*, 2007) and carbon blacks (ratio of plasticizers to natural rubber =1.03) (Chen *et al.*, 2008) at constant magnetic field of 0.8 T.

Types of MRE	Storage shear modulus, G (MPa)	Core loss factor, η_c	Reference
60 % iron particles	1.857	0.163	Chen *et al.*, (2007)
70 % iron particles	3.714	0.225	Chen *et al.*, (2007)
80 % iron particles	6.143	0.260	Chen *et al.*, (2007)
33% iron particles with 0 % carbon black	2.189	0.254	Chen *et al.*, (2008)
33% iron particles with 4 % carbon black	3.660	0.208	Chen *et al.*, (2008)
33% iron particles with 7 % carbon black	8.075	0.165	Chen *et al.*, (2008)

In case of parametrically excited system, even by applying a periodic load with amplitude very less than the critical Euler buckling load, the sandwich beam buckles and vibrate for certain amplitude and frequency of excitation. Table 2.8 shows the critical Euler buckling loads for various boundary conditions. For example, taking $\bar{P}_s$ =0.1, and $\bar{P}_d$ = 2, the maximum amplitude of periodic axial load $P(t)$ is found to be 19.512 kN which is less than the critical Euler buckling load mentioned in Table 2.8. But for certain frequency range with this amplitude of dynamic loading, the system can be found to buckle and vibrate and becomes unstable. Hence, to avoid such vibration, the study of the parametric instability regions is very important which will provide information regarding the operating amplitude and frequency for the sandwich beam. In all the figures of parametric instability regions, while the region bounded by the curves is unstable, the regions outside the curves are stable.

Table 2.8 Critical Euler buckling load of the sandwich beam for various boundary conditions.

Boundary conditions	Effective length, L_e (m) Srinath, (2007)	Critical buckling load, (kN)
Simply Supported	L	91.703
Guided-pinned	$2L$	22.926
Clamped-free	$2L$	22.926
Clamped-pinned	$0.7L$	187.15

The instability regions for the sandwich beam with MRE embedded viscoelastic core for the simply supported sandwich beam have been determined for first three modes and are shown in Fig.2.10 for principal parametric resonance condition with different magnetic field strength. Considering only viscoelastic core (i.e. core without MRE patch), the solid line shows the parametric instability regions for the first three modes of the sandwich beam for principal parametric resonance. It is noted from this figure that with decrease in $\bar{P}_d$ the unstable region decreases and the system can operate for a wide frequency range for lower value of $\bar{P}_d$. Further, there exists a critical value of $\bar{P}_d$ ($\bar{P}_{dcr}$) below which the system has no unstable region and

hence can operate at any frequency without vibration. For example, in this case $\bar{P}_{dcr}$ values are 0.55, 0.56 and 0.57 for first, second and third modes respectively for sandwich beam with viscoelastic core.

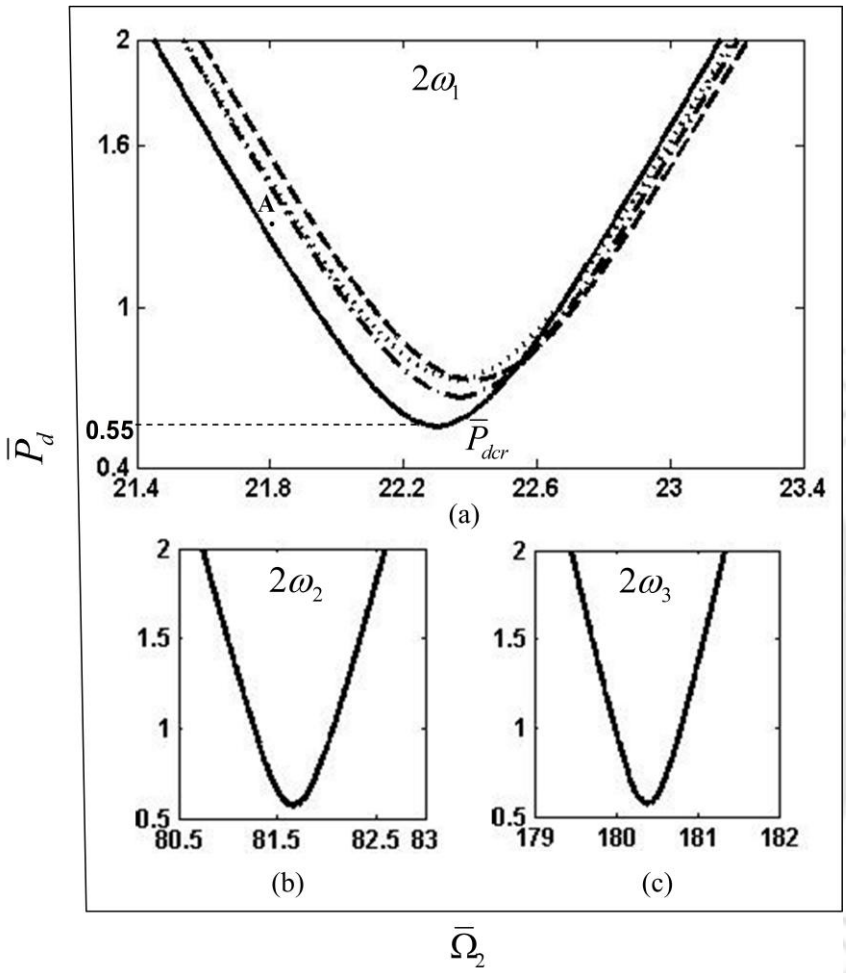

Figure 2.10 The regions of parametric instability of sandwich beam for (a) first mode, (b) second mode and (c) third mode. ——— viscoelastic core, — · — · $B_s = 0.2\text{T}$, ····· $B_s = 0.4\text{T}$ and – – – – $B_s = 0.6\text{T}$.

From Fig. 2.10 it may be observed that by using MRE patches and applying magnetic field, no instability regions have been observed for the higher modes. Also, for the first mode with increase in magnetic field strength, for MRE embedded sandwich beam the instability region decreases and shifts upwards. The instability regions occur at higher frequencies for MRE embedded beam in comparison to that of the fully viscoelastic core beam. It occurs due to the rapid and reversible change in shear modulus of the MRE with variation of magnetic field. Due to the

application of magnetic field the stiffness and damping of the beam changes which controls the vibration. In comparison to $\bar{P}_{dcr}$ of fully viscoelastic core which is 0.55 for the first mode, for core with MRE, this critical amplitude of loading $\bar{P}_{dcr}$ value increases to 0.66, 0.72 and 0.73 with increase in magnetic field strength to 0.2T, 0.4T and 0.6T, respectively. The system is stable below the above critical values for all the excitation frequencies. Hence, by suitably applying magnetic field the system vibration can be actively reduced.

Figure 2.11 (a) and (b) show the time response and phase portrait for transverse displacement of the sandwich beam with fully viscoelastic core for the frequency and amplitude of excitation corresponding to point 'A' marked in Fig. 2.10 (a) respectively. In Fig. 2.10, considering fully viscoelastic core, point 'A' is clearly in the unstable region which is in good agreement with the response curve shown in Fig. 2.11 (a) and the corresponding phase portrait as shown in Fig. 2.11 (b). For the same frequency and amplitude of axial load, Fig. 2.12 (a) and (b) show the time response and phase portrait for transverse displacement of the MRE embedded viscoelastic cored sandwich beam corresponding to the same point 'A' marked in Fig. 2.10 (a) respectively. In Fig. 2.10 (a), point 'A' is clearly in the stable region for the MRE embedded sandwich beam. This is in good agreement with the response curve and corresponding phase portrait shown in Fig. 2.12 (a) and (b).

Figure 2.13 shows the effect of percentage of iron particles on the first mode instability regions for MRE embedded sandwich beam. The sandwich beam is found to be stable for higher modes. With increase in percentage of iron particles, as the stiffness of the sandwich beam increases the instability region shifts towards right and starts at a higher frequency. Further, the $\bar{P}_{dcr}$ value increases with increase in the percentage of iron particle. Similarly, Fig. 2.14 shows the effect of percentage of carbon black on the parametric instability regions. Here, the sandwich beam consists of MRE embedded viscoelastic core with 33% of iron particles. Here also, the instability region move towards right and shifts upward with increase in percentage of carbon black. From Figs. 2.13 and 2.14, it may be observed that, by using lower percentage of iron particle, one may improve the stability of the system by adding

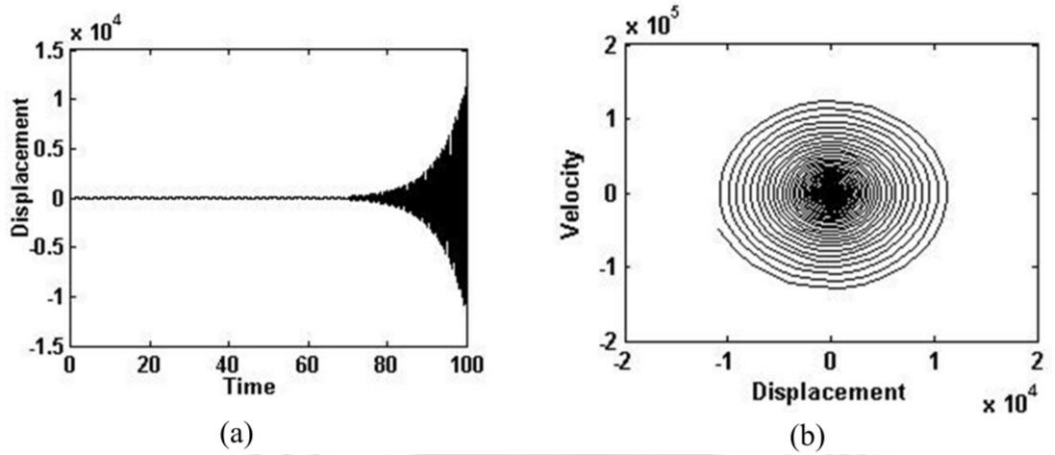

(a) (b)

Figure 2.11 (a) Time response and (b) Phase portrait of sandwich beam with viscoelastic core at point 'A' shown in Fig. 2.10 (a).

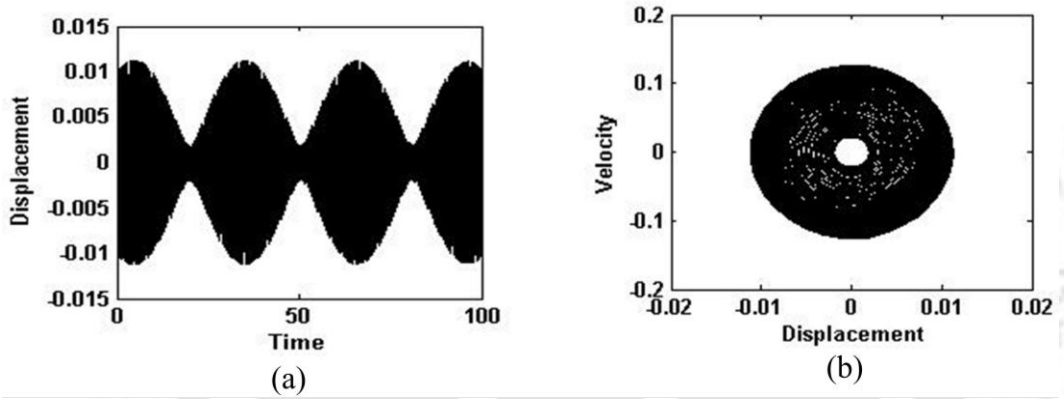

(a) (b)

Figure 2.12 (a) Time response and (b) Phase portrait of sandwich beam with MRE embedded viscoelastic core at point 'A' shown in Fig. 2.10 (a). $B_s = 0.2$T.

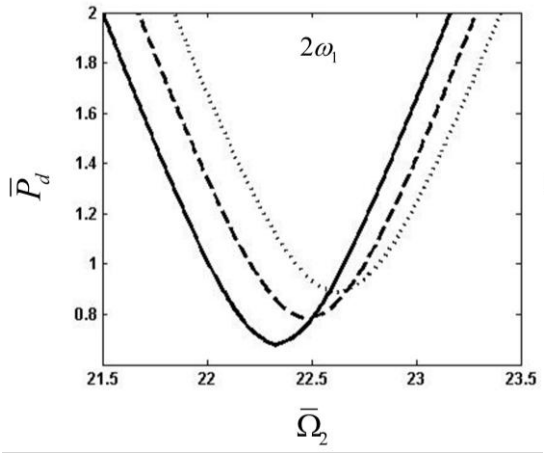

Figure 2.13. Effect of percentage of iron particles on the parametric instability regions at a constant magnetic field of 0.8T. ▬▬ 60% ▬ ▬ 70%, and ····· 80%.

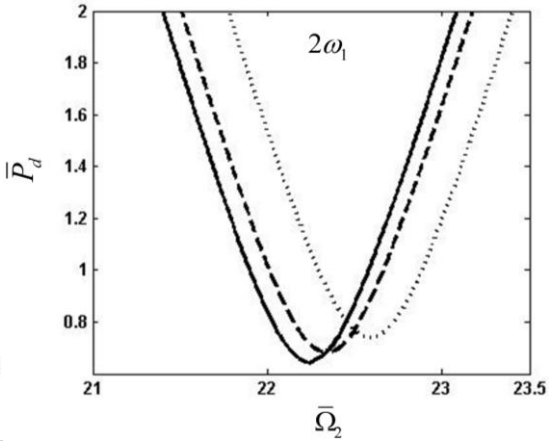

Figure 2.14. Effect of percentage of carbon black on the parametric instability regions at a constant magnetic field of 0.8T. ▬▬ 0%, ▬ ▬ 4% and ····· 7%.

carbon black. For example, the $\bar{P}_{dcr}$ value of the system with 33% iron particle with 7% carbon black is 0.74 which is higher than that of the $\bar{P}_{dcr}$ value (0.68) of the system with 60% iron particle.

Figure 2.15 shows the effect of the length of MRE patch on the parametric instability region. From this figure, it is found that with the increase in length of MRE patch the instability regions occur at a higher frequency and the $\bar{P}_{dcr}$ value increases. For the taken system parameters, the sandwich beam with fully MRE core is found to be stable. So, by changing the length of the MRE patch one can passively suppress the vibration of the sandwich beam.

For the sandwich beam with other boundary conditions such as guided-pinned, clamped-free, clamped-pinned and clamped-clamped unrestrained the effect of magnetic field, percentage of iron particles and percentage of carbon blacks have been found to be similar to those observed for the simply supported boundary condition.

Figure 2.16 shows the parametric instability regions for the above mentioned boundary conditions with pure viscoelastic (solid line) and MRE embedded viscoelastic core with 80% of iron particles (dash line) and MRE embedded viscoelastic core with 33% iron particles and 7% carbon black (dotted line),

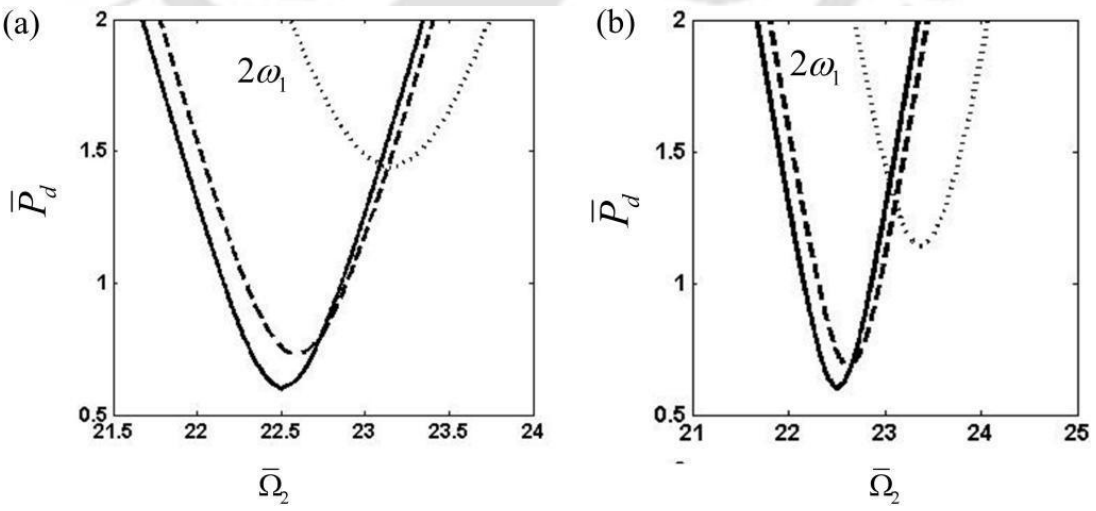

Figure 2.15 Effect of length of MRE (a) 80% of iron particles and (b) 33% of iron particles with 7% of carbon black) patch on the parametric instability regions at a magnetic field of 0.2T. —— core 1, – – – core 2 and ····· core 3.

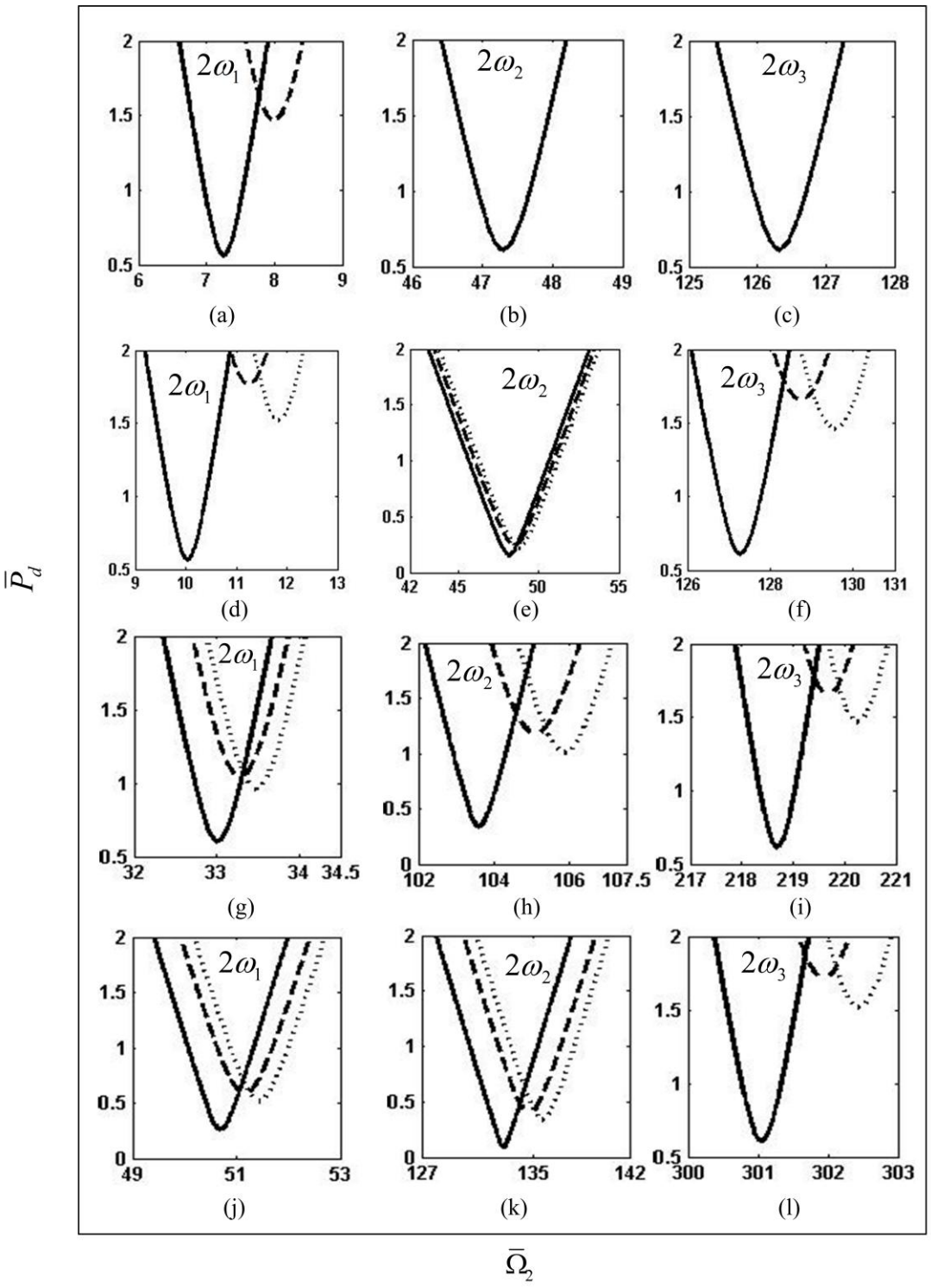

Figure 2.16 Parametric instability regions of (a)-(c) guided-pinned, (d)-(f) clamped-free, (g)-(i) clamped-pinned and (j)-(l) clamped-clamped unrestrained sandwich beams with, ——— viscoelastic core, — — ▪ MRE embedded viscoelastic core consists of 80% of iron particles and •••••••• MRE embedded viscoelastic core consists of 33% of iron particles and 7% of carbon black, subjected to a magnetic field of 0.6T.

subjected to a magnetic field of 0.6T. For guided-pinned boundary conditions as shown in Figs. 2.16 (a-c) it has been observed that while for the sandwich beam with viscoelastic core, the system has unstable region for all the three modes, for sandwich beam with MRE embedded viscoelastic core having 80% iron particles the system is stable for second and third modes. For the MRE embedded viscoelastic core having 33% iron particles and 7% carbon black, the system is stable for all the three modes. Hence, by using lower percentage of iron particle along with carbon black and by applying appropriate magnetic field one may attenuate the vibration of the sandwich beam actively.

From the instability regions for other end conditions, such as clamped-free (Fig. 2.16 (d-f)), clamped-pinned (Fig. 2.16 (g-i)) and clamped-clamped unrestrained (Fig. 2.16 (j-l)) boundary conditions, one can observe that unlike the previous two boundary conditions, here by using carbon black the unstable region increases. Hence, one should analyze the system for specific boundary condition to obtain the instability regions.

Figures 2.17 and 2.18 show the variation of instability regions with increase in the core thickness by increasing the core thickness from 4 mm to 8 mm respectively. It has been observed that for simply supported (Fig. 2.17 (a)) and clamped-guided (Fig. 2.17 (b)) end conditions with increase in core thickness higher modes become

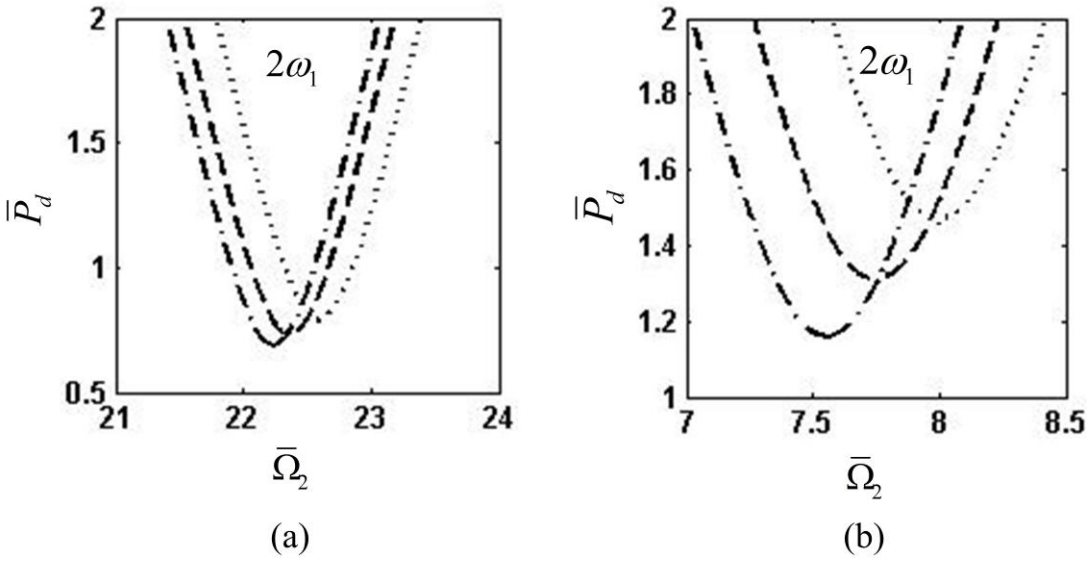

Figure 2.17 Parametric instability regions of (a) Simply supported and (b) Guided-pinned sandwich beams with variation of core thickness subjected to a magnetic field of 0.6T. — · — $2h_c$ = 4mm – – – $2h_c$ = 6mm and ····· $2h_c$ = 8mm.

stable and one obtains the instability regions only for the first mode. But for other end conditions such as clamped-free (Fig. 2.18 (a-c)), clamped-pinned (Fig. 2.18 (d-f) and clamped-clamped unrestrained (Fig. 2.18 (g-i)) sandwich beams it has been found that the instability regions also occur at higher frequencies. Similar to increase in the length of the MRE patch (Fig. 2.15), here also, with increase in core thickness, the system becomes more stable and the instability regions occur at a higher

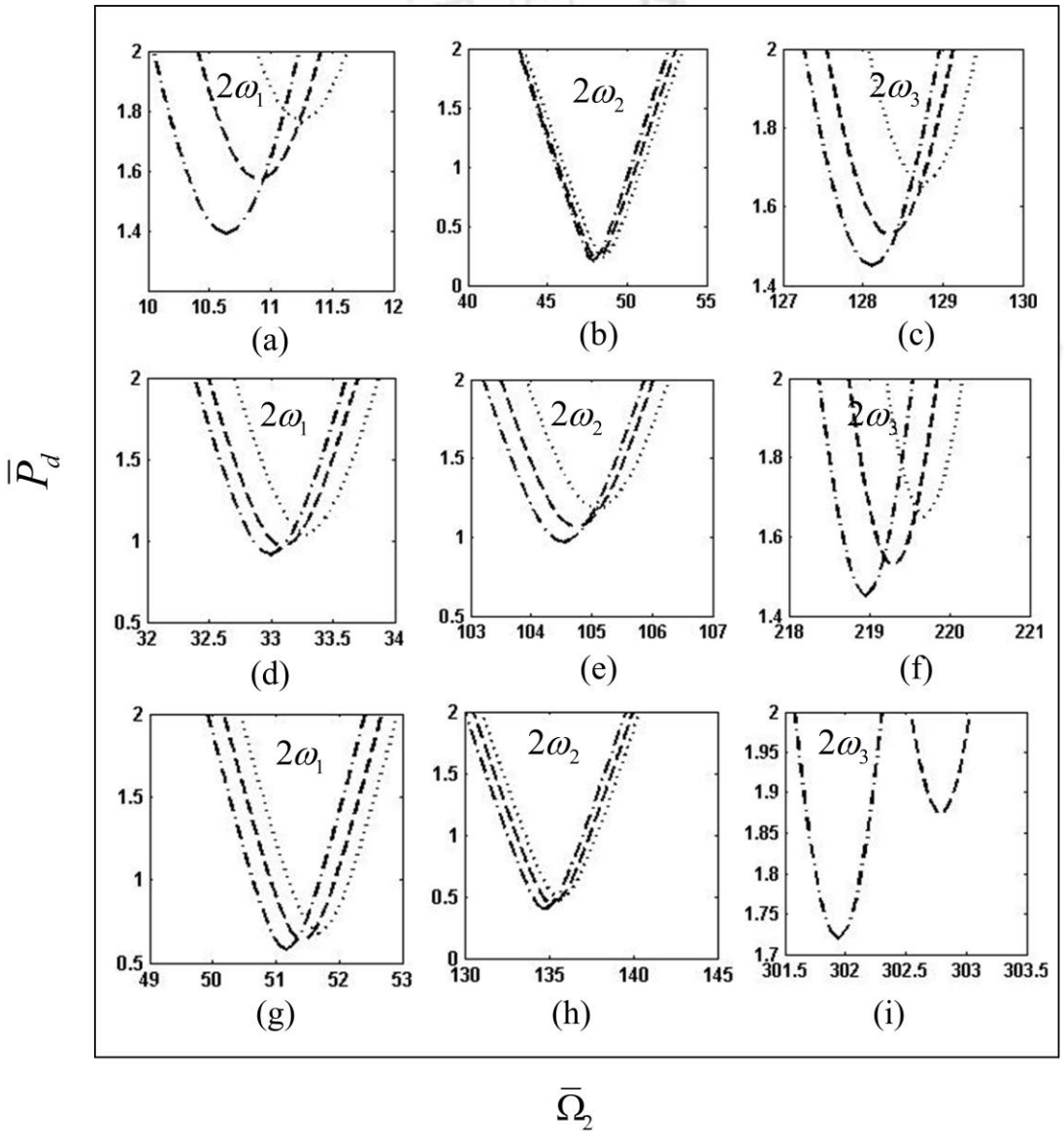

Figure 2.18 Parametric instability regions of (a)-(c) Clamped-free, (d)-(f) Clamped-pinned and (g)-(i) clamped-clamped unrestrained sandwich beams for three modes with variation of core thickness subjected to a magnetic field of 0.6T.
– · – $2h_c$=4mm, – – – $2h_c$=6mm and ····· $2h_c$=8mm.

frequency as the stiffness of the MRE embedded sandwich beam increases. The critical dynamic load amplitude $\bar{P}_{dcr}$ also increases with increase in the core thickness.

2.4.5 Comparison of Instability Regions Obtained Using Higher Order Theory

Taking same system parameters as in Fig. 2.10, and using higher order theory (Dwivedy *et al*., 2009), the modal frequencies and parametric instability regions of a simply supported (SS) and clamped-free (CF) sandwich beam have been obtained as given in Table 2.9 and Fig. 2.19. Here, both fully viscoelastic and MRE embedded viscoelastic core with 0.2 T, 0.4 T and 0.6 T magnetic fields have been considered.

From Table 2.9, it is apparent that the natural frequencies obtained by classical theory are in good agreement with those obtained by using higher order theory. But it may be noted that to obtain the first three modal frequencies using higher order theory it is required to solve at least a 12×12 matrix (144 elements) and in case of classical theory one has to solve only 3×3 matrix (9 elements). Hence to save computational time and memory in case of stiff cored sandwich beam it is advantageous to use the present method.

Figure 2.19 shows the parametric instability regions obtained by the higher-order theory for simply supported and clamped-free sandwich beams. The corresponding figures using classical theory are shown in Fig. 2.10 for simply supported and Fig. 2.16 (d)-(f) for clamped-free end conditions. From these figures it has been observed that for the same system parameters the $\bar{P}_{dcr}$ values obtained by higher order theory for the first mode are less than their corresponding values obtained by classical theory. For example, at a magnetic field of 0.6T the $\bar{P}_{dcr}$ value obtained by higher order theory for simply supported end conditions is 0.53 at $\bar{\Omega}_2$ = 23.09 and $\bar{P}_{dcr}$ value for clamped free sandwich beam is 0.34 at $\bar{\Omega}_2$ =10.224. But for the same magnetic field the $\bar{P}_{dcr}$ obtained by classical theory for the simply supported and clamped free end arrangements are 0.79 at a frequency 22.59 and 1.76 at a frequency 11.17, respectively. Also, it may be noted that in the presence of magnetic fields above 0.2

Table 2.9 Comparison of non-dimensional modal frequencies obtained by classical and higher order sandwich beam theories.

End condition	Mode	Non-dimensional modal frequencies							
		Classical theory				Higher order theory			
		Visco-elastic core	MRE embedded core with magnetic fields			Visco-elastic core	MRE embedded core with magnetic fields		
			0.2T	0.4T	0.6T		0.2T	0.4T	0.6T
SS	1	11.26	11.29	11.32	11.30	11.21	11.31	11.46	11.55
	2	40.95	41.36	41.77	41.88	40.89	41.01	41.09	41.16
	3	90.31	90.61	90.90	90.97	90.25	90.31	90.41	90.61
CF	1	5.02	5.27	5.52	5.59	5.02	5.04	5.07	5.11
	2	24.10	24.21	24.28	24.26	24.05	24.11	24.19	24.25
	3	63.64	64.00	64.30	64.38	63.50	63.62	63.75	63.85

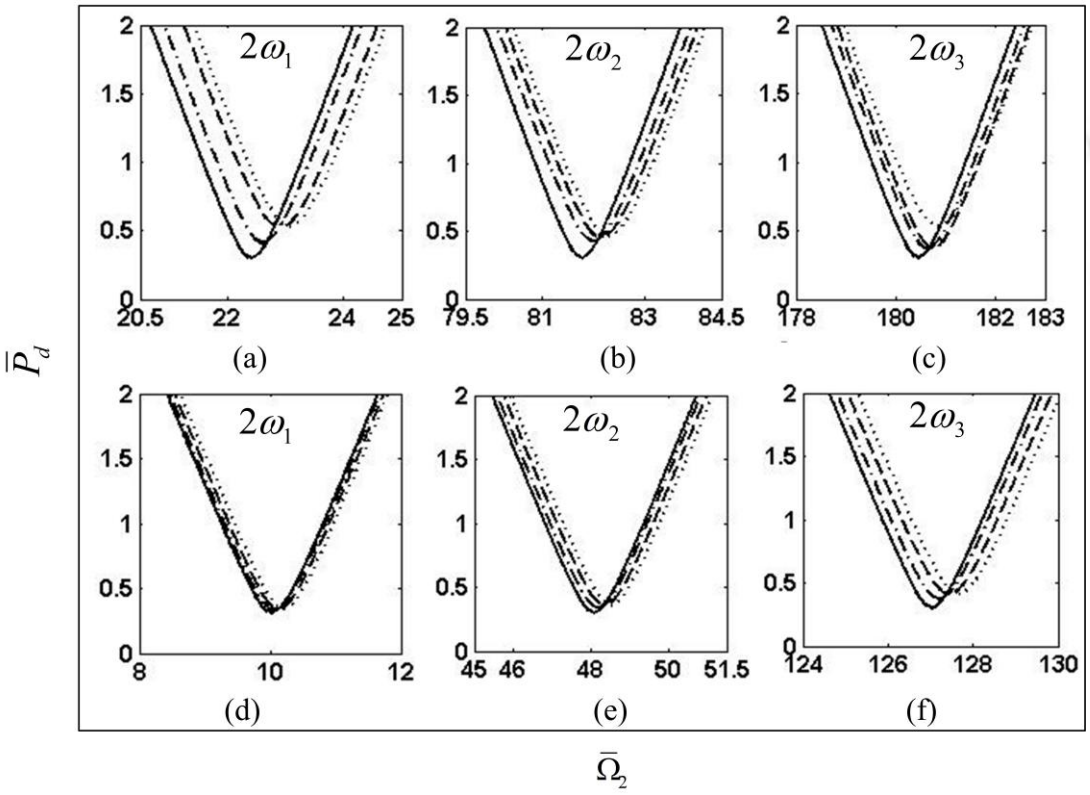

Figure 2.19 Parametric instability regions of (a)-(c) simply supported and (d)-(f) clamped free sandwich beam for first three modes, obtained by higher order theory with viscoelastic and MRE embedded viscoelastic core with different magnetic field. —— viscoelastic core, — · - 0.2T, – – – 0.4T and ····· 0.6T.

T for simply supported sandwich beam, while the system is found to be stable in second and third modes using classical theory. However in case of higher order

theory, the system is found to be unstable. This is due to the fact that as stiff core is considered in classical theory, a higher forcing is required to make the system unstable. It has been verified by solving the temporal equation of motion that the system is stable for $\bar{P}_d$ below 0.53 as predicted by classical theory. Hence the prediction of instability region using higher order theory is found to be erroneous for stiff core, but it gives a conservative value which may be useful for better design purpose.

2.4.6 Application of Present Theory for Passive and Active Vibration Reduction of Sandwich Beam

The instability regions developed in the previous subsections can be effectively used to develop passive and active vibration control strategies of the sandwich structure as explained below.

Clearly by changing the core material i.e., percentage of iron particles, carbon black in MRE, core thickness, length of MRE and viscoelastic part of the core, one obtains a new sandwich beam. This new beam can be used for passive vibration control when operated in a stable region shown in the parametric instability plots (which are plotted for various boundary conditions). For example, if it is required to design a sandwich beam which is subjected to amplitude of dynamic force $\bar{P}_d$ equal to 1.5 and frequency $\bar{\Omega}_2$ equal to 22.5, the designer or control engineer can conveniently chose a fully MRE embedded sandwich beam (core 4) or an MRE embedded viscoelastic core with MRE length equal to 2/3 of the total length as depicted in Fig. 2.15. One may clearly visualize from Fig. 2.15 that while, use of a fully viscoelastic core (core 1) or small length MRE patch (core 2) for the given operating conditions will yield unstable response of the system use of core 3 or 4 will suppress the vibration of the system. Also, by using other instability plots one may decide the optimum dimension of the sandwich beam to avoid unwanted vibration of the system for a given set of operating parameters.

Similarly, as the stiffness of the sandwich beam changes actively by applying magnetic field, using the parametric instability region for various magnetic fields,

one can actively suppress the vibration of the sandwich beam. For example, from Figs. 2.7-2.9, one may observe that by applying magnetic field, the free vibration response amplitude and settling time of the MRE embedded beam can be reduced significantly. Also, from Fig. 2.10 it can be observed that to reduce the vibration of a system actively, one should apply a suitable magnetic field so that the applied amplitude ($\bar{P}_d$) and frequency ($\bar{\Omega}_2$) of dynamic loading should be outside the instability region. Similarly, in case of various boundary conditions, Fig. 2.19 may be used to decide the appropriate magnetic field strength so that the operating amplitude and frequency lie outside the instability region.

For a given sandwich beam, to decide whether to go for active or passive vibration reduction depends on the operating amplitude and frequency of the axial load. If the point corresponding to the operating amplitude and frequency lies in the unstable region for a given range of magnetic field, then the designer should go for passive vibration control by suitably choosing proper dimension and material of the sandwich beam and replacing the existing beam by the new one. But if it is possible to have the point corresponding to the operating amplitude and frequency outside the unstable region for a given range of magnetic field, by applying suitable magnetic field one can actively control the vibration of the system.

2.5 Summary

In this chapter, the free vibration analysis and analysis for obtaining instability regions for principal parametric resonance of a three layered symmetric sandwich beam with MRE embedded viscoelastic core has been carried out based on classical sandwich beam theory. Initially, considering a viscoelastic cored sandwich beam, experiment has been performed to show that the top and bottom skins have same transverse displacement and hence classical sandwich beam theory can be used for this type of system. The theoretically obtained fundamental frequency using this theory is found to be in good agreement with the experimentally obtained frequency. Also, the modal frequencies obtained using the present analyses have been compared with three analytically and two experimentally published results and they are found to be in good agreement in most of the cases. As the principal parametric

resonances occur near twice the natural frequencies, hence the results obtained in this work may be considered to be in consistent with the experimental findings.

The parametric instability regions of MRE embedded viscoelastic core sandwich beam subjected to periodic axial load have been obtained for five different boundary conditions. The effects of various system parameters on the regions of parametric instability for first three modes of vibration have been studied. The present results have been compared with those obtained using higher order theory. It has been shown that for a MRE embedded viscoelastic cored sandwich beam it is preferable to use the present method to have less computational time and memory.

3

Stability of MRE-based Sandwich Beam Subjected to Time Varying Magnetic Field and periodic Axial Load

3.1 Introduction

Unlike in previous chapter (where a static magnetic field is applied to the system) in this chapter a dynamic magnetic field is applied to the system. This gives rise to multi-frequency excitation of the system. Hence, many different types of resonance conditions such as simple, parametric and simultaneous simple and parametric resonances are observed in this system. In this case the boundary of instability regions are obtained using method of multiple scales.

In section 3.2, the mathematical modeling of a sandwich beam subjected to time varying magnetic field has been carried out. In section 3.3, the modeling of the same system has been carried out incorporating periodic axial load. Section 3.4 presents the numerical results and discussions.

3.2 Mathematical Modeling of the Sandwich Beam Without Periodic Axial Load

A three layered MRE embedded viscoelastic cored cantilevered sandwich beam of length *L*, width *b*, mass per unit length, m with two conductive skins is shown in Fig. 3.1. The thickness of top, core and bottom layers is $2h_t$, $2h_c$ and $2h_b$, respectively. The Young's moduli of top and bottom skin materials are E_t and E_b, respectively. The corresponding moments of inertia are I_t and I_b. G_c is the shear modulus of the core. The time varying magnetic field with flux density $B(t) = B_s + B_d \cos\Omega_1 t$ is applied perpendicular to the skins and parallel to the chain like structures of the

ferrous particles inside the MRE. Here B_s is the amplitude of static magnetic field, B_d and Ω_1 are respectively, the amplitude and frequency of the dynamic magnetic field. Due to the distributed magnetic field near the skins the magnetoelastic loads are applied to the skins and the bulk dynamic flexural rigidity is affected (Zhou and Wang, 2006b). The deformed and undeformed cross section of the sandwich beam in this case is similar to that shown in Fig. (2.2).

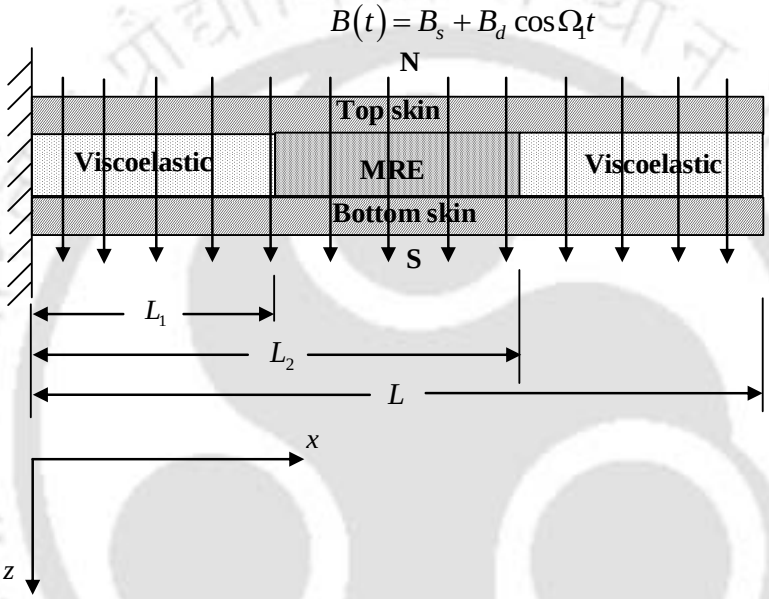

Figure 3.1 Schematic diagram of MRE embedded viscoelastic cored sandwich beam subjected to periodic magnetic field.

Following the chapter 2, the same assumptions and the expressions for kinetic energy, potential energy and non-conservative work done due to time varying magnetic field, $B(t) = B_s + B_d \cos\Omega_1 t$ the governing equations of motion are derived by applying the extended Hamilton's principle. The resulting non-dimensional equations of motion for coupled transverse and axial vibrations in terms of longitudinal displacement (u) and transverse displacement (w) are

$$\ddot{\bar{w}} + \frac{1}{mL\omega_s^2}\left[\frac{D}{L^3}\left(1+Y-\frac{B_s^{\,2}bD_t^3}{6\mu_e D}-\frac{B_d^{\,2}bD_t^3}{12\mu_e D}\right)w_{\bar{x}\bar{x}\bar{x}\bar{x}}-\frac{D}{L^2}\left(\frac{B_s^{\,2}bD_t^2}{\pi\mu_0 D}\ln\left(\frac{\bar{x}}{1-\bar{x}}\right)+\frac{B_d^{\,2}bD_t^2}{2\pi\mu_0 D}\right.\right.$$

$$\ln\left(\frac{\bar{x}}{1-\bar{x}}\right)\bar{w}_{\bar{x}\bar{x}\bar{x}}+\frac{D}{L}\left(\frac{2B_s{}^2bD_t}{\mu_0 D}+\frac{B_d{}^2bD_t}{\mu_0 D}\right)\bar{w}_{\bar{x}\bar{x}}-\frac{DY}{L^3}\bar{u}_{\bar{x}\bar{x}\bar{x}}-\frac{D}{L^3}\left(\frac{B_sB_dbD_t^3}{3\mu_e D}\bar{w}_{\bar{x}\bar{x}\bar{x}\bar{x}}+\right.$$

$$\left.\frac{2B_sB_dD_t^2L}{\pi\mu_0 D}\ln\left(\frac{\bar{x}}{1-\bar{x}}\right)\bar{w}_{\bar{x}\bar{x}\bar{x}}-\frac{4B_sB_dbD_tL^2}{\mu_0 D}\bar{w}_{\bar{x}\bar{x}}\right)\cos\bar{\Omega}_1\bar{t}-\frac{D}{L^3}\left(\frac{B_d^2bD_t^3}{12\mu_e D}\bar{w}_{\bar{x}\bar{x}\bar{x}\bar{x}}+\frac{B_d^2bD_t^2L}{2\pi\mu_0 D}\right.$$

$$\left.\ln\left(\frac{\bar{x}}{1-\bar{x}}\right)\bar{w}_{\bar{x}\bar{x}\bar{x}}-\frac{B_d^2bD_tL^2}{\mu_0 D}\bar{w}_{\bar{x}\bar{x}}\right)\cos 2\bar{\Omega}_1\bar{t}\Bigg]=0 \tag{3.1}$$

and

$$\bar{w}_{\bar{x}\bar{x}\bar{x}}-\bar{u}_{\bar{x}\bar{x}}+g_c^*\left(\frac{h_t}{h_c}\right)^2\bar{u}=0. \tag{3.2}$$

Here, $()_{,x}$ represents the differentiation with respect to x. $D=\left(E_tI_t+E_bI_b\right)$, $D_t=2h_t$. Here, $g_c^*=g_c\left(1+j\eta_c\right)$, $g_c=\left(G_c^{'}/2E_t\right)\left(h_c/h_t\right)\left(L/h_t\right)^2$ is the shear parameter, subscript $c=v$ or e depending upon viscoelastic or MRE part of the core materials, respectively. $j=\sqrt{-1}$ and η_c is the core loss factor. $Y=3\left(1+h_c/h_t\right)^2$. μ_{ej} $(j=t,b)$ and μ_0 are the permeability of the top and bottom faces and magnetic permeability in free spaces.

Solutions of equations (3.1) and (3.2) are assumed in the form,

$$\bar{w}\left(\bar{x},\bar{t}\right)=\sum_{m=1}^{r}q_m\left(\bar{t}\right)w_m\left(\bar{x}\right)\text{ and }\bar{u}\left(\bar{x},\bar{t}\right)=\sum_{k=r+1}^{s}q_k\left(\bar{t}\right)u_k\left(\bar{x}\right) \tag{3.3}$$

where, q_m and q_k are the time modulation and $w_m\left(\bar{x}\right)$ and $u_k\left(\bar{x}\right)$ are the shape functions chosen to satisfy the boundary conditions. Using single mode approximation in generalized Galerkin's method, Eqs. (3.1) and (3.2) can be reduced to the following non-dimensional temporal equation of motion.

$$\ddot{q}+\left(1+i\varepsilon\zeta\right)q+\varepsilon\left(\alpha_1\cos\bar{\Omega}_1\bar{t}+\alpha_2\cos 2\bar{\Omega}_1\bar{t}\right)q=0. \tag{3.4}$$

Due to the presence of two periodically time varying terms in the temporal equation, (which are coefficients of the response q) this is a parametrically excited equation.

Following the same non-dimensional parameters as discussed in chapter 2, the expressions for the coefficients of Eq. (3.4) are given below

$$\alpha_1 = -\frac{\bar{B}_r \delta}{\varepsilon}\left(\frac{D_t^2 \mu_0}{3\mu_e L^2}\frac{h_{22}}{h_1} + \frac{2D_t}{\pi L}\frac{h_{21}}{h_1} + 4\frac{h_{11}}{h_1}\right),\ \alpha_2 = -\frac{\bar{B}_d \delta}{\varepsilon}\left(\frac{D_t^2 \mu_0}{12\mu_e L^2}\frac{h_{22}}{h_1} + \frac{D_t}{2\pi L}\frac{h_{21}}{h_1} + \frac{h_{11}}{h_1}\right)$$

Here,

$\omega_L^2 = \frac{D}{mL^4}$, $\delta = \frac{\omega_L^2}{\omega_s^2}$, $\bar{B}_s = \frac{B_s^2 b D_t L^2}{\mu_0 D}$, $\bar{B}_d = \frac{B_d^2 b D_t L^2}{\mu_0 D}$, $\bar{B}_r = \frac{B_s B_d b D_t L^2}{\mu_0 D}$ and the book keeping parameter ε.

$$\omega_s^2 = \omega_L^2\left(\frac{h_{22}}{h_1}\right)\left[1 + Y\left(1 + \frac{h_{31}h_{13}}{h_{22}\left(h_{33} + g_c^*\left(h_c/h_t\right)^2 h_{44}\right)}\right) - \bar{B}_s\left(\frac{D_t^2\mu_0}{6\mu_e L^2} + \frac{D_t}{\pi L}\frac{h_{21}}{h_{22}} + 2\frac{h_{11}}{h_{22}}\right) - \bar{B}_d\left(\frac{D_t^2\mu_0}{12\mu_e L^2} + \frac{D_t}{2\pi L}\frac{h_{21}}{h_{22}} + \frac{h_{11}}{h_{22}}\right)\right]$$

$$h_1 = \int_0^1 \left(\bar{w}_m(\bar{x})\right)^2 d\bar{x},\ h_{11} = \int_0^1 \left(\frac{d\bar{w}_m(\bar{x})}{d\bar{x}}\right)^2 d\bar{x},$$

$$h_{21} = \int_0^1 \ln\left(\frac{\bar{x}}{1-\bar{x}}\right)\left(\frac{d^2\bar{w}_m(\bar{x})}{d\bar{x}^2}\frac{d\bar{w}_m(\bar{x})}{d\bar{x}}\right)d\bar{x},$$

$$h_{22} = \int_0^1 \left(\frac{d^2\bar{w}_m(\bar{x})}{d\bar{x}^2}\right)^2 d\bar{x},\ h_{33} = \int_0^1 \left(\frac{d\bar{u}_k(\bar{x})}{d\bar{x}}\right)^2 d\bar{x},\qquad h_{31} = \int_0^1 \left(\frac{d^2\bar{w}_m(\bar{x})}{d\bar{x}^2}\frac{d\bar{u}_k(\bar{x})}{d\bar{x}}\right)d\bar{x},$$

$$h_{13} = \int_0^1 \left(\frac{d^2\bar{u}_k(\bar{x})}{d\bar{x}^2}\frac{d\bar{w}_m(\bar{x})}{d\bar{x}}\right)d\bar{x},\ \text{and}\ h_{44} = \int_0^1 \left[\left(\frac{d\bar{u}_k(\bar{x})}{d\bar{x}}\right)^2 H_1 + \left(\frac{d\bar{u}_k(\bar{x})}{d\bar{x}}\right)^2 H_2\right]d\bar{x},$$

The expressions of H_1 and H_2 for the MRE and non-MRE parts are

$$H_1 = 1 - H\left(\bar{x} - \bar{L}_1\right) + H\left(\bar{x} - \bar{L}_2\right),\ H_2 = H\left(\bar{x} - \bar{L}_1\right) + H\left(\bar{x} - \bar{L}_2\right)$$

where H is the Heaviside function.

The shape functions used for the numerical calculations are same as those found in the work of Ray and Kar, (1995b). To obtain the solution of the temporal equation of motion (3.4), here first order method of multiple scales (Nayfeh and Mook, 1979) has been used. In this method, the displacement q can be represented in terms of different time scales $\left(T_0, T_1, T_2\right)$ and a book keeping parameter ε as

follows. The book keeping parameter ε is used in order to make the coefficients ζ, α_1 and α_2 in the same order.

$$q(\bar{t};\varepsilon) = q_0(T_0,T_1,T_2) + \varepsilon q_1(T_0,T_1,T_2) + \varepsilon^2 q_2(T_0,T_1,T_2) + O(\varepsilon^3) \tag{3.5}$$

Here, $T_n = \varepsilon^n \bar{t}$, $n = 0,1,2,3\cdots$. (3.6)

Substituting Eq. (3.5) in Eq. (3.4) and equating the coefficient of like powers of ε, yields the following equations.

Order ε^0 :

$$D_0^2 q_0 + q_0 = 0 \tag{3.7}$$

Order ε^1 :

$$D_0^2 q_1 + q_1 = -2D_0 D_1 q_0 - i\zeta q_0 - \alpha_1 \cos\left(\bar{\Omega}_1 \bar{t}\right) q_0 - \alpha_2 \cos\left(2\bar{\Omega}_1 \bar{t}\right) q_0 \tag{3.8}$$

General solutions of Eq. (3.7) can be written as

$$q_0 = A(T_1,T_2)\exp(iT_0) + \bar{A}(T,T_2)\exp(-iT_0) \tag{3.9}$$

Here, $\bar{A}(T_1,T_2)$ is the complex conjugate of $A(T_1,T_2)$.

Substituting Eq. (3.9) into Eq. (3.8) leads to

$$D_0^2 q_1 + q_1 = -2iD_1 A\exp\left(iT_0\right) - i\zeta A\exp\left(iT_0\right) - \frac{\alpha_1}{2} A\exp\left(i\left(\bar{\Omega}_1 + 1\right)T_0\right) - \frac{\alpha_1}{2}\bar{A}\exp\left(i\left(\bar{\Omega}_1 - 1\right)T_0\right)$$
$$- \frac{\alpha_2}{2} A\exp\left(i\left(2\bar{\Omega}_1 + 1\right)T_0\right) - \frac{\alpha_2}{2}\bar{A}\exp\left(i\left(2\bar{\Omega}_1 - 1\right)T_0\right) + cc \tag{3.10}$$

Here, *cc* stands for the complex conjugate of the preceding terms. In this case, one may observe that the solution of Eq. (3.10) contains secular or small divisor terms when the non-dimensional frequency of magnetic field strength ($\bar{\Omega}_1$) is nearly equal to 1. This will lead to a simple resonance condition. In this case, one may use detuning parameter σ to express the nearness of $\bar{\Omega}_1$ to 1, as

$$\bar{\Omega}_1 = 1 + \varepsilon\sigma, \quad \text{and} \quad \sigma = O(1) \tag{3.11}$$

Substituting Eq. (3.11) into Eq. (3.10), and equating the secular and small-divisor terms to zero will yield the following equation.

$$-2iD_1 A - i\zeta A - \frac{\alpha_2}{2}\bar{A}\exp(i2\sigma T_1) = 0 \tag{3.12}$$

Substituting Eq. (3.12) into $\frac{d}{d\bar{t}} = D_0 + \varepsilon D_1 + \varepsilon^2 D_2 + O(\varepsilon^2)$, gives

$$2i\frac{dA}{d\bar{t}} + \varepsilon i\zeta A + \frac{\alpha_2}{2}\bar{A}\exp(i2\sigma T_1) = 0 \tag{3.13}$$

Putting $A = \left(B_r + iB_i\right)\exp\left(i\varepsilon\sigma\bar{t}\right)$, where B_r and B_i the real and imaginary parts, in Eq. (3.13) and separating the real and imaginary parts yield the following equations.

$$2\frac{dB_r}{d\bar{t}} + \varepsilon\zeta B_r - \left(2\sigma + \varepsilon\frac{\alpha_2}{2}\right)B_i = 0 \tag{3.14}$$

$$2\frac{dB_i}{d\bar{t}} + \varepsilon\zeta B_i + \left(2\sigma - \varepsilon\frac{\alpha_2}{2}\right)B_r = 0 \tag{3.15}$$

Substituting $\left(B_r, B_i\right) = (b_r, b_i)\exp(\gamma\tau)$ into the Eqs. (3.14) and (3.15) yields the following equations.

$$2\gamma b_r + \varepsilon\zeta b_r - \left(2\sigma + \varepsilon\frac{\alpha_2}{2}\right)b_i = 0 \tag{3.16}$$

$$2\gamma b_i + \varepsilon\zeta b_i + \left(2\sigma - \varepsilon\frac{\alpha_2}{2}\right)b_r = 0 \tag{3.17}$$

For steady state trivial response, γ is equal to zero. One may obtain the expression for the transition curves by finding the value of σ from the above two equations. Neglecting the term $O(\varepsilon^3)$ one may write the expression for transition curves of the second order expansion when $\bar{\Omega}_1 \approx 1$ as

$$\bar{\Omega}_1 = 1 \pm \frac{\varepsilon^2}{4}\sqrt{(\alpha_2)^2 - 4\zeta^2} \tag{3.18}$$

3.3 Mathmatical Modeling of the Sandwich Beam with Time Varying Magnetic Field and Periodic Axial Load

Figure 3.2 shows a MRE embedded viscoelastic cored clamped-free sandwich beam which is subjected to time varying magnetic field with flux density $B(t) = B_s + B_d\cos\Omega_1 t$ and a periodic axial load, $P(t) = P_s + P_d\cos\Omega_2 t$ where, P_s is the amplitude of static load, P_d and Ω_2 are respectively the amplitude and frequency of the dynamic axial load.

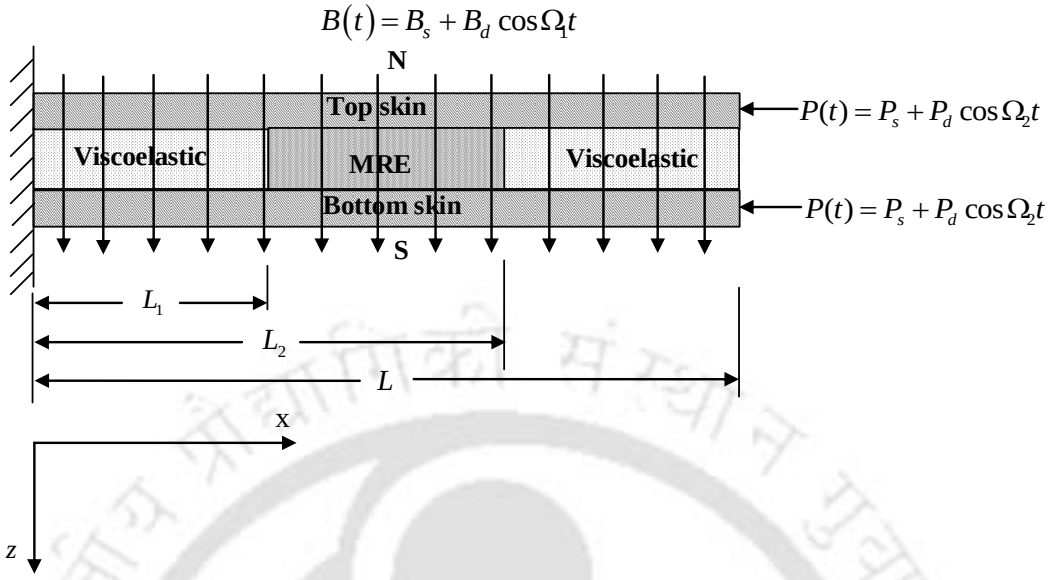

Figure 3.2 Schematic diagram of MRE embedded viscoelastic cored sandwich beam subjected to periodic magnetic field and axial load.

Following the similar procedure discussed above the non-dimensional equations of motion for coupled transverse and axial vibrations in terms of longitudinal displacement (u) and transverse displacement (w) are

$$\ddot{\bar{w}} + \frac{1}{mL\omega_s^2}\left[\frac{D}{L^3}\left(1+Y-\frac{B_s{}^2bD_t^3}{6\mu_e D}-\frac{B_d{}^2bD_t^3}{12\mu_e D}\right)w_{\bar{x}\bar{x}\bar{x}\bar{x}}-\frac{D}{L^2}\left(\frac{B_s{}^2bD_t^2}{\pi\mu_0 D}\ln\left(\frac{\bar{x}}{1-\bar{x}}\right)+\frac{B_d{}^2bD_t^2}{2\pi\mu_0 D}\right.\right.$$
$$\left.\ln\left(\frac{\bar{x}}{1-\bar{x}}\right)\right)\bar{w}_{\bar{x}\bar{x}\bar{x}}+\frac{D}{L}\left(\frac{2B_s{}^2bD_t}{\mu_0 D}+\frac{B_d{}^2bD_t}{\mu_0 D}\right)\bar{w}_{\bar{x}\bar{x}}-\frac{DY}{L^3}\bar{u}_{\bar{x}\bar{x}\bar{x}}-\frac{D}{L^3}\left(\frac{B_sB_dbD_t^3}{3\mu_e D}\bar{w}_{\bar{x}\bar{x}\bar{x}\bar{x}}+\right.$$
$$\frac{2B_sB_dD_t^2L}{\pi\mu_0 D}\ln\left(\frac{\bar{x}}{1-\bar{x}}\right)\bar{w}_{\bar{x}\bar{x}\bar{x}}-\left.\left.\frac{4B_sB_dbD_tL^2}{\mu_0 D}\bar{w}_{\bar{x}\bar{x}}\right)\cos\bar{\Omega}_1\bar{t}-\frac{D}{L^3}\left(\frac{B_d^2bD_t^3}{12\mu_e D}\bar{w}_{\bar{x}\bar{x}\bar{x}\bar{x}}+\frac{B_d^2bD_t^2L}{2\pi\mu_0 D}\right.\right.$$
$$\left.\left.\ln\left(\frac{\bar{x}}{1-\bar{x}}\right)\bar{w}_{\bar{x}\bar{x}\bar{x}}-\frac{B_d^2bD_tL^2}{\mu_0 D}\bar{w}_{\bar{x}\bar{x}}\right)\cos 2\bar{\Omega}_1\bar{t}+\frac{D}{L^3}\left(\bar{P}_s+\bar{P}_d\cos\bar{\Omega}_2\bar{t}\right)w_{\bar{x}\bar{x}}\right]=0. \quad (3.19)$$

and

$$\bar{w}_{\bar{x}\bar{x}\bar{x}}-\bar{u}_{\bar{x}\bar{x}}+g_c^*\left(\frac{h_t}{h_c}\right)^2\bar{u}=0. \quad (3.20)$$

Using single mode approximation in generalized Galerkin's method, Eqs. (3.19) and (3.20) can be reduced to the following non-dimensional temporal equation of motion.

$$\ddot{q}+\left(1+i\varepsilon\zeta\right)q+\varepsilon\left(\alpha_1\cos\bar{\Omega}_1\bar{t}+\alpha_2\cos 2\bar{\Omega}_1\bar{t}+\alpha_3\cos\bar{\Omega}_2\bar{t}\right)q=0. \qquad (3.21)$$

Due to the presence of three periodically time varying terms in the temporal equation (which are coefficients of the response q) this is a parametrically multi-frequency excited equation. The shape functions used for the numerical calculations are same as those found in the work of Ray and Kar, (1995b).

As the expressions for the coefficients α_1 and α_2 are given in the above section the expression for the coefficients α_3 is

$$\alpha_3=-\frac{\bar{P}_d\delta}{\varepsilon}\frac{h_{11}}{h_1}\text{, here, }\bar{P}_s=\frac{P_sL^2}{D}\text{ and }\bar{P}_d=\frac{P_dL^2}{D}\text{ .}$$

$$\omega_s^2=\omega_L^2\left(\frac{h_{22}}{h_1}\right)\left[1+Y\left(1+\frac{h_{31}h_{13}}{h_{22}\left(h_{33}+g_c^*\left(h_c/h_t\right)^2h_{44}\right)}\right)-\bar{B}_s\left(\frac{D_t^2\mu_0}{6\mu_eL^2}+\frac{D_t}{\pi L}\frac{h_{21}}{h_{22}}+2\frac{h_{11}}{h_{22}}\right)\right.$$
$$\left.-\bar{B}_d\left(\frac{D_t^2\mu_0}{12\mu_eL^2}+\frac{D_t}{2\pi L}\frac{h_{21}}{h_{22}}+\frac{h_{11}}{h_{22}}\right)-\bar{P}_s\frac{h_{11}}{h_{22}}\right]$$

To obtain the solution of the temporal equation of motion (3.21), here second order method of multiple scales (Nayfeh and Mook, 1979) has been used. In this method, the displacement q can be represented in terms of different time scales $\left(T_0,T_1,T_2\right)$ and a book keeping parameter ε as follows. The book keeping parameter ε is used in order to make the coefficients ζ, α_1, α_2 and α_3 in the same order.

$$q(\bar{t};\varepsilon)=q_0(T_0,T_1,T_2)+\varepsilon q_1(T_0,T_1,T_2)+\varepsilon^2q_2(T_0,T_1,T_2)+O(\varepsilon^3) \qquad (3.22)$$

Here, $T_n=\varepsilon^n\bar{t}$, $n=0,1,2,3\cdots$.Taking, $D_0=\frac{\partial}{\partial T_0}$, $D_1=\frac{\partial}{\partial T_1}$, $D_2=\frac{\partial}{\partial T_2}$, solving the Eq. (3.21) and equating the coefficient of like powers of ε, yields the following equations.

Order ε^0 :

$$D_0^2q_0+q_0=0 \qquad (3.23)$$

Order ε^1 :

$$D_0^2q_1+q_1=-2D_0D_1q_0-i\zeta q_0-\alpha_1\cos\left(\bar{\Omega}_1\bar{t}\right)q_0-\alpha_2\cos\left(2\bar{\Omega}_1\bar{t}\right)q_0-\alpha_3\cos\left(\bar{\Omega}_2\bar{t}\right)q_0 \qquad (3.24)$$

Order ε^2 :

$$D_0^2 q_2 + q_2 = -2D_0 D_1 q_1 - D_1^2 q_0 - 2D_0 D_2 q_0 - i\zeta q_1 - \alpha_1 \cos\left(\bar{\Omega}_1 \bar{t}\right) q_1 - \alpha_2 \cos\left(2\bar{\Omega}_1 \bar{t}\right) q_1$$
$$-\alpha_3 \cos\left(\bar{\Omega}_2 \bar{t}\right) q_1 \tag{3.25}$$

General solutions of Eq. (3.23) can be written as

$$q_0 = A(T_1, T_2)\exp(iT_0) + \bar{A}(T, T_2)\exp(-iT_0) \tag{3.26}$$

Here, $\bar{A}(T_1, T_2)$ is the complex conjugate of $A(T_1, T_2)$.

Substituting Eq. (3.26) into Eq. (3.24) leads to

$$D_0^2 q_1 + q_1 = -2iD_1 A\exp\left(iT_0\right) - i\zeta A\exp\left(iT_0\right) - \frac{\alpha_1}{2} A\exp\left(i\left(\bar{\Omega}_1 + 1\right)T_0\right)$$
$$-\frac{\alpha_1}{2}\bar{A}\exp\left(i\left(\bar{\Omega}_1 - 1\right)T_0\right) - \frac{\alpha_2}{2} A\exp\left(i\left(2\bar{\Omega}_1 + 1\right)T_0\right) - \frac{\alpha_2}{2}\bar{A}\exp\left(i\left(2\bar{\Omega}_1 - 1\right)T_0\right)$$
$$-\frac{\alpha_3}{2} A\exp\left(i\left(\bar{\Omega}_2 + 1\right)T_0\right) - \frac{\alpha_3}{2}\bar{A}\exp\left(i\left(\bar{\Omega}_2 - 1\right)T_0\right) + cc \tag{3.27}$$

Here, *cc* stands for the complex conjugate of the preceding terms. In this case, one may observe that the solution of Eq. (3.27) contains secular or small divisor terms when the non-dimensional frequency of external axial loading ($\bar{\Omega}_2$) is nearly equal to 2 and/or non-dimensional frequency of magnetic field strength ($\bar{\Omega}_1$) is nearly equal to 1. Hence one may have three different resonance conditions viz. (i) $\bar{\Omega}_2 \approx 2$ and $\bar{\Omega}_1$ is away from 1, (ii) $\bar{\Omega}_1 \approx 1$ and $\bar{\Omega}_2$ is away from 2 and (iii) $\bar{\Omega}_2 \approx 2$ and $\bar{\Omega}_1 \approx 1$ simultaneously. These three conditions are discussed in the following subsections.

3.3.1 Principal parametric resonance case ($\bar{\Omega}_2 \approx 2$ and $\bar{\Omega}_1$ away from 1)

In this case, one may use detuning parameter σ to express the nearness of frequencies for the resonance conditions, as

$$\bar{\Omega}_2 = 2 + 2\varepsilon\sigma, \text{ and } \sigma = O(1) \tag{3.28}$$

Substituting Eq. (3.28) into Eq. (3.27) and eliminating the secular or small divisor terms yields

$$2iD_1A+i\zeta A+\frac{\alpha_3}{2}\bar{A}\exp(i2\sigma T_1)=0 \tag{3.29}$$

The particular solution of the Eq. (3.27) after eliminating the secular or small divisor terms is

$$q_1=\frac{\alpha_1}{2\left[\left(\bar{\Omega}_1+1\right)^2-1\right]}\left(A\exp i(\bar{\Omega}_1+1)\bar{t}\right)+\frac{\alpha_1}{2\left[\left(\bar{\Omega}_1-1\right)^2-1\right]}\left(A\exp i\left(\bar{\Omega}_1-1\right)\bar{t}\right)$$
$$+\frac{\alpha_2}{2\left[\left(2\bar{\Omega}_1+1\right)^2-1\right]}\left(A\exp i(2\bar{\Omega}_1+1)\bar{t}\right)+\frac{\alpha_2}{2\left[\left(2\bar{\Omega}_1-1\right)^2-1\right]}\left(A\exp i(2\bar{\Omega}_1-1)\bar{t}\right)$$
$$+\frac{\alpha_3}{2\left[\left(\bar{\Omega}_2+1\right)^2-1\right]}\left(A\exp i(\bar{\Omega}_2+1)\bar{t}\right)+cc \tag{3.30}$$

Substituting Eqs. (3.29) and (3.30) into the Eq. (3.25) and eliminating the secular or small divisor terms yields

$$2iD_2A+D_1^2A+\Gamma A=0 \tag{3.31}$$

where,

$$\Gamma=\frac{1}{4}\left(\frac{\alpha_1^2}{\bar{\Omega}_1^2+2\bar{\Omega}_1}\right)+\frac{1}{4}\left(\frac{\alpha_1^2}{\bar{\Omega}_1^2-2\bar{\Omega}_1}\right)+\frac{1}{4}\left(\frac{\alpha_2^2}{4\bar{\Omega}_1{}^2+4\bar{\Omega}_1}\right)+\frac{1}{4}\left(\frac{\alpha_2^2}{4\bar{\Omega}_1{}^2-4\bar{\Omega}_1}\right)+\frac{1}{4}\left(\frac{\alpha_3^2}{\bar{\Omega}_2^2+2\bar{\Omega}_2}\right)$$

From Eq. (3.29), one may obtain

$$D_1^2A=\frac{\zeta^2A}{4}+\left(\frac{\alpha_3}{4}\right)^2A-\frac{\alpha_3}{4}\left(i\zeta+2\sigma\right)\bar{A}\exp(2i\sigma T_1) \tag{3.32}$$

Substituting Eqs. (3.32) into Eq. (3.31), gives

$$2iD_2A+\left(\frac{\zeta^2}{4}+\left(\frac{\alpha_3}{4}\right)^2+\Gamma\right)A-\frac{\alpha_3}{4}\left(i\zeta+2\sigma\right)\bar{A}\exp(2i\sigma T_1)=0 \tag{3.33}$$

Substituting Eqs. (3.32) and (3.33) to Eq. $d/d\bar{t}=D_0+\varepsilon D_1+\varepsilon^2D_2+O(\varepsilon^2)$, one may obtain the following equation

$$2i\frac{dA}{d\bar{t}}+\left(i\varepsilon\zeta+\varepsilon^2\left[\frac{\zeta^2}{4}+\left(\frac{\alpha_3}{4}\right)^2+\Gamma\right]\right)A+\frac{\alpha_3}{2}\left(\varepsilon-\frac{\varepsilon^2}{2}\left[i\zeta+2\sigma\right]\right)\bar{A}\exp(2i\sigma T_1)=0 \tag{3.34}$$

Putting, $A=(B_r+iB_i)\exp(i\varepsilon\sigma\bar{t})$, where B_r, and B_i are real and imaginary parts, in Eq. (3.34) and separating the real and imaginary parts yield the following equations.

$$2\frac{dB_r}{d\bar{t}}+\left(\varepsilon\zeta-\varepsilon^2\frac{\alpha_3}{4}\zeta\right)B_r+\left[-2\sigma-\varepsilon\frac{\alpha_3}{2}+\varepsilon^2\left(\frac{\alpha_3}{2}\sigma\right)+\varepsilon^2\left(\frac{\zeta^2}{4}+\left(\frac{\alpha_3}{4}\right)^2+\Gamma\right)\right]B_i=0 \tag{3.35}$$

$$2\frac{dB_i}{d\bar{t}}+\left(\varepsilon\zeta+\varepsilon^2\frac{\alpha_3}{4}\zeta\right)B_i+\left[2\sigma-\varepsilon\frac{\alpha_3}{2}+\varepsilon^2\left(\frac{\alpha_3}{2}\sigma\right)-\varepsilon^2\left(\frac{\zeta^2}{4}+\left(\frac{\alpha_3}{4}\right)^2+\Gamma\right)\right]B_r=0 \tag{3.36}$$

Substituting $(B_r,B_i)=(b_r,b_i)\exp(\gamma\bar{t})$ into the Eqs. (3.35) and (3.36) yields the following equations.

$$2\gamma b_r+\left(\varepsilon\zeta-\varepsilon^2\frac{\alpha_3}{4}\zeta\right)b_r+\left[-2\sigma-\varepsilon\frac{\alpha_3}{2}+\varepsilon^2\left(\frac{\alpha_3}{2}\sigma\right)+\varepsilon^2\left(\frac{\zeta^2}{4}+\left(\frac{\alpha_3}{4}\right)^2+\Gamma\right)\right]b_i=0 \tag{3.37}$$

$$2\gamma b_i+\left(\varepsilon\zeta+\varepsilon^2\frac{\alpha_3}{4}\zeta\right)b_i+\left[2\sigma-\varepsilon\frac{\alpha_3}{2}+\varepsilon^2\left(\frac{\alpha_3}{2}\sigma\right)-\varepsilon^2\left(\frac{\zeta^2}{4}+\left(\frac{\alpha_3}{4}\right)^2+\Gamma\right)\right]b_r=0 \tag{3.38}$$

For steady state trivial response, γ is equal to zero. One may obtain the expression for the transition curves by finding the value of σ from the above two equations. Neglecting the terms $O(\varepsilon^3)$ one may write the expression for transition curves of the second order expansion when $\Omega_2\approx 2$ as

$$\bar{\Omega}_2=2\pm\frac{\varepsilon}{4}\left[\sqrt{\left(\varepsilon^2\left(\zeta^2+\left(\frac{\alpha_3}{2}\right)^2+4\Gamma\right)^2-16\varepsilon^2\left(\zeta^2-\frac{\alpha_3^2}{4}\right)\right)}+\varepsilon^2\left(\zeta^2+\left(\frac{\alpha_3}{2}\right)^2+4\Gamma\right)\right] \tag{3.39}$$

3.3.2 Simple resonance case ($\bar{\Omega}_1\approx 1$ and $\bar{\Omega}_2$ away from 2)

Following the method similar to that described in section 3.3.1, for this simple resonance case $\bar{\Omega}_1\approx 1$ ($\bar{\Omega}_1=1+\varepsilon\sigma$) and Ω_2 is away from 2, the transition curves emanating from $\bar{\Omega}_1\approx 1$ may be written as

$$\bar{\Omega}_1 = 1 \pm \frac{\varepsilon}{8}\left[\sqrt{\left(\varepsilon^2\left(\zeta^2+\left(\frac{\alpha_2}{2}\right)^2+4\Gamma\right)^2-16\varepsilon^2\left(\zeta^2-\frac{\alpha_2^2}{4}\right)\right)}+\varepsilon^2\left(\zeta^2+\left(\frac{\alpha_2}{2}\right)^2+4\Gamma\right)\right] \tag{3.40}$$

Here, $\Gamma = \frac{1}{4}\left(\frac{\alpha_1^2}{\bar{\Omega}_1^2+2\bar{\Omega}_1}\right)+\frac{1}{4}\left(\frac{\alpha_2^2}{4\bar{\Omega}_1{}^2+4\bar{\Omega}_1}\right)+\frac{1}{4}\left(\frac{\alpha_3^2}{\bar{\Omega}_2{}^2+2\bar{\Omega}_2}\right)+\frac{1}{4}\left(\frac{\alpha_3^2}{\bar{\Omega}_2^2-2\bar{\Omega}_2}\right)$

3.3.3 Simultaneous resonance case ($\bar{\Omega}_1 \approx 1$ and $\bar{\Omega}_2 \approx 2$)

In this resonance condition when the system is excited simultaneously by the external force and the magnetic field the frequency of excitation can be given by $\bar{\Omega} = \bar{\Omega}_2 = 2\bar{\Omega}_1 = 2 + 2\varepsilon\sigma$. Following the method similar to that described in section 3.3.1 and 3.3.2, the expression for the transition curves can be given by

$$\bar{\Omega} = 2 \pm \frac{\varepsilon}{4}\left[\sqrt{\left(\varepsilon^2\left(\zeta^2+\left(\frac{\alpha_2+\alpha_3}{2}\right)^2+4\Gamma\right)\right)^2-16\varepsilon^2\left(\zeta^2-\left(\frac{\alpha_2+\alpha_3}{2}\right)^2\right)}+\varepsilon^2\left(\zeta^2+\left(\frac{\alpha_2+\alpha_3}{2}\right)^2+4\Gamma\right)\right] \tag{3.41}$$

Here, $\Gamma = \frac{1}{4}\left(\frac{\alpha_1^2}{\bar{\Omega}_1^2+2\bar{\Omega}_1}\right)+\frac{1}{4}\left(\frac{\alpha_1^2}{\bar{\Omega}_1^2-2\bar{\Omega}_1}\right)+\frac{1}{4}\left(\frac{\alpha_2^2}{4\bar{\Omega}_1{}^2+4\bar{\Omega}_1}\right)+\frac{1}{4}\left(\frac{\alpha_2\alpha_3}{\bar{\Omega}_1^2+2\bar{\Omega}_1}\right)$
$+\frac{1}{4}\left(\frac{\alpha_2\alpha_3}{4\bar{\Omega}_1^2+4\bar{\Omega}_1}\right)+\frac{1}{4}\left(\frac{\alpha_3^2}{\bar{\Omega}_2^2+2\bar{\Omega}_2}\right)$

3.4 Numerical Results and Discussions

3.4.1 Instability Regions of a Sandwich Beam Subjected to Time Varying Magnetic Field for Simple Resonance Case.

In this section the numerical investigation has been carried out to determine the instability regions for simple resonance case of a sandwich beam subjected to time varying magnetic field. For this purpose, the MRE based on natural rubber containing different percentage of iron particles and carbon blacks in nano size are considered for sandwich beams with simply supported and clamped free end

conditions. It has been observed from the experiment (Chen *et al.*, 2007) that for same magnetic field strength, with increase in percentage of iron particles, the shear modulus and loss factor increases. For same percentage of iron particle, with increase in percentage of carbon black, though the shear modulus increases, the loss factor decreases (Chen *et al.*, 2008).

For numerical simulation, following physical parameters have been taken. The span of the sandwich beam, $L = 500$ mm; width, $b = 50$ mm; the top and bottom skins thickness, $2h_t = 2h_b = 1$ mm, the core thickness, $2h_c = 3$ mm. The top and bottom aluminum skins have Young's modulus 72 GPa and density 2700 kg/m^3. The zero field Young's modulus and shear modulus are same for both MRE and non-MRE parts in core.

Figure 3.3 illustrates the variation modal frequencies for the system without magnetic field and with magnetic field strength of 0.8 T. Here, the properties of MRE based on natural rubber containing 80% of iron particles have been taken (Chen *et al.*, 2007).

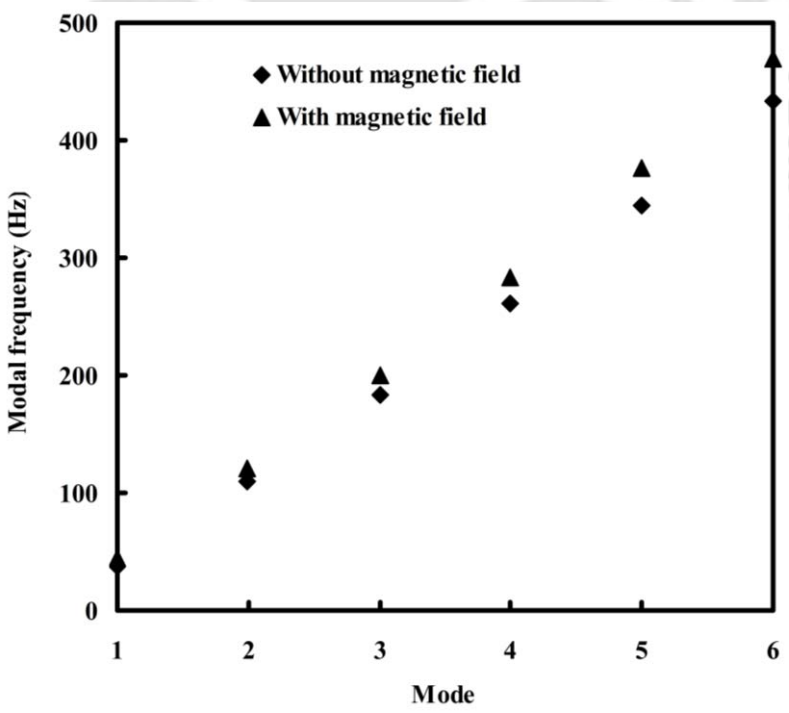

Figure 3.3 Modal frequencies of a simply supported sandwich beam without and with magnetic field.

It can be seen that the natural frequencies corresponding to all the modes increase with the application of magnetic field. The results show significant effect of the magnetic field on the higher modal frequencies, while the effect is small on the lower modes. The increase in the modal frequencies with increasing magnetic field can be attributed to increase in the complex shear modulus of the MRE and thus the increase in the stiffness of the sandwich beam under a higher magnetic field. This confirms the potential of the MRE to control the vibration of the sandwich beam by actively shifting the natural frequencies or the resonance conditions by applying magnetic field.

In the following subsections vibration control of sandwich beams with simply supported and cantilevered end conditions have been studied.

3.4.1.1 Stability Analysis of Simply Supported Sandwich Beam

It may be noted from Eq. (3.4) that by applying a time varying magnetic field, the governing equation of the system becomes that of a parametrically excited system with two frequency excitations. Hence, one may study the parametric instability region which will give an idea of the amplitude and frequency of the alternating magnetic filed to have stable vibration free system. Considering two types of MRE viz., MRE containing 80% iron particles and MRE containing 33% iron particles with 7 % carbon black, Figs. 3.3 (a) and (b) show the instability regions of the sandwich beam for various skin thicknesses. The region bounded by the curves is unstable, the regions out side the curves are stable. The unstable and stable regions for the sandwich beam with 0.1 mm skin thickness have been represented by letter U and S, respectively in Fig. 3.4 (a).

It has been observed that the instability region decreases with increase in skin thickness (Fig. 3.4). It may also be noticed that, by using less percentage of iron particle with carbon black in MRE, the critical $\bar{B}_d$ value (below which the system becomes stable for all frequencies $\bar{\Omega}_1$) marginally decreases (Fig. 3.4 (b)). This is due to the fact that though the shear modulus of MRE increases with carbon black, the core loss factor decreases.

Figure 3.5 shows the free vibration response of a sandwich beam with skin thickness of 1mm. This corresponds to the point marked 'B' in Fig.3.4 (a). As the point is out side the instability region, the system is supposed to be stable. This fact is validated from the time response shown in Fig. 3.5. One may clearly observe that by applying the magnetic field, the system response can be reduced. Hence, one can control the free vibration of MRE embedded viscoelastic core sandwich beam with the application of magnetic field.

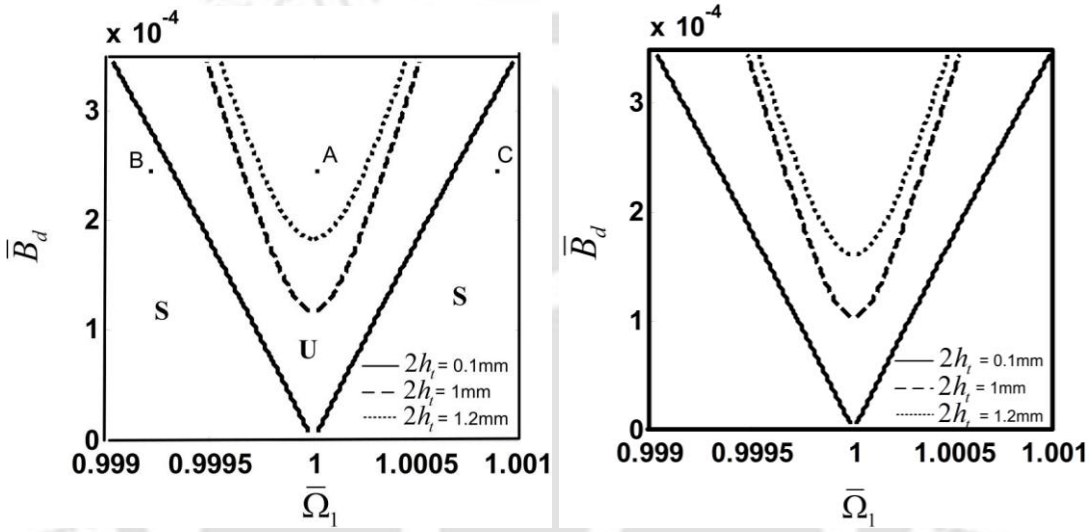

Figure 3.4 Effect of skin thickness on the instability regions of the sandwich beam with MRE embedded core, subjected to dynamic magnetic field. (a) MRE containing 80% of iron particles (b) MRE containing 33% of iron particles and 7% of carbon black.

Now taking the same amplitude of magnetic field strength, if one increases the frequency of the applied magnetic field, the system may be unstable. For example, taking frequency $\bar{\Omega}_1$ corresponding to point A as marked in Fig. 3.4 (a), Fig. 3.6 (a) shows the time response for the transverse displacement of the sandwich beam with MRE embedded core. In Fig. 3.4 (a), point 'A' is clearly in the unstable region which is in good agreement with the response curve shown in Fig. 3.6 (a). For the same amplitude of magnetic field strength, Fig. 3.6 (b) and (c) show the time response for transverse displacement of the system corresponding to the points 'B' and 'C' respectively (marked as shown in Fig.3.4 (a)). Clearly these points are in

stable regions and are in good agreement with the response curves shown in Figs. 3.6 (b) and (c).

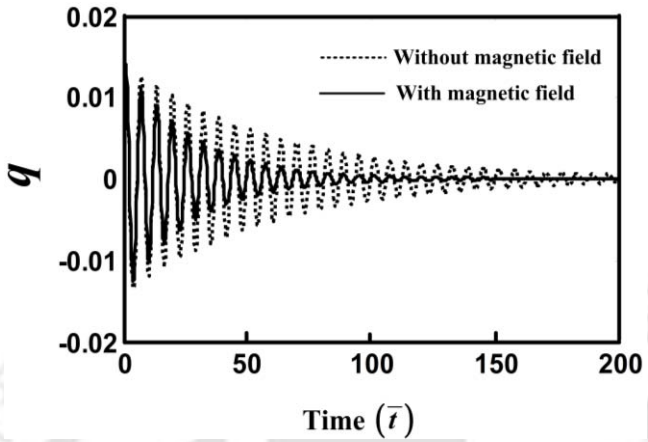

Figure 3.5 Time response of the sandwich beam without magnetic field and with magnetic field strength of 0.6 T ($2h_t = 2h_b = 1$ mm) corresponding to point B in Fig. 3.4 (a).

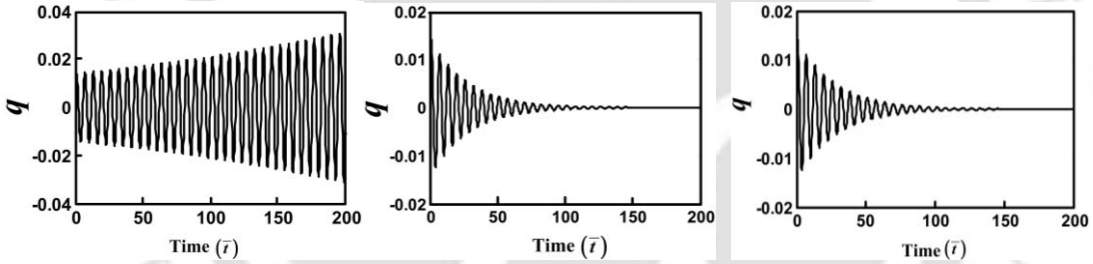

(a) (b) (c)

Figure 3.6 Time response of the sandwich beam with skin thickness equal to 1.2 mm, corresponding to (a) point A, (b) point B and (c) point C in Fig. 3.4 (a).

The effects of percentage of iron particles and carbon black on the instability regions are shown in Figs. 3.7 (a) and (b) respectively. From Fig. 3.7 (a) one may observe that with increase in percentage of iron particles the instability regions decreases as the core loss factor and the shear modulus of the MRE increases with increase in magnetic field. But with increase in percentage of carbon black the instability region increases as shown in Fig. 3.7 (b). In case of MRE containing carbon black, though the shear modulus increases the core loss factor decreases with increase in carbon black. So the passive vibrations control of the sandwich beam is possible by changing the MRE patch according to the requirements.

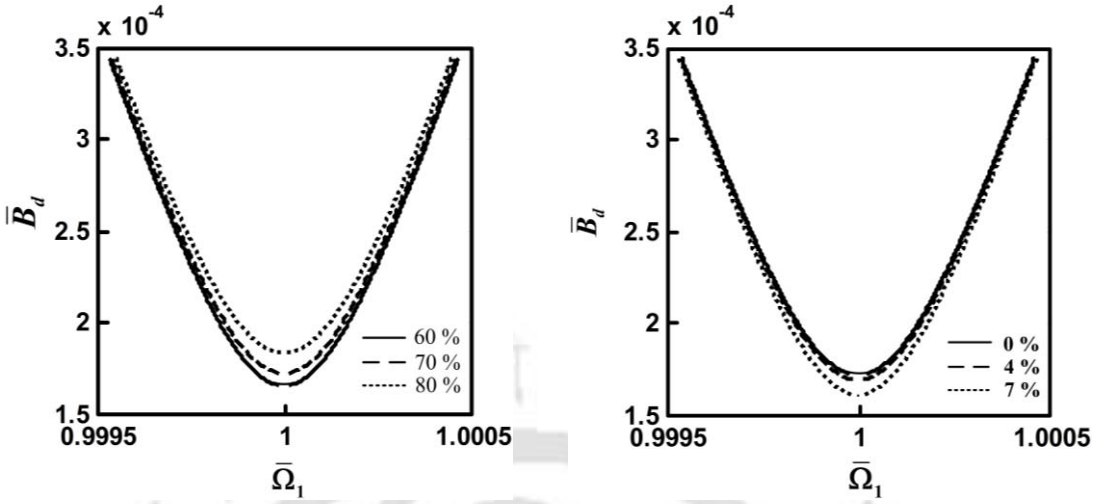

(a) (b)

Figure 3.7 Effect of (a) percentage of iron particles and (b) percentage of carbon black on the instability regions of the sandwich beam with MRE embedded core subjected to time varying magnetic field.

3.4.1.2 Stability Analysis of Clamped free Sandwich Beam

In this subsection the free vibration response and parametric instability regions of a cantilevered sandwich beam with MRE patch have been determined considering the same dimensions of the beam as given in the previous subsection. Figure 3.8 (a) shows the instability region of this system with MRE containing 80% iron particles. Similar to simply supported case with increase in skin thickness the stability of the system improves. Similarly Fig. 3.8 (b) shows the instability region for various skin thicknesses for a sandwich beam with MRE patch containing 33% iron particles with 7% carbon blacks. As in this arrangement the system becomes lighter than the previous one the instability region marginally decreases. In order to control the free vibration of the system, one should apply a magnetic field whose amplitude and frequencies are out side the instability region. To demonstrate this, Fig. 3.9 shows the free vibration response of a cantilevered sandwich beam with and without magnetic field. Here the skin thickness is taken as 1mm and other system parameters are same as in Fig. 3.8 (a). For the system with magnetic field, the considered amplitude and frequency of the magnetic field corresponds to the point marked ‘B’

in Fig. 3.8 (a). One may clearly observe that by suitably applying the magnetic field, the system response can be reduced.

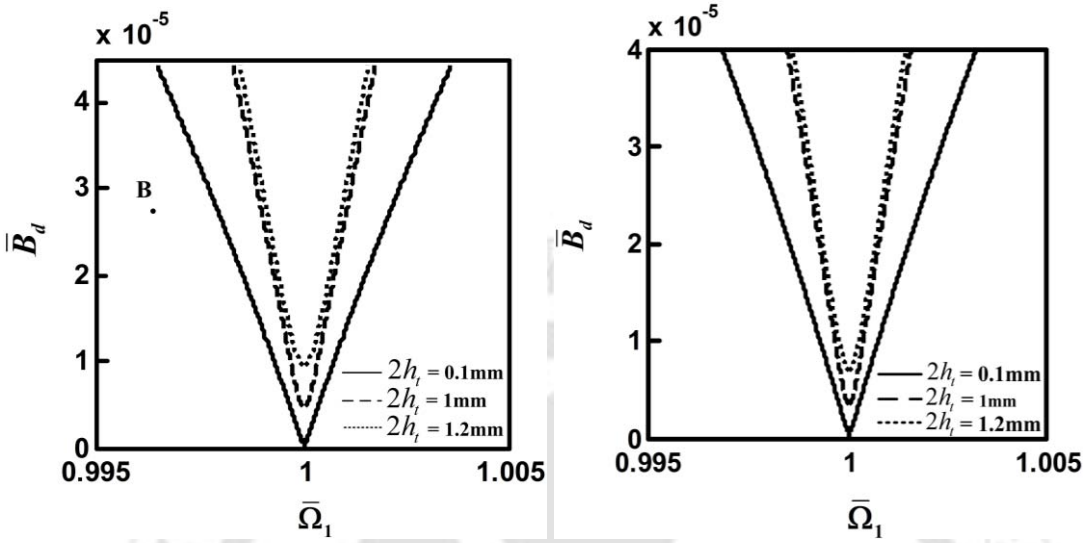

Figure 3.8 Effect of skin thickness on the instability regions of the sandwich beam with MRE patch (a) containing 80% of iron particles (b) containing 33% of iron particles and 7% of carbon black.

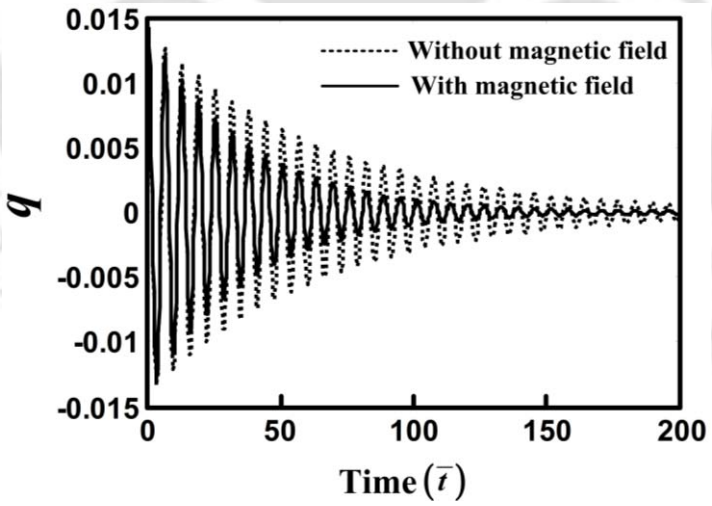

Figure 3.9 Time response of the sandwich beam without magnetic field and with magnetic field strength of 0.6 T ($2h_t = 2h_b = 1$ mm) corresponding to point B in Fig. 3.8 (a).

Figure 3.10 (a) shows the effect of variation of percentage of iron particles and Fig. 3.10 (b) shows the variation of percentage of carbon black on the instability regions. Like the previous case, here also one may take suitable value of the

amplitude and frequency of the magnetic field, percentage of iron particles and carbon black to attenuate the vibration of the system. The vibration reduction can be performed actively by using suitable magnetic field, or by passively with the help of suitable MRE embedded viscoelastic cored sandwich beam. From the instability regions of simply supported and cantilevered sandwich beam, it is observed that the lower critical dynamic amplitude of magnetic field below which the system remain stable for all frequency range is more in case of simply supported sandwich beam.

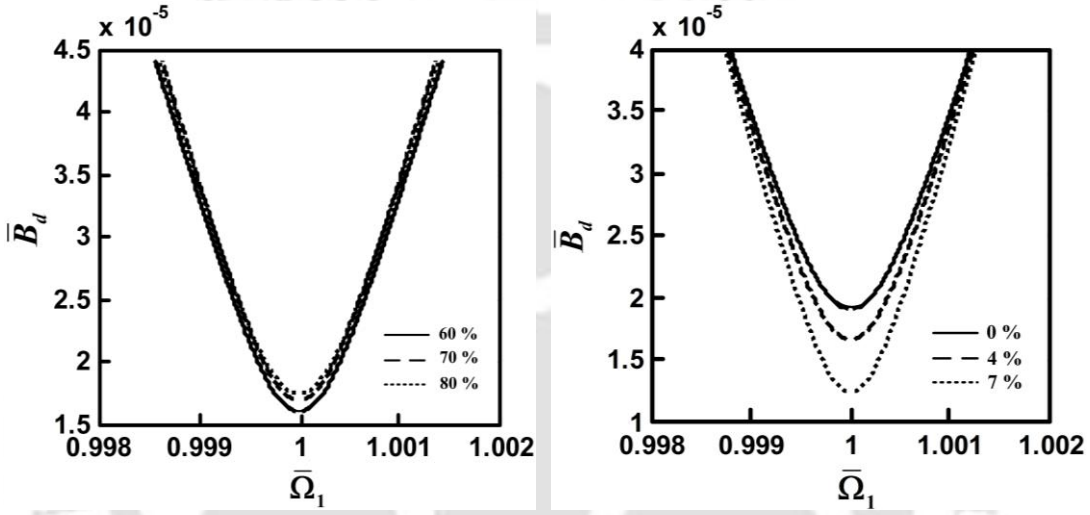

(a) (b)

Figure 3.10 Effect of (a) percentage of iron particles and (b) percentage of carbon black on the instability regions of the sandwich beam with MRE embedded core.

3.4.2 Instability Regions of a Sandwich Beam Subjected to Time Varying Magnetic Field and Periodic Axial Load

In this section the instability regions are determined for three resonance cases viz. simple, parametric and simultaneous simple and parametric resonance cases of a sandwich beam subjected to both time varying magnetic field and axial load. The effects of various key parameters such as skin thickness, static magnetic field B_s, static axial force P_s, amplitude of transverse periodic magnetic field B_d, amplitude of axial periodic load P_d, percentage of iron particles and percentage of nano-sized carbon blacks on the instability regions of the sandwich beam are studied.

The dimensions and material properties of the sandwich beam are given as follows. To keep the Euler buckling strength approximately same for the simply supported and clamped free end conditions, the spans of the beam (L) is taken as 950 mm for simply supported and 500 mm for clamped free end conditions. Other physical parameters, width, $b = 30\,\text{mm}$; the top and bottom skins thicknesses, $2h_t = 2h_b = 0.1\,\text{mm}$, the core thickness, $2h_c = 2\,\text{mm}$ are same for both the boundary conditions. The top and bottom aluminum skins have Young's modulus, $E_t = E_b = 72\,\text{GPa}$, densities, $\rho_t = \rho_b = 2700\,\text{kg m}^{-3}$ and permeabilities $\mu_e = \mu_{et} = \mu_{eb}$ = 1.25665e-6. Magnetic permeability in free spaces μ_0 =4πe-7 (Zhou and Wang, 2006b). The zero fields shear modulus and Young's modulus of both MRE and non-MRE parts are same (chapter 2).

Considering the amplitude of dynamic magnetic field B_d equal to zero, the modal frequencies are given in Table 3.1 which are found to be in good agreement with those obtained by Zhou and Wang, (2006b). The present system reduces to that of chapter 2 (i.e., absence of dynamic magnetic field case) and hence same frequencies could be noticed. It may be noted that in Zhou and Wang, (2006b), a higher order theory has been taken and in the present work classical sandwich beam theory has been taken. The advantage of using classical thory over the higher order theory is the less computational time and memory requirements and simplicity in analysis procedure.

Table 3.1 Comparison of the modal frequencies obtained in the present analysis with those obtained by Zhou and Wang, (2006b).

Magnetic field	Modal frequencies (Hz)		
	Mode	Present Analysis with $B_d = 0$	Zhou and Wang, (2006b), [21, Fig. 4a]
1Tesla	1	67.338	68.816
	2	144.923	152.441
	3	222.145	225.08

In the following subsections the instability regions of sandwich beams with simply supported and clamped free end conditions have been studied for the three resonance cases. In section 3.4.2.1 the results for the case with non-dimensional

frequency of magnetic field $\bar{\Omega}_1 \approx 1$ and non-dimensional frequency of external axial loading $\bar{\Omega}_2$ away from 2 are presented. In section 3.4.2.2 the results for the case with $\bar{\Omega}_2 \approx 2$ and $\bar{\Omega}_1$ away from 1 are presented and in section 3.4.2.3 the results for the case with $\bar{\Omega}_1 \approx 1$ and $\bar{\Omega}_2 \approx 2$ are presented.

One may use the instability regions developed in this work for suppressing the vibration of the system. For example for a sandwich beam with 0.1mm skin thickness the system is unstable at $\bar{B}_d$ = 4 with a frequency of $\bar{\Omega}_1$=1 (Fig. 3.11(a)), and hence the system will vibrate. Now to suppress this vibration one may change only the frequency of the AC component of the magnetic field (e.g., $\bar{\Omega}_1$=0.9 or $\bar{\Omega}_1$=1.08). Similarly for a sandwich beam with 0.5mm thickness ($\bar{B}_d$ = 4, $\bar{\Omega}_1$=1) to suppress this vibration one may either decrease the amplitude of AC component of the magnetic field (e.g., $\bar{B}_d$ =2.4) or change the frequency of the AC component of the magnetic field (e.g., $\bar{\Omega}_1$=0.9 or $\bar{\Omega}_1$=1.08). In a similar way one may interpret the instability region developed in this work for attenuation or control of vibration by suitably changing the system parameters.

3.4.2.1 Simple Resonance due to Magnetic Field ($\bar{\Omega}_1 \approx 1$ and $\bar{\Omega}_2$ away from 2)

In this case, the system is subjected to magnetic field with a frequency nearly equal to the natural frequency of the system and the frequency of external axial loading is away from the principal parametric instability zone. Thus, the instability regions are independent of P_d .

Initially a simply supported sandwich beam has been considered for the analysis. Figures 3.11(a) and (b) show the effect of skin thickness of a simply supported sandwich beam on the transition curves with MRE containing 80% of iron particles and MRE containing 33% of iron particles with 7% of carbon black, respectively. With increase in skin thickness the instability region decreases as the skins strengthen the bulk flexural rigidities of the sandwich beam. From Fig. 3.11(a) it is noted that with decrease in $\bar{B}_d$ the unstable region decreases and the system can operate for a wide frequency range for lower value of $\bar{B}_d$. Further, there exists a

critical value of $\bar{B}_d$ ($\bar{B}_{dcr}$) as shown in Fig. 3.11(a) below which the system has no unstable region and hence can operate at any frequency without vibration. By using less percentage of iron particles with carbon black in MRE, the critical $\bar{B}_d$ value below which the system becomes stable for frequency $\bar{\Omega}_1$, marginally decreases which is clearly illustrated by the comparison of $\bar{B}_{dcr}$ values for different MRE patch as given in Table 3.2. This is due to the fact that, though the shear modulus of MRE increases with carbon black, the loss factor decreases. From Fig. 3.11 it may also be observed that the system with higher skin thickness remain stable for all frequency range for higher value of $\bar{B}_d$.

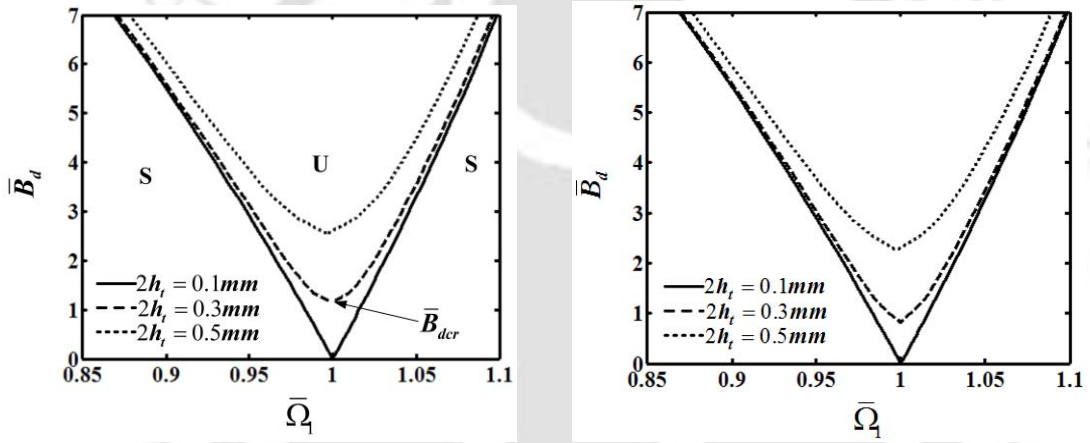

Figure 3.11 Effect of skin thickness on the instability regions of the sandwich beam with (a) MRE containing 80% of iron particles and (b) MRE containing 33% of iron particles and 7% of carbon black. $P_s = 1N$ and $B_s = 0$.

The results presented in Fig. 3.12 clearly illustrate the influence of static axial force P_s and static magnetic field B_s on the transition curves. Comparing Figs. 3.12(a) and (b), with increase in static axial load P_s from 5N to 10N the area of instability regions increases and the critical value of $\bar{B}_d$ decreases. This is due to the fact that with increase in P_s, the compressive force in the skins makes the system less stiff. One may also observe that with increase in iron particles from 60% to 80% in MRE the instability regions decreases but with increase in carbon black from 4% to 7% in MRE containing 33% of iron particles the instability regions increases.

Table 3.2 Comparison of $\bar{B}_{dcr}$ for different skin thicknesses with different MRE patch.

Skin thickness (mm)	$\bar{B}_{dcr}$	
	Core with MRE patch containing 80% of iron particles	Core with MRE patch containing 33% of iron particles and 7% of carbon black
0.1	0	0
0.3	1.152	0.829
0.5	2.549	2.264

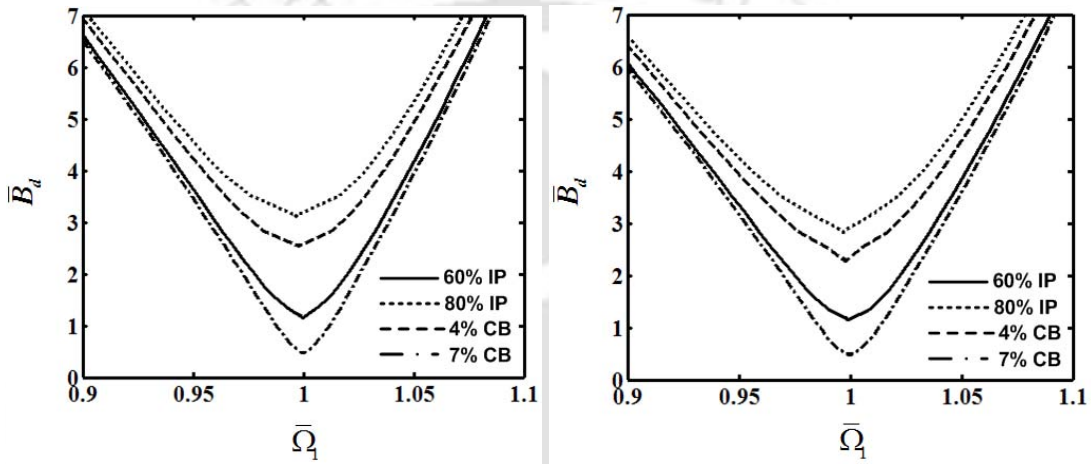

(a) (b)

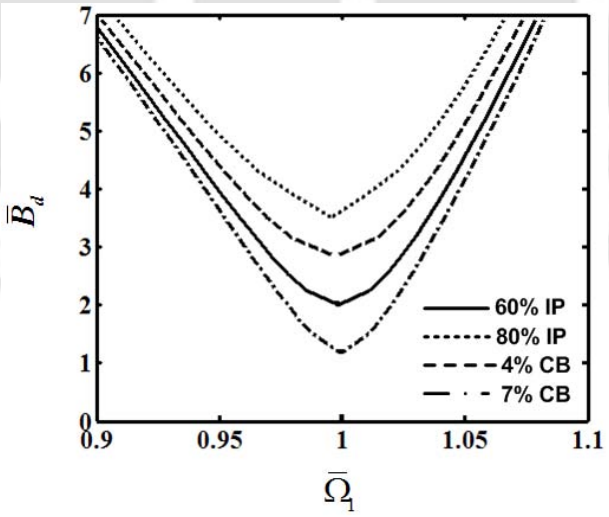

(c)

Figure 3.12 Influence of static axial load P_s and static magnetic field B_s on instability regions: (a) P_s =5N and B_s =0.1T, (b) P_s =10N and B_s =0.1T, and (c) P_s =5N and B_s =0.2T

This can be attributed to the relatively increase in the loss factor with increase in percentage of iron particles and decrease in the loss factor of the MRE with increase in carbon blacks.

Comparing Fig. 3.12(a) and Fig. 3.12(c) it is observed that with increase in static transverse magnetic field density B_s from 0.1T to 0.2T, the width of the instability regions decreases and the critical value of $\bar{B}_d$ increases. Here the critical values of $\bar{B}_d$ are more in comparison to that in case of change of static load which is given in Table 3.3. This can be related to the fact that the relative variation in the beam stiffness could be greater than that of the beam subjected to variation of the static load. It should be noted that due to the increase of field dependant shear modulus of the MRE patches with magnetic field, the stiffness of the beam changes.

Table 3.3 Values of critical dynamic magnetic field, $\bar{B}_{dcr}$ of the simply supported sandwich beam with different MRE patch.

MRE patch with	$\bar{B}_{dcr}$		
	Static load (5 N) and Static magnetic field (0.1T)	Static load (10 N) and Static magnetic field (0.1T)	Static load (5 N) and Static magnetic field (0.2T)
60% IP	1.16	1.158	2.001
80%IP	3.123	2.854	3.512
33% IP and 4% CB	2.536	2.266	2.836
33% IP and 7% CB	0.462	0.46	1.162

Now considering a clamped free MRE embedded sandwich, since similar trends in the instability regions are observed as in case of simply supported boundary condition for the variation of the skin thickness, the instability regions are not plotted but the critical values of $\bar{B}_{dcr}$ are given in Table 3.4. Like simply supported case, here also the instability regions decreases and the critical amplitude of dynamic magnetic field $\bar{B}_{dcr}$ increase with increase in skin thickness.

Figure 3.13 shows the instability regions of a clamped-free sandwich beam subjected to static axial force P_s and static magnetic field B_s. The values of $\bar{B}_{dcr}$ with

the variation of P_s and B_s, are presented in the Table 3.5. Since, $\bar{B}_{dcr}$ depends on the length of the beam, in this case the maximum value of $\bar{B}_{dcr}$ decreases in comparison to that of the simply supported case. From Tables 3.3 and 3.5 it is observed that the $\bar{B}_{dcr}$ values in case of simply supported sandwich beam are more than that of the clamped free end condition. Hence, to obtain the instability regions one should analyze the system for specific boundary condition.

Table 3.4 Comparison of $\bar{B}_{dcr}$ for different skin thicknesses with different MRE patch for a clamped-free sandwich beam.

Skin thickness (mm)	$\bar{B}_{dcr}$	
	Core with MRE patch containing 80% of iron particles	Core with MRE patch containing 33% of iron particles and 7% of carbon black
0.1	0	0
0.3	0.953	0.687
0.5	2.115	1.878

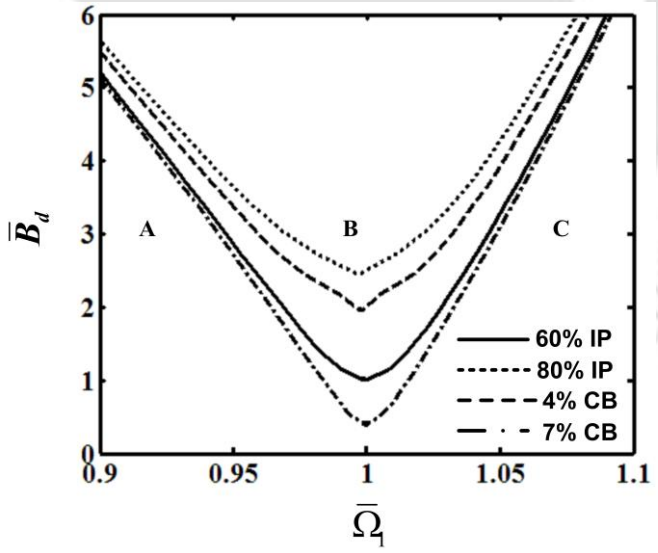

Figure 3.13 Transition curves for a clamped free sandwich beam subjected to static axial load, P_s =10N and static magnetic field B_s =0.1T.

Figure 3.14 shows the time response of a clamped-free sandwich beam considering two different cores with MRE patch containing 60% and 80% of iron particles. This corresponds to the point marked ‘A’ in Fig. 3.13. As the point is out

side the instability region, the system is supposed to be stable which is validated from the time response shown in Fig. 3.14. One may clearly observe that by increasing the percentage of iron particles in MRE patch, the system response can be reduced for the same magnetic field and frequency corresponding to the point A. The settling time is reduced from $\bar{t}$ =100 to $\bar{t}$ =60.

Table 3.5 Values of critical dynamic magnetic field, $\bar{B}_{dcr}$ of the clamped free sandwich beam with different MRE patch.

MRE patch with	$\bar{B}_{dcr}$		
	Static load (5 N) and Static magnetic field (0.1T)	Static load (10 N) and Static magnetic field (0.1T)	Static load (5 N) and Static magnetic field (0.2T)
60% IP	1.063	0.993	1.63
80%IP	2.897	2.447	3.272
33% IP and 4% CB	2.324	1.942	2.941
33% IP and 7% CB	0.424	0.394	1.069

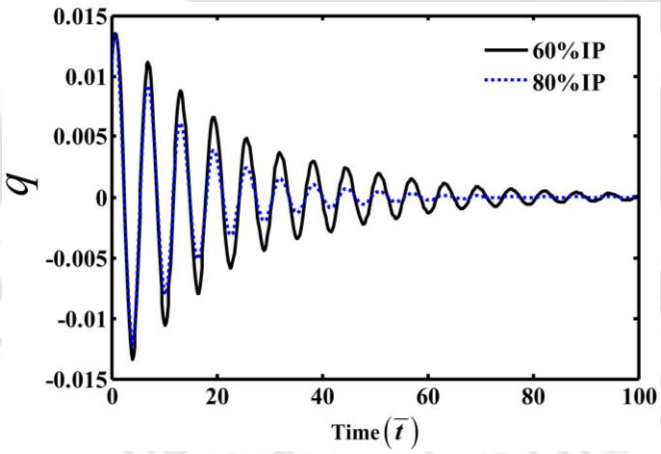

Figure 3.14 Time response at point A for MRE patches containing 60% and 80% of iron particles; key as in Fig. 3.13.

Now taking the same amplitude of magnetic field strength, if one increases the frequency of the applied magnetic field $\bar{\Omega}_1$, the system may be unstable. For example, taking frequency $\bar{\Omega}_1$ corresponding to point B as marked in Fig. 3.13, Fig. 3.15 (a) shows the time response for the transverse displacement of the clamped-free sandwich beam with MRE embedded core. In Fig. 3.13, point 'B' is clearly in the

unstable region which is in good agreement with the response curve shown in Fig. 3.15 (a). For the same amplitude of magnetic field strength, Fig. 3.15 (b) shows the time response for transverse displacement of the system corresponding to the points 'C', as marked in Fig. 3.13. Clearly this point is in stable region and is in good agreement with the response curve shown in Fig. 3.15(b). The time response is obtained by numerically solving the temporal Eq. (3.4).

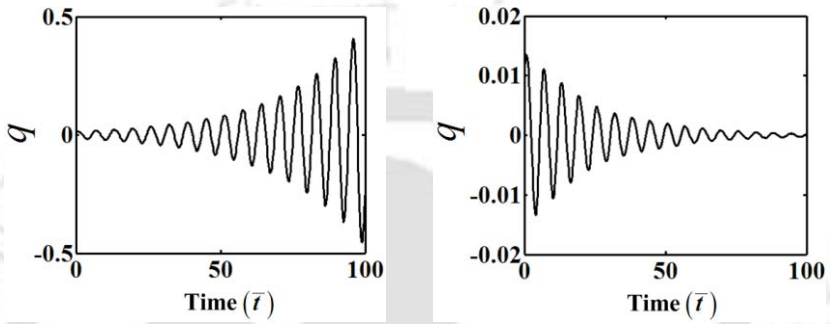

(a) (b)

Figure 3.15 Time responses for (a) point B and (b) point C; key as in Fig. 3.13.

3.4.2.2 Principal parametric resonance ($\bar{\Omega}_2 \approx 2$ and $\bar{\Omega}_1$ away from 1)

In this subsection, effect of percentage of iron particles, percentage of carbon black, static axial force and static magnetic field has been investigated for the simply supported and clamped free boundary conditions when the system is excited at a frequency $\bar{\Omega}_2 \approx 2$ (i.e. nearly equal to twice the fundamental frequency) and $\bar{\Omega}_1$ is away from 1.

The influence of skin thickness on the transition curves of a simply supported sandwich beam with MRE containing 80% of iron particles and MRE containing 33% of iron particles with 7% of carbon black respectively are shown in Figs. 3.16 (a) and (b). With increase in skin thickness the instability region decreases. From Fig. 3.16(a) it is observed that there exists a critical value of $\bar{P}_d$ ($\bar{P}_{dcr}$) below which the system has no unstable region and hence the system can operate at any frequency without vibration. Also it may be noted that, by using less percentage of iron particle with carbon black in MRE, the critical value of dynamic load $\bar{P}_d$ (below which the

system becomes stable for the frequency $\bar{\Omega}_2$) marginally decreases. This is due to the fact that though the shear modulus of MRE increases with carbon black, the loss factor decreases. The critical values of dynamic load $\bar{P}_{dcr}$ are given in Table 3.6.

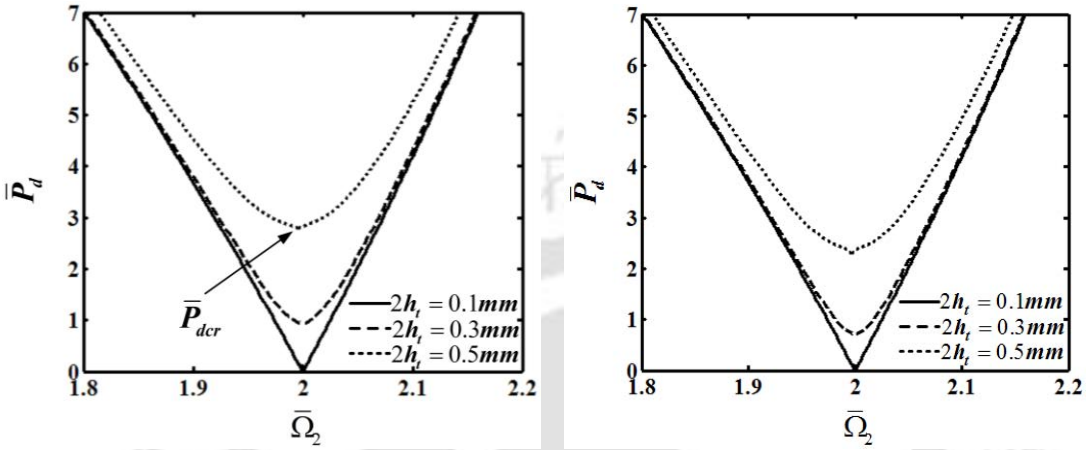

Figure 3.16 Effect of skin thickness on the instability regions of the simply supported sandwich beam with (a) MRE containing 80% of iron particles and (b) MRE containing 33% of iron particles and 7% of carbon black. $P_s = 1N$ and $B_s = 0$.

Table 3.6. Comparison of $\bar{P}_{dcr}$ for different skin thicknesses with different MRE patch.

Skin thickness (mm)	$\bar{P}_{dcr}$	
	Core with MRE patch containing 80% of iron particles	Core with MRE patch containing 33% of iron particles and 7% of carbon black
0.1	0	0
0.3	0.9	0.7
0.5	2.8	2.3

Figure 3.17 is plotted for various combinations of B_s and B_d to compare the results of present case with the case where the dynamic magnetic field (AC component) is not considered (chapter 2). It may be noted that in chapter 2, instability regions were found by using a different method. The instability regions with $B_d = 0$ are found to be in good agreement with chapter 2. From Fig. 3.17 one may observe that while application of static ($B_d = 0$) or dynamic magnetic field

improves the stability of the system by decreasing the instability region, application of static magnetic field (DC component) has more stabilizing effect than the dynamic (AC component) magnetic field.

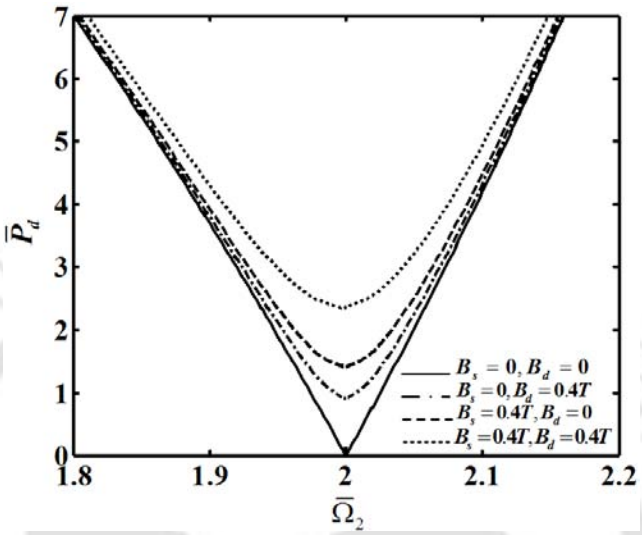

Figure 3.17 Transition curves of a simply supported sandwich beam with MRE containing 80% of iron particles for different combinations of B_s and B_d values. $2h_t = 0.1$ mm, $P_s = 1$ N.

Figure 3.18 shows the instability regions for different static load and magnetic fields for four different types of MRE patch. The corresponding critical values of dynamic load $\bar{P}_{dcr}$ for these cases are given in Table 3.7. It has been observed that with increase in percentage of iron particles the stability of the system improves and the $\bar{P}_{dcr}$ value increases. But for the same percentage of iron particle with increase in percentage of carbon black, $\bar{P}_{dcr}$ decreases. Also it may be noted that doubling the static load has an effect in decreasing $\bar{P}_{dcr}$ values whereas doubling the magnetic field has an effect in increasing $\bar{P}_{dcr}$ values. Hence one can effectively increase the magnetic field for active vibration reduction as it improves the stability of the system significantly.

The effect of skin thickness on the instability regions for the clamped free sandwich beam are found to be similar to simply supported case and the instability regions in this case also decrease with increase in skin thickness as the critical

dynamic load $\bar{P}_{dcr}$ increases. Table 3.8 presents the variation of critical dynamic load $\bar{P}_{dcr}$ for MRE with 80% iron particles and 33% iron particle with 7% carbon black. It is observed that, in the former case, one can have higher $\bar{P}_{dcr}$. This may be due to the fact that in the later case, though the shear modulus is more, the loss factor is less.

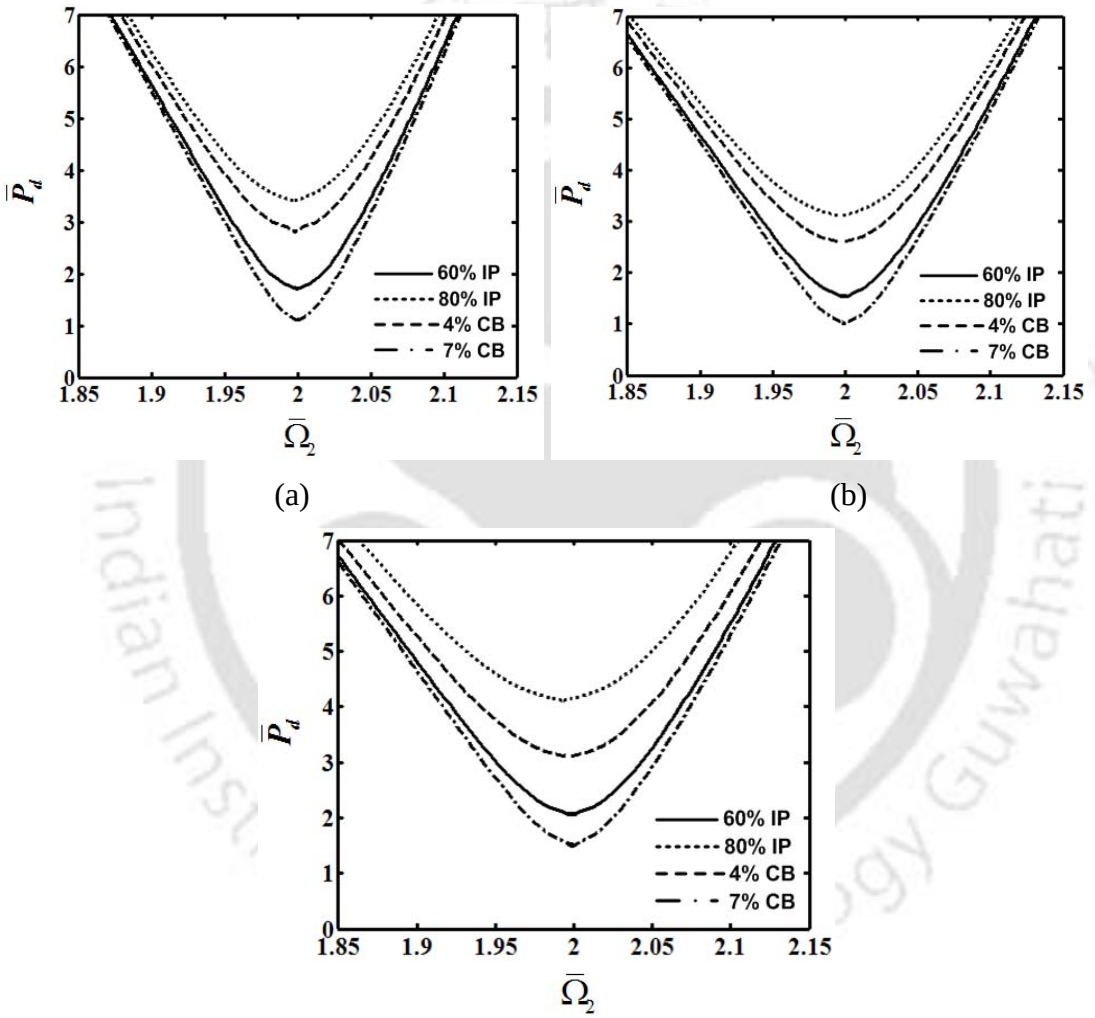

Figure 3.18 Influence of static axial load, P_s and static magnetic field B_s on instability regions (a) P_s = 5N and B_s = 0.1T, (b) P_s = 10N and B_s = 0.1T, and (c) P_s = 5N and B_s = 0.2T.

Table 3.7 Values of critical dynamic axial force, $\bar{P}_{dcr}$ of the simply supported sandwich beam with different MRE patch.

MRE patch with	$\bar{P}_{dcr}$		
	Static load (5 N) and Static magnetic field (0.1T)	Static load (10 N) and Static magnetic field (0.1T)	Static load (5 N) and Static magnetic field (0.2T)
60% IP	1.7	1.5	2.2
80%IP	3.4	3.1	4.1
33% IP and 4% CB	2.8	2.6	3.1
33% IP and 7% CB	1.1	1.0	1.7

Table 3.8 Comparison of $\bar{P}_{dcr}$ for different skin thicknesses with different MRE patch.

Skin thickness (mm)	$\bar{P}_{dcr}$	
	Core with MRE patch containing 80% of iron particles	Core with MRE patch containing 33% of iron particles and 7% of carbon black
0.1	0	0
0.3	0.9	0.69
0.5	2.7	2.25

The influence of P_s and B_s on the instability regions for the clamped free boundary conditions are found to be similar to the that of a simply supported beam and the values of critical dynamic load $\bar{P}_{dcr}$ for different MRE patches are presented in Table 3.9. With the increase in static magnetic field the shear modulus of the MRE increases which causes the increase in overall stiffness of the system and hence the critical value of dynamic load $\bar{P}_d$ increases. The increase of $\bar{P}_{dcr}$ makes the system more stable and hence the system can operate at a wide range of frequency without any vibration. Here, with increase in iron particles from 60% to 80% in MRE the instability regions decreases but with increase in carbon black from 4% to 7% in MRE containing 33% of iron particles the instability regions increases. This is due to the relative increase of loss factor with increase in percentage of iron particles and decrease of the loss factor of MRE with increase in percentage of blacks.

Table 3.9 Values of critical dynamic axial force, $\bar{P}_{dcr}$ of the clamped free sandwich beam with different MRE patch.

MRE patch with	$\bar{P}_{dcr}$		
	Static load (5 N) and Static magnetic field (0.1T)	Static load (10 N) and Static magnetic field (0.1T)	Static load (5 N) and Static magnetic field (0.2T)
60% IP	1.692	1.483	2.1
80%IP	3.573	3.076	4.096
33% IP and 4% CB	2.785	2.567	3.098
33% IP and 7% CB	1.098	0.987	1.654

3.4.2.3 Simultaneous Principal Parametric and Simple Resonance ($\bar{\Omega}_2 \approx 2$ and $\bar{\Omega}_1 \approx 1$)

In this case the system is subjected to dynamic magnetic field with a frequency nearly equal to the natural frequency of the system and an external axial loading with a frequency nearly equal to twice the fundamental frequency. Hence the system is subjected to simultaneous principal parametric resonance due to external axial loading and simply resonance due to the magnetic field. The instability regions are plotted for simply supported and clamped free boundary conditions.

Figures 3.19 (a) and (b) show the influence of dynamic magnetic field on the instability regions for simply supported sandwich beam. It is observed that with increase in magnetic field the stability of the system improves. The critical value of dynamic load, $\bar{P}_{dcr}$ increases and the instability regions moves upward. The values of $\bar{P}_{dcr}$ for simply supported sandwich beam are given in Table 3.10. From this table it is observed that the value of $\bar{P}_{dcr}$ increases by 27.14% with the variation of dynamic magnetic field from 0.2T to 0.6T for the beam having the MRE patch containing 80% of iron particles. This characteristic indicates that the applied magnetic field increases the flexural rigidity of the sandwich beam due to field dependant shear modulus of MRE. Similar to previous resonance conditions, here also the instability regions decrease with increase in percentage of iron particles and increases with increase in carbon black. Also for the same boundary condition, the influence of static axial load on the instability regions is shown in Figs. 3.19(c) and (d) and the

critical dynamic magnetic field, $\bar{B}_{dcr}$ obtained in this resonance condition are given in Table 3.10. It is noticed that the value of $\bar{B}_{dcr}$ decreases by 23.76% at a dynamic load of $\bar{P}_d = 1N$ and with variation of static load from 5N to 10N for simply supported sandwich beam having the MRE patch containing 80% of iron particles.

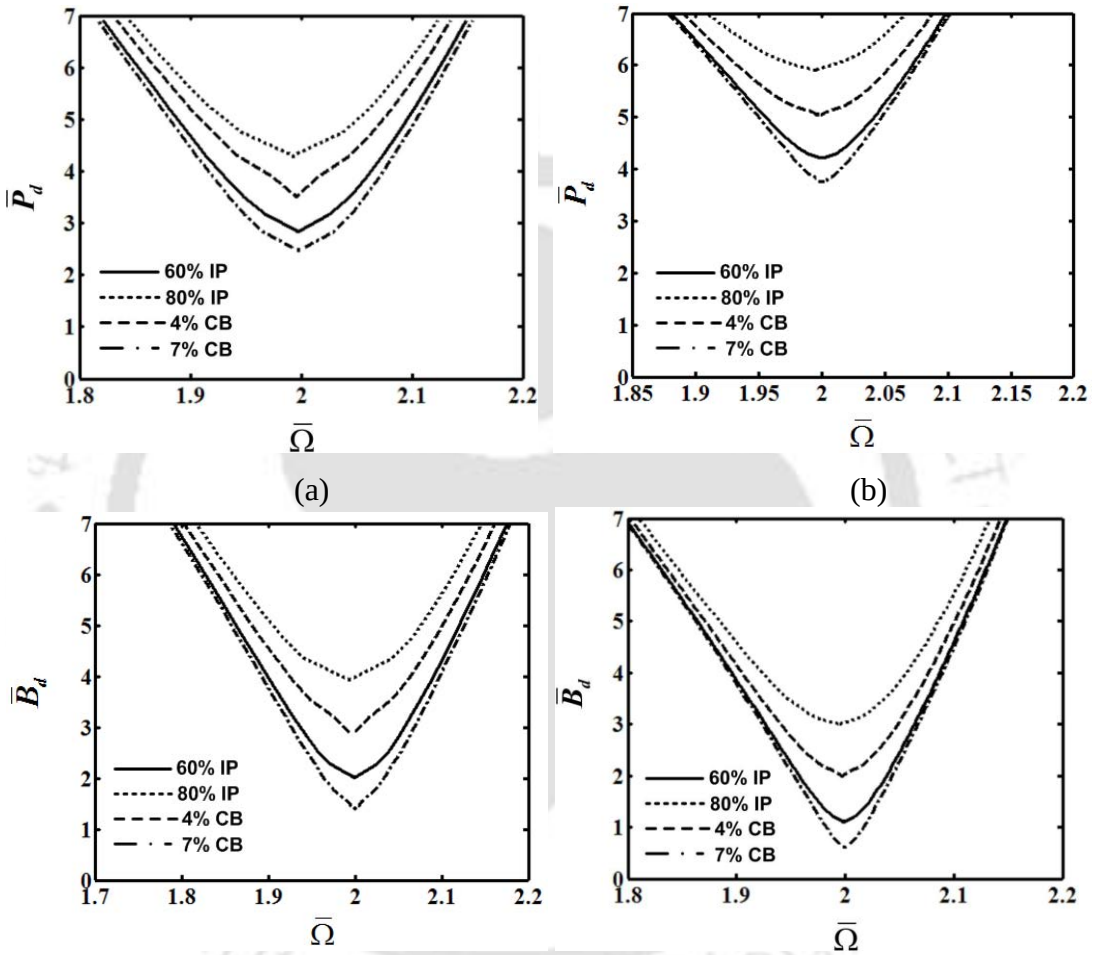

Figure 3.19 Influence of dynamic magnetic field B_d and static axial load P_s on the transition curves for simply supported sandwich beam. (a) P_s = 1N, B_d = 0.2T; (b) P_s = 1N, B_d = 0.6T; (c) P_d = 1N, P_s = 5N and (d) P_d = 1N, P_s = 10N.

Similar to simply supported case, for the clamped free sandwich beam Figs. 3.20 (a), (b), (c) and (d) show the instability regions due to dynamic magnetic field and axial load. The corresponding critical values are given in Table 3.11. It is observed that the value of $\bar{P}_{dcr}$ increases by 8% with the variation of dynamic magnetic field

Table 3.10 Values of critical dynamic axial force, $\bar{P}_{dcr}$ and critical dynamic magnetic field, $\bar{B}_{dcr}$ of a simply supported sandwich beam with different MRE patches for combination resonance case.

MRE patch with	$\bar{P}_{dcr}$ (P_s = 1N)		$\bar{B}_{dcr}$ (P_d = 1N)	
	$B_d = 0.2$T	$B_d = 0.6$T	P_s = 5N	P_s = 10N
60% IP	2.836	4.2	2.006	1.1
80%IP	4.299	5.9	3.935	3.00
33% IP and 4% CB	3.512	5.0	2.854	2.00
33% IP and 7% CB	2.506	3.7	1.344	0.6

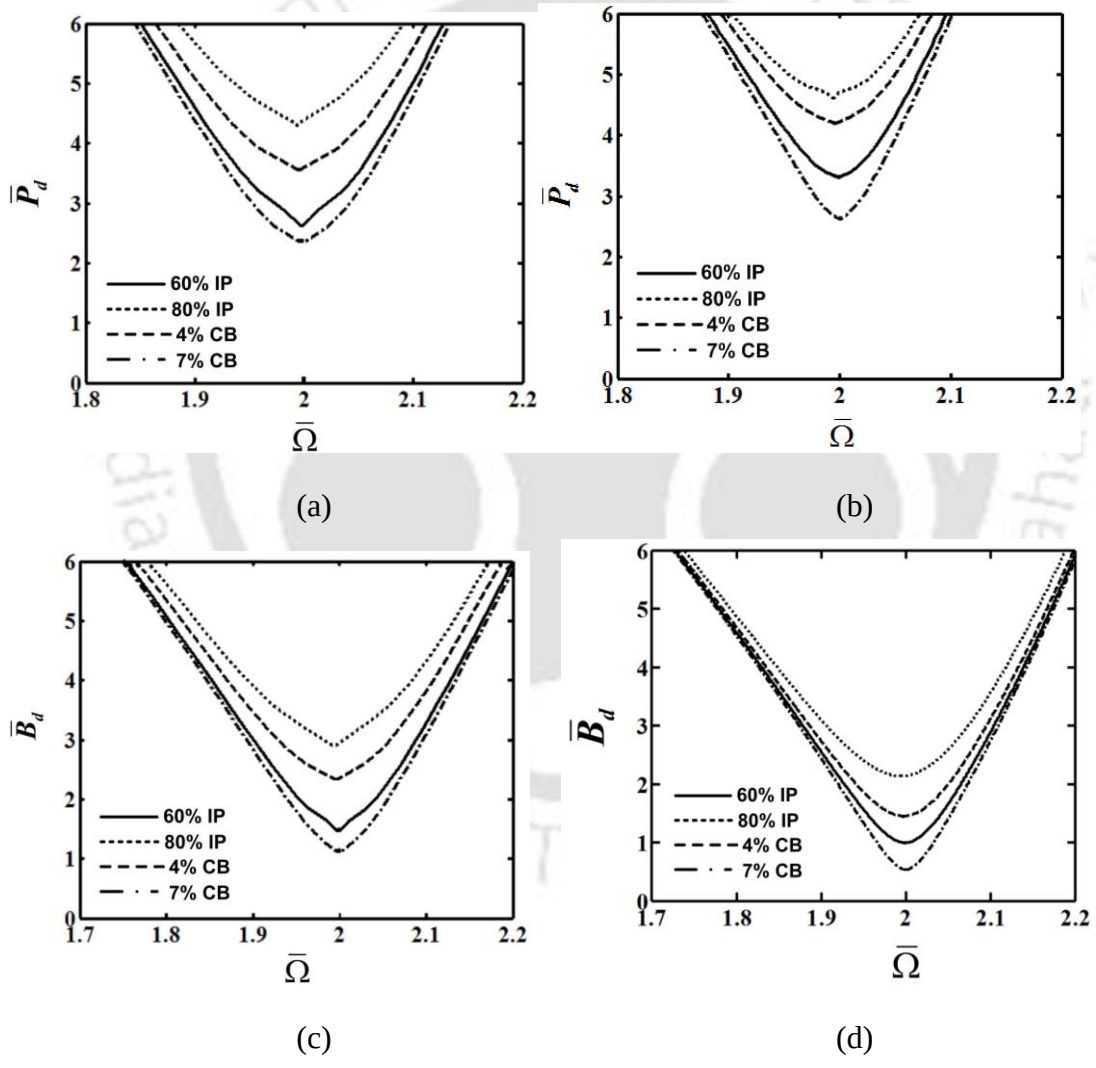

Figure 3.20 Influence of dynamic magnetic field B_d and static axial load P_s on the transition curves for clamped free sandwich beam. (a) P_s = 1N, B_d = 0.2T; (b) P_s = 1N, B_d = 0.6T; (c) P_d = 1N, P_s = 5N and (d) P_d = 1N, P_s = 10N.

from 0.2T to 0.6T for the beam having the MRE patch containing 80% of iron particles. Also for sandwich beam with MRE patch containing 80% of iron particles it is noticed that the value of $\bar{B}_{dcr}$ decreases by 3.67% at a dynamic load of $P_d = 1N$ and varying the static load from 5N to 10N.

Table 3.11 Values of critical dynamic axial force, $\bar{P}_{dcr}$ and critical dynamic magnetic field, $\bar{B}_{dcr}$ of a simply supported sandwich beam with different MRE patches for combination resonance case.

MRE patch with	$\bar{P}_{dcr}$ (P_s = 1N)		$\bar{B}_{dcr}$ (P_d = 1N)	
	$B_d = 0.2$T	$B_d = 0.6$T	P_s = 5N	P_s = 10N
60% IP	2.604	3.3	1.431	0.994
80%IP	4.232	4.6	2.894	2.131
33% IP and 4% CB	3.501	4.2	2.323	1.449
33% IP and 7% CB	2.331	2.6	1.086	0.528

3.5 Summary

In this chapter an attempt has been made to study the different resonance cases of the MRE embedded viscoelastic cored sandwich beam subjected to time varying magnetic field with and without applying periodic axial load. Two types of MREs are taken for the analysis. Using first order method of multiple scales the instability regions of a simply supported and clamped free sandwich beam has been carried out to show the reduction of free vibration response of a sandwich beam by applying time varying magnetic field.

Then the stability of the sandwich beam with MRE embedded viscoelastic core subjected to time varying transverse magnetic field and axial periodic load has been carried out. The temporal equation of motion, which contains two frequency parametric excitation terms, is solved using second-order method of multiple scales. Instability regions are found for three different resonance conditions viz., simple resonance, principal parametric resonance and simultaneous principal parametric and simple resonance. It has been noticed that with the increase in skin thickness the flexural rigidity of the sandwich beam increases and the instability regions decreases.

4

Dynamic Analysis of Rotating and Non-rotating MRE Embedded Sandwich Beam using Finite Element Method

4.1 Introduction

Vibration attenuation of machines and structures incorporating active or passive sandwich beam with MR materials in the viscoelastic core is an important aspect of investigation. The number, location and length of the MRE patches in non-MRE viscoelastic core influences the performance of a sandwich beam as it changes the dynamic properties of the sandwich beam under the application of magnetic field. Since it is difficult to apply classical sandwich beam models developed in chapter 2 for complex situations therefore, numerical techniques such as finite element method is extremely useful in such situations. It should be noted that in chapter 2 analytical method is employed for solution. In this chapter finite element method (FEM) has been used to study the dynamic behaviour of rotating and non-rotating sandwich beam. Though the analysis has been carried out for simple sandwich beam, the developed elemental mass, stiffness and force vectors can be used conveniently for any structural components.

In section 4.2, the modeling of a non-rotating sandwich beam with conductive skins subjected to static magnetic filed has been carried out using FEM. In section 4.3, the analysis has been carried out for the same system subjected to a periodic axial load. In section 4.4, the mathematical formulation of a rotating sandwich beam has been carried out using FEM. In section 4.5, the numerical results have been discussed for both rotating and non-rotating MRE based sandwich beam.

4.2 Finite Element Formulation of a MRE Embedded Sandwich Beam

Figure 4.1(a) shows the schematic diagram of a sandwich beam with fully MRE core and Fig. 4.1(b) shows that of a MRE embedded viscoelastic cored sandwich beam. Here the viscoelastic patches are of lengths L_1 and L_3 and a MRE patch of length L_2. N and S stands for the north and south pole of the magnets used to apply magnetic field. B_s is the magnetic flux density applied to the sandwich beam. Figure 4.1(c) shows the deformed and undeformed configuration of an element of the sandwich beam.

The following assumptions are considered for modeling the sandwich beam.

1. The top and bottom skins obey Euler-Bernoulli beam theory.
2. The MRE and non-MRE core materials are only subjected to shear deformation.
3. The MRE part of the core is only affected by the magnetic field while the non-MRE parts of the core are not affected by the magnetic field.
4. The zero field Young's modulus and shear modulus are same for both MRE and non-MRE parts in core.
5. Considering anti-plane concept the transverse displacement w is considered to be uniform on a cross section.
6. Perfect bonding between layers of the sandwich beam has been assumed.

As shown in Fig. 4.1(b) and (c) the top, bottom and core layers thickness are h_t, h_b and h_c respectively, and the corresponding longitudinal displacements of the mid-planes in the x-direction are u_t, u_b and u_c. Referring to the Fig. 4.1(c), the strain and displacement relation in the axial and transverse directions can be expressed as

$$\frac{\partial u_j}{\partial x} = \frac{\partial u_{0j}}{\partial x} - z_j \frac{\partial^2 w}{\partial x^2}, \quad j = \text{t, b} \tag{4.1}$$

where u_j is the axial displacement of skin j, which is at a distance z_j from the mid-plane of the skin j in z direction. The shear strain γ_c in the core can be derived from (Mead and Markus, 1969),

$$\gamma_c = \frac{\partial w}{\partial x} + \frac{\partial u_c}{\partial z} \tag{4.2}$$

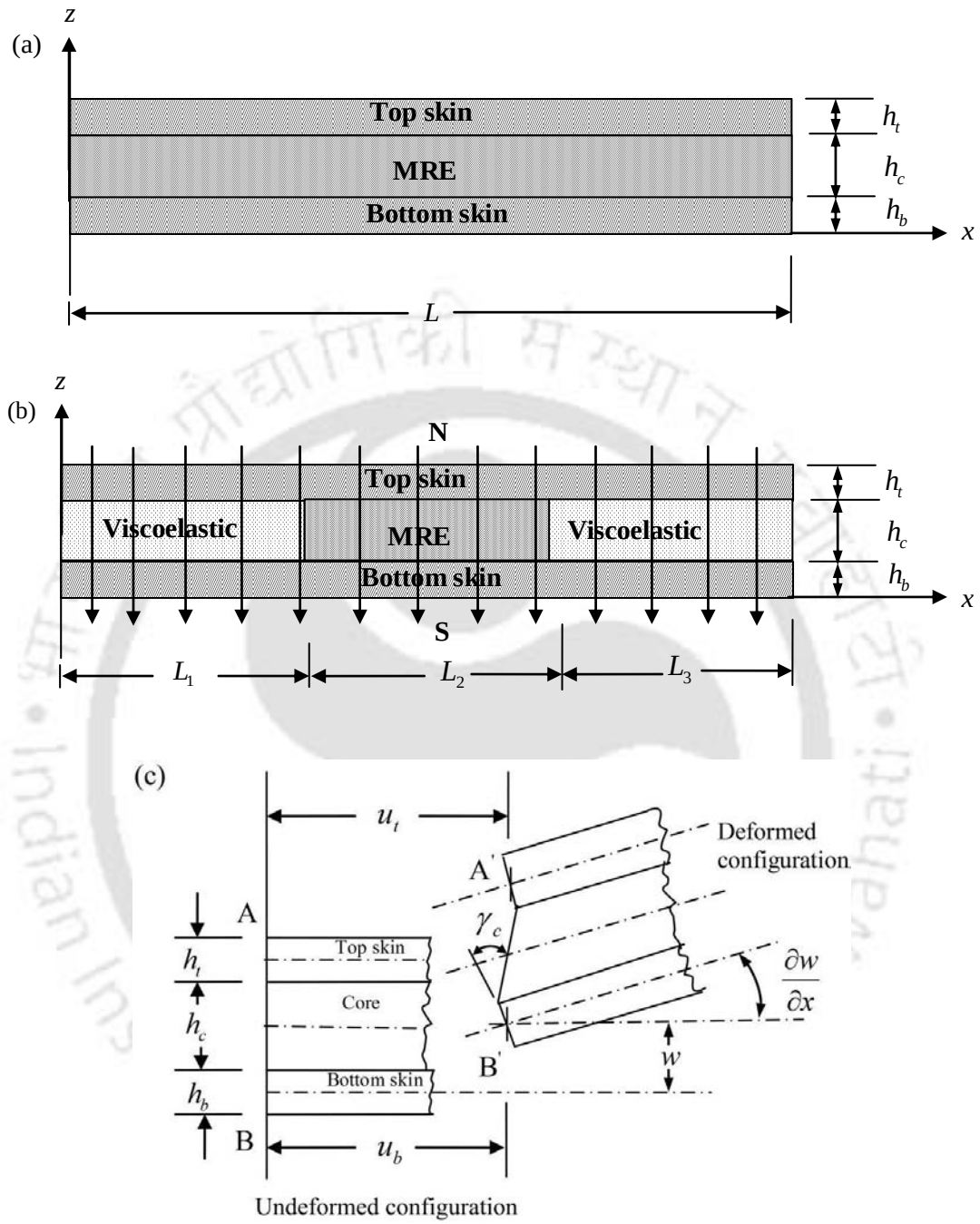

Figure 4.1 (a) Fully MRE cored sandwich beam, (b) MRE embedded viscoelastic cored sandwich beam and (c) Deformed and undeformed configurations of a sandwich beam.

where,

$$\frac{\partial u_c}{\partial z} = \frac{(h_t + h_b)}{2h_c}\frac{\partial w}{\partial x} + \frac{(u_t - u_b)}{h_c}. \tag{4.3}$$

Substituting Eq. (4.3) in Eq. (4.2), the obtained shear strain as a function of the layers thickness is

$$\gamma_c = \frac{H}{h_c}\frac{\partial w}{\partial x} + \frac{\left(u_t - u_b\right)}{h_c} \tag{4.4}$$

where, $H = h_c + \dfrac{\left(h_t + h_b\right)}{2}$.

The strain energy contributions due to bending and extension of top and bottom skins of the sandwich beam, U_{tb} can be expressed as

$$U_{tb} = \frac{1}{2}\int_0^L \left(E_t A_t \left(\frac{\partial u_t}{\partial x}\right)^2 + E_b A_b \left(\frac{\partial u_b}{\partial x}\right)^2 \right) dx + \frac{1}{2}\int_0^L \left(E_t I_t + E_b I_b\right)\left(\frac{\partial^2 w}{\partial x^2}\right)^2 dx \tag{4.5}$$

where, I_t and I_b are the second moment of inertia at the centroid of the top and bottom elastic skins. A_t and A_b are the cross sectional areas of top and bottom skins. It has been assumed that the normal strain of the core is negligible, and the core deforms due to shear only. Then the strain energy U_c is obtained as

$$U_c = \frac{1}{2}\int_0^L G_c^* A_c \gamma_c^2 dx \tag{4.6}$$

where, the complex shear modulus $G_c^* = G_c^{'}\left(1 + i\eta_c\right)$, $G_c^{'}$ is the storage shear modulus, $i = \sqrt{-1}$ and η_c is the core loss factor. Now substituting the shear strain of Eq. (4.4) in Eq. (4.6), the obtained expression as follows

$$U_c = \frac{1}{2}\int_0^L G_c^* A_c \left[\frac{H}{h_c}\frac{\partial w}{\partial x} + \frac{u_t - u_b}{h_c}\right]^2 dx \tag{4.7}$$

Here the expressions for magnetoelastic loads (horizontal force n_j and the distributed moment m_j^m due to magnetic field are same as that discussed in chapter 2. The external energy due to the above mentioned magnetoelastic loads can be given by

$$U_m = \int_0^L \left[n_t u_t + n_b u_b + m_t^m w_{,x} + m_b^m w_{,x} \right] dx \tag{4.8}$$

where, n_t, and n_b are the horizontal forces and m_t^m and m_b^m are the distributed moments in top and bottom skins respectively due to the application of magnetic field.

The total strain energy *U* of the sandwich beam is expressed as the sum of those due to top, bottom and middle layers, such that

$$U = U_{tb} + U_c - U_m \tag{4.9}$$

The total kinetic energy of the sandwich beam can be obtained by adding the kinetic energy due to the transverse displacement of all the layers, axial displacements of top and bottom skins and the rotation due to shear strain of the MRE embedded viscoelastic core.

$$T = \frac{1}{2}\int_0^L \left(m\left(\frac{\partial w}{\partial t}\right)^2 + m_t\left(\frac{\partial u_t}{\partial t}\right)^2 + m_b\left(\frac{\partial u_b}{\partial t}\right)^2 + \rho_c I_c\left(\frac{H}{h_c}\frac{\partial^2 w}{\partial x \partial t} + \frac{\left(\partial u_t/\partial t\right) - \left(\partial u_b/\partial t\right)}{h_c}\right)^2 \right) dx \tag{4.10}$$

where, $m = m_t + m_c + m_b$. m_t, m_c and m_b are the mass per unit length of the top, core and bottom layers respectively. The above equations are also applicable for MRE embedded sandwich beam with either a fully MRE core or multiple MRE patch embedded core.

In modeling of the sandwich beam using FEM, a standard beam element with two end nodes (Fig.4.2) with four degrees of freedom (DOF) for each node is considered. The DOF include the transverse displacement *w*, axial displacement of top skin u_t, axial displacement of bottom skin u_b and the rotational displacement φ of the beam. The elemental displacement vector consists of two nodal displacement vectors as:

$$\left\{q^e\right\} = \left\{q^i \;\; q^j\right\}^{\mathrm{T}} = \left\{w^i, \varphi^i, u_t^i, u_b^i, w^j, \varphi^j, u_t^j, u_b^j\right\}^{\mathrm{T}} \tag{4.11}$$

The elemental displacement "u", can be determined in terms of displacements of two nodes as:

$$u = \begin{Bmatrix} w \\ u_t \\ u_b \end{Bmatrix} = \begin{Bmatrix} [N_w] \\ [N_{ut}] \\ [N_{ub}] \end{Bmatrix} \left\{q^e\right\} \tag{4.12}$$

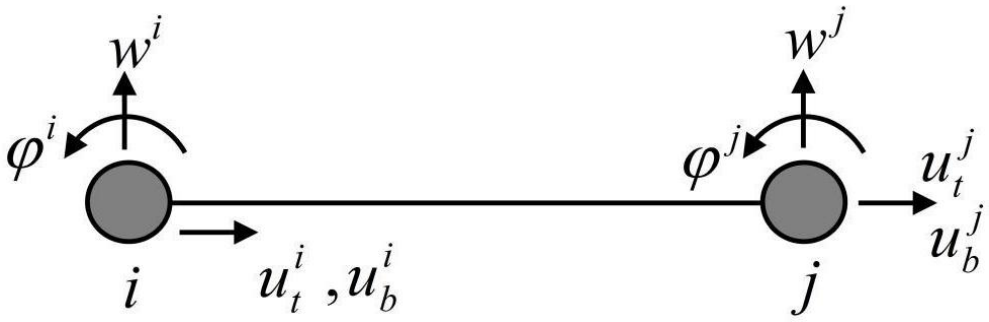

Figure 4.2 Beam element with two end nodes and four DOF for each node.

where, $[N_w]$ and $[N_{uj}]$ (where $j = t, b$) are commonly used linear and cubic polynomial beam shape functions. The shape functions are (Rao, 2005)

$$\left.\begin{aligned}
[N_w] &= \left\{1-\frac{3x^2}{l_e^2}+\frac{2x^3}{l_e^3} \quad x-\frac{3x^2}{l_e}+\frac{x^3}{l_e^2} \quad 0 \quad 0 \quad \frac{3x^2}{l_e^2}+\frac{2x^3}{l_e^3} \quad -\frac{x^2}{l_e}+\frac{x^3}{l_e^2} \quad 0 \quad 0\right\} \\
[N_{ut}] &= \left\{0 \quad 0 \quad 1-\frac{x}{l_e} \quad 0 \quad 0 \quad 0 \quad \frac{x^2}{l_e} \quad 0\right\} \\
[N_{ub}] &= \left\{0 \quad 0 \quad 0 \quad 1-\frac{x}{l_e} \quad 0 \quad 0 \quad 0 \quad \frac{x^2}{l_e}\right\}
\end{aligned}\right\} \tag{4.13}$$

The derived potential energy Eq. (4.9) and kinetic energy Eq. (4.10) terms can be rewritten in nodal displacement variables for one element with length l_e as follows:

$$U^e = \frac{1}{2}\{q^e\}^T [K^e]\{q^e\}$$

$$[K^e] = [K_u^e] + [K_s^e] - [K_m^e]$$

where,

$$[K_u^e] = \int_0^{l_e} E_t A_t \left[\frac{dN_{ut}}{dx}\right]^{\mathrm{T}} \left[\frac{dN_{ut}}{dx}\right] dx + \int_0^{l_e} E_b A_b \left[\frac{dN_{ub}}{dx}\right]^{\mathrm{T}} \left[\frac{dN_{ub}}{dx}\right] dx + \int_0^{l_e} \left(E_t I_t + E_b I_b\right) \left[\frac{d^2 N_w}{dx^2}\right]^{\mathrm{T}} \left[\frac{d^2 N_w}{dx^2}\right] dx$$

$$[K_s^e] = \int_0^{le} G_c^* A_c \left[\frac{H}{h_c}\left[\frac{dN_w}{dx}\right] + \frac{N_{ut} - N_{ub}}{h_c}\right]^{\mathrm{T}} \left[\frac{H}{h_c}\left[\frac{dN_w}{dx}\right] + \frac{N_{ut} - N_{ub}}{h_c}\right] dx$$

$$\left[K_m^e\right]=\left(\frac{B_s^2bh_t}{\mu_{et}}\right)\int_0^{le}\left[\frac{dN_{ut}}{dx}\right]^{\mathrm{T}}\left[\frac{dN_{ut}}{dx}\right]dx+\left(\frac{B_s^2bh_b}{\mu_{eb}}\right)\int_0^{le}\left[\frac{dN_{ub}}{dx}\right]^{\mathrm{T}}\left[\frac{dN_{ub}}{dx}\right]dx+\left(\frac{\pi B_s^2bh_t}{2\mu_0}\right)$$

$$\int_0^{le}\left(\frac{1}{\ln\left(1/\left(l_e-x\right)\right)}\right)\left[\frac{dN_{ut}}{dx}\right]^T\left[\frac{dN_w}{dx}\right]dx+\left(\frac{\pi B_s^2bh_b}{2\mu_0}\right)\int_0^{le}\left(\frac{1}{\ln\left(1/\left(l_e-x\right)\right)}\right)$$

$$\left[\frac{dN_{ub}}{dx}\right]^T\left[\frac{dN_w}{dx}\right]dx-\left(\frac{B_s^2b\left(h_t^2+h_b^2\right)}{2\pi\mu_0}\right)\int_0^{le}\ln\left(\frac{1}{l_e-x}\right)\left[\frac{d^2N_w}{dx^2}\right]^T\left[\frac{dN_w}{dx}\right]dx$$

$$+\left(\frac{B_s^2b\left(h_t+h_b\right)}{\mu_0}\right)\int_0^{le}\left[\frac{dN_w}{dx}\right]^T\left[\frac{dN_w}{dx}\right]dx-\left(\frac{B_s^2b}{12}\left(\frac{h_t^3}{\mu_{et}}+\frac{h_b^3}{\mu_{eb}}\right)\right)\int_0^{le}\left[\frac{d^3N_w}{dx^3}\right]^T\left[\frac{dN_w}{dx}\right]dx$$

The kinetic energy term can be rewritten in nodal displacement variables for one element with length l_e as follows:

$$T^e=\frac{1}{2}\left\{\dot{q}^e\right\}^{\mathrm{T}}\left[M^e\right]\left\{\dot{q}^e\right\} \tag{4.14}$$

where, $\left[M^e\right]=\int_0^{l_e}\left(m\left[N_w\right]^{\mathrm{T}}\left[N_w\right]+m_t\left[N_{ut}\right]^{\mathrm{T}}\left[N_{ut}\right]+m_b\left[N_{ub}\right]^{\mathrm{T}}\left[N_{ub}\right]\right.$

$$\left.+\rho_cI_c\left[\frac{H}{h_c}\left[\frac{dN_w}{dx}\right]+\frac{N_{ut}-N_{ub}}{h_c}\right]^{\mathrm{T}}\left[\frac{H}{h_c}\left[\frac{dN_w}{dx}\right]+\frac{N_{ut}-N_{ub}}{h_c}\right]\right)dx$$

Upon substituting the expressions for kinetic energy T and potential energy U into Lagrange's principle, described as

$$\frac{d}{dt}\left(\frac{\partial L}{\partial\dot{q}_i}\right)-\frac{\partial L}{\partial q_i}=Q_i,\quad i=1,2,3,.....n \tag{4.15}$$

where, Lagrangian, $L=T-U$ and n is the total DOF considered in the formulation and Q_i is the generalized force corresponding to the ith DOF, the governing equations of motion for the partially or fully treated MRE sandwich beam element in the finite element form can be obtained as

$$\left[M^e\right]\left\{\ddot{q}^e\right\}+\left[K^e\right]\left\{q^e\right\}=\left\{F^e\right\}. \tag{4.16}$$

Here, $\left[M^e\right]$and$\left[K^e\right]$are the elemental mass and stiffness matrices, respectively and

F^e is the elemental force vector. Assembling the mass and the stiffness matrices and force vector for all the elements yields the global governing equation of motion of MRE embedded sandwich beam as follows:

$$[M]\{\ddot{q}\}+[K]\{q\}=\{F\} \tag{4.17}$$

where, $[M],[K]$ and F are the global mass and stiffness matrices and global force vector, respectively.

For the MRE embedded sandwich beam, the matrices $[M]$and$[K]$ are formulated by imposing compatibility conditions which are identical transverse displacements $w^1\big|_{x=L_1}=w^2\big|_{x=L_1}$, $w^2\big|_{x=L_1+L_2}=w^3\big|_{x=L_1+L_2}$ and axial displacements $u_j^1\big|_{x=L_1}=u_j^2\big|_{x=L_1}$, $u_j^2\big|_{x=L_1+L_2}=u_j^3\big|_{x=L_1+L_2}$ and the slopes $\varphi^1\big|_{x=L_1}=\varphi^2\big|_{x=L_1}$, $\varphi^2\big|_{x=L_1+L_2}=\varphi^3\big|_{x=L_1+L_2}$ at the interfaces of the viscoelastic material and MRE patches within the core of the sandwich beam (Fig. 4.1(b)). Each MRE patch is modeled independently and then coupled with the adjacent non-MRE patches.

In free vibration studies taking F =0 in Eq. (4.17), the natural frequencies and loss factors are calculated by finding the eigenvalues of $[M]^{-1}[K]$matrix. While the square root of the real part of the eigenvalues gives the modal frequencies of the system, the loss factor is obtained from the ratio of the imaginary part to real part of the eigenvalues.

To study the forced vibration response, a harmonically varying point load of amplitude F_0 and frequency Ω_e is assumed to be applied at the n^{th} node. Assuming the solution $\{q\}=\{q_0\sin\Omega_e t\}$, Eq. (4.17) reduces to the following form.

$$\left([K]-\Omega_e{}^2[M]\right)\{q_0\}=\{0\,0\cdots F_0\sin\Omega_e t\,0\,0\cdots\}^{\mathrm{T}} \tag{4.18}$$

For each frequency of excitation Ω_e, the displacement amplitude q_0 is calculated by solving Eq. (4.18).

4.3 Finite Element Formulation of a MRE Embedded Sandwich Beam Subjected to Periodic Axial Force

Figure 4.3 shows the sandwich beam subjected to a time varying axial force, $P(t) = P_s + P_d \cos(\Omega_2 t)$.

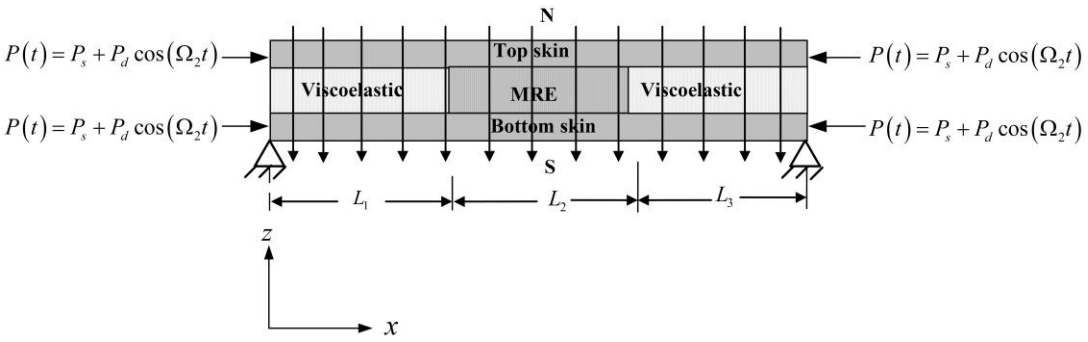

Figure 4.3 MRE embedded viscoelastic cored sandwich beam subjected to time varying axial load.

Here the expressions for kinetic energy potential energy and magnetoelastic loads due to magnetic field are same as that discussed in the previous section.

The non-conservative work done due to periodic axial load is:

$$W = \frac{1}{2}\int_0^L P(t)\left(\frac{\partial w}{\partial x}\right)^2 dx \tag{4.19}$$

This can be rewritten in nodal displacement variables for one element with length l_e as follows:

$$W^e = \frac{1}{2}\{q^e\}^{\mathrm{T}} P(t)\left[F_f^e\right]\{q^e\} \tag{4.20}$$

where, $\left[F_f^e\right] = \int_0^{l_e}\left[\frac{dN_w}{dx}\right]^{\mathrm{T}}\left[\frac{dN_w}{dx}\right]dx$

Upon substituting the expressions for kinetic energy T^e, potential energy U^e and the work done into Hamilton's principle, described as

$$\delta\int_{t_1}^{t_2}\left(T^e - U^e + W^e\right)dt = 0 \tag{4.21}$$

The governing equations of motion for the un-damped partially or fully treated MRE sandwich beam element in the finite element form can be obtained as

$$\left[M^e\right]\{\ddot{q}\}+\left[K^e\right]\{q\}-\left(P_s+P_d\cos\Omega t\right)\left[F_f^e\right]\{q\}=0 \tag{4.22}$$

$\left[M^e\right]$ and $\left[K^e\right]$ are the elemental mass and stiffness matrices. Assembling the all elemental matrices for all the elements, the global governing equation of motion of MRE embedded sandwich beam as follows:

$$[M]\{\ddot{q}\}+[K]\{q\}-\left(P_s+P_d\cos\Omega_2 t\right)\left[F_f\right]\{q\}=0 \tag{4.23}$$

Considering the damping effect of MRE on the sandwich beam the equation of motion can be rewritten as.

$$[M]\{\ddot{q}\}+[K]\{q\}+[C]\{q\}-\left(P_s+P_d\cos\Omega_2 t\right)\left[F_f\right]\{q\}=0 \tag{4.24}$$

where, $[C]=i\eta_c[K_s]$, here η_c is the loss factor of the MRE.

To reduce the size of the matrix the Guyan reduction method is used. In this method, DOF of the FE model are designated as either slaves or masters (Cook *et al.*, 2007). Here the transverse displacement is considered as master DOF and others as slave DOF. The Eq. (4.23) without force term can be partitioned according to master DOF $\{\bar{q}_m\}$ and slave DOF $\{\bar{q}_s\}$ as follows

$$\left(\begin{bmatrix}K_{mm} & K_{ms}\\ K_{ms}^T & K_{ss}\end{bmatrix}-\omega^2\begin{bmatrix}M_{mm} & M_{ms}\\ M_{ms}^T & M_{ss}\end{bmatrix}\right)\begin{Bmatrix}\bar{q}_m\\ \bar{q}_s\end{Bmatrix}=\begin{Bmatrix}0\\ 0\end{Bmatrix} \tag{4.25}$$

Solving the lower partition and substituting into upper partition and following the procedure given in Cook *et al.*, (2007), one can obtain

$$\{q_s\}=-\left[K_{ss}\right]^{-1}\left[K_{ms}\right]^T\{q_m\} \tag{4.26}$$

The entire set of DOF is expressed in terms of masters DOF by the equation,

$$q=\begin{Bmatrix}q_m\\ q_s\end{Bmatrix}=[T]\{q_m\}\ \text{where}\ [T]=\begin{bmatrix}I\\ -K_{ss}^{-1}K_{ms}^T\end{bmatrix} \tag{4.27}$$

The Eq. (4.24) can be written as

$$\left[M_r\right]\{\ddot{q}_m\}+\left[K_r\right]\{q_m\}+\left[C_r\right]\{q_m\}-\left(P_s+P_d\cos\Omega_2 t\right)\left[F_{fr}\right]\{q_m\}=0 \tag{4.28}$$

where,

$$\left[M_r\right]=[T]^T[M][T],\left[K_r\right]=[T]^T[K][T],\left[C_r\right]=[T]^T[C][T]\ \text{and}\left[F_{fr}\right]=[T]^T\left[F_f\right][T]$$

4.3.1 Dynamic Stability Analysis

For the analysis of stability of sandwich beams the method developed by Bolotin, (1964), is applied to obtain the relation for the dynamic instability of the system. Considering the damping effect of MRE on the sandwich beam the equation of motion can be rewritten as.

$$[M_r]\{\ddot{q}_m\}+[K_r]\{q_m\}+[C_r]\{q_m\}-(P_s+P_d\cos\Omega_2 t)[F_{fr}]\{q_m\}=0 \quad (4.29)$$

The static and dynamic loads P_s and P_d can be represented in terms of the static buckling load P_{cr} as, $P(t)=\alpha P_{cr}+\beta P_{cr}\cos\Omega_2 t$, where α and β are the static load factor and dynamic load factor, respectively. Now Eq. (4.34) can be rewritten as,

$$[M_r]\{\ddot{q}_m\}+[K_r]\{q_m\}+[C_r]\{q_m\}-(\alpha P_{cr}+\beta P_{cr}\cos\Omega_2 t)[F_{fr}]\{q_m\}=0 \quad (4.30)$$

The above equation is a Mathieu-Hill equation with a periodic coefficient. The periodic motion of the system is usually the boundary case of vibrations with unboundedly increasing amplitudes. Therefore it is important to study the dynamic instability of the system and determination of the boundaries of the dynamic instability regions. The first-order trivial solution of the Eq. (4.30) with period of 2*T*, where $T=\dfrac{2\pi}{\Omega_2}$ are expressed as,

$$q_m=\{A\}\sin\frac{\Omega_2 t}{2}+\{B\}\cos\frac{\Omega_2 t}{2} \quad (4.31)$$

Here, $\{A\}$ and $\{B\}$ are vectors independent of time, *t*. Substituting the Eq. (4.31) into Eq. (4.30) leads to the eigenvalue equations in matrix form;

$$\begin{vmatrix} [K_r]-(\alpha P_{cr}-\beta P_{cr})[F_{fr}]-\dfrac{\Omega_2^2}{4}[M_r] & -\dfrac{\Omega_2}{2}[C_r] \\ \dfrac{\Omega_2}{2}[C_r] & [K_r]-(\alpha P_{cr}+\beta P_{cr})[F_{fr}]-\dfrac{\Omega_2^2}{4}[M_r] \end{vmatrix}=0 \quad (4.32)$$

This equation is referred as the equation of boundary frequencies. The above equation is used to find the boundaries of parametric instability regions of the system.

4.4 Dynamic Model of a MRE Cored Rotating Sandwich Beam

In this section the dynamic model of a rotating MRE cored sandwich beam has been studied. The geometry of a rotating sandwich beam with MRE core and conductive aluminum skins subjected to magnetic field (B_s) and time varying axial force $\left(P(t) = P_s + P_d \cos(\Omega_2 t)\right)$ is shown in Fig. 4.4(a). The setting angle θ is the angle between the mid-plane of the sandwich beam and the plane of rotation as shown in Fig. 4.4(c) which is similar to that shown in the work of Hoa, (1979). r is the hub radius.

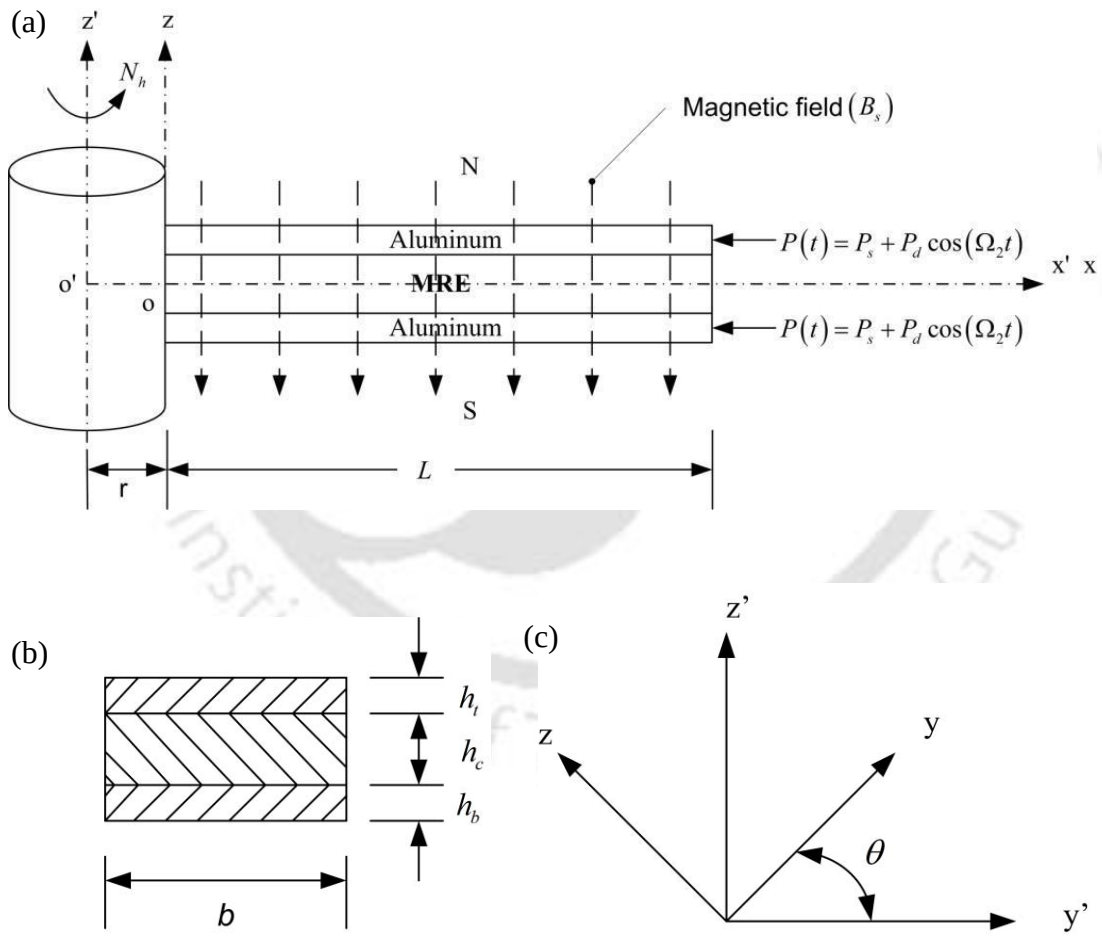

Figure 4.4 (a) Rotating sandwich beam with MRE core subjected to magnetic field and periodic axial load (b) cross section of the sandwich beam (c) setting angle definition.

Here the expressions for kinetic energy, potential energy and work done due to periodic axial load and magnetoelastic loads due to magnetic field are same as that discussed in the previous section 4.2. Work done of a rotating beam due to the centrifugal forces can be expressed as (Lin and Chen, 2003)

$$W_c^e = -\frac{1}{2}\int_0^{l_e} A\sigma_x \left(\frac{\partial w}{\partial x}\right)^2 dx + \frac{1}{2}\int_0^{l_e} \rho A N_h^2 \sin^2\theta w^2 dx \tag{4.33}$$

where, N_h is the rotating speed in rad/sec, A is the cross section area of sandwich beam, ρ is the mass density of the system and σ_x is the radial stress created by centrifugal forces acting on any section at a distance x from the left end of the element:

$$\sigma_x = \rho N_h^2 \left[-rx - nl_e x - \frac{x^2}{2} + rl_e\left(N-n\right) + \frac{1}{2}l_e^2\left(N^2-n^2\right)\right] \tag{4.34}$$

Here, N is the total number of elements of the sandwich beam and n is the number of elements before and not including the element under consideration.

The work done due to periodic axial load $P(t)$ can be written as,

$$W_f^e = \frac{1}{2}\int_0^{l_e} P(t)\left(\frac{\partial w}{\partial x}\right)^2 dx \tag{4.35}$$

Here, $P(t) = \alpha P_{cr} + \beta P_{cr}\cos\Omega_2 t$, where, $P_s = \alpha P_{cr}$ and $P_d = \beta P_{cr}$. α and β are the static and dynamic load factors, respectively. P_{cr} is the critical buckling load.

The work done by the magnetoelastic load and moments, centrifugal forces and periodic axial load can be rewritten as:

$$W^e = \{q\}^{\mathrm{T}}\left[K_m^e\right]\{q\} + \frac{1}{2}\{q\}^{\mathrm{T}}\left[K_c^e\right]\{q\} + \frac{1}{2}\{q\}^{\mathrm{T}} P(t)\left[F_f^e\right]\{q\} \tag{4.36}$$

The expressions for the matrices, $\left[M^e\right]$, $\left[K_u^e\right]$, $\left[K_s^e\right]$, $\left[K_m^e\right]$ and $\left[F_f^e\right]$ are same as that mentioned in section 4.2. The expression for the matrix $\left[K_c^e\right]$ is as follows

$$\left[K_c^e\right] = -\int_0^{l_e} A\sigma_x \left[\frac{dN_w}{dx}\right]^{\mathrm{T}}\left[\frac{dN_w}{dx}\right]dx + \int_0^{l_e} \rho A N_h^2 \sin^2\theta \left[N_w\right]^{\mathrm{T}}\left[N_w\right]dx$$

Upon substituting the expressions for elemental kinetic energy T^e, potential energy U^e and work done due to external forces into Hamilton's principle, described as

$$\delta\int_{t_1}^{t_2}\left(T^e - U^e + W^e\right)dt = 0 \tag{4.37}$$

The governing equations of motion for the MRE based sandwich beam element in the finite element form can be obtained as

$$\left[M^e\right]\left\{\ddot{q}^e\right\} + \left[K^e\right]\left\{q^e\right\} - \beta P_{cr}\cos\Omega_2 t\left[F_f^e\right]\left\{q^e\right\} = 0 \tag{4.38}$$

where, $\left[K^e\right] = \left[K_u^e\right] + \left[K_s^e\right] + \left[K_m^e\right] - \left[K_c^e\right] - \alpha P_{cr}\left[F_f^e\right]$

Assembling the all elemental matrices for all the elements, the global governing equation of motion of MRE embedded sandwich beam as follows:

$$[M]\{\ddot{q}\} + [K]\{q\} - \beta P_d\cos\Omega_2 t\left[F_f\right]\{q\} = 0 \tag{4.39}$$

Since MRE is a viscoelastic material it provides damping effects on the sandwich beam. The equation of motion can be rewritten as.

$$[M]\{\ddot{q}\} + [K]\{q\} + [C]\{q\} - \beta P_d\cos\Omega_2 t\left[F_f\right]\{q\} = 0 \tag{4.40}$$

where, $[C] = i\eta_c[K_s]$ is the damping effect on the sandwich beam and η_c is the loss factor of the MRE.

To reduce the size of the matrix the Guyan reduction method as discussed in the section 4.3 is used and the Eq. (4.39) and Eq. (4.40) can be written as

$$\left[M_r\right]\{\ddot{q}_m\} + \left[K_r\right]\{q_m\} - \beta P_{cr}\cos\Omega_2 t\left[F_{fr}\right]\{q_m\} = 0 \tag{4.41}$$

$$\left[M_r\right]\{\ddot{q}_m\} + \left[K_r\right]\{q_m\} + \left[C_r\right]\{q_m\} - \beta P_d\cos\Omega_2 t\left[F_{fr}\right]\{q_m\} = 0 \tag{4.42}$$

where,

$$\left[M_r\right] = [T]^T[M][T], \left[K_r\right] = [T]^T[K][T], \left[C_r\right] = [T]^T[C][T] \text{ and } \left[F_{fr}\right] = [T]^T\left[F_f\right][T]$$

The above equations (4.41) and (4.42) are the Mathieu-Hill equation with a periodic coefficient for a system without and with damping effect of MRE. The modal frequencies of the system are obtained by finding the real part of the square root of eigenvalues of the $\left[M\right]^{-1}\left[K\right]$. The loss factor of the system is determined by finding

the ratio of the imaginary and real part of the complex modal frequency of the system.

4.4.1 Dynamic Stability Analysis

Following the same procedure discussed in the subsection 4.3.1, the expressions for finding the stability boundaries are as follows:

4.4.1.1 Without Damping Effect of MRE

The eigenvalue equations without damping effect of MRE to obtain the instability regions;

$$\left| [K_r] \pm \beta P_{cr} [K_{fr}] - \frac{\Omega_2^2}{4} [M_r] \right| = 0 \tag{4.43}$$

4.4.1.2 With Damping Effect of MRE

The eigenvalue equations in matrix form with damping effect of MRE;

$$\begin{vmatrix} [K_r] + \beta P_{cr} [K_{fr}] - \frac{\Omega_2^2}{4} [M_r] & -\frac{\Omega_2}{2} [C_r] \\ \frac{\Omega_2}{2} [C_r] & [K_r] - \beta P_{cr} [K_{fr}] - \frac{\Omega_2^2}{4} [M_r] \end{vmatrix} = 0 \tag{4.44}$$

Hereafter, the equations (4.43) and (4.44) are referred as the equation of boundary frequencies. The above equations are used to find the boundaries of principal instability regions of a MRE cored sandwich beam with and without damping effect of MRE.

4.5 Results and Discussions

4.5.1 Dynamic Properties of Sandwich Beam

Using FE formulation a code has been developed using MATLAB to determine the free vibration characteristics such as natural frequencies and loss factors and the forced vibration responses of the sandwich beam. Initially the results from finite element formulation are validated by comparing the results with those obtained by conducting experiments on sandwich beams with viscoelastic core. For MRE embedded sandwich beam the results obtained from FE analysis are compared with

the results obtained from the analytical formulation discussed in chapter 2. Then parametric studies have been carried out to investigate the dynamical properties of the system in terms of natural frequencies and loss factors for a wide range of system parameters. The influences of magnetoelastic loads due to conductive skins, and number, length and locations of MRE patches on the transverse vibration response are also investigated.

4.5.1.1 Validation of the Developed Finite Element Formulation

Case 1. Figure 4.5 shows the experimental set up used to find the natural frequencies of a clamped-free viscoelastic cored sandwich beam. Brüel and Kjaer made PULSE analyzer software (type 3560 D, version 13.1.0) has been used for finding the natural frequencies. Here two sandwich beam samples with span, $L = 500\,\text{mm}$; width, $b = 30\,\text{mm}$ and the top and bottom skins thickness, $h_t = h_b = 2\,\text{mm}$, core thicknesses $h_c = 6\,\text{mm}$ and $h_c = 18$ mm have been taken for experimental validation. The beam samples are fabricated from commercial grade aluminum sheets as skins and commercial grade rubber sheets as core. The accelerometers are set one below another at fixed positions on the top and bottom skins of the test specimen. The impact hammer is used to apply impulse force to obtain a wide range of frequency. Before using the impact hammer the driving and measurement points are carefully located to identify three modes of vibration of the beam within the desired frequency range (Banerjee *et al.*, 2007). Using the impact hammer the sandwich beam is excited at specified driving points. The accelerometers (type 4396, sensitivity-9.88 and 9.9mv/ms^{-2}) attached to the sandwich beam recorded the response signals. Further these signals are processed by the signal analyzer. Using the PULSE analyzer software the frequency response functions are plotted against frequency from which the natural frequencies are identified. The first three natural frequencies obtained by the experiments are presented in Table 4.1.

Also the natural frequencies are obtained using the developed finite element code. To know the Young's modulus of the aluminium and rubber, the tensile test has been conducted on the INSTRON-8801, an universal testing machine (100 kN capacity). The Young's modulus of aluminum is found to be 69.53 GPa (chapter 2).

The density of the aluminium is 2618.025 kg/m^3. The shear modulus of rubber is found to be 1.886 MPa. The density of the rubber is 1800 kg/m^3.

Figure 4.5 Experimental Set-up.

Table 4.1 presents the comparison of the natural frequencies obtained from the FE formulation and those obtained from experimental measurements. Here the maximum difference is found to be 9.8 % in second mode for the beam with core thickness of 18 mm. It is observed that while in first mode the natural frequency obtained by FEM has a higher value in comparison to that of the experimental one, in other two modes the experimental natural frequencies have higher values than the FEM result. It has been observed that with increase in core thickness the natural frequency increases.

Table 4.1 Comparison of natural frequencies of a fully viscoelastic cored clamped free sandwich beam derived from the FEM with the frequencies measured by experiment.

Core thickness (mm)	Mode	Natural frequencies (Hz)		% of difference
		Experimental	FEM	
6	1	18.00	19.19	6.2
	2	83.50	77.36	7.3
	3	166.00	161.79	2.5
18	1	25.50	26.12	2.4
	2	97.00	87.43	9.8
	3	173.00	167.22	3.3

Case 2. In this case a symmetric sandwich beam is considered taking the material and geometric properties as in the work of Howson and Zare, (2005). The natural frequencies obtained from the present finite element analysis are compared with those obtained by Howson and Zare, (2005) for three different end conditions as given in Table 4.2 which are found to be in good agreement with the results of Howson and Zare (2005).

Table 4.3 shows a comparison of natural frequencies obtained from the present finite element model and the results of Banerjee *et al.*, (2007). The geometric and material properties are same as that given in Banerjee *et al.*, (2007). The differences in the natural frequencies are found to be small. This is due to the modeling of top and bottom skins. In the present model the effect of both shear and rotary inertia of the skins are not considered which have been considered by Banerjee *et al.*, (2007).

Table 4.2 Comparison of the modal frequencies (Hz) obtained by present model and Howson and Zare, (2005) for three different end conditions of sandwich beam.

End conditions		Modal frequencies (Hz)				
		Mode 1	Mode 2	Mode 3	Mode 4	Mode 5
Simply supported	Present Analysis	57.146	223.919	465.932	772.133	1111.10
	Howson and Zare, (2005)	57.136	219.585	465.172	768.177	1106.68
Cantilever	Present Analysis	33.754	199.126	513.174	909.954	1355.30
	Howson and Zare, (2005)	33.754	198.992	512.307	907.299	1349.65
Clamped-Clamped	Present Analysis	34.669	93.522	178.472	285.810	412.095
	Howson and Zare, (2005)	34.597	93.100	177.155	282.784	406.325

Table 4.3 Comparison of the modal frequencies (Hz) obtained by present model and Banarjee *et al.*, (2007) of a cantilevered sandwich beam.

Mode	Modal frequencies (Hz)	
	Present Analysis	Banerjee *et al.*, (2007), Example 1
1	291.15	291.50
2	1692.1	1684.48
3	4675.2	4623.98
4	9125.5	8945.18

Case 3. In the third example MRE embedded sandwich beam as shown in Fig. 4.1(b) is considered with both clamped-free and simply supported end conditions. Here the MRE patch which is one third of the span of the beam is placed at the middle of the core. The physical parameters and material properties are as follows. The span of the beam, $L = 416$ mm; width, 30 mm; the top and bottom skins thickness, $h_t = h_b = 1$ mm, the core thickness, $h_c = 3$ mm. The top and bottom aluminum skins have Young's modulus 72 GPa and density 2700 kg/m^3. The permeability of air gap, $\mu_0 = 4\pi \times 10^{-7}$ and for aluminum skin the permeability, $\mu_e = 1.2566650 \times 10^{-6}$. The zero fields shear modulus and Young's modulus of both MRE and non-MRE parts are same. The properties of the MRE (contains 80% iron particles) used for the analysis (Chen *et al*., 2007).

In this case the obtained natural frequencies by FEM are given in Table 4.4 which are compared with the results obtained from the analytical model developed in chapter 2 for the first three modes under different magnetic field strength. The results obtained in both these methods are found to be in close agreement. It is observed that while maximum percentage difference (8.16%) occurs for the simply supported boundary condition, for the clamped free boundary condition the difference is very small. In both these end conditions with increase in magnetic field strength the natural frequency increases.

Case 4. In this example, a simply supported fully MRE cored sandwich beam used in the theoretical and experimental work of Sun *et al.*, (2003) has been compared with the results obtained from the finite element analysis (Table 4.5). Results have also been compared with the analytical work presented in chapter 2. The dimensions and material properties considered are length, $L = 400$ mm, skins thickness $h_t = h_b = 1$ mm, core thickness, $h_c = 1$ mm, width, $b = 25$ mm and Young's modulus of top and bottom skins $E_t = E_b = 70$ GPa, density of skin materials $\rho_t = \rho_b = 2700$ kg/m^3, Storage modulus of MRE core $G_c^{'} = 0.621$ MPa (at 0 Oe) and $G_c^{'} = 1.167$ MPa (at 900 Oe), and density of core $\rho_c = 3.5$ kg/m^3. It is observed that the theoretical results of Sun *et al.*, (2003) are not in good agreement

with their experimental results but the present results obtained using FEM are in very good agreement with the experimental results of Sun *et al.*, (2003) and the analytical work discussed in Chapter 2.

Table 4.4 Comparison of natural frequencies of MRE embedded simply supported and clamped free sandwich beams obtained from present FE formulation and the analytical method presented in chapter 2.

End conditions	Magnetic field density, B_s (T)	Mode	Natural frequencies (Hz)		% of difference
			Finite element formulation	Analytical method (chapter 2)	
Simply supported	0	1	36.36	33.97	6.57
		2	77.56	77.35	0.27
		3	130.20	130.30	0.07
	0.2	1	37.06	34.40	7.17
		2	85.87	88.29	2.74
		3	140.73	141.26	0.37
	0.4	1	38.51	35.54	7.91
		2	89.18	92.87	3.97
		3	145.16	145.46	0.20
	0.6	1	39.96	36.86	8.16
		2	90.50	93.97	3.69
		3	146.98	146.43	0.37
Clamped free	0	1	14.42	14.44	0.29
		2	51.83	51.03	0.49
		3	105.01	106.09	1.23
	0.2	1	15.36	15.34	0.45
		2	53.43	53.83	0.81
		3	116.79	118.25	1.35
	0.4	1	16.81	16.59	0.60
		2	54.34	54.52	1.26
		3	121.42	122.80	1.72
	0.6	1	16.91	16.65	0.65
		2	55.17	54.68	1.46
		3	123.17	123.84	1.92

Case 5. In this example the natural frequencies obtained from the present analysis are compared with the experimental results of Choi, (2009) for a fully MRE cored simply supported sandwich beam subjected to magnetic field of 0.3T. The

material and geometric properties taken are same as those of Choi, (2009) and are as follows. The density and Young's modulus of aluminum are 2500 kg/m^3 and 60 GPa respectively. The density of MRE is 3100 kg/m^3. The storage shear modulus and loss factor for 0.3 T magnetic field are 4.7 MPa and 0.17 respectively. The obtained modal frequencies are presented in the Table 4.6. These results are found to be in good agreement with the experimental work of Choi, (2009). These four examples where the results obtained from FE analysis have been compared with the experimental and other theoretical work validate the FE formulation carried out in this work.

Table 4.5 Comparison of fundamental frequencies with experimentally obtained fundamental frequencies of Sun *et al.*, (2003) and analytical method (chapter 2).

Magnetic Field (Oe)	Fundamental frequency (Hz)			
	Present Analysis	Sun *et al.*, (2003) Theoretical	Sun *et al.*, (2003) Experimental	Analytical method (Chapter 2)
0	34.347	22.23	31.373	34.016
900	41.278	23.24	41.176	40.499

Table 4.6 Comparison of modal frequencies of a fully MRE cored simply supported sandwich beam with those of Choi, (2009).

Magnetic field density, B_s (T)	Mode	fundamental frequency (Hz)	
		Present work	Choi, (2009), Fig. 6.7(a)
0.3	1	84.47	73.09
	2	169.53	175.17

In the next sections parametric studies have been carried out considering the same physical parameters and material properties of the sandwich beam discussed in case 3 of this section.

4.5.1.2 Effect of Magnetoelastic Loads due to Conductive Skins

From literature it is observed that the Lorenz body force caused by the vibration of the beam, subjected to magnetic field will induce tensile deformation and the surface

stress caused by the Maxwell's stress jumps will generate flexural moment distribution on the beam with conductive skins (Zhou and Wang, 2006b). Here to study the effect of magnetoelastic loads due to conductive skins, a fully MRE cored clamped-free sandwich beam with conductive aluminum skins subjected to magnetic field of 0.6T has been considered. Also assuming the skin material to be nonconductive but having other properties same as that of the system of the conductive skins, the natural frequencies for this case has been determined and plotted in Fig. 4.4.

The span of the MRE embedded sandwich beam is divided into 32 elements for FE formulation. Figure 4.6 shows the variations in modal frequencies of the sandwich beam subjected to zero magnetic field and magnetic field of 0.6T without magnetoelastic load and magnetic field of 0.6T with magnetoelastic load on the skins. It has been observed that the modal frequencies of the beam are influenced by the conductive and nonconductive skins under the application of magnetic field. It may be noted that in case of nonconductive skins as no magnetoelastic loads act on the skins the increase in modal frequencies are mainly due to the change in shear modulus of MRE part which actively increases the stiffness of the system.

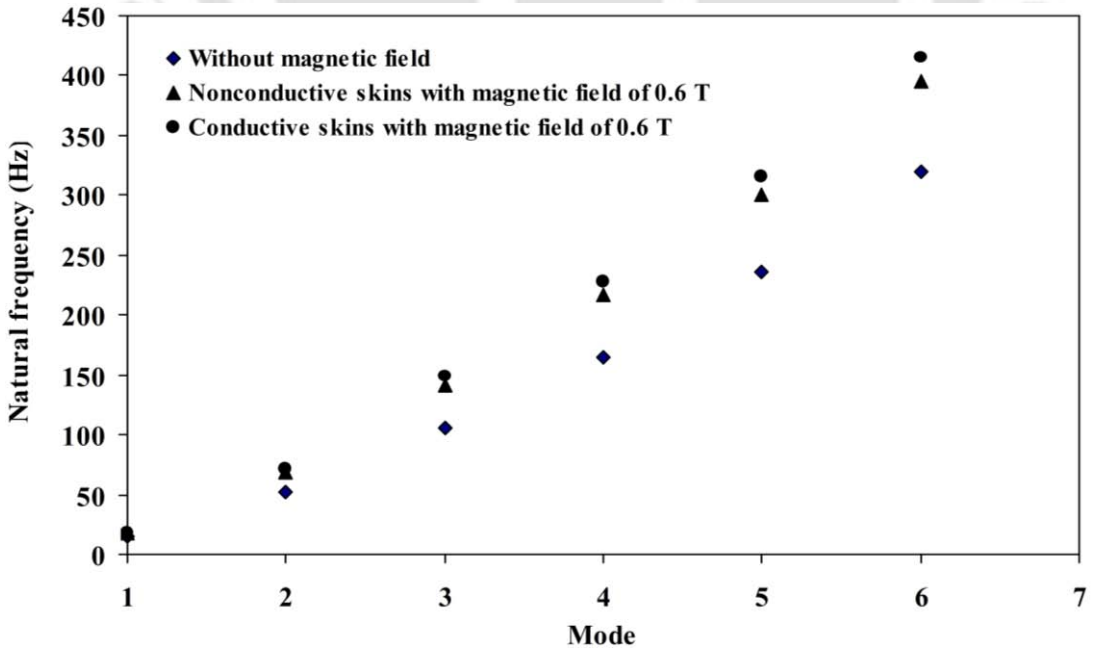

Figure 4.6 Influence of magnetoelastic loads on the modal frequencies.

4.5.1.3 Effect of Magnetic Field Strength and Beam Configurations on Natural Frequencies

To study the effect of magnetic field and beam configurations on natural frequencies, in addition to the full MRE cored sandwich beam, three more configurations of MRE embedded sandwich beam as shown in Fig. 4.7 have been considered with simply supported (SS) and clamped free (CF) boundary conditions. The hatched portion in Fig. 4.7 represents the MRE patch in the core and the remaining parts of the core are of viscoelastic material. In these three configurations though the total MRE patch length is same the individual patch lengths and their locations are different in each configuration. The span of the MRE embedded sandwich beam is divided into 32 parts of equal length.

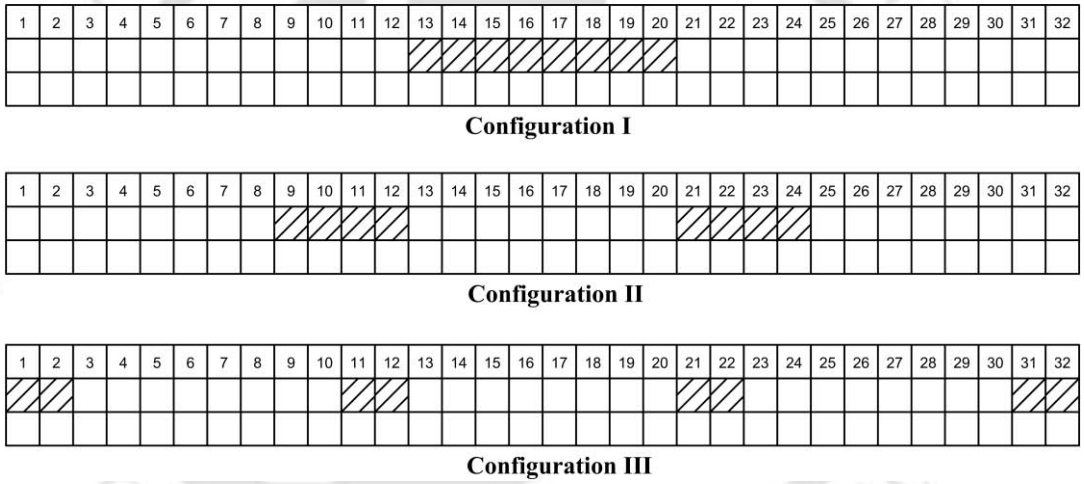

Figure 4.7 Three different configurations of MRE embedded viscoelastic cored sandwich beam.

Effect of Beam Configurations on Natural Frequencies

Table 4.7 presents the variation of natural frequencies for fully MRE cored sandwich beam along with the above mentioned three configurations with a magnetic field of 0.6T for SS and CF end conditions. It is observed that the natural frequencies of the partially MRE cored sandwich beam are less than those of the fully MRE embedded cored sandwich beam. This is due to the fact that the stiffness of the sandwich beam increases with increase in length of the MRE patch. One may also note that depending on the mode of vibration, the natural frequency of a

particular configuration differs from the other configurations. Also depending on boundary conditions the natural frequencies are different for different configurations. Comparing the frequencies of both the boundary conditions the natural frequencies of cantilever beam is less than that of the simply supported beam. It can be related to the relative changes in the stiffness of the beam. In other words, even though the mass of the beam is same in all the configurations, the increase in stiffness would be relatively larger in case of simply supported boundary condition. For simply supported sandwich beam with configuration III the natural frequency is found to be more than the other two configurations, I and II as the beam has more stiffness at the two ends due to presence of MRE patches at these two ends.

Table 4.7 Influence of boundary conditions on the natural frequencies of the fully MRE core and different configurations of MRE embedded sandwich beams at a magnetic field of 0.6T

End conditions	Configuration	Mode					
		1	2	3	4	5	6
Simply Supported	Full MRE core	55.84	115.50	187.73	267.93	358.39	460.35
	I	38.50	88.96	140.08	213.32	296.90	383.08
	II	40.45	81.14	154.30	214.38	286.02	393.06
	III	42.67	89.93	158.95	216.09	298.68	401.95
Clamped free	Full MRE core	17.81	71.15	148.23	227.68	316.10	413.65
	I	15.90	54.26	121.18	180.73	252.44	347.78
	II	16.01	57.51	110.81	188.22	262.22	338.87
	III	15.71	56.27	112.41	187.10	258.38	341.89

Effect of Magnetic Field on Natural Frequencies

The effect of magnetic field strength on the first six modal frequencies for the different configurations of MRE embedded sandwich beam for a simply supported end condition is given in Table 4.8.

It is observed that in all the modes in all configurations the natural frequencies increase with increase in magnetic field. For a particular magnetic field except in the second and fifth modes in all other modes while the third configuration has highest,

the first configuration has the lowest natural frequency. As the effect of magnetoelastic loads on the skins in all configurations are same, this change in natural frequencies can be attributed to the local stiffening of the MRE core with application of magnetic field.

Table 4.8 Variations of natural frequencies with magnetic field for simply supported sandwich beam.

B_s (T)	Configuration	Mode					
		1	2	3	4	5	6
0.2	I	36.72	84.81	135.91	205.59	286.66	374.42
	II	38.12	79.19	145.01	206.39	279.28	380.81
	III	40.24	85.24	147.71	206.68	287.34	385.92
0.4	I	37.08	87.72	138.62	211.07	294.05	380.42
	II	39.93	80.25	151.90	213.25	283.79	389.73
	III	41.96	88.57	156.18	213.47	295.59	397.85
0.6	I	38.50	88.96	140.08	213.32	296.90	383.08
	II	40.45	81.14	154.30	214.38	286.02	393.06
	III	42.67	89.93	158.95	216.09	298.68	401.95

For example, in the second mode of first configuration a node is formed at the middle of the sandwich beam and thus the system will behave as two simply supported and clamped beam of span $L/2$. In second configuration as MRE patch is not at the middle, the beam can be modelled as two SS beam with a span of $L/2$. Similarly in the third configuration as the MRE patches are placed at both the ends the system will behave as two clamped SS beams. This explains the reason for having lowest natural frequency in the second configuration in the second mode. Similar analogy may be used for explaining for the fifth mode.

4.5.1.4 Influence of Location of MRE Patch

In this section the influence of location of the MRE patch is investigated by considering four different locations (LI, LII, LIII and LIV) as shown in Fig.4.8. Here, to model the case of clamped free end conditions the left end of the beam is fixed and the right end is made free for numerical analysis. Also these results are compared with those obtained for the configuration I (CI) as discussed in section 4.5.1.3. The obtained natural frequencies and loss factors corresponding to first six

modes of all these cases are presented in Tables 4.9 and 4.10 under a magnetic field strength of 0.6T. One may observe from these tables that in case of simply supported boundary condition due to symmetry the natural frequencies and loss factors for location LI and LIV and also for LII and LIII are same. But in case of clamped free end condition (which is not symmetric in nature) the natural frequencies and loss factors are different.

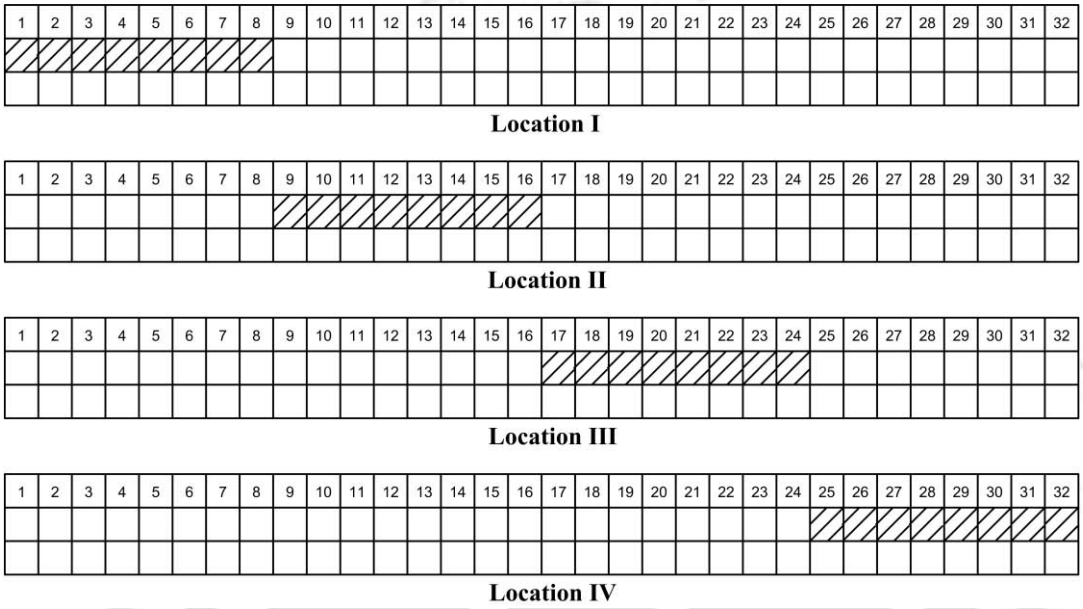

Figure 4.8 Different locations of MRE patches in the core.

Table 4.9 Influence of location of MRE patch on the natural frequencies of different configurations of MRE embedded sandwich beam at a magnetic field of 0.6T.

End conditions	Mode	Natural frequencies (Hz)				
		CI	LI	LII	LIII	LIV
Simply Supported	1	38.50	43.14	38.42	38.42	43.14
	2	88.96	90.15	84.63	84.63	90.15
	3	140.08	143.52	146.69	146.69	143.52
	4	213.32	211.66	211.80	211.80	211.66
	5	296.90	296.08	291.52	291.52	296.08
	6	383.08	390.59	387.98	387.98	390.59
Clamped free	1	15.90	15.96	16.19	15.59	15.13
	2	54.26	61.07	55.28	56.15	55.44
	3	121.18	115.44	118.92	112.66	115.14
	4	180.73	175.39	179.74	185.36	177.32
	5	252.44	250.53	257.65	258.60	253.18
	6	347.78	340.85	342.78	344.47	346.29

Also it may be observed that in case of locations LI and LIV (in which the MRE patches are placed at the boundary edges of the simply supported case) the natural frequencies and loss factors are higher compare to other locations. But such variations are not observed in case of clamped-free end conditions. The results show that the natural frequencies and loss factors are affected by the location of the MRE patch.

Table 4.10 Influence of location of MRE patch on the loss factors of different configurations of MRE embedded sandwich beam at a magnetic field of 0.6T.

End conditions	Mode	Loss factors				
		I	LI	LII	LIII	LIV
Simply Supported	1	0.18991	0.19562	0.19095	0.19095	0.19562
	2	0.16809	0.19179	0.16668	0.16668	0.19179
	3	0.15356	0.16686	0.16020	0.16020	0.16686
	4	0.14084	0.13874	0.13715	0.13715	0.13874
	5	0.12258	0.12163	0.11822	0.11822	0.12163
	6	0.09704	0.10717	0.10130	0.10130	0.10717
Clamped free	1	0.08486	0.08946	0.08174	0.08868	0.09325
	2	0.12929	0.15825	0.13652	0.12393	0.12674
	3	0.15604	0.16554	0.15711	0.14702	0.14085
	4	0.14683	0.14554	0.14307	0.15086	0.12949
	5	0.12550	0.12458	0.12904	0.13086	0.11367
	6	0.11428	0.10917	0.11030	0.11571	0.10149

4.5.1.5 Forced Vibration Response of the MRE Embedded Viscoelastic Cored Sandwich Beam

In this section the frequency response of simply supported sandwich beams are determined to study the effect of magnetoelastic loads on skins, length and location of MRE patch and magnetic field strength on the vibration response of the system. An external harmonic force $F_0 \sin \Omega_e t$ with amplitude of F_0=1N is applied at the centre of the beam and the transverse vibration response at this point is determined for a wide range of frequency Ω_e. The frequency response curves are obtained by solving the Eq. (4.18) which are shown in Figs. 4.9-4.11.

Figure 4.9 shows the transverse vibration response of the simply supported MRE embedded sandwich beam shown in Fig. 4.1(a) for three cases. In the first case (case

I) no magnetic field is applied and in the second case (case II) a magnetic field of 0.6T is applied to the system considering nonconductive skins of the sandwich beam. In the third case (case III) the skin is considered to be conductive but having all other properties same as that in case II. It has been observed that in case I (Fig. 4.9) the response amplitude is maximum and in case II it decreases by application of magnetic field as the shear modulus of the MRE core increases which in turn increases the stiffness of the beam.

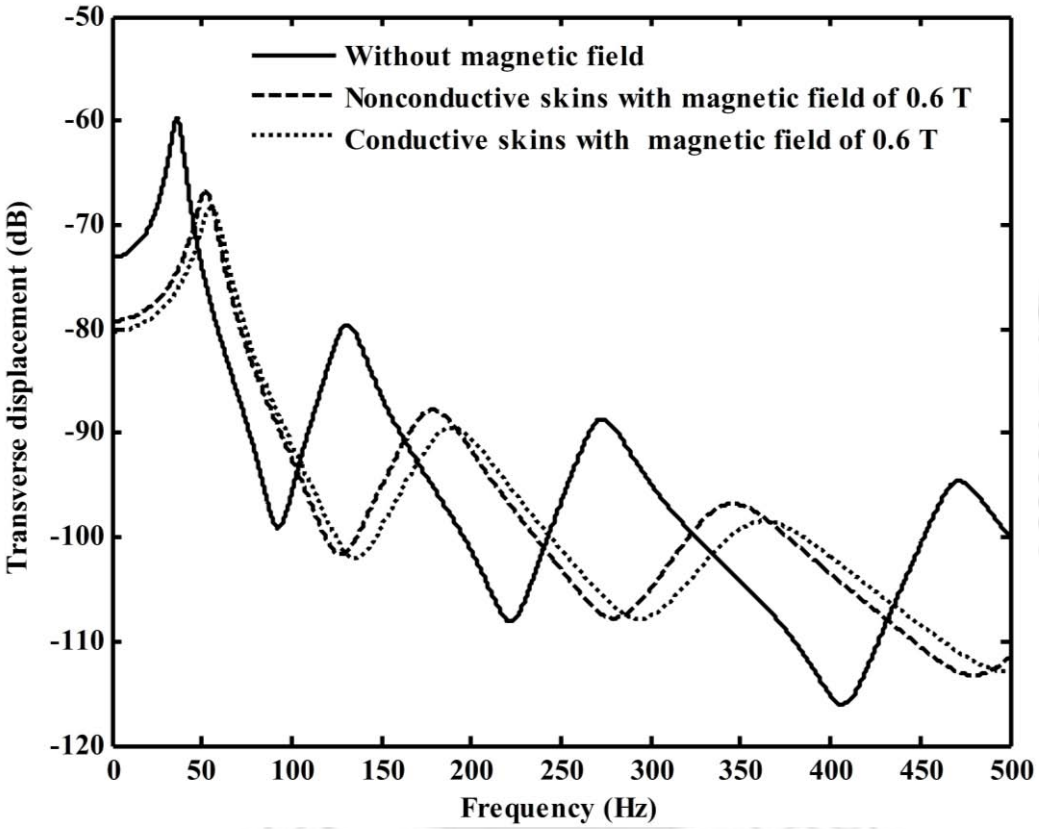

Figure 4.9 Transverse vibration response of a fully MRE cored simply supported sandwich beam with the consideration of magnetoelastic loads on skins.

In case III the response amplitude further decreases as the dynamic flexural rigidity of the beam increases due to the magnetoelastic loads induced in the skins along with the increase of shear modulus of the MRE core. It may be noted that the peaks in the frequency response curve corresponds to the resonance conditions near the modal frequencies. As discussed in previous section due to increase in the

stiffness, the modal frequencies increases with increase in magnetic field and has a higher value for a conductive skins than that for a nonconductive skins.

Figure 4.10 shows the influence of magnetic field on the transverse vibration response of a simply supported MRE embedded sandwich beam with configuration III (Fig. 4.7) subjected to a harmonic force $F_0 \sin \Omega_e t$ with amplitude of 1N acting at the centre of the beam.

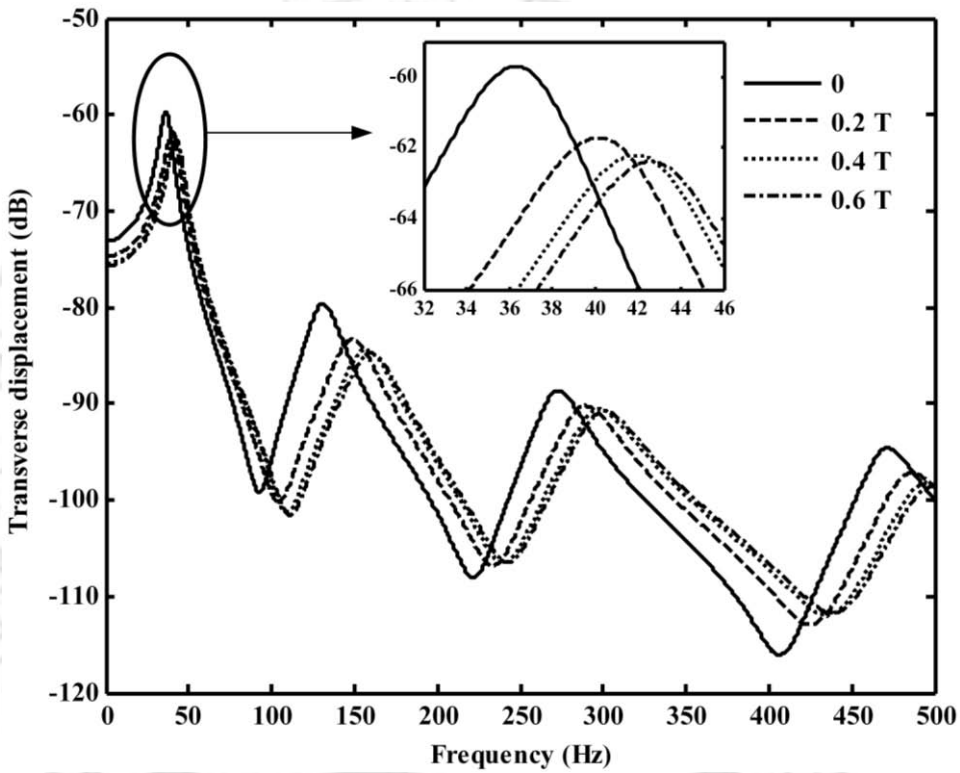

Figure 4.10 Transverse vibration response of configuration III of a simply supported MRE embedded viscoelastic cored sandwich beam subjected to various magnetic fields.

It is observed that (Fig. 4.10) the peak amplitudes decrease with the increase in the magnetic field. This is due to the combined effect of magnetoelastic load on skins and the increase in shear modulus of the MRE patch with the application of magnetic field. Hence one may actively reduce the vibration by suitably applying magnetic field.

Figure 4.11 shows the transverse vibration response of simply supported MRE embedded sandwich beams with different configurations subjected to magnetic field of 0.6T and a harmonic force of 1N amplitude at the centre of the beam. From this

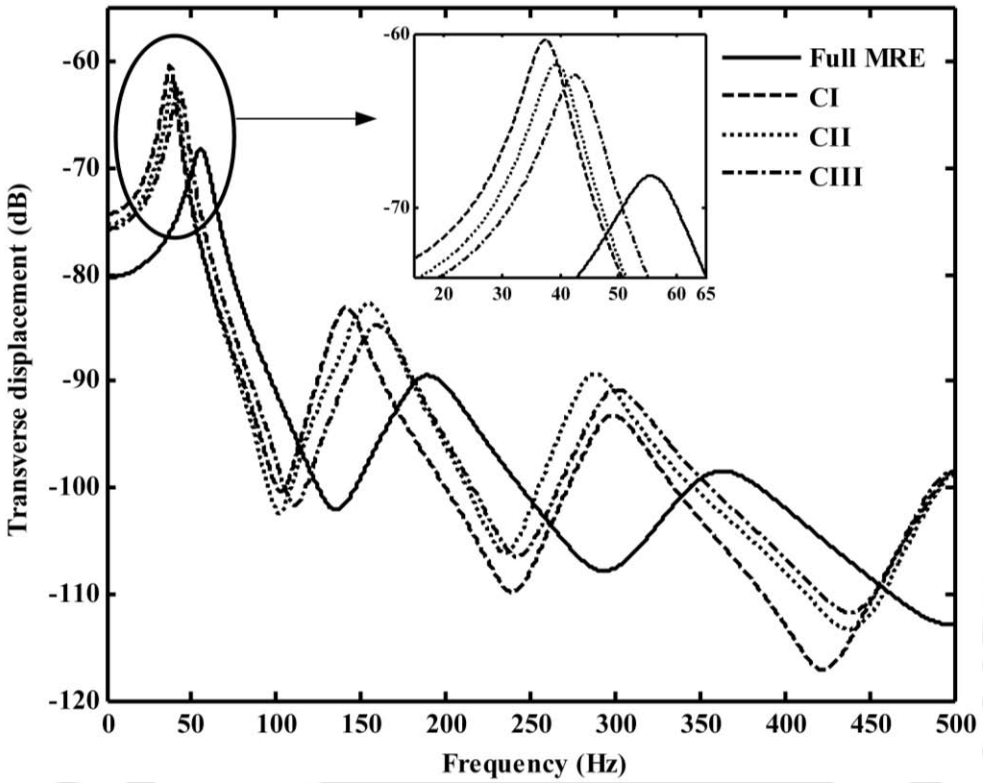

Figure 4.11 Transverse vibration response of fully MRE core and MRE embedded cored sandwich beam at a magnetic field of 0.6 T for simply supported boundary conditions.

figure it is observed that in the first mode the largest peak occurs in the configuration I and lowest peak occurs for the sandwich beam with fully MRE core. This is due to the fact that the configuration I has the lowest loss factor and the sandwich beam with fully MRE core has the highest loss factor for the fundamental mode. But one may observe that the same configuration does not have highest or lowest peak at other modal frequencies. For example, in case of second and third modes the largest peak occurs for the configuration II due to the change of dynamic properties of the MRE embedded sandwich beam. In configuration I as the MRE patch is at the middle (i.e., at the nodal position) the response amplitude in second mode of vibration is less than that of the configuration II. Also in case of third mode as this patch is in between two nodal positions the response amplitude is found to be less than that of configuration II and III. In configuration III as the MRE patches are placed at the ends and with the application of magnetic field the ends get stiffened and the beam behaves as a clamped-clamped beam. Therefore, the response

amplitude is found to be less than that of configuration II and I in case of second mode. Thus, the vibration can be suppressed actively by changing the magnetic field or passively by suitably applying the MRE patch at different locations depending on the frequency range in which the system is operating.

4.5.2 Dynamic Stability of the Various Configurations of Sandwich Beam

Using the expressions of the developed finite element model a MATLAB code has been developed to obtain the natural frequency, loss factor, parametric instability and dynamic response of a simply supported MRE embedded sandwich beams for different configurations. Upon performing the convergence study, it has been decided to use 32 elements in FE analysis.

In the present numerical analysis a symmetric sandwich beam with MRE embedded core has been considered for simply supported end conditions. The geometric and material properties of the sandwich beam are same as that discussed in subsection 4.5.1.1, case 3. Following expressions for the shear storage modulus and loss factor of natural rubber based MRE (containing 80% of iron particles) have been used which are obtained by curve fitting (Appendix A) the experimentally obtained data of Chen *et al*., (2007) up to the saturated magnetic field strength of 0.6 T.

$$G_c^{'} = \left(-6.9395B_s^6 - 9.1077B_s^5 + 71.797B_s^4 - 93.422B_s^3 + 38.778B_s^2 + 2.43B_s + 2.7006\times10^6\right)\text{Pa}$$

$$\eta_c = 5.3485B_s^6 - 17.787B_s^5 + 22.148B_s^4 - 12.185B_s^3 + 2.3522B_s^2 + 0.1526B_s + 0.228$$

In this work, along with the full length MRE core sandwich beam (Fig. 4.1(a)) seven other different types of MRE embedded sandwich beam structures have been considered for numerical analysis as shown in Fig. 4.7 and Fig. 4.8. Figure 4.7 shows three different configurations (CI, CII and CIII) of the sandwich beam having the same total MRE patch length but with different individual patch length and locations. Similarly, Fig. 4.8 shows four different sandwich beam configurations LI, LII, LIII and LIV having the same MRE patch length but with different MRE patch locations.

4.5.2.1 Effect of Magnetic Field and Static Load Factor on Modal Frequencies and Loss Factor of Different Sandwich Beam Configurations

The variation of modal frequencies and loss factors of a fully MRE cored sandwich beam with magnetic field is shown in Fig. 4.12, where the static load factor α is zero. It is noted that the modal frequencies of first three modes increase with the strength of the applied magnetic field (Fig. 4.12 (a)). Figure 4.12 (b) shows the effect of magnetic field strength on the loss factor. In all the three modes, the loss factor initially increases and then decreases with increase in magnetic field strength. It is because that the stiffness of the sandwich beams increases with the magnetic field strength due to the increase in complex shear modulus of MRE (Appendix A, Fig. A1), where as its loss factor decrease with increase in magnetic field strength (Appendix A, Fig. A2).

Figure 4.13 (a) shows the variation of the modal frequencies with the static load factor α. The modal frequencies in all the three modes decrease with the increase in static load factor. Figure 4.13 (b) shows the influence of α on the loss factor where one may observe that in all the modes the loss factor increases with increase in the static load factor. It may be noted that initially the loss factor of the sandwich beam is less than that of the MRE and with increase in α, this value increases significantly. For example with $B_s = 0.6\text{T}$, loss factor for MRE is equal to 0.26 (Appendix A, Fig. A2) and with $\alpha = 0$ the loss factor of the sandwich beam is 0.19, 0.14 and 0.1 for first, second and third mode respectively. The corresponding values for $\alpha = 1$ are 0.37, 0.21 and 0.135.

The effect of variation of magnetic field strength on the fundamental frequency and loss factor for the different configurations of a MRE embedded viscoelastic cored sandwich beam is shown in Fig. 4.14. It can be seen from the Fig. 4.14 (a) that the fundamental frequency increases with increase in magnetic field. Also it can be observed that at higher magnetic field the fundamental frequency of CII is more than CI. Similarly the fundamental frequency of CIII is more than CI and CII. For full length MRE core sandwich beam the fundamental frequency at higher magnetic field is larger than the other configurations. Increase in the frequency with increase in magnetic field can be attributed to the increase in the complex shear modulus of

the MRE patch which increases the stiffness of the sandwich beam. Also the distribution of MRE patches in the core increases the stiffness of the beam.

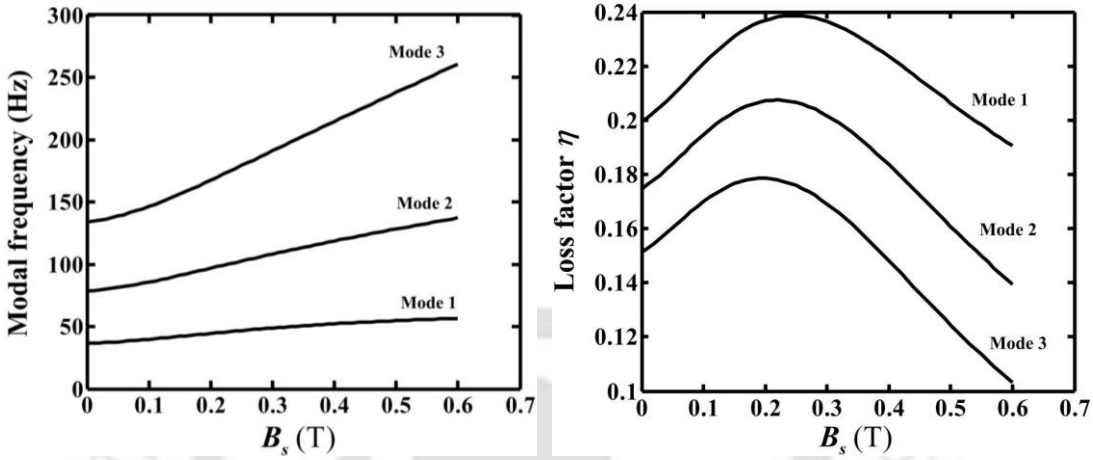

(a) (b)

Figure 4.12 Influence of magnetic field on (a) modal frequencies and (b) modal loss factors of a fully treated MRE core sandwich beam ($P(t) = 0$).

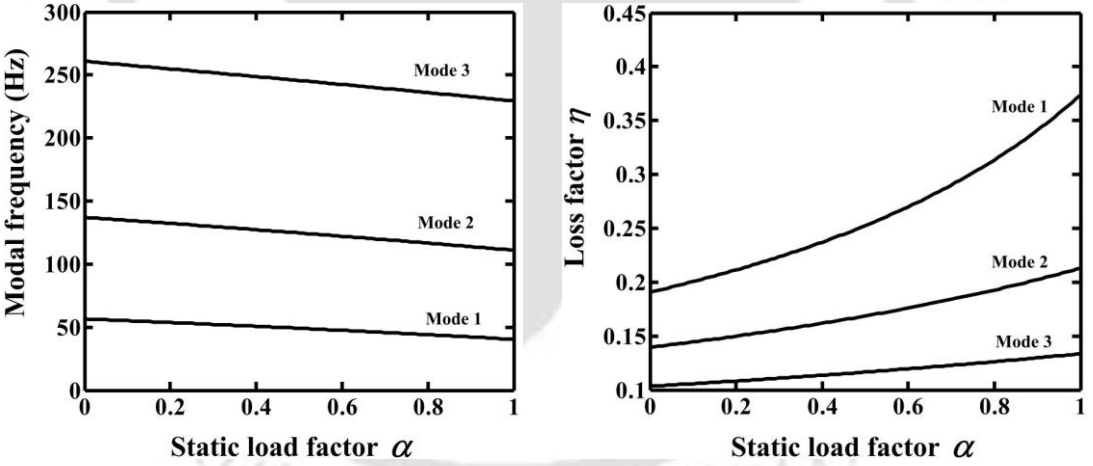

(a) (b)

Figure 4.13 Influence of static load factor on (a) modal frequencies and (b) modal loss factors of a fully treated MRE core sandwich beam ($B_0 = 0.6\text{T}$).

Figure 4.14 (b) shows the influence of magnetic field strength on the loss factor for the different configurations of a sandwich beam. In all the configurations, the loss factor initially increases and then decreases as the magnetic field strength increases. This trend is much obvious for the configurations CIII and fully MRE core of sandwich beam and less evident for the configurations CI and CII. As the

loss factor is merely the ratio of dissipated energy to the total strain energy which initially increases and then decreases as shown in Fig. A2 (Appendix A), so the dissipated energy and hence the loss factor of the system as shown in Fig. 4.14 (b) initially increases and then decreases with increase in magnetic field.

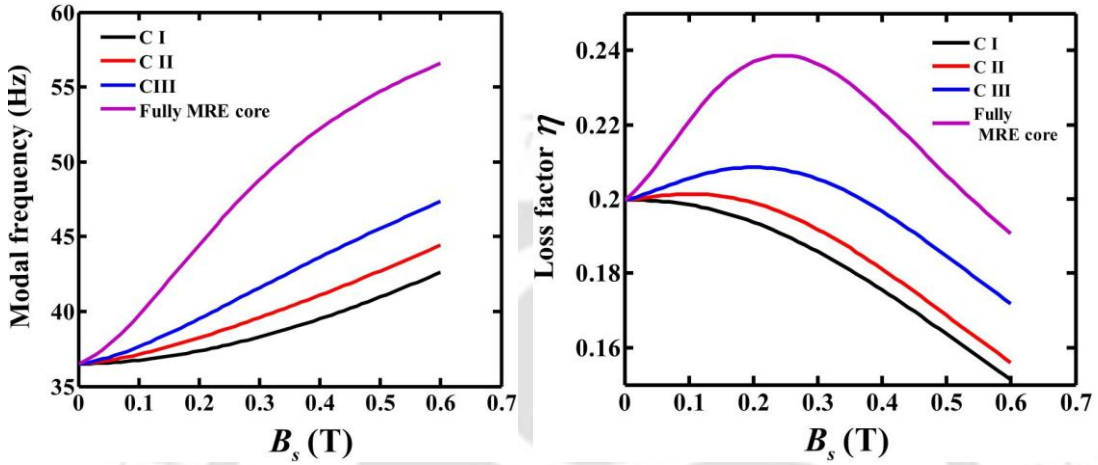

(a) (b)

Figure 4.14 Dependence of (a) fundamental frequency and (b) loss factor on magnetic field for different configurations of sandwich beam ($P(t) = 0$).

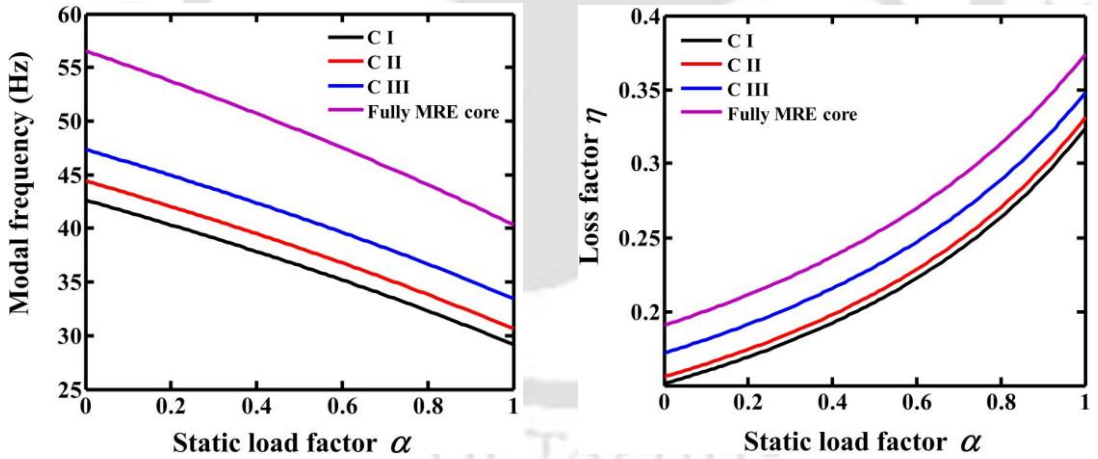

(a) (b)

Figure 4.15 Dependence of (a) fundamental frequency and (b) loss factor on static load factor for different configurations of sandwich beam ($B_s = 0.6\text{T}$).

The influence of static load factor on the fundamental frequency and loss factor for the different configurations of a MRE embedded viscoelastic cored sandwich beam is shown in Fig. 4.15. As shown in Fig. 4.15(a) the fundamental frequency in all the configurations decreases with the increase in static load factor. The influence

of static load factor α on the loss factor is shown in Fig. 4.15(b). It can be observed that in all configurations the loss factor increases with static load factor. This can be attributed to the fact that for the same dissipated energy the total strain energy decreases with increase in static load factor α.

Figure 4.16 shows the effect of variation of magnetic field strength on the fundamental frequency and loss factor for the different configurations of the sandwich beam shown in Fig. 4.8. The results have also been compared with those of the configuration CI and the fully treated MRE core of sandwich beam. Here similar trend has been observed as in Fig.4.14. One may observe that due to symmetry, the fundamental frequencies and loss factors for location LI and LIV and also for LII and LIII are same as shown in Fig. 4.16 (a) and (b) respectively. Also it can be observed that at higher magnetic field the fundamental frequencies and loss factors of LI and LIV in which the MRE patches are located at the support ends are more than those of LII and LIII.

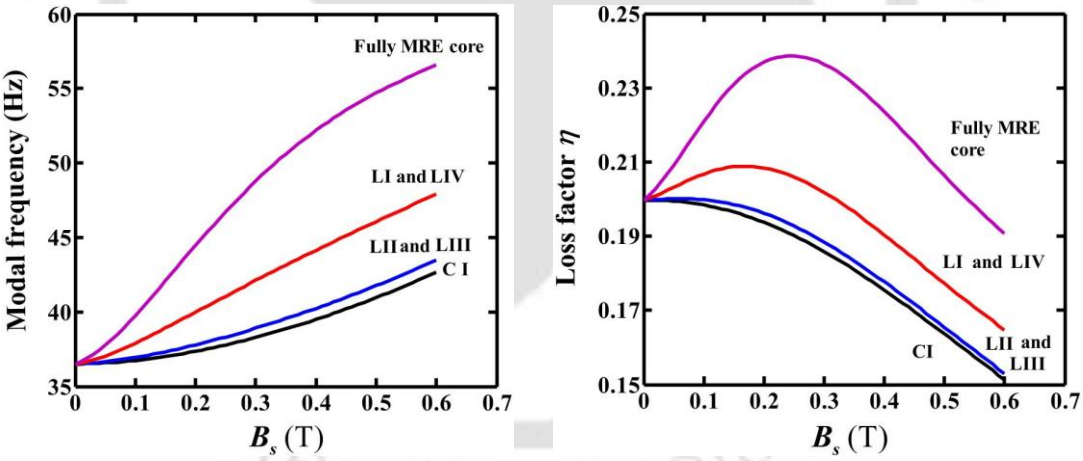

(a) (b)

Figure 4.16 Variation of (a) fundamental frequency and (b) loss factor with magnetic field for different configurations CI, LI, LII, LIII, LIV and fully treated MRE core sandwich beam ($P(t) = 0$).

The influence of static load factor on the fundamental frequency and loss factor for the same configurations discussed in previous is shown in Fig. 4.17. It is observed that in all configurations fundamental frequency decreases and loss factor increases with increase in static load factor. Here also due to symmetry the

fundamental frequencies and loss factors for location LI and LIV and also for LII and LIII are same.

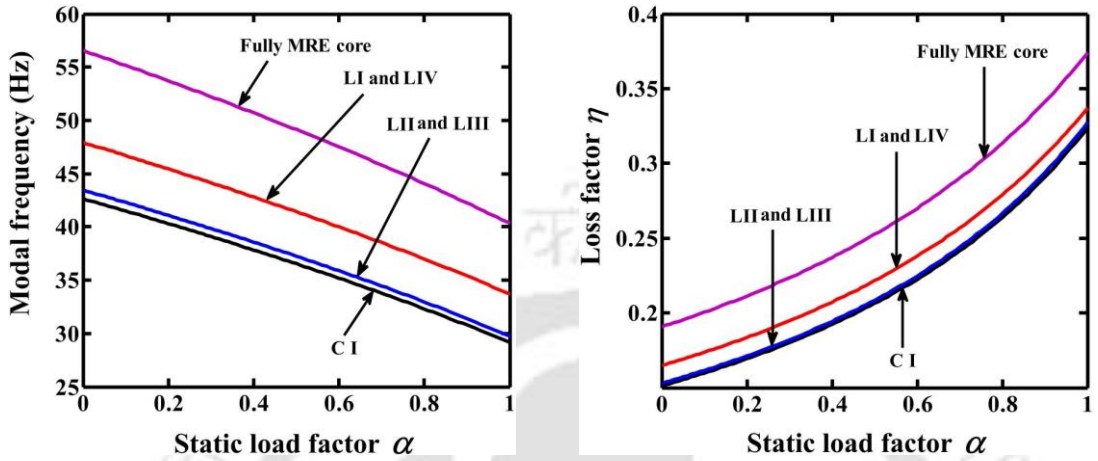

(a) (b)

Figure 4.17 Dependence of first mode (a) frequency and (b) loss factor on static load factor for different locations CI, LI, LII, LIII, LIV and fully treated MRE core sandwich beam ($B_s = 0.6$).

4.5.2.2 Study of Parametric Instability Regions

In this subsection, the stability of a MRE embedded viscoelastic cored sandwich beam subjected to periodic axial load has been investigated considering various system parameters and different configurations for the simply supported end condition.

Figure 4.18 shows the instability regions of the system with configurations CI for $\alpha = 0, B_0 = 0.2\text{T}$. To validate these instability regions the time response corresponding to the three points A, B and C which lie in the stable, unstable and stable regions respectively have been plotted as shown in Fig.4.19. Clearly Fig. 4.19 (a) and (c) show that the response corresponding to the point A and C are stable and that corresponding to point B is unstable as the response increases with time. It may be noted that the response amplitude and settling time corresponding to point C is found to be more than that of the point A. Further in Fig. 4.19 (a) the time response corresponding to configuration CIII is also plotted which shows the response amplitude and settling time for configuration CIII is less than that of CI. Hence in

this way by properly locating the MRE patch one may passively reduce the vibration of the system.

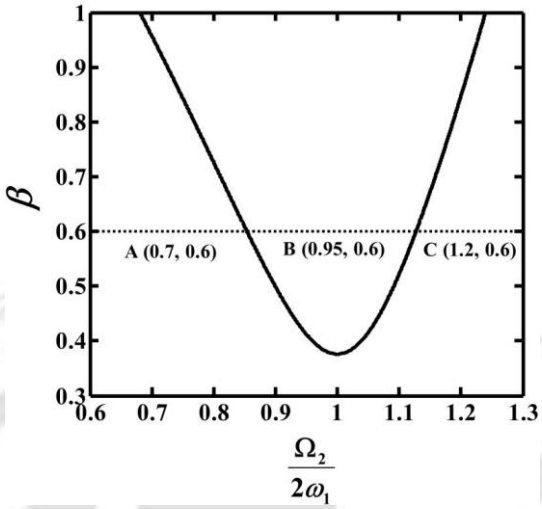

Figure 4.18 Parametric instability region of a sandwich beam (configuration CI, $\alpha = 0$ and $B_0 = 0.2\mathrm{T}$).

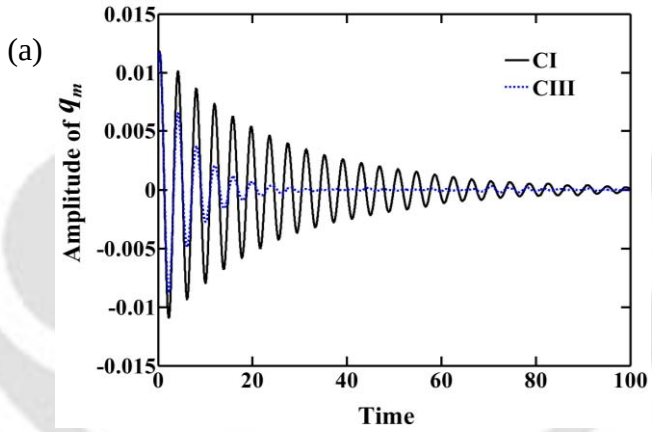

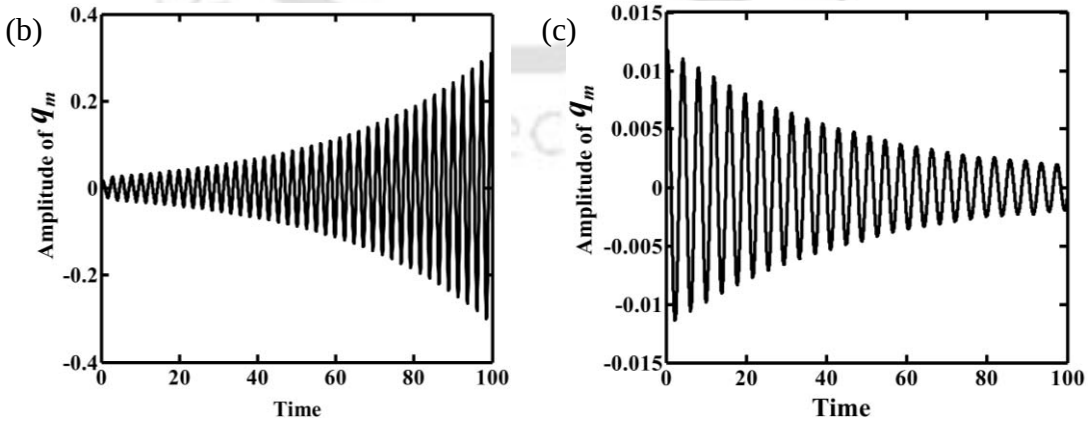

Figure 4.19 (a) Time response at point A for configurations CI and CIII; key as in Fig. 4.18. (b) Time response for point B and (c) time response for point C; key as in Fig. 4.18.

The effect of magnetic field B_s and static load factor α on the first principal instability regions for different configurations of a sandwich beam for the simply supported end condition have been determined and are shown in Figs.4.20. Figure 4.20 shows the variation of instability regions for different configurations, CI, CII, CIII and fully MRE cored sandwich beam with different values of magnetic field strength and static load factor. Considering the instability boundary line of configuration CI (Fig.4.20 (a)), it can be observed that with decrease in dynamic load factor β the unstable region decreases and the system can operate for a wide

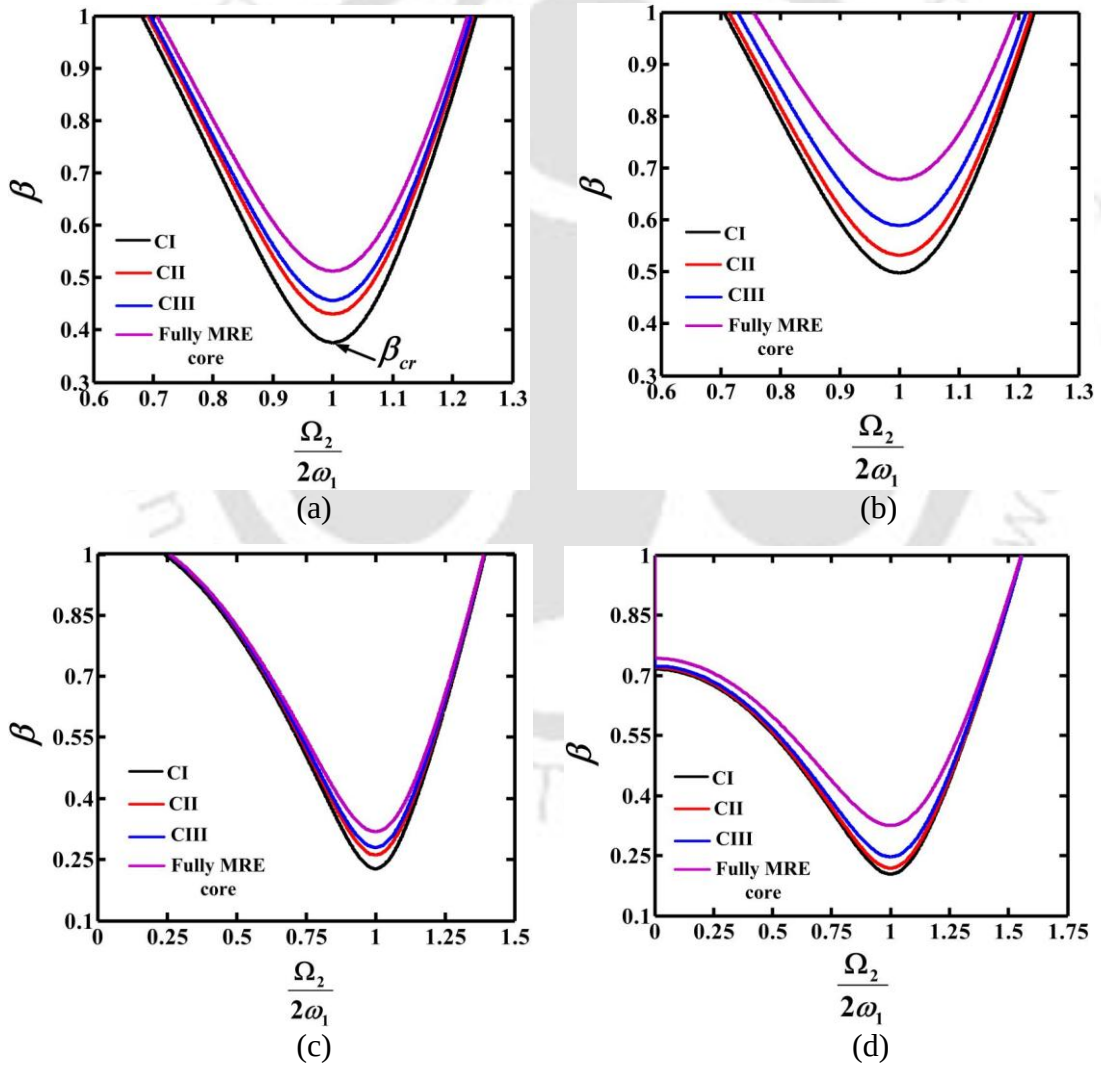

Figure 4.20 principal parametric instability regions of a sandwich beam with different configuration (a) $\alpha = 0, B_s = 0.2\text{T}$, (b) $\alpha = 0, B_s = 0.6\text{T}$, (c) $\alpha = 0.4, B_s = 0.2\text{T}$ and (d) $\alpha = 0.6, B_s = 0.6\text{T}$.

frequency range for lower value of β. Further, there exists a critical value of β (β_{cr}) below which the system has stable region and hence can operate at any frequency without vibration.

It is observed that for the same value of α and B_s while the fully MRE cored sandwich beam has the least instability region, the instability region of configuration CIII is less than that of the configurations CII which is less than that of CI. It can be attributed to the fact that the instability region in the first case is least as the length of the MRE patch is more in this case. Also, though the total length of the MRE patch is same in configurations CI, CII and CIII, due to their relative location, in case of CIII the stiffness is higher in comparison to CII which is more than that of CI. Further one can actively increase the stiffness of the sandwich beam by applying magnetic field.

For constant value of static load factor α, from Fig. 4.20 (a) and (b) it is observed that with increase in magnetic field strength the instability regions decreases and moves upward. Hence in this case the system remains stable for a higher value of dynamic load factor β. This is because that the stiffness of the beam changes as the shear modulus of MRE increases with the application of magnetic field. Similarly, for same value of magnetic field (Fig. 4.20 (a) and (c)) with increase in static load factor α, it is observed that the stability of the system deteriorates as the width and β_{cr} of the instability regions increases. One may get similar observation by comparing Fig. 4.20 (b) and (d) which have been plotted for higher amplitude of magnetic field and static load factor.

The critical values of dynamic load factor β_{cr} for different configurations with different system parameters are presented in the Table 4.11. Considering the case $\alpha = 0$ and $B_s = 0.2\text{T}$ the value of $\beta_{cr} = 0.375$ for the configuration CI but for the same system parameter the value of β_{cr} is 0.456 for the configuration CIII. So the configuration CIII of sandwich beam can be operated at a higher value of dynamic load for a wide range of frequency. Similarly considering the case $\alpha = 0.6$ and $B_s = 0.6\text{T}$ the value of β_{cr} is 0.203 for the configuration CI but for the

same system parameter the value of β_{cr} is 0.246 for the configuration CIII. In case of configuration CIII the operating range of dynamic load decreases with increase in static load factor α .

Table 4.11 Values of critical dynamic load factor, β_{cr} for different configurations of a simply supported sandwich beam.

Configuration	β_{cr}			
	$\alpha = 0,$ $B_s = 0.2\text{T}$	$\alpha = 0.4,$ $B_s = 0.2\text{T}$	$\alpha = 0,$ $B_s = 0.6\text{T}$	$\alpha = 0.6,$ $B_s = 0.6\text{T}$
CI	0.375	0.227	0.497	0.203
CII	0.43	0.261	0.532	0.218
CIII	0.456	0.279	0.588	0.246
Fully MRE core	0.512	0.318	0.677	0.325

Figure 4.21 shows the influence of location of the MRE patch on the stability of the sandwich beam which has been obtained for four different configurations, LI, LII, LIII and LIV (Fig. 4.7). These results are also compared with those obtained for the configuration CI and fully MRE cored sandwich beam. Comparing the Fig. 4.21 (a) and (b), the instability regions decreases with increase in magnetic field for all the locations of the sandwich beam. From Fig.4.21 (c) and (d) one may observe that with increase in static load factor α , while the width of the instability regions increases the value of β_{cr} decreases making the system more unstable. One may observe that due to symmetry the instability regions of simply supported end condition are same for location LI and LIV and also for LII and LIII. For the same system parameters the instability regions of locations LI and LIV are less than that of the locations LII and LIII. This is because that stiffness and damping capacity of the locations LI and LIV increase due to the location of MRE patches at the boundary edges of the simply supported sandwich beam as presented in Fig. 4.16.

The variation of critical dynamic load factors β_{cr} for different locations with different system parameters are shown in the Table 4.12. Considering the case $\alpha = 0 \text{ and } B_s = 0.2\text{T}$ the value of $\beta_{cr} = 0.485$ for the configurations LI and LIV but for the same system parameter the value of β_{cr} is 0.444 for the configurations LII

and LIII. So for the configurations LI and LIV the system can be operated for a higher value of dynamic load for a wide range of frequency. Similarly considering the case $\alpha = 0.6$ and $B_s = 0.6\text{T}$ the value of β_{cr} is 0.257 for the configurations LI and LIV but for the same system parameter the value of β_{cr} is 0.224 for the configurations LII and LIII. In case of configurations LII and LIII the operating range of dynamic load decreases as compare to configurations LI and LIV with increase in static load factor α.

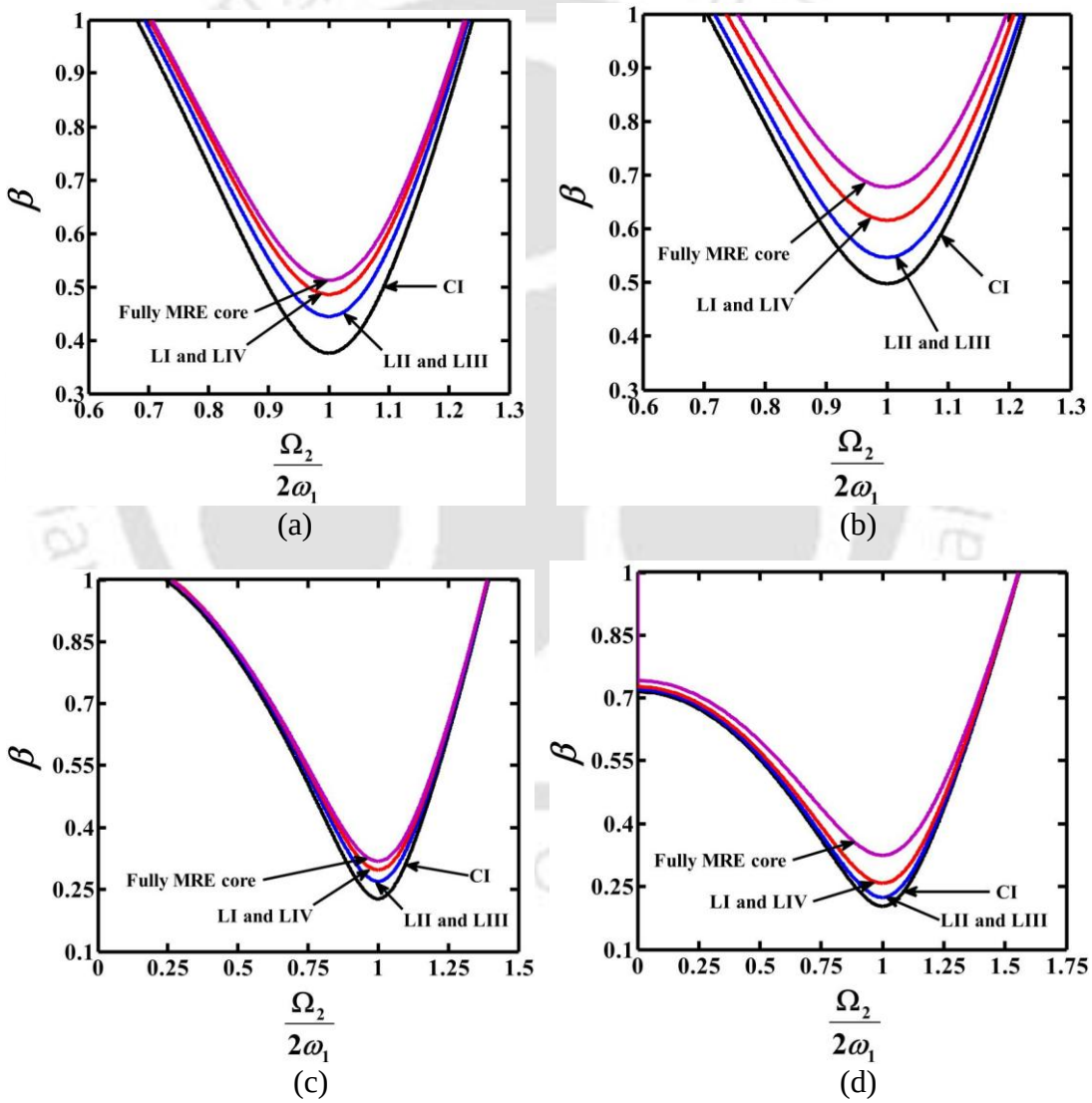

Figure 4.21 Principal parametric instability regions of a sandwich beam with different locations of MRE patch (a) $\alpha = 0, B_s = 0.2\text{T}$, (b) $\alpha = 0, B_s = 0.6\text{T}$, (c) $\alpha = 0.4, B_s = 0.2\text{T}$ and (d) $\alpha = 0.6, B_s = 0.6\text{T}$.

Table 4.12 Values of critical dynamic load factor, β_{cr} for different locations of a simply supported sandwich beam.

Location	β_{cr}			
	$\alpha = 0,$ $B_s = 0.2\text{T}$	$\alpha = 0.4,$ $B_s = 0.2\text{T}$	$\alpha = 0,$ $B_s = 0.6\text{T}$	$\alpha = 0.6,$ $B_s = 0.6\text{T}$
CI	0.375	0.227	0.497	0.203
LI	0.485	0.297	0.615	0.257
LII	0.444	0.269	0.546	0.224
LIII	0.444	0.269	0.546	0.224
LIV	0.485	0.297	0.615	0.257
Fully MRE core	0.512	0.318	0.677	0.325

4.5.3 Numerical Results and Discussions of a Rotating Sandwich Beam

In this section considering the rotating MRE cored sandwich beam as shown in Fig. 4.4(a), the dynamic characteristics such as fundamental frequency, loss factor and dynamic stability of the system have been studied using various system parameters. A MATLAB code has been developed for this purpose and to validate the developed code, the resonant frequencies without considering the axial load are compared with those obtained from the previous literature.

Table 4.13 shows the comparison of resonant frequencies of MRE cored rotating sandwich beam with different rotating speeds obtained from the present model and the results of Putter and Manor, (1978) and Lin and Chen, (2003). It can be seen that the present results are in good agreement with those of Putter and Manor [35] and Lin and Chen, (2003).

4.5.3.1 Study of Frequencies and Loss Factors of a Rotating MRE Cored Sandwich Beam

In the present numerical analysis, a rotating symmetric sandwich beam with MRE core has been considered for clamped-free end condition. The geometric and material properties of the sandwich beam are same as the properties discussed in 4.5.1.1, case 3. The properties of MRE are same as discussed in section 4.5.2. The effects of rotational speed (N_h) on fundamental frequency and loss factor for various magnetic field (B_s) are shown in Fig. 4.22. It can be observed that the

Table 4.13 Comparisons of non-dimensional modal frequencies $\left(\omega\sqrt{\rho AL^4/EI}\right)$ of a rotating sandwich beam, where $\Omega_1^{'}=\Omega_1\sqrt{\rho AL^4/EI}$, $R=r/L$, $\theta=90^{o}$ and $B_s=0$.

	$\Omega_1^{'}$	Mode 1		Mode 2	
		R = 0	R = 1	R = 0	R = 1
Present analysis	2	3.671	4.442	22.826	23.570
Lin and Chen [42]		3.623	4.403	22.528	23.282
Putter and Manor [35]		3.612	4.401	22.526	23.280
Present analysis	5	4.322	7.529	25.209	29.035
Lin and Chen [42]		4.075	7.415	24.952	28.927
Putter and Manor [35]		4.074	7.412	24.95	28.924
Present analysis	10	5.182	13.294	32.973	44.325
Lin and Chen [42]		5.052	13.261	32.124	43.238
Putter and Manor [35]		5.049	13.258	32.12	43.227

fundamental frequency increases and system loss factor decreases by increasing of the rotational speed and magnetic field (Fig. 4.22). This increase in frequency is due to stiffening effect. The effect of the setting angle is illustrated in Fig. 4.23. It shows that the fundamental frequency decreases and the loss factor increases with an increase in setting angle. This can be followed from Eq. (4.38) that the stiffness of the system decreases with increase in setting angle. Fig. 4.24 shows the influence of hub radius to beam length ratio r/L on the fundamental frequency and loss factor. It can be observed that the fundamental frequency increases and the system loss factor decreases as the r/L increases. In all the above three cases the fundamental frequency increases with increase in magnetic field. It may be noted that the loss factor of the system is the ratio of the imaginary and real part of the complex modal frequency. The imaginary part of the complex modal frequency is a function of loss factor of MRE core which remain almost constant. As the real part of the complex eigenvalue increases or decreases depending on the rotational speed and magnetic field for a particular system, hence the loss factor decreases or increases as shown in Figs. 4.22-4.24.

The influence of static load (P_s) on the fundamental frequency and loss factor of the rotating MRE cored sandwich beam is shown in Figs.4.25-4.28. From Fig. 4.25

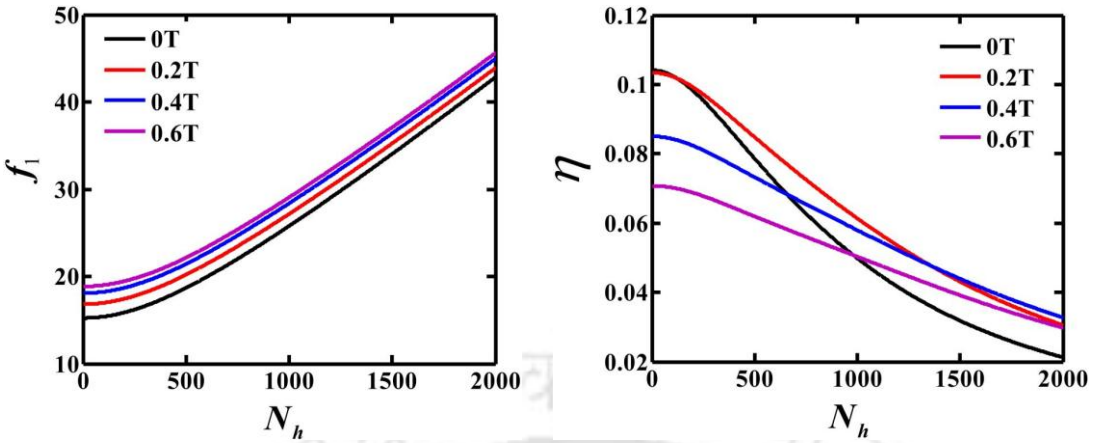

Figure 4.22 The influence of rotating speed N_h (rpm) and magnetic field strength B_s on (a) fundamental frequency f_1(Hz) and (b) system loss factor η; $r/L=0$, $\alpha=0$ and $\theta=0$.

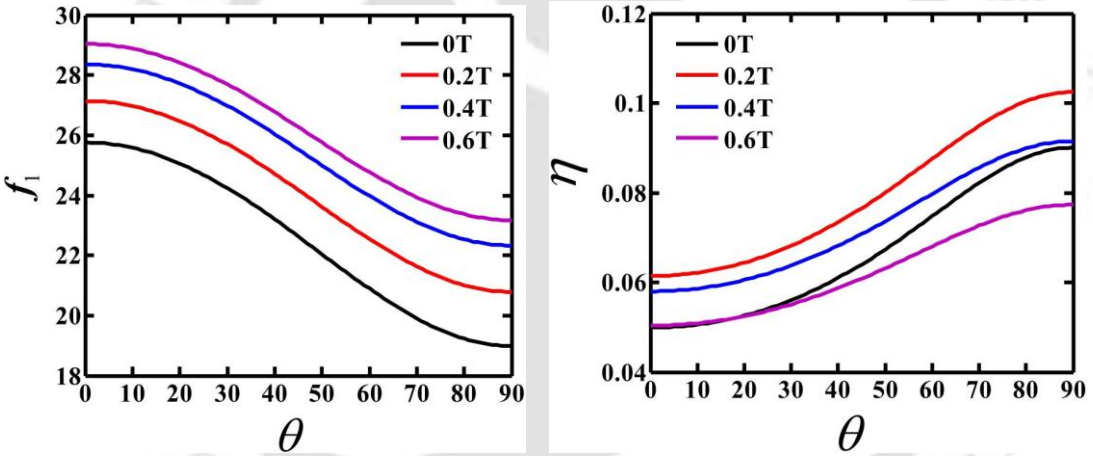

Figure 4.23 The influence of setting angle θ (degrees) and magnetic field strength B_s on (a) fundamental frequency f_1(Hz) and (b) system loss factor η; $N_h=1000$ rpm, $r/L=0$ and $\alpha=0$.

(a) it can be observed that the fundamental frequency significantly decreases as the static load factor α increases. For example increasing α =0 to α =0.8, decreases the fundamental frequency from 18.86 Hz to 11.24 HZ for a magnetic field of 0.6T. Hence it may be observed that for a combination of magnetic field and static load factor the fundamental frequency of the system can be changed significantly which will help in actively reducing the system response amplitude. Figure 4.25 (b) shows the influence of static load factor on system loss factor. It shows that the system loss

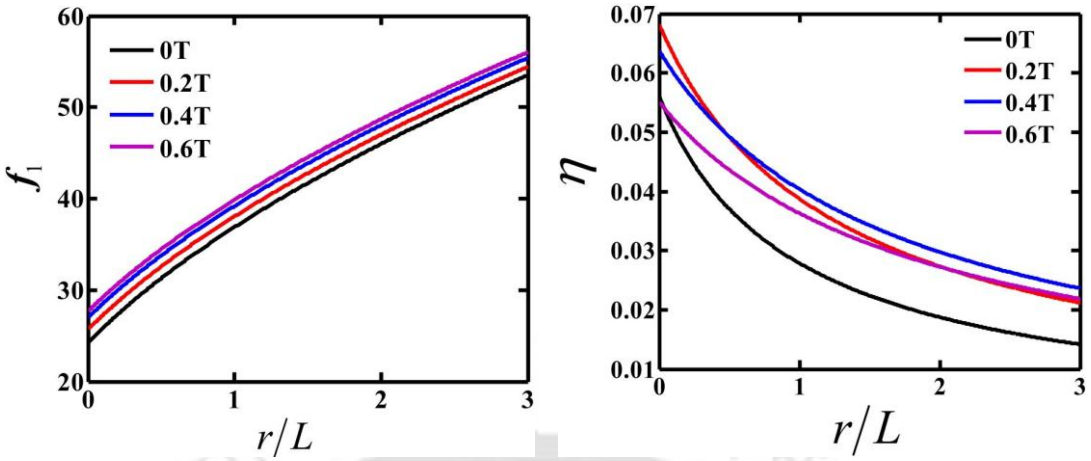

(a) (b)

Figure 4.24 The influence of hub radius to beam length r/L and magnetic field strength B_s on (a) fundamental frequency f_1(Hz) and (b) system loss factor η; $N_h = 1000$ rpm, $\theta = 30^o$ and $\alpha = 0$.

factor increases for higher values of static load factor. The influence of static load factor on resonant frequency and system loss factor for different rotating speed is shown in Fig. 4.26. The resonant frequency decreases and the loss factor increases with increase in static load factor. For a constant magnetic field, the results show significant change in the fundamental frequency with static load factor for the system without rotation and this change is very small for the higher rotational speed.

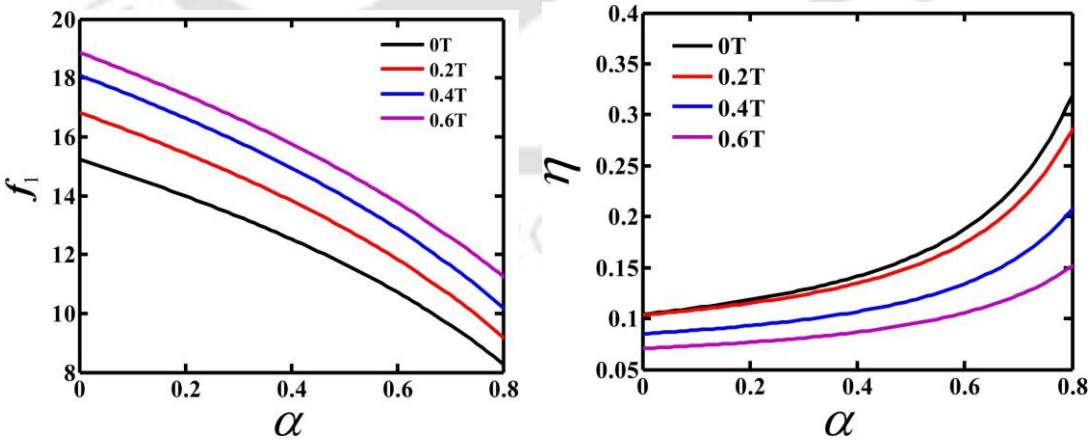

(a) (b)

Figure 4.25 The effect of static load factor on (a) fundamental frequency f_1(Hz) and (b) system loss factor η for different magnetic field strength B_s; $N_h = 0$, $r/L = 0$ and $\theta = 0^o$.

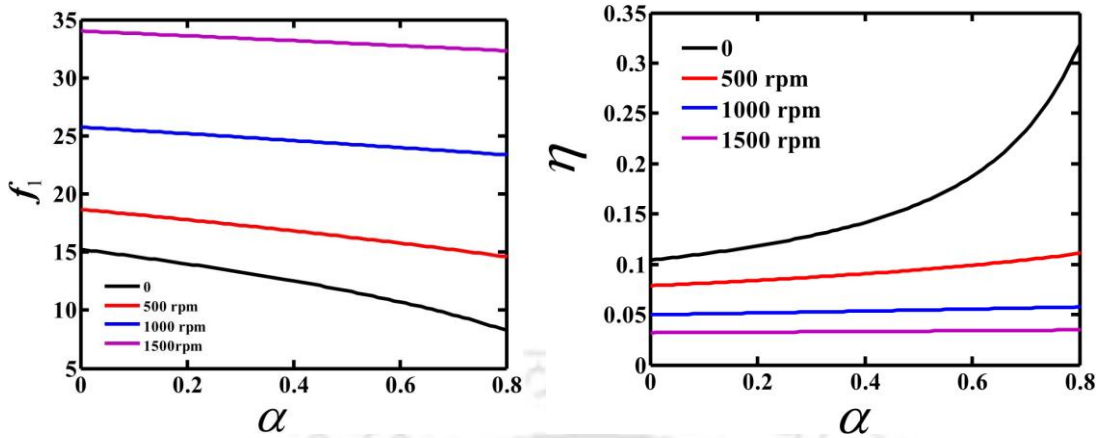

(a) (b)

Figure 4.26 The effect of static load factor on (a) fundamental frequency f_1(Hz) and (b) system loss factor η for different rotating speed N_h; $B_s = 0$, $r/L = 0$ and $\theta = 0^o$.

Figure 4.27 shows the influence of static load factor on fundamental frequency and system loss factor for different setting angle. The fundamental frequency decreases and system loss factor increases as the static load factor increases. Also it can be observed that the fundamental frequency decreases and system loss factor increases with increases in setting angle. The effect of static load factor on fundamental frequency and system loss factor for different hub radius to beam length ratio r/L is shown in Fig. 4.28. The fundamental frequency decreases and the loss factor increases with increase in static load factor. It can be seen that the

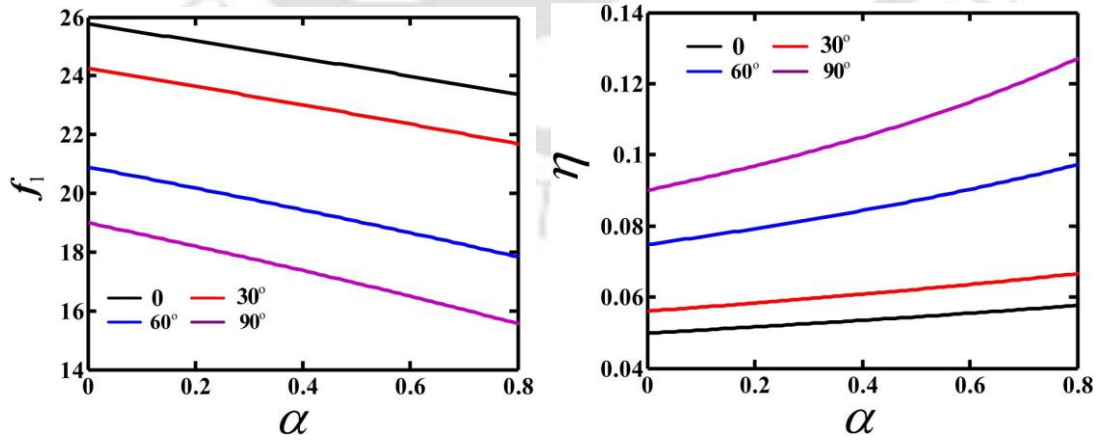

(a) (b)

Figure 4.27 The effect of static load factor on (a) fundamental frequency f_1(Hz) and (b) system loss factor η for different setting angle θ; $B_s = 0$, $N_h = 1000$ rpm and $r/L = 0$.

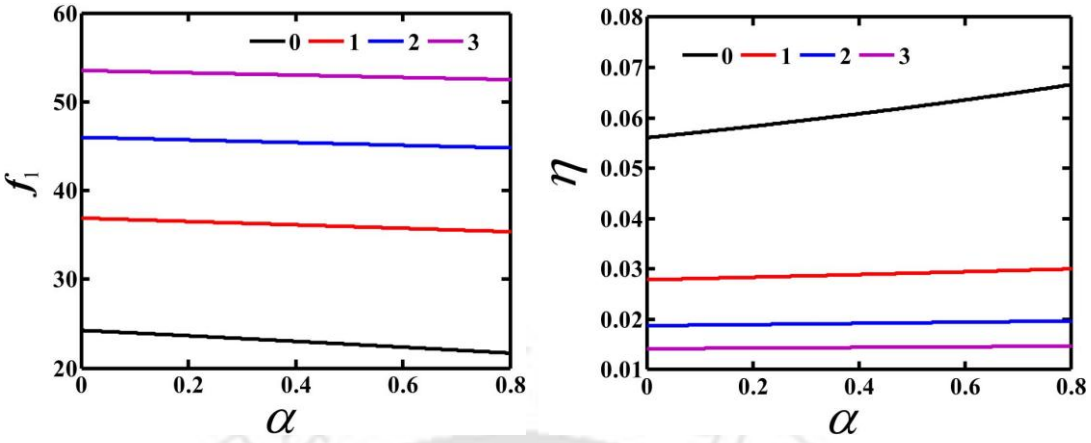

(a) (b)

Figure 4.28 The effect of static load factor on (a) fundamental frequency f_1 (Hz) and (b) system loss factor η for different hub radius to beam length ratio r/L; $B_s = 0$, $N_h = 1000$ rpm and $\theta = 30^o$.

fundamental frequency increases and system loss factor decreases with increase in hub radius to beam length ratio r/L. It may be noted that in all these cases as the variation of fundamental frequency or loss factor with different system parameters like static load factor, rotational speed, magnetic field, setting angle and r/L ratio is not linear, it is difficult to intuitively predict the fundamental frequency without actually finding the eigenvalues using the developed global mass and stiffness matrices.

4.5.3.2 Stability of the MRE cored Rotating Sandwich Beam

In this subsection, the stability of a MRE cored rotating sandwich beam subjected to periodic axial load has been investigated by determining the parametric instability regions for the clamped free end condition. The instability regions of the sandwich beam are investigated with and without considering the damping effect of MRE. The influence of various system parameters such as magnetic field strength, rotating speed, setting angle, hub radius to beam length ratio, static load and dynamic load on instability regions (Figs. 4.29-4.31) is investigated. In all these figures, while the regions bounded by the curves are unstable, the regions outside the curves are stable.

Parametric Instability Regions without Damping Effect of MRE

Figure 4.29 (a) shows the effect of magnetic field on the instability regions of a rotating MRE cored sandwich beam considering the loss factor of the MRE core to be zero. It can be seen that the width of instability regions decreases and occurs at higher frequencies with increase in magnetic field. The decrease in width of instability regions and the increase in the frequency with increase in magnetic field can be attributed to the increase in the complex shear modulus of the MRE patch which increases the stiffness of the sandwich beam. The effect of rotational speed on

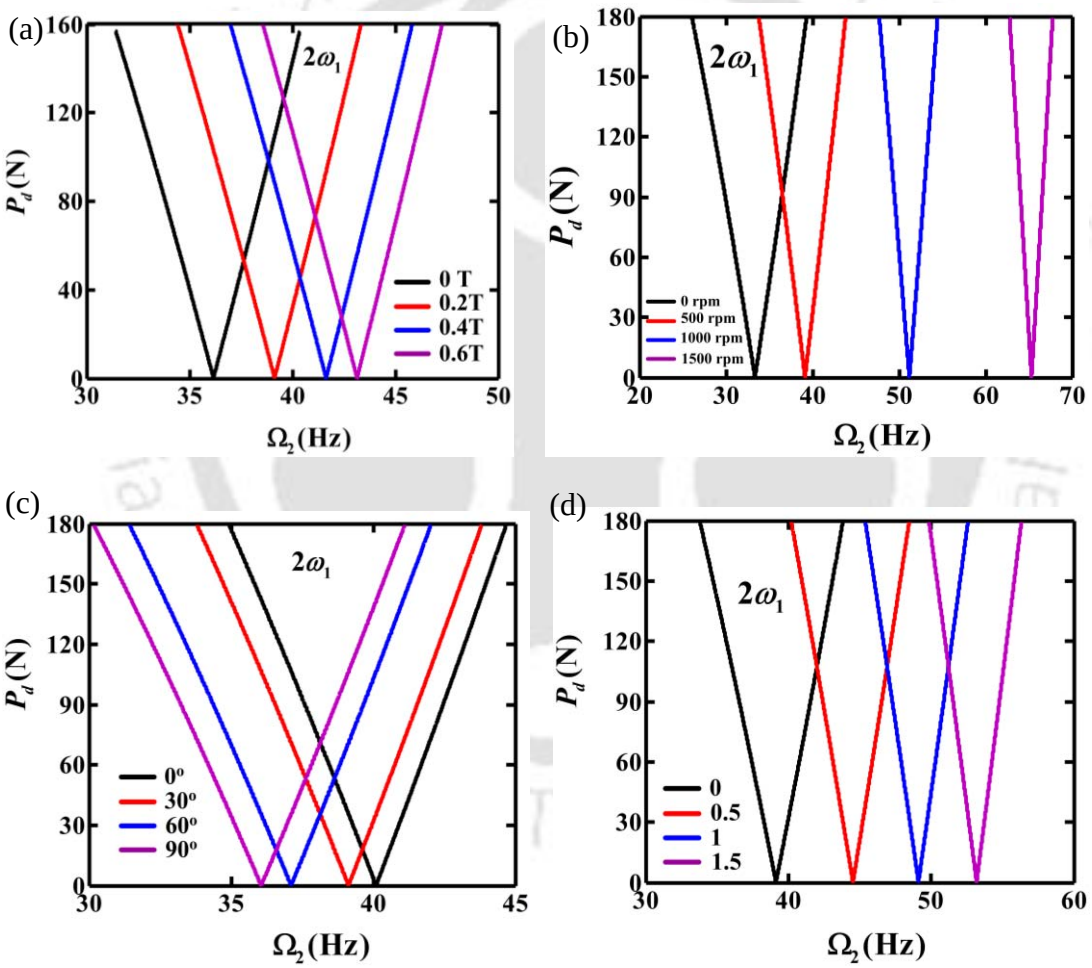

Figure 4.29 Parametric instability regions of a rotating sandwich beam without damping (a) effect of magnetic field: $r/L=0$, $N_h=500\,\text{rpm}$ and $\theta=30^{\circ}$ (b) effect of rotating speed: $r/L=0$, $B_s=0.2\text{T}$ and $\theta=30^{\circ}$ (c) effect of setting angle: $B_s=0.2\text{T}$, $N_h=500\,\text{rpm}$ and $r/L=0$ (d) effect of hub radius to beam length ratio: $B_s=0.2\text{T}$, $N_h=500\,\text{rpm}$ and $\theta=30^{\circ}$.

the instability regions at a constant magnetic field $B_s = 0.2\text{T}$ is investigated and is shown in Fig. 4.29 (b). It shows that increase in the rotational speed increases the excitation frequency Ω_2 at which the system becomes unstable, so that the instability region shifts to the right. Also, it can be observed that the width of the instability region decreases with increase in rotating speed. This is due to the increase in stiffness of the beam which makes the sandwich beam more stable.

Figure 4.29 (c) shows the effect of the setting angle on the instability regions of a rotating MRE cored sandwich beam at a constant magnetic field $B_s = 0.2\text{T}$. The instability regions shift to the left due to the decrease of the resonant frequency with increase in setting angle. Also it can be observed that the width of the instability regions increases with increase in setting angle. Consequently, the larger setting angle makes the rotating MRE cored sandwich beam more unstable.

The effects of the hub radius to length ratio on the instability regions of this system at a constant magnetic field $B_s = 0.2\text{T}$ are presented in Fig. 4.29 (d). With increase in hub radius to length ratio the stiffness of the rotating sandwich beam increases so that the resonant frequency increases and the instability region move towards right. Also it can be seen that the width of the instability region decreases with increase in hub radius to length ratio. So the larger hub radius to length ratio makes the rotating MRE cored sandwich beam more stable.

Figure 4.30 shows the influence of static load factor α on the instability regions of the MRE cored rotating sandwich beam for different system parameters and a constant magnetic field $B_s = 0.2\text{T}$. It can be observed that in all the cases the instability regions shift to the left due to the decrease of the resonant frequency with increase in static load factor α. Also it can be observed that the width of the instability regions increases with increase in static load factor. Consequently, the larger static load factor makes the rotating MRE cored sandwich beam more unstable. From all these the figures it can be observed that by changing the system parameters the instability regions can be changed to make the system stable.

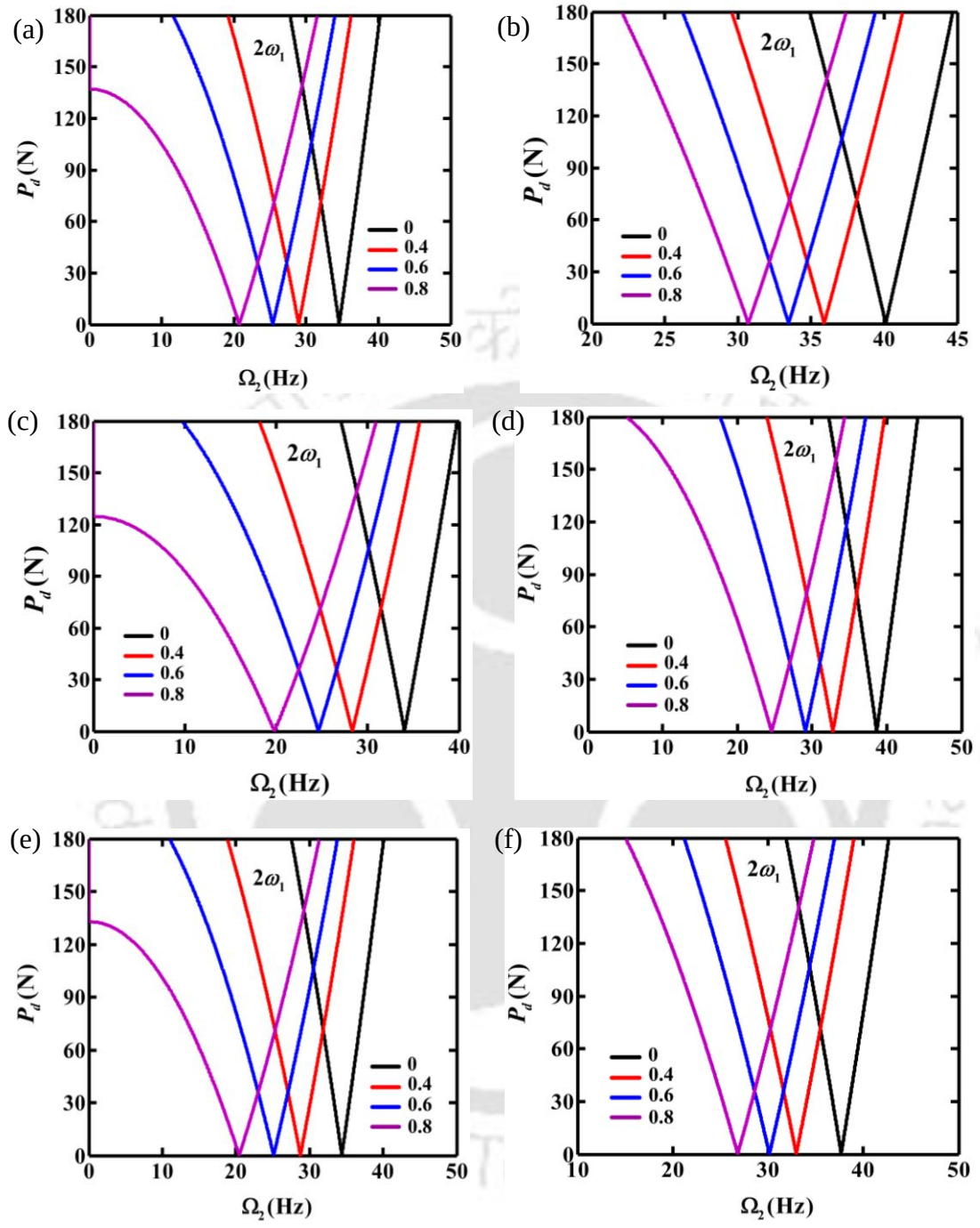

Figure 4.30 Effect of static load factor α on parametric instability regions of a rotating sandwich beam without damping (a) $B_s = 0.2\text{T}$, $r/L = 0$, $N_h = 200\,\text{rpm}$ and $\theta = 0^\circ$ (b) $B_s = 0.2\text{T}$, $N_h = 500\,\text{rpm}$, $\theta = 0^\circ$ and $r/L = 0$ (c) $B_s = 0.2\text{T}$, $r/L = 0$, $N_h = 200\,\text{rpm}$ and $\theta = 60^\circ$ (d) $B_s = 0.6\text{T}$, $N_h = 200\,\text{rpm}$ $r/L = 0$ and $\theta = 0^\circ$ (e) $B_s = 0.2\text{T}$, $r/L = 0$, $N_h = 200\,\text{rpm}$ and $\theta = 30^\circ$ (f) $B_s = 0.2\text{T}$, $r/L = 1.5$, $N_h = 200\,\text{rpm}$ and $\theta = 30^\circ$.

Parametric Instability Regions with Damping Effect of MRE

Damping of sandwich beams with MRE core plays a vital role in the dynamic behavior analysis of structures by controlling the resonant vibrations and thus reducing of the bounded instability regions. This damping depends on the core material properties.

The effect of magnetic field B_s on the first principal instability regions of a MRE cored rotating sandwich beam with damping have been determined considering different system parameters and are shown in Figs.4.31. Figure 4.31 (a) shows the instability regions for the system parameters $N_h = 200\,\text{rpm}$, $\alpha = 0.8$, $r/L = 0$ and $\theta = 60^{\circ}$ with variation of magnetic field. It is observed that with decrease in dynamic load P_d the unstable region decreases and the system can operate for a wide frequency range for lower value of dynamic load. Further, there exists a critical value of P_d (P_{dcr}) below which the system has stable region and hence can operate at any frequency without vibration. From Fig. 4.31 (a) it can be observed that with increase in magnetic field the instability regions decreases, shifts towards right and the P_{dcr} value increases. This is because that the stiffness of the beam increases as the shear modulus and loss factor of MRE increases with the application of magnetic field. Now taking the same system parameters and increasing the speed to 500 rpm the instability regions are determined which are shown in Fig. 4.31 (b). The values of P_{dcr} are presented in the Table 4.14. Now comparing the Fig. 4.31 (a) and (c), with decrease of static load factor to 0.2 the instability regions are decreases. Also, the system becomes more stable as the values of P_{dcr} increases. Similarly comparing the instability regions shown in Figs. 4.31 (a) and (d), it can be observed that with increase in ratio of hub radius to beam length the instability regions decreases and move upward as the effective stiffness and damping increases. The values of P_{dcr} for different magnetic fields increase so that the system can operate at higher dynamic loads. The values of P_{dcr} for the above discussed cases are presented in the Table 4.14.

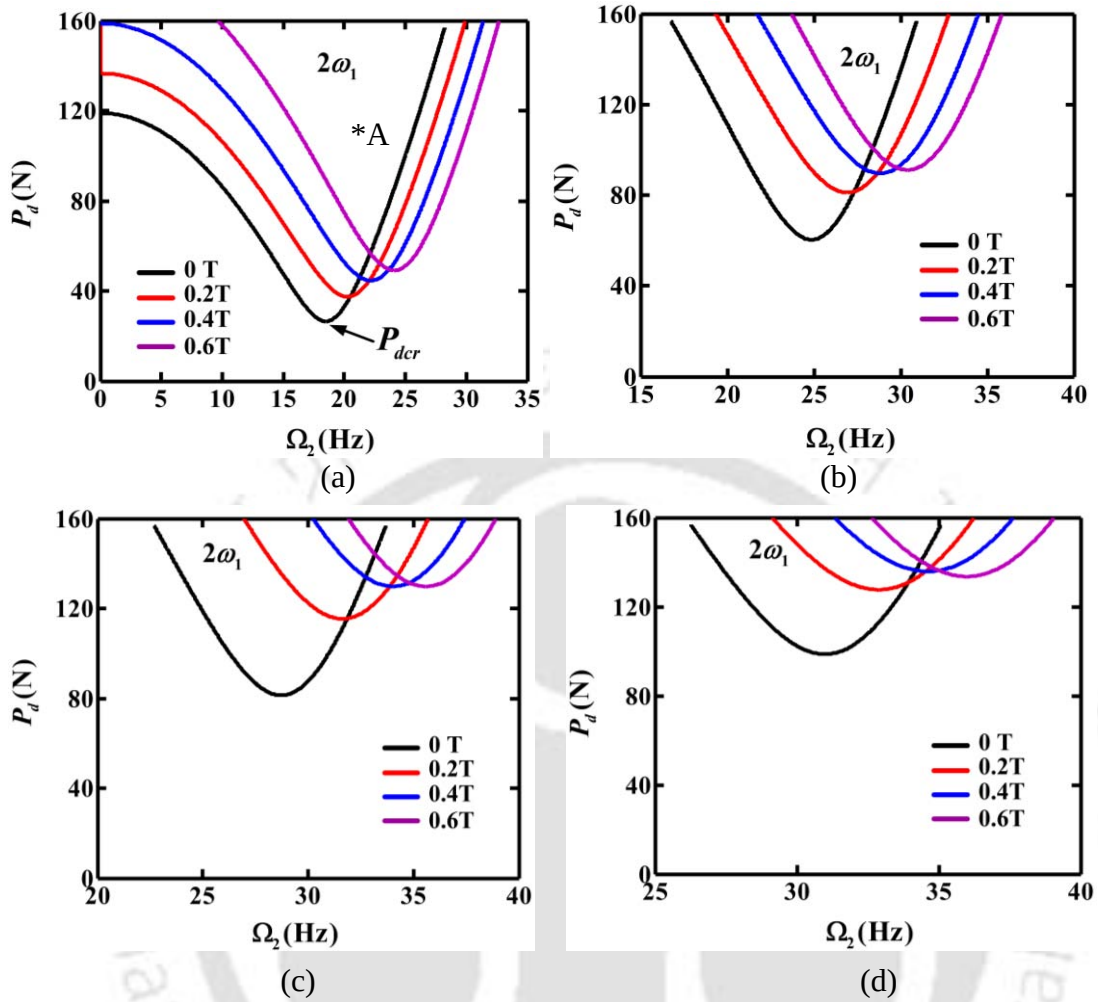

Figure 4.31 Parametric instability regions of a rotating sandwich beam with damping (a) $N_h = 200\,\text{rpm}$, $\alpha = 0.8$, $r/L = 0$ and $\theta = 60^o$ (b) $N_h = 500\,\text{rpm}$, $\alpha = 0.8$, $r/L = 0$ and $\theta = 60^o$ (c) $N_h = 200\,\text{rpm}$, $\alpha = 0.2$, $r/L = 0$ and $\theta = 60^o$ (d) $N_h = 200\,\text{rpm}$, $\alpha = 0.8$, $r/L = 1.5$ and $\theta = 60^o$.

Table 4.14 Values of critical dynamic load, P_{dcr} of instability regions of the MRE cored rotating sandwich beam for different system parameters with variation of magnetic field.

	P_{dcr} (N)			
B_s (T)	$N_h = 200\,\text{rpm}$, $\alpha = 0.8$, $r/L = 0$, $\theta = 60^o$	$N_h = 500\,\text{rpm}$, $\alpha = 0.8$, $r/L = 0$, $\theta = 60^o$	$N_h = 200\,\text{rpm}$, $\alpha = 0.2$, $r/L = 0$, $\theta = 60^o$	$N_h = 200\,\text{rpm}$, $\alpha = 0.8$, $r/L = 1.5$, $\theta = 60^o$
0	26.36	60.25	81.28	98.54
0.2	37.44	80.97	115.4	127.5
0.4	44.47	89.52	129.7	135.7
0.6	48.96	91.02	129.7	133.5

To validate the instability regions time response curves have been plotted (Fig. 4.32) corresponding to three points of Fig. 4.29 (a). For system parameters $B_s = 0.2\text{T}$ and $P_d = 90\text{N}$, clearly from Fig. 4.32 (a) and (c) (which corresponds to $\Omega_2 = 35\,\text{Hz}$ and $\Omega_2 = 43\text{Hz}$ respectively) are found to be stable and similarly for $\Omega_2 = 38\,\text{Hz}$ (Fig. 4.32 (b)) the response is found to be unstable.

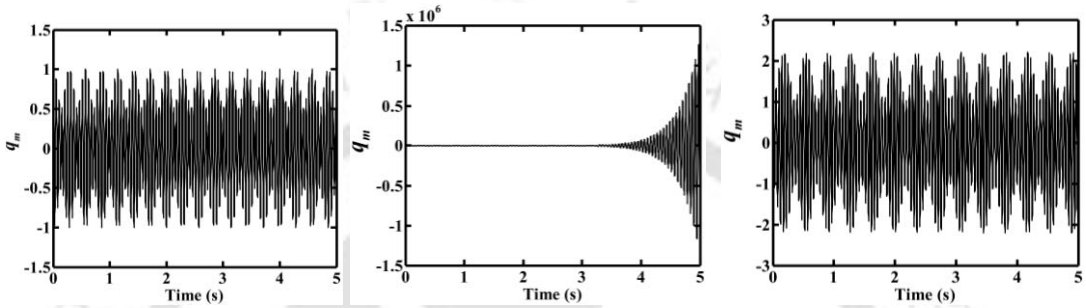

(a) (b) (c)

Figure 4.32 Time response at three points in Fig. 4.29, (a) $P_d = 90\text{N}$, $\Omega_2 = 35\,\text{Hz}$ (b) $P_d = 90\text{N}$, $\Omega_2 = 38\,\text{Hz}$ and (c) $P_d = 90\text{N}$, $\Omega_2 = 43\text{Hz}$ for a magnetic field of 0.2 T.

Figure 4.33 (a) shows the time response of a point chosen from Fig. 4.31 (a) ($\Omega_2 = 3\,\text{Hz}$ and $P_d = 100\text{N}$) of the rotating MRE-based sandwich beam without magnetic field. The point is in stable region. It can be observed that due to the damping effect of MRE the response amplitude exponentially decreases and reach a steady state solution. While the transient response shows higher amplitude for the system with 0.6 T magnetic fields, in the steady state the response amplitude decreases significantly with application of magnetic field. Figure 4.33 (b)-(e) shows the time response of a point marked A in Fig. 4.31 (a) for different magnetic field. The point is in unstable region with parameters $\Omega_2 = 22\,\text{Hz}$ and $P_d = 100\text{N}$. It can be observed from Fig. 4.33 (b)-(e) that the response amplitude exponentially increases which validate the unstable state predicted in Fig. 4.31 (a). Now to bring the system to a stable state one may increase the rotational speed and use a magnetic field as shown in Fig. 4.31 (b).

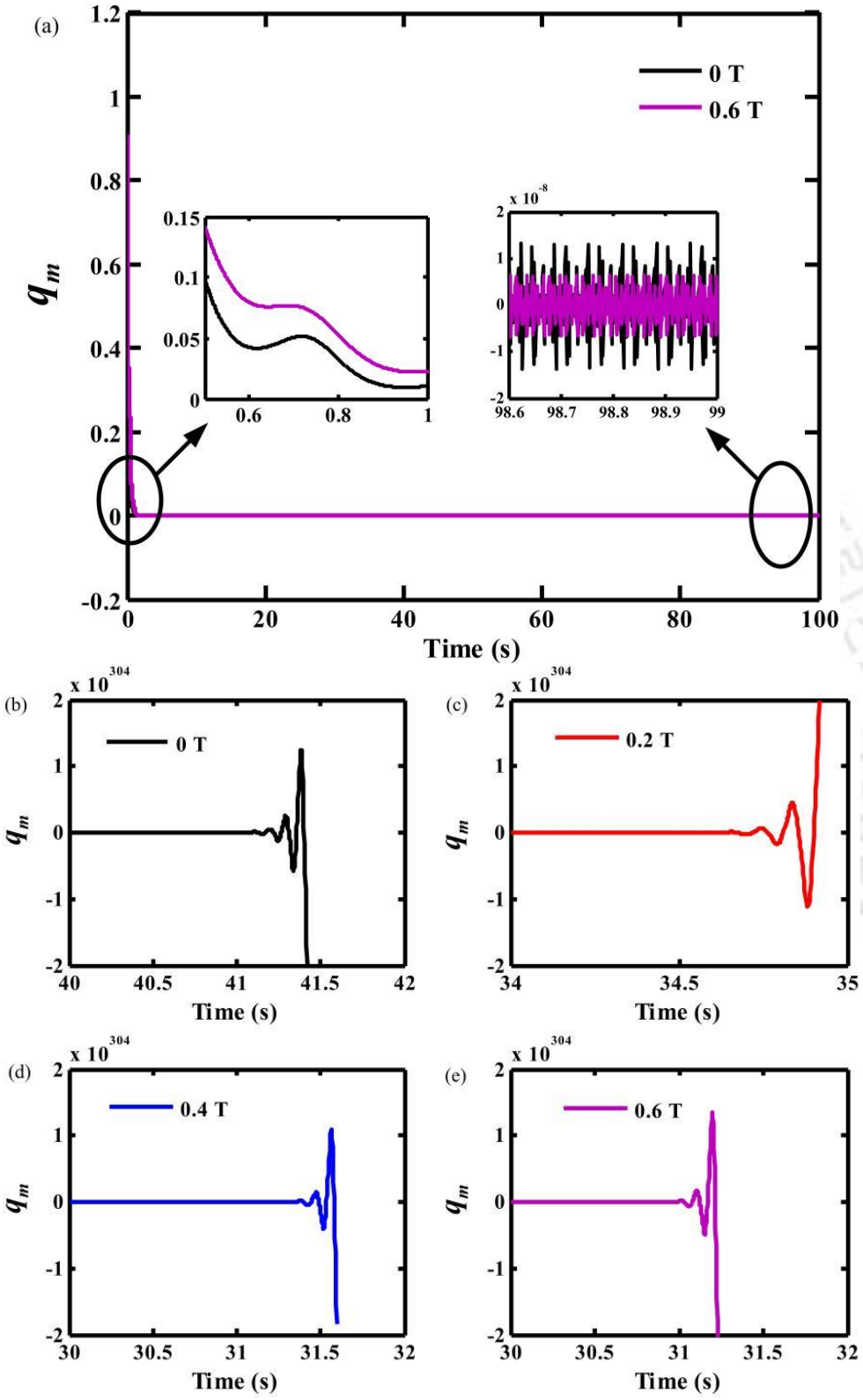

Figure 4.33 (a) Time response at a point ($\Omega_2 = 3\text{Hz}$, $P_d = 100\text{N}$) in Fig. 4.31 (a) without and with magnetic field 0.6 T. (b)-(e) Time response at the point A marked in Fig. 4.31 (a) for different magnetic field.

4.6 Summary

Using the finite element method the mathematical modeling of rotating and non-rotating MRE embedded sandwich beam has been carried out. It is observed that the natural frequencies and the loss factors of the MRE embedded sandwich structure are strongly influenced by the location, length and number of the MRE patch in addition to the magnetic field and the boundary conditions. It is shown that the transverse vibration response of the system are considerably reduced passively by using conductive skins and conveniently placing number of MRE patches in the core and actively reduced by applying magnetic field of suitable amplitude.

In case of rotating sandwich beam the variation of fundamental frequency and loss factor along with instability regions for different system parameters such as magnetic field, rotational speed, setting angle, hub radius to length of beam ratio and static load factor have been investigated.

5

Dynamic Analysis of Sandwich Beam with Composite Skins and Flexible MRE Core using FEM

5.1 Introduction

Sandwich structures with composite material skins are now widely used in the aerospace industry. They offer great advantages compared to metal alloys, such as reduction in weight, increase in strength, and greater resistance to corrosion. In this chapter MRE embedded sandwich beam with nonconductive composite skins has been considered. In section 5.2, the finite element formulation of a sandwich beam with composite skins and flexible MRE core has been carried out. In section 5.3, numerical analysis has been carried out to study the free and forced vibration and parametric instability regions of this structure for different system parameters.

5.2 Finite Element Formulation

A three layer symmetric sandwich beam of length L and width b, with two nonconductive composite skins and a MRE core is shown in Fig. 5.1 (a). Figure 5.1 (b) shows the sandwich beam subjected to magnetic field, B_s and periodic axial load, $P(t)$. For modelling of sandwich beam with MRE embedded soft core and nonconductive composite skins, the top, bottom and core layers thicknesses h_t, h_b and h_c are considered to be very small compared to the length of the beam. The composite skins have independent transverse displacements. The transverse displacement through the depth of beam is considered as linear variation. Rotary inertia and longitudinal kinetic energy of core are considered. There is no slippage between the interfaces between two layers.

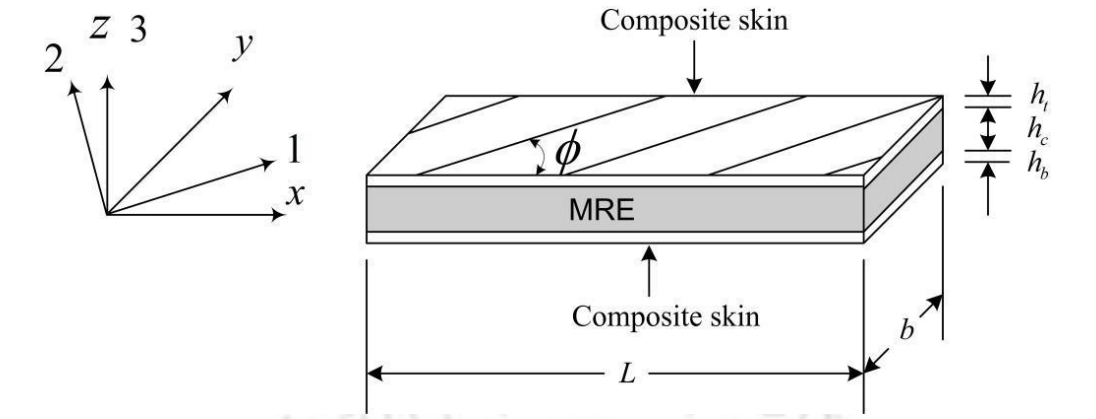

(a)

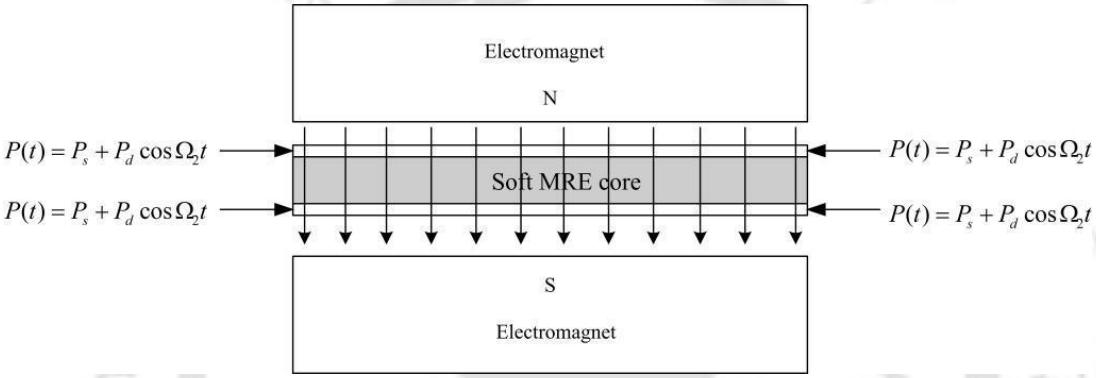

(b)

Figure 5.1 (a) Fully MRE cored composite sandwich beam and (b) composite sandwich beam subjected to magnetic field and periodic axial load.

The geometric coordinates in composite sandwich beam are shown in the Fig. 5.1. To model the mechanical behaviour of sandwich beam, kinematics relations of the faces and core, compatibility conditions of the interface layer, and the constitutive relations of the faces and core are considered. For the skins,

$$\varepsilon_{xt} = \frac{\partial u_t}{\partial x} = \frac{\partial u_{ot}}{\partial x} - (z - e_t)\frac{\partial^2 w_t}{\partial x^2} \qquad \frac{h_c}{2} \le z \le \frac{h_c}{2} + h_t \qquad e_t = \frac{h_t + h_c}{2} \tag{5.1}$$

$$\varepsilon_{xb} = \frac{\partial u_b}{\partial x} = \frac{\partial u_{ob}}{\partial x} - (z + e_b)\frac{\partial^2 w_b}{\partial x^2} \qquad -h_b - \frac{h_c}{2} \le z \le -\frac{h_c}{2} \qquad e_b = \frac{h_b + h_c}{2} \tag{5.2}$$

where, u_t and u_b the longitudinal displacements of the top and bottom skins, u_{ot} and u_{ob} are the longitudinal displacements of the neutral axis of the top and bottom skins respectively. ε_{xt} and ε_{xb} are the axial strains of top and bottom skins respectively. w_t and w_b are the transverse displacement of the top and bottom skins

z_t and z_b are the vertical coordinate of top and bottom skins which are measured from the centre line of the respective skin. Assuming, the core transverse and axial displacements are linearly dependent on coordinate *z*. The axial strain can be written as,

$$\varepsilon_{xc} = \frac{\partial u_c}{\partial x} = \left(\frac{\frac{\partial u_{0t}}{\partial x} + \frac{\partial u_{0b}}{\partial x}}{2} + \frac{h_t \frac{\partial^2 w_t}{\partial x^2} - h_b \frac{\partial^2 w_b}{\partial x^2}}{4} \right) + \left(\frac{\frac{\partial u_{0t}}{\partial x} - \frac{\partial u_{0b}}{\partial x}}{h_c} + \frac{h_t \frac{\partial^2 w_t}{\partial x^2} + h_b \frac{\partial^2 w_b}{\partial x^2}}{2h_c} \right) z \tag{5.3}$$

where, u_c and ε_{xc} are the axial displacement and strain of the core respectively. Appling the classical theory of the beam for face sheets, the strain-displacement relations can be calculated as,

$$\varepsilon_{zt} = \frac{\partial w_t}{\partial z} = 0,\ \varepsilon_{zb} = \frac{\partial w_b}{\partial z} = 0,\ \gamma_{xzt} = 2\varepsilon_{xzt} = 0,\ \gamma_{xzb} = 2\varepsilon_{xzb} = 0 \text{ and } \varepsilon_{zc} = \frac{\partial w_c}{\partial z} = \frac{w_t - w_b}{h_c}$$

$$\gamma_c = 2\varepsilon_{xzc} = \frac{\partial w_c}{\partial x} + \frac{\partial u_c}{\partial z} = \left(\frac{u_{0t} - u_{0b}}{h_c} + \frac{\left(h_t + h_c\right)\frac{\partial w_t}{\partial x} + \left(h_b + h_c\right)\frac{\partial w_b}{\partial x}}{2h_c} \right) + \left(\frac{\frac{\partial w_t}{\partial x} - \frac{\partial w_b}{\partial x}}{h_c} \right) z \tag{5.4}$$

where, ε_{zt}, ε_{zb} and ε_{zc} are the transverse strains of top skin, bottom skin and core respectively. γ_{xzt}, γ_{xzb} and γ_c are the shear strains of top skin, bottom skin and core respectively.

Now ignoring the stress in *y* direction: $\tau_{xy} = \tau_{zy} = \sigma_{yy} = 0.\ \gamma_{zy} = 0,\ \gamma_{xy} \neq \varepsilon_{yy} \neq 0$

The potential energy of top layer can be written as:

$$U_t = \frac{1}{2}\int_{Vt} \left(\sigma_{xt}\varepsilon_{xt} + \sigma_{zt}\varepsilon_{zt} + \tau_{xzt}\gamma_{xzt} \right) dV \tag{5.5}$$

The stress-strain relations for top composite face can be written as (Kaw, 1997):

$$\begin{Bmatrix} \sigma_{xt} \\ \sigma_{zt} \\ \tau_{xzt} \end{Bmatrix} = \begin{bmatrix} \bar{Q}_{11})_t & \bar{Q}_{13})_t & \bar{Q}_{15})_t \\ \bar{Q}_{13})_t & \bar{Q}_{33})_t & \bar{Q}_{35})_t \\ \bar{Q}_{15})_t & \bar{Q}_{35})_t & \bar{Q}_{55})_t \end{bmatrix} \begin{Bmatrix} \varepsilon_{xt} \\ \varepsilon_{zt} \\ \gamma_{xzt} \end{Bmatrix} \tag{5.6}$$

where $\bar{Q}_{ij}\big)_t$, are the elements of transformed reduced stiffness matrix of the top face. By using strain-displacement, stress-strain relations, the strain energy of top face is written as:

$$U_t = \frac{\bar{Q}_{11}\big)_t}{2}\int_0^L \left(A_t\left(\frac{\partial u_{0t}}{\partial x}\right)^2 + I_t\left(\frac{\partial^2 w_t}{\partial x^2}\right)^2 \right) dx \tag{5.7}$$

where, A_t and I_t are area and moment of inertia of top face, respectively. Similarly, the potential energy of bottom skin can be obtained as:

$$U_b = \frac{\bar{Q}_{11}\big)_b}{2}\int_0^L \left(A_b\left(\frac{\partial u_{0b}}{\partial x}\right)^2 + I_b\left(\frac{\partial^2 w_b}{\partial x^2}\right)^2 \right) dx \tag{5.8}$$

where, $\bar{Q}_{11}\big)_b$, A_t and I_t are element of transformed reduced stiffness matrix, area and moment of inertia of bottom skin, respectively.

Assuming the core material is isotropic (Kallio, 2005); its stress-strain relationship can be written as (Kaw, 1997):

$$\begin{Bmatrix} \sigma_{xc} \\ \sigma_{zc} \\ \tau_{xzc} \end{Bmatrix} = \begin{bmatrix} Q_{11}\big)_c & Q_{13}\big)_c & 0 \\ Q_{13}\big)_c & Q_{33}\big)_c & 0 \\ 0 & 0 & Q_{55}\big)_c \end{bmatrix} \begin{Bmatrix} \varepsilon_{xc} \\ \varepsilon_{zc} \\ \gamma_{xzc} \end{Bmatrix} \tag{5.9}$$

where $Q_{ij}\big)_c$, are stiffness coefficients. By using strain-displacement and stress-strain relation, the potential energy of core is written as:

$$U_c = \frac{1}{2}\int_0^L \Bigg[Q_{11}\big)_c \Bigg(A_c \left(\frac{\frac{\partial u_{0t}}{\partial x} + \frac{\partial u_{0b}}{\partial x}}{2} + \frac{h_t\frac{\partial^2 w_t}{\partial x^2} - h_b\frac{\partial^2 w_b}{\partial x^2}}{4} \right)^2 + I_c \left(\frac{\frac{\partial u_{0t}}{\partial x} - \frac{\partial u_{0b}}{\partial x}}{h_c} + \frac{h_t\frac{\partial^2 w_t}{\partial x^2} + h_b\frac{\partial^2 w_b}{\partial x^2}}{2h_c} \right)^2 \Bigg) + 2Q_{13}\big)_c A_c \left(\frac{\frac{\partial u_{0t}}{\partial x} + \frac{\partial u_{0b}}{\partial x}}{2} + \frac{h_t\frac{\partial^2 w_t}{\partial x^2} - h_b\frac{\partial^2 w_b}{\partial x^2}}{4} \right) \left(\frac{w_t - w_b}{h_c} \right) +$$

$$Q_{33})_c A_c \left(\frac{w_t - w_b}{h_c}\right)^2 + Q_{55})_c \left(A_c \left(\frac{u_{0t} - u_{0b}}{h_c} + \frac{(h_t + h_c)\frac{\partial w_t}{\partial x} + (h_b + h_c)\frac{\partial w_b}{\partial x}}{2h_c} \right)^2 \right.$$

$$\left. + I_c \left(\frac{w_t - w_b}{h_c}\right)^2 \right] dx \tag{5.10}$$

The kinetic energy of the beam due to extension, bending and rotation is:

$$T = \frac{1}{2}\int_0^L \left[\rho_t A_t \left(\frac{\partial u_{0t}}{\partial t}\right)^2 + \rho_b A_b \left(\frac{\partial u_{0b}}{\partial t}\right)^2 + \rho_t A_t \left(\frac{\partial w_t}{\partial t}\right)^2 + \rho_b A_b \left(\frac{\partial w_b}{\partial t}\right)^2 + \rho_t I_t \left(\frac{\partial^2 w_t}{\partial x \partial t}\right)^2 \right.$$

$$+ \rho_b I_b \left(\frac{\partial^2 w_b}{\partial x \partial t}\right)^2 + \rho_c A_c \left(\frac{\frac{\partial u_{0t}}{\partial t} + \frac{\partial u_{0b}}{\partial t}}{2} + \frac{h_t \frac{\partial w_t}{\partial t} - h_b \frac{\partial w_b}{\partial t}}{4} \right)^2 + \rho_c I_c \left(\frac{\frac{\partial u_{0t}}{\partial t} - \frac{\partial u_{0b}}{\partial t}}{h_c} \right.$$

$$\left. \left. + \frac{h_t \frac{\partial^2 w_t}{\partial x \partial t} + h_b \frac{\partial^2 w_b}{\partial x \partial t}}{2h_c} \right)^2 + \rho_c A_c \left(\frac{\frac{\partial w_t}{\partial t} + \frac{\partial w_b}{\partial t}}{2} \right)^2 + \rho_c I_c \left(\frac{\frac{\partial w_t}{\partial t} - \frac{\partial w_b}{\partial t}}{h_c} \right)^2 \right] dx \tag{5.11}$$

In the FEM modelling of the sandwich beam a standard beam element with two end nodes with six degrees of freedom (DOF) for each node is considered as shown in Fig. 5.2. The DOF include the transverse, axial and rotational displacements of top and bottom composite faces of the sandwich beam.

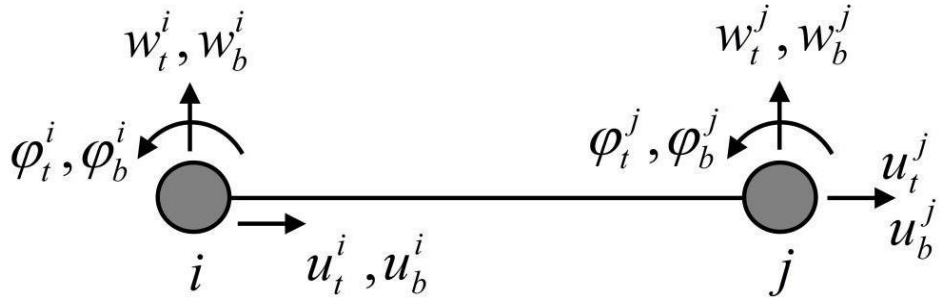

Figure 5.2 Beam element with two end nodes and six DOF for each node.

The axial and transverse displacements of an element can be determined in terms of the displacements of the two nodes as follows:

$$u(x,t) = N_u(x)q(t) \text{ and } w(x,t) = N_w(x)q(t) \tag{5.12}$$

where $q(t)$ is the displacement vector for an element as:

$$q(t)=\left\{w_t^i\ \varphi_t^i\ u_t^i\ w_b^i\ \varphi_b^i\ u_b^i\ w_t^j\ \varphi_t^j\ u_t^j\ w_b^j\ \varphi_b^j\ u_b^j\right\}^{\mathrm{T}}$$

and N_w and N_u are common linear and cubic polynomial beam shape functions. The shape functions are (Rao, 2005),

$$\left.\begin{aligned}
N_{wt}&=\left\{1-\frac{3x^2}{l_e^2}+\frac{2x^3}{l_e^3}\ \ x-\frac{3x^2}{l_e}+\frac{x^3}{l_e^2}\ \ 0\ 0\ 0\ 0\ \ \frac{3x^2}{l_e^2}+\frac{2x^3}{l_e^3}\ \ -\frac{x^2}{l_e}+\frac{x^3}{l_e^2}\ \ 0\ 0\ 0\ 0\right\}\\
N_{ut}&=\left\{0\ 0\ 1-\frac{x}{l_e}\ \ 0\ 0\ 0\ 0\ 0\ \ \frac{x}{l_e}\ \ 0\ 0\ 0\right\}\\
N_{wb}&=\left\{0\ 0\ 0\ 1-\frac{3x^2}{l_e^2}+\frac{2x^3}{l_e^3}\ \ x-\frac{3x^2}{l_e}+\frac{x^3}{l_e^2}\ \ 0\ 0\ 0\ 0\ \ \frac{3x^2}{l_e^2}+\frac{2x^3}{l_e^3}\ \ -\frac{x^2}{l_e}+\frac{x^3}{l_e^2}\ \ 0\right\}\\
N_{ub}&=\left\{0\ 0\ 0\ 0\ 0\ 1-\frac{x}{l_e}\ \ 0\ 0\ 0\ 0\ 0\ \ \frac{x}{l_e}\right\}
\end{aligned}\right\} \tag{5.13}$$

The derived potential energy and kinetic energy terms can be rewritten in nodal displacement variables for an element with length l_e as follows:

$$U^e=\frac{1}{2}\left\{q^e\right\}^T\left[K^e\right]\left\{q^e\right\} \tag{5.14}$$

The stiffness matrix $\left[K^e\right]$ for one element is obtained by summation of the stiffness matrices of the top face, bottom face and core, as:

$$\left[K_u^e\right]=\left[K_t^e\right]+\left[K_b^e\right]+\left[K_s^e\right] \tag{5.15}$$

where, $\left[K_t^e\right]$,$\left[K_b^e\right]$ and $\left[K_s^e\right]$ are the stiffness matrices for the top face, bottom face and core, respectively.

$$\left[K_t^e\right]=\left(\hat{Q}_{11}\right)_t A_t\int_0^{l_e}\left[\frac{\partial N_{ut}}{\partial x}\right]^{\mathrm{T}}\left[\frac{\partial N_{ut}}{\partial x}\right]dx+\left(\bar{Q}_{11}\right)_t I_t\int_0^{l_e}\left[\frac{\partial^2 N_{wt}}{\partial x^2}\right]^{\mathrm{T}}\left[\frac{\partial^2 N_{wt}}{\partial x^2}\right]dx$$

$$\left[K_b^e\right]=\left(\hat{Q}_{11}\right)_b A_b\int_0^{l_e}\left[\frac{\partial N_{ub}}{\partial x}\right]^{\mathrm{T}}\left[\frac{\partial N_{ub}}{\partial x}\right]dx+\left(\bar{Q}_{11}\right)_b I_b\int_0^{l_e}\left[\frac{\partial^2 N_{wb}}{\partial x^2}\right]^{\mathrm{T}}\left[\frac{\partial^2 N_{wb}}{\partial x^2}\right]dx$$

$$\left[K_s^e\right]=\left(Q_{11}\right)_c A_c\int_0^{l_e}\left[\frac{\frac{\partial N_{ut}}{\partial x}+\frac{\partial N_{ub}}{\partial x}}{2}+\frac{h_t\frac{\partial^2 N_{wt}}{\partial x^2}-h_b\frac{\partial^2 N_{wb}}{\partial x}}{4}\right]^{\mathrm{T}}\left[\frac{\frac{\partial N_{ut}}{\partial x}+\frac{\partial N_{ub}}{\partial x}}{2}\right.$$

$$+\frac{h_t\frac{\partial^2 N_{wt}}{\partial x^2}-h_b\frac{\partial^2 N_{wb}}{\partial x}}{4}\Bigg]dx+Q_{11}\Big)_c I_c\int_0^{l_e}\Bigg[\frac{\frac{\partial N_{ut}}{\partial x}-\frac{\partial N_{ub}}{\partial x}}{h_c}+\frac{h_t\frac{\partial^2 N_{wt}}{\partial x^2}+h_b\frac{\partial^2 N_{wb}}{\partial x}}{2h_c}\Bigg]^{\mathrm{T}}$$

$$\Bigg[\frac{\frac{\partial N_{ut}}{\partial x}-\frac{\partial N_{ub}}{\partial x}}{h_c}+\frac{h_t\frac{\partial^2 N_{wt}}{\partial x^2}+h_b\frac{\partial^2 N_{wb}}{\partial x}}{2h_c}\Bigg]dx+Q_{13}\Big)_c A_c\int_0^{l_e}\Bigg[\frac{\frac{\partial N_{ut}}{\partial x}+\frac{\partial N_{ub}}{\partial x}}{2}+$$

$$\Bigg[\frac{h_t\frac{\partial^2 N_{wt}}{\partial x^2}-h_b\frac{\partial^2 N_{wb}}{\partial x^2}}{4}\Bigg]^{\mathrm{T}}\Bigg[\frac{N_{wt}-N_{wb}}{h_c}\Bigg]dx+Q_{33}\Big)_c A_c\int_0^{l_e}\Bigg[\frac{N_{wt}-N_{wb}}{h_c}\Bigg]^{\mathrm{T}}\Bigg[\frac{N_{wt}-N_{wb}}{h_c}\Bigg]dx+$$

$$Q_{55}\Big)_c A_c\int_0^{l_e}\Bigg[\frac{N_{ut}-N_{ub}}{h_c}+\frac{\left(h_t+h_c\right)\frac{\partial N_{wt}}{\partial x}+\left(h_b+h_c\right)\frac{\partial N_{wb}}{\partial x}}{2h_c}\Bigg]^{\mathrm{T}}\Bigg[\frac{N_{ut}-N_{ub}}{h_c}$$

$$+\frac{\left(h_t+h_c\right)\frac{\partial N_{wt}}{\partial x}+\left(h_b+h_c\right)\frac{\partial N_{wb}}{\partial x}}{2h_c}\Bigg]dx+Q_{55}\Big)_c I_c\int_0^{l_e}\Bigg[\frac{w_t-w_b}{h_c}\Bigg]^{\mathrm{T}}\Bigg[\frac{w_t-w_b}{h_c}\Bigg]dx$$

The kinetic energy can be rewritten in nodal displacement variables for an element with length l_e as follows:

$$T^e=\frac{1}{2}\left\{\dot{q}^e\right\}^T\left[M^e\right]\left\{\dot{q}^e\right\} \tag{5.16}$$

where $\left[M^e\right]$ is the elemental mass matrix for one element.

$$\left[M^e\right]=\rho_t A_t\int_0^{l_e}\left[N_{ut}\right]^{\mathrm{T}}\left[N_{ut}\right]dx+\rho_b A_b\int_0^{l_e}\left[N_{ub}\right]^{\mathrm{T}}\left[N_{ub}\right]dx+\rho_t A_t\int_0^{l_e}\left[N_{wt}\right]^{\mathrm{T}}\left[N_{wt}\right]dx$$

$$+\rho_b A_b\int_0^{l_e}\left[N_{wb}\right]^{\mathrm{T}}\left[N_{wb}\right]dx+\rho_t I_t\int_0^{l_e}\Bigg[\frac{\partial N_{wt}}{\partial x}\Bigg]^{\mathrm{T}}\Bigg[\frac{\partial N_{wt}}{\partial x}\Bigg]dx+\rho_b I_b\int_0^{l_e}\Bigg[\frac{\partial N_{wb}}{\partial x}\Bigg]^{\mathrm{T}}\Bigg[\frac{\partial N_{wb}}{\partial x}\Bigg]dx$$

$$+\rho_c A_c\int_0^{l_e}\Bigg[\frac{N_{ut}+N_{ub}}{2}+\frac{h_t\frac{\partial N_{wt}}{\partial x}-h_b\frac{\partial N_{wb}}{\partial x}}{4}\Bigg]^{\mathrm{T}}\Bigg[\frac{N_{ut}+N_{ub}}{2}+\frac{h_t\frac{\partial N_{wt}}{\partial x}-h_b\frac{\partial N_{wb}}{\partial x}}{4}\Bigg]dx$$

$$+\rho_c I_c \int_0^{l_e} \left[\frac{N_{ut}-N_{ub}}{h_c} + \frac{h_t \frac{\partial N_{wt}}{\partial x} + h_b \frac{\partial N_{wb}}{\partial x}}{2h_c} \right]^{\mathrm{T}} \left[\frac{N_{ut}-N_{ub}}{h_c} + \frac{h_t \frac{\partial N_{wt}}{\partial x} + h_b \frac{\partial N_{wb}}{\partial x}}{2h_c} \right] dx$$

$$+\rho_c A_c \int_0^{l_e} \left[\frac{N_{wt}+N_{wb}}{2} \right]^{\mathrm{T}} \left[\frac{N_{wt}+N_{wb}}{2} \right] dx + \rho_c I_c \int_0^{l_e} \left[\frac{N_{wt}-N_{wb}}{h_c} \right]^{\mathrm{T}} \left[\frac{N_{wt}-N_{wb}}{h_c} \right] dx$$

Employing Hamilton's principle, described as

$$\delta \int_{t_1}^{t_2} \left(T^e - U^e + W^e \right) dt = 0 \tag{5.17}$$

the governing equations of motion of the sandwich beam element in the finite element form are derived for the following loading conditions.

5.2.1 Sandwich Beam Subjected to a Transverse Harmonic Force on the Top Skin

The work done by the transverse harmonic force Q_t due to transverse displacement of the top skin can be written as,

$$W = \int_0^L Q_t w_t dx \tag{5.18}$$

The work done by transverse harmonic force can be rewritten in nodal displacement variables for an element with length l_e as follows:

$$W^e = \frac{1}{2} \{q^e\}^{\mathrm{T}} \left[F_t^e \right] \{q^e\} \tag{5.19}$$

where, $\left[F_t^e \right]$ is the force vector for one element.

$$\{F_t^e\} = \left\{ 0 \quad 0 \quad . \quad . \quad 0 \quad \int_0^{l_e} Q_t \left[N_{wt} \right]^e dx \quad 0 \quad 0 \quad 0 \quad 0 \quad 0 \right\} \tag{5.20}$$

The governing equations of motion for the sandwich beam element in the finite element form can be obtained as

$$\left[M^e \right] \{\ddot{q}^e\} + \left[K^e \right] \{q^e\} = \{F_t^e\} \tag{5.21}$$

$\left[M^e \right]$ and $\left[K^e \right]$, are the elemental mass and stiffness matrices, respectively and $\{F_t^e\}$ is the elemental force vector. Assembling the mass and the stiffness matrices

and force vector for all the elements, yields the global governing equation of motion of MRE embedded sandwich beam as follows:

$$[M]\{\ddot{q}\}+[K]\{q\}=\{F_t\} \tag{5.22}$$

where, $[M],[K]$ and $\{F_t\}$ are the global mass and stiffness matrices and global force vector, respectively. For the MRE embedded sandwich beam, the matrices $[M]$and$[K]$ are formulated by imposing compatibility conditions which are identical transverse and axial displacements and the slopes at the interfaces of the MRE and non MRE patches within the core of the sandwich beam. The frequency response at an observing point, subjected to the point force at given excitation location is investigated. Assuming that a harmonic transverse point load, $Q_t = Q_0 e^{i\omega t}$, is applied at the tip point of the beam. In the harmonic excitation, the vector of the nodal degrees of freedom is considered as $\{q\}=\{q_0\}e^{i\omega t}$. Using Eq. (5.21) and above considerations, the frequency response is obtained as:

$$\left(-\omega^2[M]+[K]\right)\{q_0\}=\left\{0 \quad . \quad . \quad . \quad 0 \quad Q_0[N_{wt}]\right\|_{x=L} \quad 0 \quad 0 \quad 0 \quad 0 \quad 0\Big\}^{\mathrm{T}} \tag{5.23}$$

5.2.2 Sandwich Beam Subjected to Periodic Axial Load

The work done by the periodic axial load $P(t)$ due to independent transverse displacements of the top and bottom skins can be written as,

$$W=\frac{1}{2}\int_0^L P(t)\left(\frac{\partial w_t}{\partial x}\right)^2 dx+\frac{1}{2}\int_0^L P(t)\left(\frac{\partial w_b}{\partial x}\right)^2 dx \tag{5.24}$$

Using critical Euler's buckling load P_{cr}, the periodic axial load can be written as, $P(t)=\alpha P_{cr}+\beta P_{cr}\cos\Omega_2 t$, where, $P_s=\alpha P_{cr}$ and $P_d=\beta P_{cr}$. α and β are the static and dynamic load factors, respectively.

The Eq. (5.24) can be rewritten in nodal displacement variables for an element with length l_e as follows:

$$W^e=\frac{1}{2}P(t)\{q^e\}^{\mathrm{T}}\left[F_f^e\right]\{q^e\} \tag{5.25}$$

where, $\left[F_f^e\right]$is the geometric stiffness matrix for one element.

$$\left[F_f^e\right]=\int_0^{l_e}\left[N_{wt}\right]^{\mathrm{T}}\left[N_{wt}\right]dx+\int_0^{l_e}\left[N_{wb}\right]^{\mathrm{T}}\left[N_{wb}\right]dx \tag{5.26}$$

The governing equations of motion for the sandwich beam element in the finite element form can be obtained as

$$\left[M^e\right]\left\{\ddot{q}^e\right\}+\left[K^e\right]\left\{q^e\right\}-\beta P_{cr}\cos\Omega_2 t\left[F_f^e\right]\left\{q^e\right\}=0 \tag{5.27}$$

where, $\left[K^e\right]=\left[K_u^e\right]-\alpha P_{cr}\left[F_f^e\right]$.

Assembling the all elemental matrices for all the elements, the global governing equation of motion of MRE embedded sandwich beam as follows:

$$[M]\{\ddot{q}\}+[K]\{q\}-\beta P_{cr}\cos\Omega_2 t\left[F_f\right]\{q\}=0 \tag{5.28}$$

Since MRE is a viscoelastic material it provides damping effects on the sandwich beam. The equation of motion can be rewritten as.

$$[M]\{\ddot{q}\}+[K]\{q\}+[C]\{q\}-\beta P_{cr}\cos\Omega_2 t\left[F_f\right]\{q\}=0 \tag{5.29}$$

where, $[C]=i\eta_c[K_S]$ is the damping effect on the sandwich beam and η_c is the loss factor of the MRE.

To reduce the size of the matrix the Guyan reduction method as discussed in the chapter 4 is used and the Eq. (5.28) and Eq. (5.29) can be written as

$$\left[M_r\right]\{\ddot{q}_m\}+\left[K_r\right]\{q_m\}-\beta P_{cr}\cos\Omega_2 t\left[F_{fr}\right]\{q_m\}=0 \tag{5.30}$$

$$\left[M_r\right]\{\ddot{q}_m\}+\left[K_r\right]\{q_m\}+\left[C_r\right]\{q_m\}-\beta P_d\cos\Omega_2 t\left[F_{fr}\right]\{q_m\}=0 \tag{5.31}$$

where,

$\left[M_r\right]=[T]^T[M][T],\left[K_r\right]=[T]^T[K][T],\left[C_r\right]=[T]^T[C][T]$ and $\left[F_{fr}\right]=[T]^T\left[F_f\right][T]$

The above Eqs. (5.30) and (5.31) are the Mathieu-Hill equation with a periodic coefficient for a system without and with damping effect of MRE.

5.2.3 Dynamic stability analysis

For the analysis of stability of sandwich beams the method discussed in the previous chapter is used and the equations for obtaining the instability regions are given below.

5.2.3.1 *Without Damping Effect of MRE*

The eigenvalue equations without damping damping effect of mre to obtain the instability regions;

$$\left|\left[K_r\right] \pm \beta P_{cr}\left[K_{fr}\right] - \frac{\Omega_2^2}{4}\left[M_r\right]\right| = 0 \tag{5.32}$$

5.2.3.2 *With Damping Effect of MRE*

The eigenvalue equations in matrix form with damping effect of MRE;

$$\begin{vmatrix} \left[K_r\right] + \beta P_{cr}\left[F_{fr}\right] - \frac{\Omega_2^2}{4}\left[M_r\right] & -\frac{\Omega_2}{2}\left[C_r\right] \\ \frac{\Omega_2}{2}\left[C_r\right] & \left[K_r\right] - \beta P_{cr}\left[F_{fr}\right] - \frac{\Omega_2^2}{4}\left[M_r\right] \end{vmatrix} = 0 \tag{5.33}$$

Hereafter, the Eqs. (5.32) and (5.33) are referred as the equation of boundary frequencies. The above equations are used to find the boundaries of principal instability regions of the system with and without damping effect of MRE.

5.3 Results and Discussions

The properties of a three layer sandwich beam with composite skins are strongly influenced by many core materials and structure related parameters such as beam geometry and boundary conditions. The dynamic characteristics of the sandwich beam can be improved and actively changed by a MRE core with the application of magnetic field. In this section, first the proposed finite element formulation is validated. Then the formulation is used to investigate the dynamic characteristics of the MRE based sandwich beam with conductive faces. The effect of various system parameters such as magnetic field, fibre angle and other system parameters has been studied.

5.3.1 Validation of the Developed Finite Element Formulation

Case 1. To validate the FE formulation, experiments for the free and forced vibration of sandwich beams with soft flexible foam core and aluminum skins have been carried out. The same experimental set up discussed in chapter 4 is used to find

the natural frequencies of the sandwich beams. Here two sandwich beam samples with span, $L = 435\,\text{mm}$; width, $b = 30\,\text{mm}$, the top and bottom skins thickness, $h_t = h_b = 2\,\text{mm}$, core thicknesses $h_c = 12\,\text{mm}$ and $h_c = 20$ mm have been taken for experimental validation. Figure 5.3 shows the clamped free sandwich beam. The accelerometers are set one below another at the free end on the top and bottom skins of the test specimen. Following the same experimental procedure discussed in chapter 4, the free vibration time and frequency response are obtained using PULSE analyser software as shown in Fig. 5.4 for the specimen with 12mm core thickness.

Figure 5.3 Sandwich beam with flexible foam core

It is found that, the transverse displacements of the top and bottom skins have different amplitude having 180^0 phase difference between them. This is due to the fact that the thickness of the foam core changes during deflection of the beam. Hence, the assumption of having unequal transverse displacement in the top and bottom skin in a soft cored sandwich beam is validated. Similar observations have been made for the specimen with 20 mm core thickness.

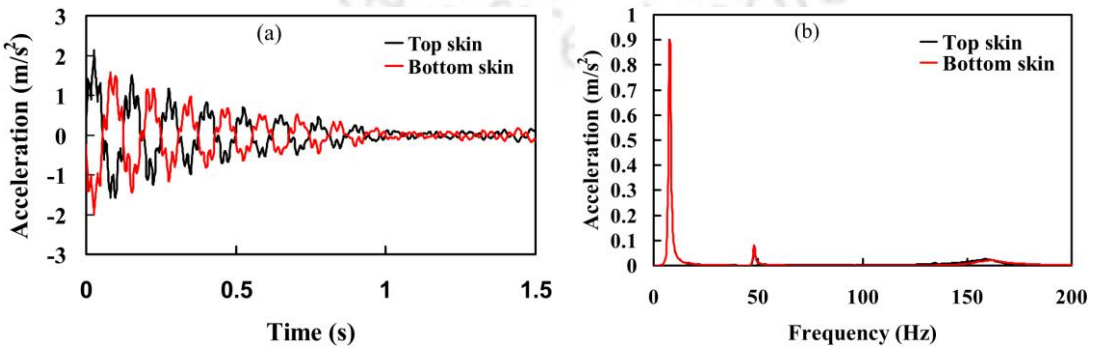

Figure 5.4 (a) Time response and (b) frequency response of sandwich beam with soft foam core of 12 mm thickness.

The variation of natural frequencies for both the specimens is given in Table 5.1 which have been compared with the developed finite element code. The same material properties of aluminum discussed in chapter 4 are taken. The properties of foam core such as density, Young's modulus and shear modulus are 38 kg/m^{3,} 20.513 KPa and 8.9187 KPa, respectively. The frequencies obtained from the present model are compared with the experimental result and are presented in Table 5.1. It is observed that the difference of natural frequency obtained by FEM and the experiment are relatively small.

Table 5.1 Comparison of natural frequencies obtained from present experiment and FE analysis of a fully flexible foam cored clamped free sandwich beam.

Core thickness (mm)	Mode	Natural frequencies (Hz)	
		Experimental	FEM
12	1	7.50	9.47
	2	48.00	57.09
	3	161.00	158.87
20	1	8.00	9.55
	2	45.00	56.56
	3	128.00	156.91

Case 2. In this case, modal frequencies obtained from the present model are compared with that of the Ahmed, (1972) and Hwu *et al.*, (2004). The dimensions and the properties of materials of the sandwich beam are taken from Ahmed, (1972), which are $L = 711.2$ mm, $h_t = h_b = 0.4572$ mm, $h_c = 12.7$ mm, $E_t = E_b = 68.9$ GPa, $\rho_t = \rho_b = 2680$ kg/m^3, $\rho_c = 32.8$ kg/m^3 and $G_c = 0.08274$ GPa. Here E_t and E_b are the Young's modulus of isotropic skins. The frequencies obtained from the FE formulations are presented in Table 5.2. The frequencies obtained by FE model using higher order theory are found to be in good agreement with those obtained by Ahmed, (1972) and Hwu *et al.*, (2004). FE model using higher order theory yields higher values of natural frequencies which are in the expected line. This validates the developed code using FE formulation for the sandwich beam.

Case 3. For numerical analysis a cantilevered sandwich beam of length L = 230 mm and width b = 30 mm, with MRE core and graphite-epoxy skins has been

considered. The thickness of top skin, core and bottom skin are h_t = 0.1 mm, h_c =3 mm and h_b =0.1 mm, respectively. Material properties of the composite skins are taken from Pradeep *et al*., (2007) and are presented in Table 5.3.

Table 5.2 Comparison of modal frequencies (Hz).

Mode	Ahmed [14]	Hwu et al [15]	Present FE formulation
1	32	32	36
2	193	193	211
3	499	509	538
4	888	923	944
5	1320	1402	1393

Table 5.3 Material properties of composite skins of the sandwich beam

Young's Modulus (GPa)	Density ρ (kg/m^3)	Poisson's ratio	Shear Modulus (GPa)
E_1 = 137, E_2 = 8.96	1600	ν_{12} = 0.3	G_{12} = 7.1

Here, E_1, E_2, ν_{12} and G_{12} are the Young's modulus in direction 1, Young's modulus in direction 2, Poisson's ratio and in plane shear modulus respectively. Here the properties of the MRE material developed in the present work are taken for analysis (chapter 6). The shear storage modulus $\left(G_c^{'}\right)$ and shear loss modulus $\left(G_c^{''}\right)$ of fabricated isotropic MREs (chapter 6) are expressed by the following second-order polynomial functions with respect to the magnetic field intensity B_s.

$$G_c^{'} = 0.104B_s^2 + 0.098B_s + 0.301\times10^6 \text{ Pa}$$

$$G_c^{''} = 0.0024B_s^2 + 0.005B_s + 0.0415\times10^6 \text{ Pa}$$

Taking the above physical dimensions and material properties of the sandwich beam, the obtained modal frequencies are compared with the frequencies obtained from the FE analysis carried out by Sastri, (2012) using classical sandwich beam theory. These results are presented in Table 5.4. Though the results are found to be sufficiently close, the natural frequencies obtained using the flexible core are found to be higher than those obtained using classical theory. This is due to the fact that in

case of classical sandwich beam theory only the strain energy due to shear deformation of the core has been considered and in case of flexible core in addition to shear deformation strain energy due to transverse and axial deformations have also been considered. It is observed that at the higher modes the modal frequencies are strongly influenced by magnetic field.

Table 5.4 Comparison of modal frequencies (Hz) with Sastri (2012).

Fiber orientation ϕ (degree)	Magnetic field density, B_s (T)	Mode No.	Modal frequencies (Hz)	
			Sastri, (2012)	Present
0	0	1	12.79	12.93
		2	39.11	39.54
		3	68.51	69.11
		4	97.55	98.61
		5	128.03	129.93
		6	159.79	162.96
	0.5	1	14.03	14.21
		2	43.06	43.59
		3	75.96	76.65
		4	108.04	109.20
		5	141.51	143.53
		6	176.06	179.37
90	0	1	7.39	7.66
		2	29.23	29.71
		3	59.83	60.38
		4	88.75	89.20
		5	117.68	118.07
		6	146.04	146.39
	0.5	1	7.60	7.90
		2	31..42	31.99
		3	65.31	66.02
		4	97.86	98.45
		5	130.35	130.85
		6	162.17	162.60

5.3.2 Free Vibration Analysis

The modal frequencies and loss factors of the system are calculated from the stiffness and mass matrices (Eq. 5.28). Since the core shear modulus is the complex

value, the eigenvalues are complex. The ratio of imaginary part to the real part of the each eigenvalue is the loss factor and the square root of the real part represents the natural frequency.

The effects of magnetic field (B_s), fibre angle (ϕ) and static load factor (α) on modal frequency and loss factor of the composite sandwich beam is studied. Figure 5.5 shows the effect of magnetic field on modal frequency and loss factor. It can be observed that the modal frequencies increases and system loss factor decreases by increasing the magnetic field. This increase in frequency is due to stiffening effect of composite sandwich beam. The shear modulus of MRE increases with increase in magnetic field which increases the stiffness of the bean. The effect of fibre angle is illustrated in Fig. 5.6. It shows that the modal frequencies and loss factors decrease with increase in fibre angle. This could be due to the strength and stiffness of the lamina decreases with increase in fiber angle. Figure 5.7 shows the influence of static load factor on the modal frequency and loss factor of the composite sandwich beam. It can be observed that the modal frequencies decreases and the system loss factors increases as static load factor increases. From all the above three cases it can be observed that the system modal frequency and loss factors can be changed with the variation of the magnetic field, fiber orientation and static load factor.

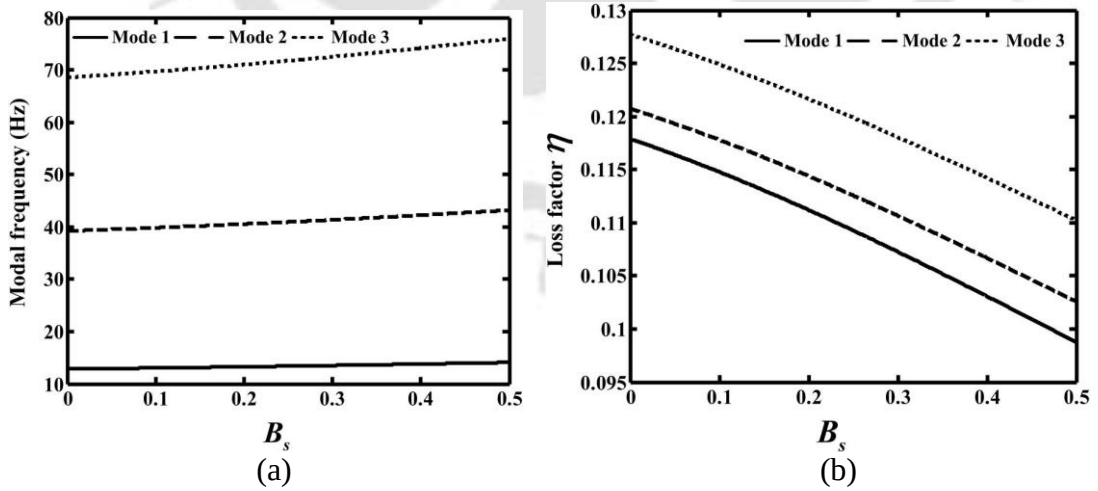

Figure 5.5 Effect of magnetic field B_s on (a) modal frequencies and (b) loss factor of the sandwich beam; $\phi = 0$.

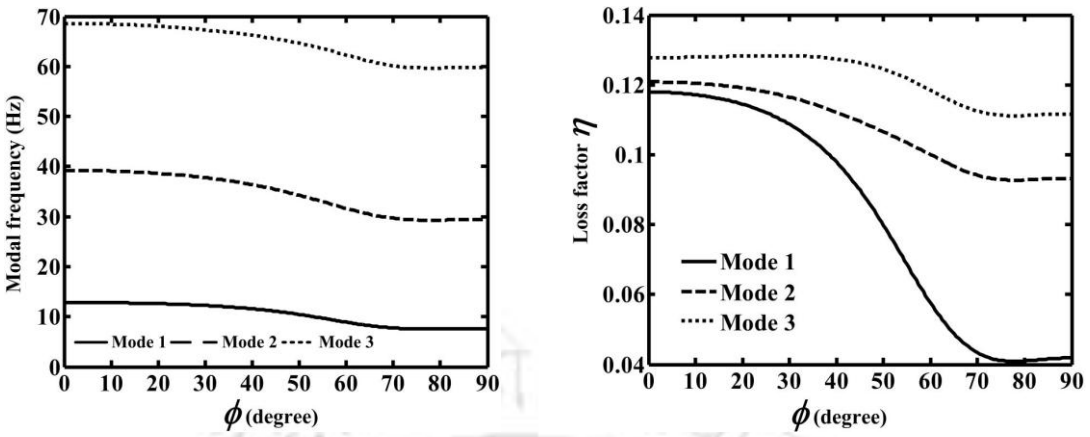

(a) (b)

Figure 5.6 Effect of composite skin fibre angle ϕ on (a) modal frequencies and (b) loss factor of the sandwich beam ($B_s = 0$).

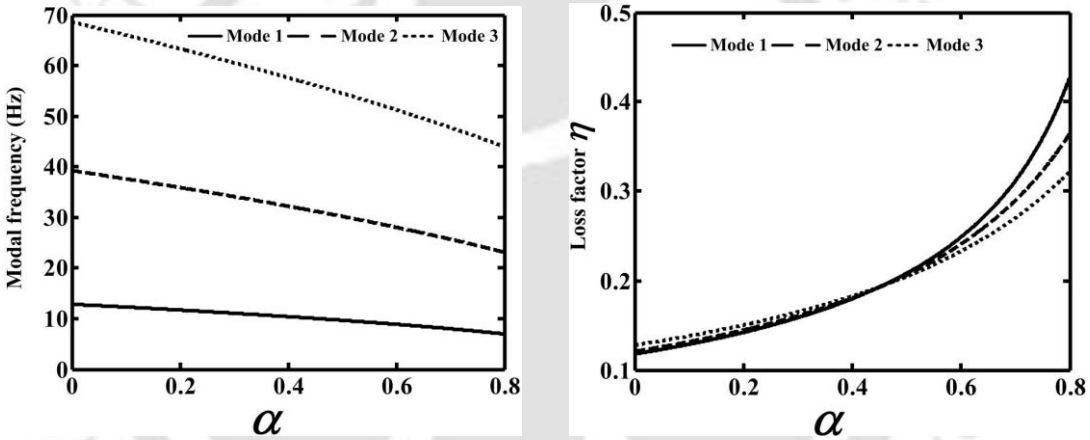

(a) (b)

Figure 5.7 Effect of static load factor α on (a) modal frequencies and (b) loss factor of the sandwich beam ($B_s = 0$ and $\phi = 0$).

5.3.3 Frequency Response Analysis

In this section the frequency response of composite sandwich beam with MRE core is presented. All of these results are obtained for neutral axis of each skins at the tip point of the composite sandwich beam. In anti-plane core situations, transverse displacement through the depth of beam is considered constant, whereas in this analysis linear variation of the transverse displacement is assumed. Transverse displacements of two skins (top and bottom), for the isotropic soft core are obtained and presented in Fig. 5.8. Fig. 5.8 shows that independency of the transverse displacement in top and bottom skins, results in none equal transverse displacement in the case of soft-core.

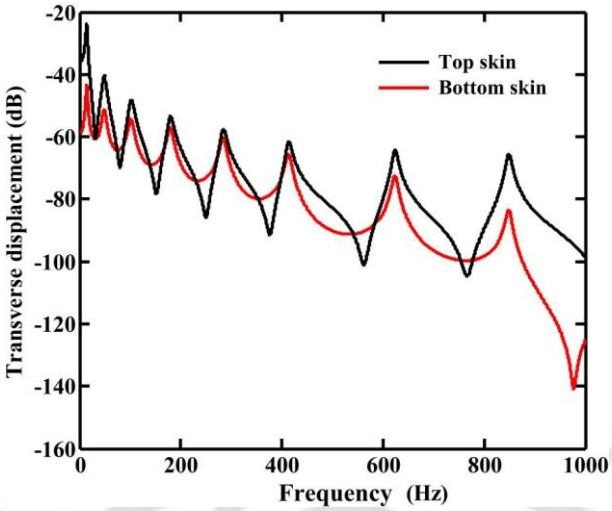

Figure 5.8 Frequency response of neutral axis tip point of skins of composite sandwich beam with soft isotropic MRE core; $B_s = 0$ and $\phi = 0$.

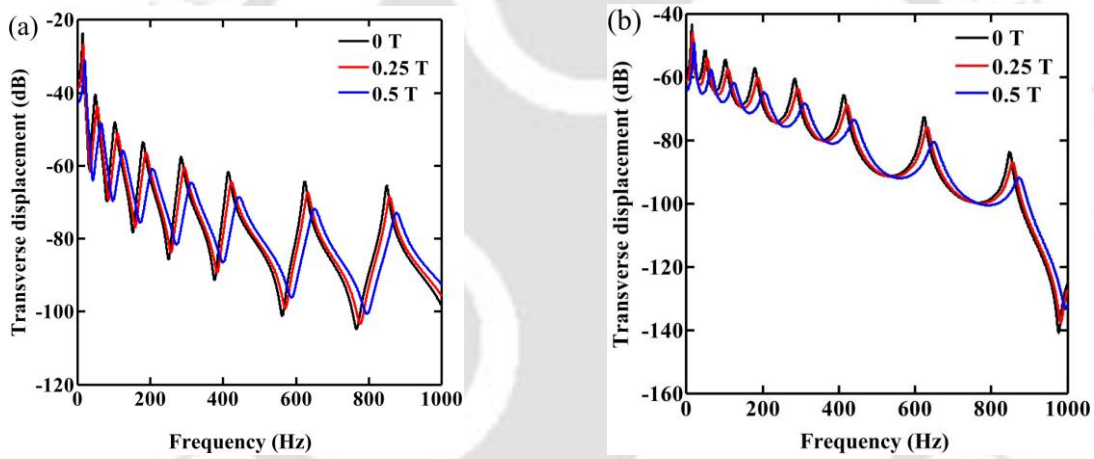

Figure 5.9 Frequency response of (a) top skin and (b) bottom skin with different magnetic field. $\phi = 0$.

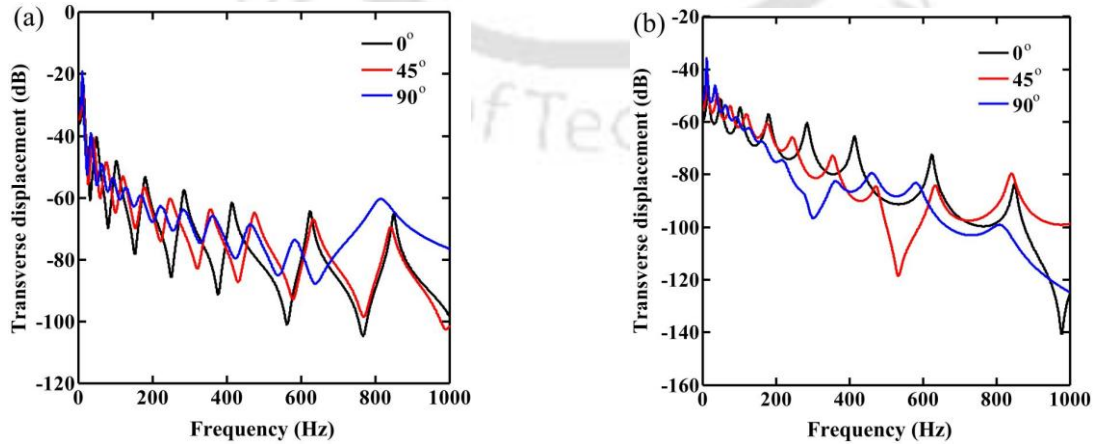

Figure 5.10 Frequency response of (a) top skin and (b) bottom skin with different fibre angle. $B_s = 0$.

Figure 5.9 (a) and (b) shows the transverse displacements of the top and bottom skins respectively, with variation of magnetic field for the isotropic soft core. It can be seen that with increase in magnetic field the resonance frequencies are shifting towards right. Also the effect of fiber angle on the frequency response of top and bottom skins is shown in Fig. 5.10 (a) and (b) respectively. But with increase in fiber angle the resonance frequencies are shifting towards left.

5.3.4 Sability Analysis of the composite Sandwich Beam Subjected to Periodic Axial Load

In this section, the stability of a MRE cored composite sandwich beam subjected to periodic axial load has been investigated by determining the parametric instability regions for the clamped free end condition. The instability regions are investigated with and without considering the damping effect of the MRE core. The influence of various system parameters such as magnetic field strength, fiber angle, static load and dynamic load on instability regions is investigated.

5.3.4.1 Stability Analysis without Damping Effect of MRE

In this section the instability regions are investigated without considering the damping effect of the MRE core. Figure 5.11 (a) shows the effect of magnetic field on the instability regions of a MRE cored composite sandwich beam with composite skins fiber angle $\phi = 0$ and static load factor $\alpha = 0$. It can be seen that the width of instability regions decreases and occurs at higher frequencies with increase in magnetic field. This attributed to the increase in the complex shear modulus of the MRE patch which increases the stiffness of the sandwich beam. Also the periodic dynamic load increases with increase in magnetic field as the Euler's critical buckling load increases. So the system can operate at higher dynamic load. For the same amplitude of magnetic fields and static load factor with composite skins fiber angle, $\phi = 60^{o}$ the instability regions are shown in Fig. 5.11 (b). The dynamic axial load decreases as the strength and stiffness of the composite skins decreases with increases in fiber angle. Also the instability regions occur at lower frequencies even though the magnetic field increases.

Now comparing the Figs. 5.11 (a) and (c), with increase in static load factors to 0.8 the instability regions increases and the excitation frequency Ω_2 at which the system becomes unstable decreases. Figure 5.11 (d) shows the instability regions of the composite sandwich beam for the same magnetic fields but $\phi = 60^o$ and $\alpha = 0.8$. It can be observed that due to both increases in fiber angle and the static load factor, the excitation frequency Ω_2 further decreases as compared to the Fig. 5.9 (c) and the instability regions increase.

Figure 5.12 (a) shows the influence of static load factor α on the instability regions of the MRE cored composite sandwich beam for different system parameters and a constant magnetic field $B_s = 0.5\text{T}$ and $\phi = 60^o$. With increase in static load factor the instability regions increases and shifts towards left. Consequently, the larger static load factor makes the composite sandwich beam more unstable.

The effect of composite skins fiber angle on the instability regions at a constant magnetic field $B_s = 0.5\text{T}$ is investigated and is shown in Fig. 5.12 (b). It shows that increase in the fiber angle decreases the excitation frequency Ω_2 at which the system becomes unstable, so that the instability region shifts to the left. But the dynamic axial load decreases with increase in fiber angle as the Euler's buckling load decreases. As the strength and stiffness of the 90^o fiber angle composite skins are less, the system should be operated at a lower dynamic axial load.

5.3.4.2 Stability Analysis with Damping effect of MRE

It has already been seen that the damping of sandwich beam with MRE core plays a vital role in the dynamic behavior analysis of structures by controlling the resonant vibrations and thus reducing the bounded instability regions. This damping depends on the core material properties. The instability regions of the MRE cored composite sandwich beam considering damping effect of MRE are investigated and shown in Figs. 5.13 and 5.14. Due to the damping effect of MRE the critical values of dynamic axial load P_{dcr} increases and the instability regions decreases. Therefore the system can operate for a wide frequency range for lower value of dynamic load. The

values of critical dynamic axial loads P_{dcr} of the instability regions shown in Figs. 5.13 and 5.14 are presented in the Table. 5.5 and 5.6.

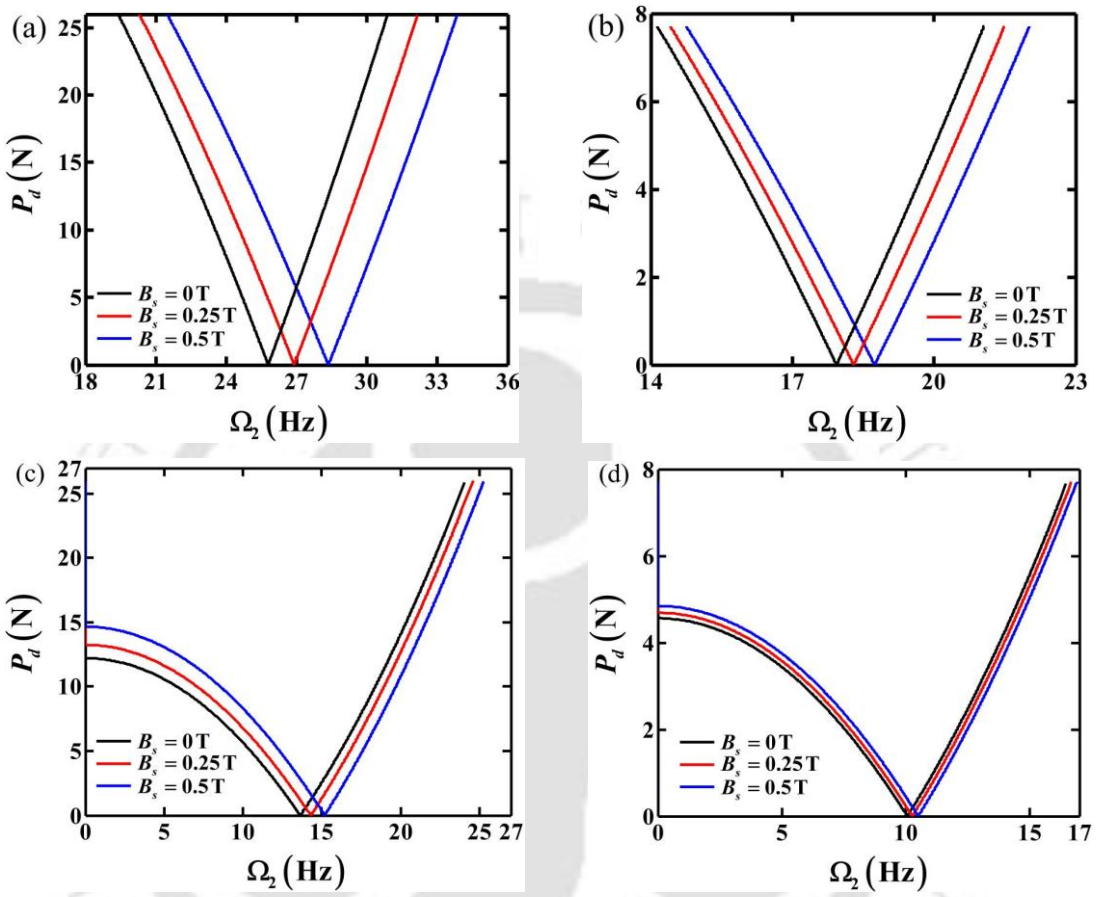

Figure 5.11 Instability regions of composite sandwich beam (a) $\alpha = 0$ and $\phi = 0$, (b) $\alpha = 0$ and $\phi = 60^o$, (c) $\alpha = 0.8$ and $\phi = 0$ and (d) $\alpha = 0.8$ and $\phi = 60^o$.

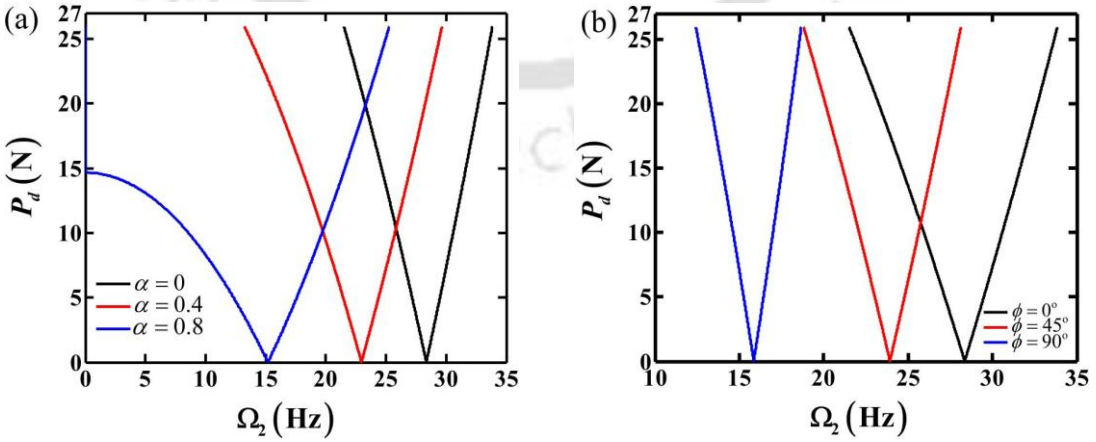

Figure 5.12 Instability regions of composite sandwich beam (a) effect of static load factor α, $B_s = 0.5$T and $\phi = 0$, (b) effect of fibre angle, $B_s = 0.5$ and $\alpha = 0$.

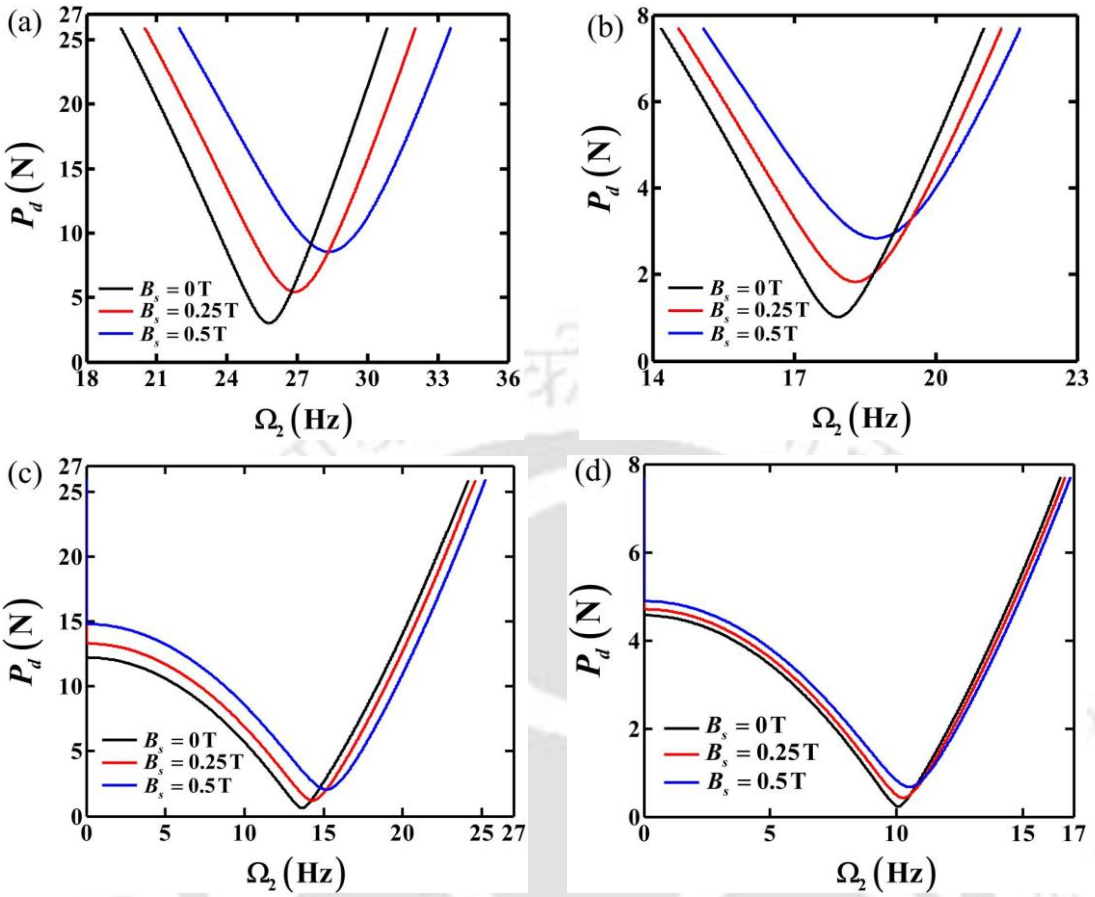

Figure 5.13 Instability regions of composite sandwich beam (a) $\alpha = 0$ and $\phi = 0$, (b) $\alpha = 0$ and $\phi = 60^o$, (c) $\alpha = 0.8$ and $\phi = 0$ and (d) $\alpha = 0.8$ and $\phi = 60^o$.

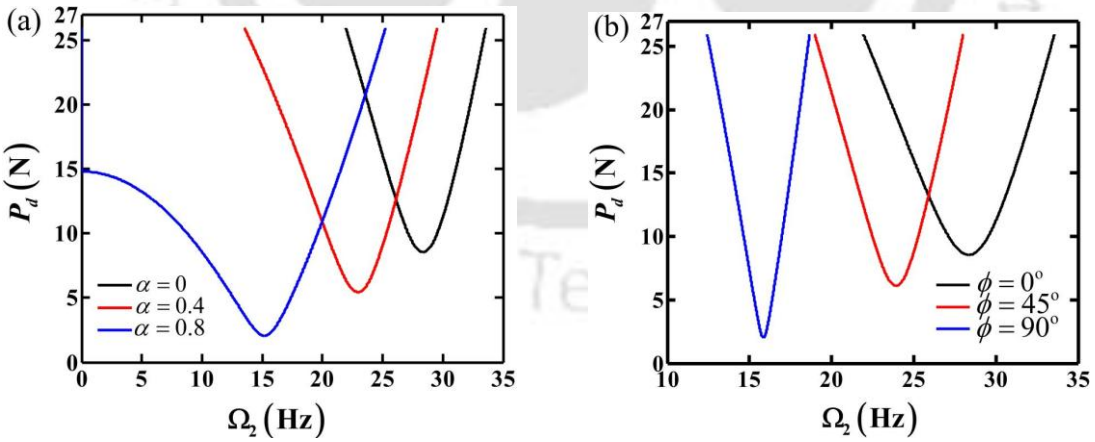

Figure 5.14 Instability regions of composite sandwich beam (a) effect of static load factor α, $B_s = 0.5$T and $\phi = 0$, (b) effect of fibre angle, $B_s = 0.5$T and $\alpha = 0$.

From the Table 5.5 it can be observed that with increase in magnetic field the P_{dcr} increases as the loss factor of MRE increases which results the decrease in

instability regions. Fig 5.14(a) shows the damping effect of MRE at a constant magnetic field on the stability of the composite sandwich beam. It can be seen that the value of P_{dcr} decreases with increase in static load factor which is presented in Table 5.6. Fig 5.14(b) shows the damping effect of MRE at a constant magnetic field on the stability of the composite sandwich beam. Here also it can be observed that the value of P_{dcr} decreases with increase in fiber angle which is presented in Table 5.6. With the damping effect of MRE the P_{dcr} increases, so that the system can operate at higher dynamic load without any vibration.

Table 5.5 Values of critical dynamic load, P_{dcr} of instability regions of the MRE cored composite sandwich beam for different system parameters with variation of magnetic field shown in Fig. 5.11.

Magnetic field, B_s (T)	P_{dcr} (N)			
	$\alpha=0,\phi=0^o$	$\alpha=0,\phi=60^o$	$\alpha=0.8,\phi=0^o$	$\alpha=0.8,\phi=60^o$
0	2.53	0.966	0.594	0.227
0.25	4.949	1.776	1.184	0.42
0.5	8.531	2.828	2.048	0.678

Table 5.6 Values of critical dynamic load, P_{dcr} of instability regions of the MRE cored composite sandwich beam for different system parameters shown in Fig.5.12.

	$B_s=0.5\text{T},\ \phi$=0			$B_s=0.5\text{T},\alpha$=0		
	$\alpha=0$	$\alpha=0.4$	$\alpha=0.8$	$\phi=0^o$	$\phi=45^o$	$\phi=90^o$
P_{dcr} (N)	8.531	5.149	2.048	8.531	5.454	1.864

5.3.5 Comparision of Instability Regions

The instability regions obtained from classical theory based FE formulation (Bhanu, 2012) are compared with the present higher order theory based FE formulation for different system parameters. In classical theeory based formulation the potential energy of the core is considered only due to shaer deformation. But in the present higher order theory based formulation along with the potential energy due to shear deformation, the poential energy due to axial and transverse deformation of the core has been considered. From the Fig. 5.15 it has been observed that at lower excitation

frequencies there is a small difference in the dynamic axial load. But the difference is very small at higher excitation frequencies. From Fig. 5.16 it can be seen that the difference in instability regions are very small. This occurs, as certain effects are ignored in case of classical sandwich beam theory compared to higher order theory.

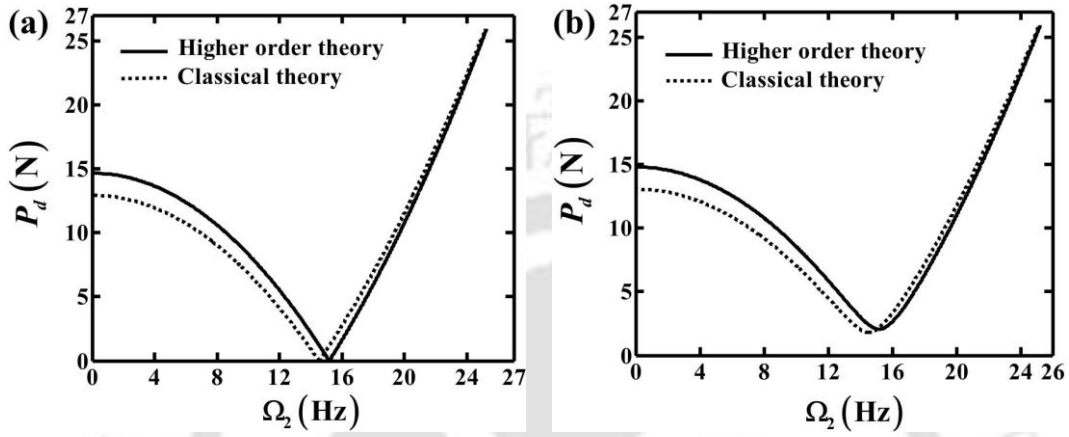

Figure 5.15 Instability regions obtained from FE formulation using classical and higher order sandwich beam theories: (a) without damping effect of MRE and (b) with damping effect of MRE ; $\alpha = 0.8, B_s = 0.5\text{T}$ and $\phi = 0$.

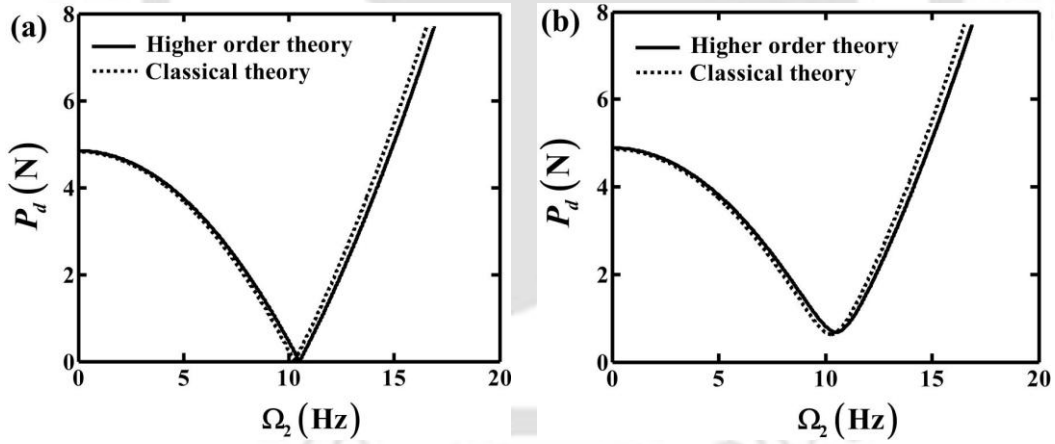

Figure 5.16 Instability regions obtained from FE formulation using classical and higher order sandwich beam theories: (a) without damping effect of MRE and (b) with damping effect of MRE ; $\alpha = 0.8, B_s = 0.5\text{T}$ and $\phi = 60^{\circ}$.

5.4 Summary

In this chapter, the higher order theory for the sandwich beam has been used in the FE formulation of a composite skin sandwich beam with flexible MRE core. The free and forced vibration response of the composite sandwich beam has been studied

for different system parameters such as magnetic field, composite skin fiber angle. For the systems with periodic axial loading and static magnetic field, harmonic balance method is used to determine the instability regions for the principal parametric resonance of first mode for various system parameters. Also the instability regions obtained from present higher order theory based FE formulation are compared with that obtained from classical theory based FE formulation.

6

Experimental Vibration Analysis of Magnetorheological Elastomer Cored Sandwich Beams

6.1 Introduction

The present chapter deals with the experimental vibration analysis of MRE cored sandwich beam. Two different isotropic MREs have been fabricated with and without addition of carbon blacks into the silicon matrix. Microscopic and morphological analysis, thermo-gravimetric analysis (TGA), Magnetic field verses magnetic moment (MH) measurement, thermo-mechanical analysis (TMA) tests, dynamic-mechanical analysis (DMA) tests, tensile test and magneto-rheological test of MRE are carried out to characterize the fabricated MREs. These MREs are embedded into sandwich beams to study its free and forced vibration. In the section 6.2, the fabrication of silicone rubber based soft isotropic MREs has been discussed. Various tests are performed to characterize the fabricated MREs and the observations are discussed in the section 6.3. In section 6.4, the MRE cored sandwich beams are fabricated with two different skin and core thicknesses. An experimental set up is fabricated to investigate the vibration response of the MRE embedded sandwich beam under the magnetic field. From the vibration response the modal frequencies are obtained and compared with the results obtained from the analytical and finite element model.

6.2 Fabrication of Isotropic MREs

To fabricate isotropic MREs, carbonyl iron particles (CIP), room temperature vulcanized (RTV) silicone, catalyst and carbon black are used (Fig. 6.1). The

carbonyl iron powder is purchased from BASF, Germany. These particles are fine, mechanically hard powder and the size distribution: are of d10=1.5 µm, d50= 5 µm and d90=10 µm. The RTV silicone, catalyst (CAT-13219), Shin-Etsu Chemical Co. Ltd.) and carbon black are provided by Swastika Constant Care, Kolkata, India.

Two samples are fabricated viz. MRE without carbon black and MRE with carbon black. During fabrication of MRE without carbon black, first the 40 % V carbonyl iron powders are mixed with 60 % V RTV silicone and catalyst and then stirred for 45 minutes to achieve even dispersion. Similarly, the MRE with carbon black is fabricated. First the 7% V carbon blacks are mixed with the 40% V carbonyl iron powders and then this mixture is added to the 53% V RTV silicone and catalyst and stirred until all the materials are mixed thoroughly (Fig. 6.2).

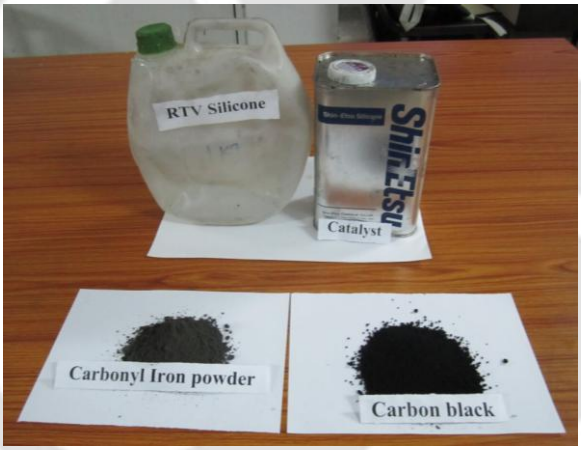

Figure 6.1 Different material components for preparation of MRE

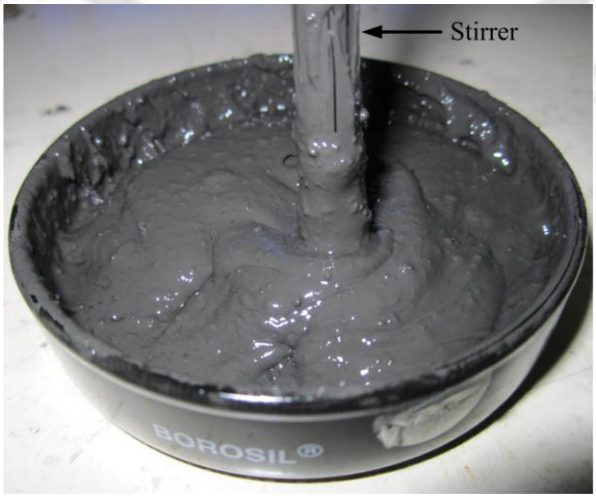

Figure 6.2 Mixing of different components

Then the air bubbles are pulled out by placing these mixtures in a vacuum chamber. Then the mixture is poured into the aluminum mould after the removal of air bubbles (Fig. 6.3). The RTV silicone is mixed with liquid catalyst in the ratio of 10:1. These samples are used for experimental study of the present investigation.

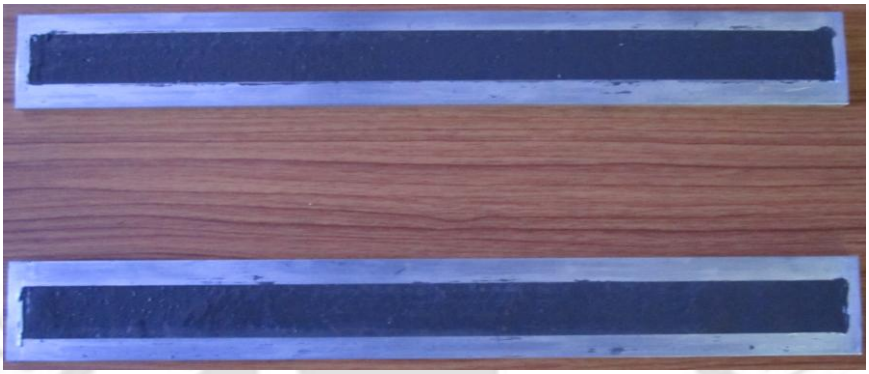

Figure 6.3 Aluminium moulds filled with mixture of different components

6.3 Characterisation of MREs

In this section the magnetic, thermal and mechanical properties of the developed MREs are characterized. Also different analyses are done to study different properties.

6.3.1 Morphological and Microstructure Analysis

The surface morphology of the MREs is studied using ΣIGMA Field Emission Scanning Electron Microscope (FE-SEM) (Make: Carl Zeiss NTS GmbH). Two sample specimens of 5mm×5mm are prepared and are examined under high voltage (10kV) with 1 kX times magnification. Figure 6.4 shows the photograph of ΣIGMA Field Emission Scanning Electron Microscope along with coating unit.

Figure 6.4 (a) and (c) illustrate the SEM based morphological structure of the fabricated MRE without and with carbon black. It shows the randomly dispersed carbonyl iron particles in a silicone polymeric elastomer matrix without and with carbon black. Energy dispersive X-ray (EDX) analyzer is equipped with scanning electron microscope (Make: LEO 1430VP), analyze the composition of the samples of MRE without and with carbon black which are shown in Figs. 6.5(b) and (d) respectively.

(a) (b)

Figure 6.4 (a) Scanning Electron Microscope (b) coating unit.

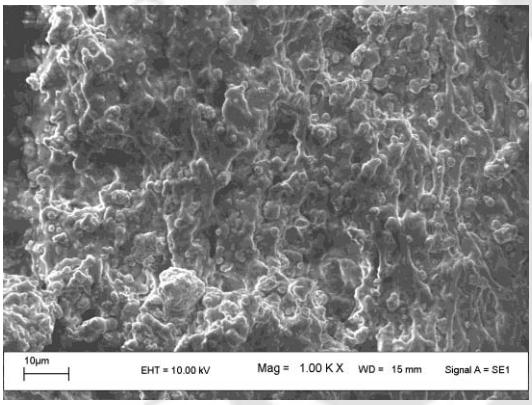

(a)

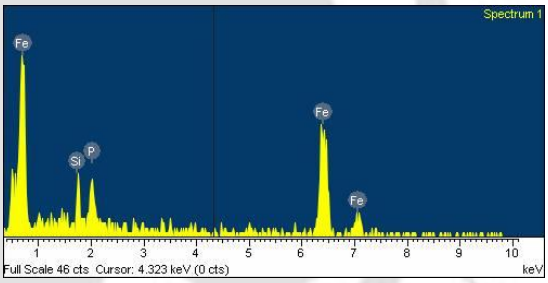

(b)

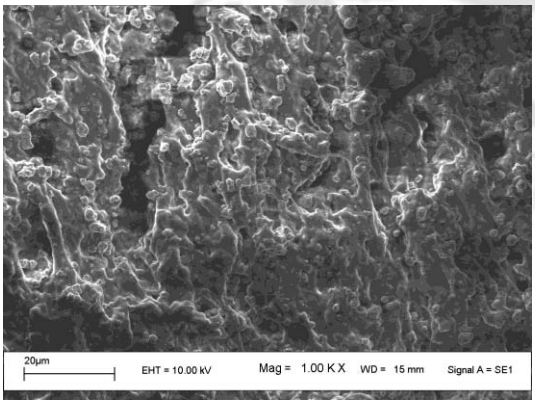

(c)

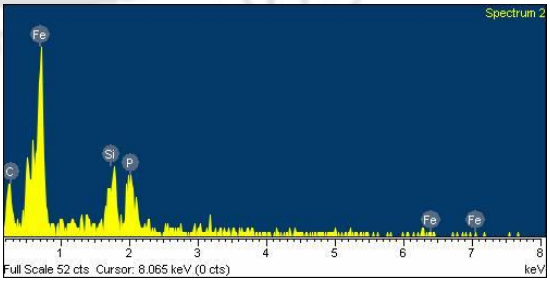

(d)

Figure 6.5 (a) SEM micrograph and (b) EDX of the surface of the fabricated MRE without carbon black (c) SEM micrograph and (d) EDX of the surface of the fabricated MRE with carbon black.

6.3.2 Magnetic Characteristics of the MREs

The magnetic field verses magnetisation (Hysteresis loop) is carried out to study the magnetic characteristics of MREs with and without carbon black. This is carried out on a Vibrating Sample Magnetometer (VSM) (Lake Shore Cryotronics, Inc. Series: 7410). MREs are cut into small rectangular pieces to provide a suitable sample of weight 0.03-0.04gm and then the test is performed. Figure 6.6 shows the photograph of the VSM instrument.

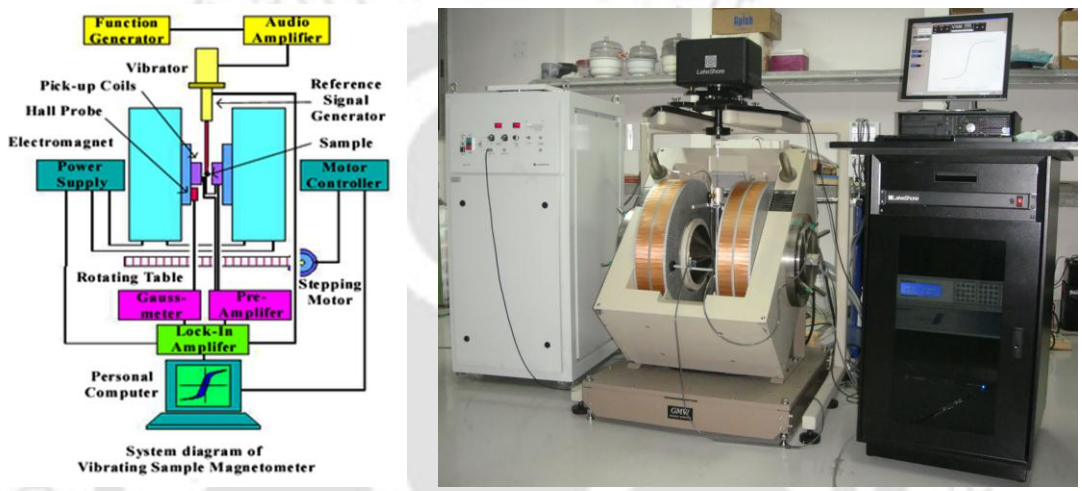

(a) (b)

Figure 6.6 (a) Schematic diagram and (b) Photograph of Vibrating Sample Magnetometer (VSM) instrument.

Figure 6.7 show the magnetic field verses magnetic moment (Hysteresis loop) of MREs with and without carbon black. Hysteresis develops as the magnetic field increases. It is observed that the hysteresis loop from saturation is a characteristic of the specimen. The hysteresis properties of MREs are not much influenced by the addition of carbon black. The hysteresis loop is narrow with high saturation moment, low remanent magnetization and low coercive magnetic field which characterises the fabricated MREs as the soft ferromagnetic materials.

6.3.3 Thermal Analysis

Investigation of thermal properties of MREs is indispensible for various applications in an environment subjected to temperature variation.

Thermo-Gravimetric Analysis (TGA)

Thermo-gravimetric analysis (TGA) is carried out to investigate the thermal behaviour and also the effect of temperature on the MREs. TG measurement is carried out on a NETZSCH STA 449 F3, Jupiter® instrument. The MREs are cut into small pieces to provide a suitable sample size of about 5-10 mg. TG curve is recorded on MREs at a heating rate of 10 ^{o}C/min under Argon atmosphere (60 ml/min) from room temperature to 1200 ^{o}C. Figure 6.8 shows the photograph of the TGA instrument.

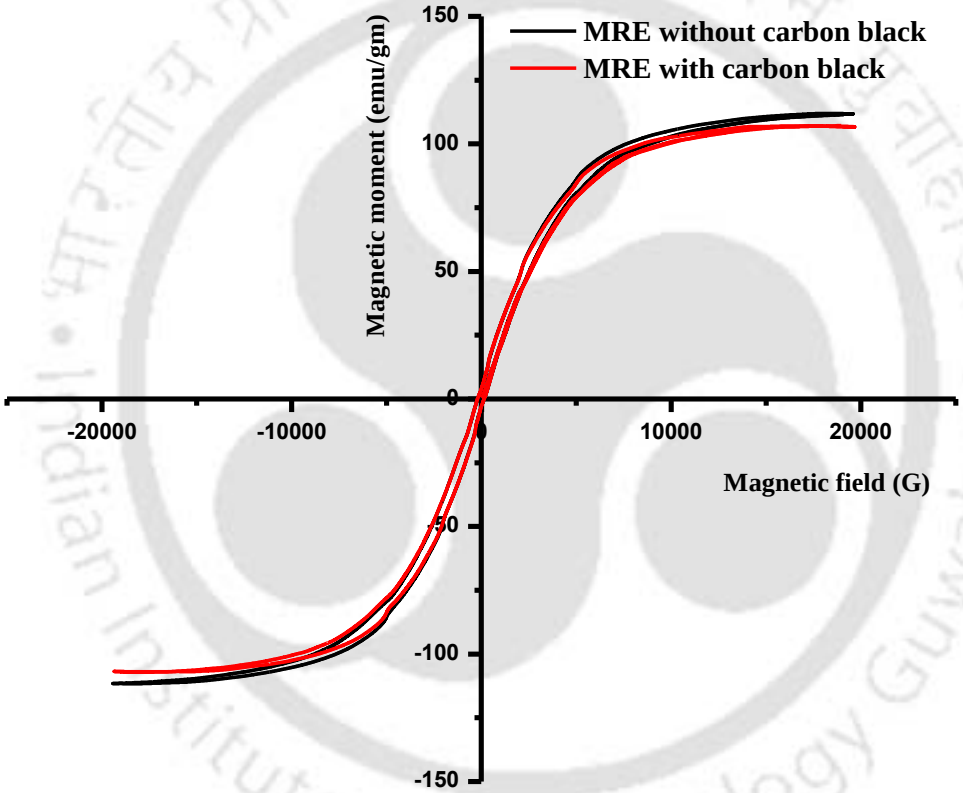

Figure 6.7 Hysteresis loops of MREs.

Both the types of MREs are used for TG analysis. Figure 6.9 (a) and (b) show the TG and DTG curves of MREs without and with carbon black respectively. It may be noted that TG curve shows the percentage variation of mass with temperature and the DTG curve shows its first derivative. The two curves are shown in each graph, one represents the mass loss and other represents the rate of mass loss with time. The DTG curve is obtained by carrying out the first derivative of the TGA curve with time. The total mass losses of MRE without and with carbon black

are 21.12% and 18.79% respectively. From DTG curves it is observed that the time rate of mass loss is more in MRE without carbon black. Hence, addition of carbon black attenuates the time rate of mass loss.

Figure 6.8 Photograph of TGA instrument.

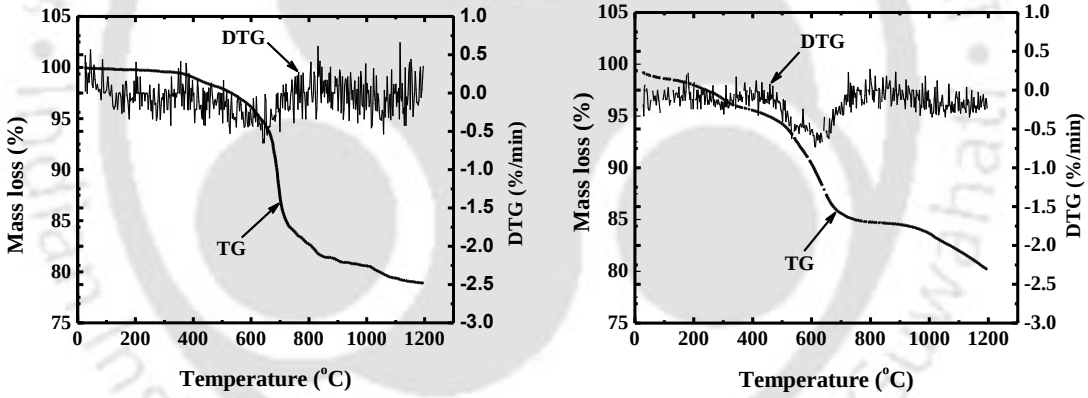

(a) (b)

Figure 6.9 TG and DTG curves of MRE (a) without carbon black and (b) with carbon black.

Thermo Mechanical Analysis (TMA)

Thermo mechanical analysis is carried out for both the types of MREs for studying the coefficient of thermal expansion (CTE). The Thermo Mechanical Analyzer (TMA) (EXSTAR TMA/SS 6000, SII Seiko Instrument Inc.) with a macro compression alumina probe is shown in Fig. 6.10. Calibration of the instrument is done using zinc standard. The samples of MRE with and without carbon black of 5mm × 5mm are prepared and tested on TMA. Data are collected at a heating rate of 10^{o}C/min from room temperature to 250^{o}C while the compressive load is adjusted to

0.1N. The coefficients of thermal expansion obtained from the experiment are shown in Fig. 6.11. It can be seen that the CTE values corresponding to temperature is less in case of MRE with carbon black compare to the MRE without carbon black. It is observed that the addition of carbon black influences the CTE of MRE.

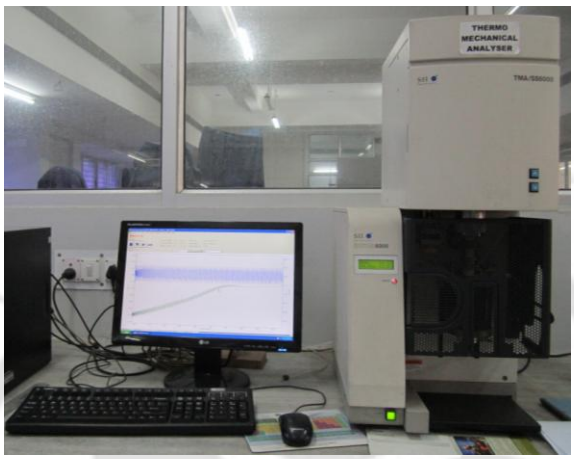

Figure 6.10 Photograph of DMA/TMA instrument.

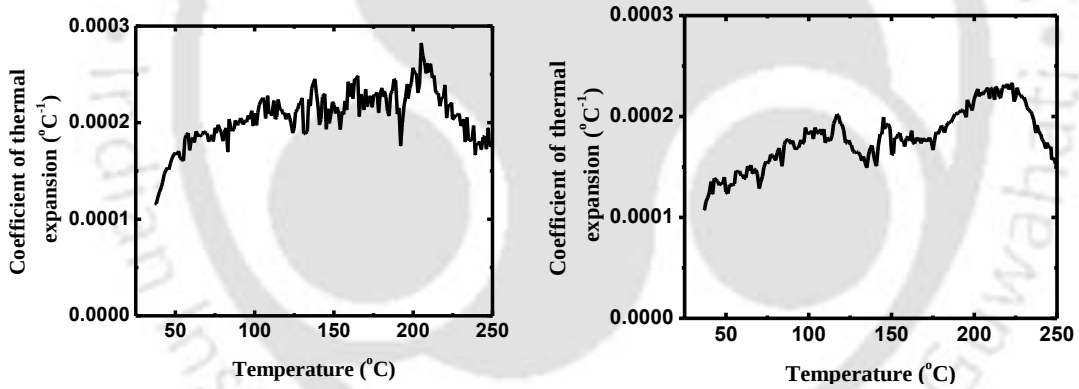

Figure 6.11 Variation of coefficient of thermal expansion of MRE with temperature (a) without carbon black and (b) with carbon black.

To investigate further the effects of temperature and other influencing factors that may affect the linear thermal expansion mechanism of MRE, TMA analysis under tensile load is carried out in the same equipment. Data are collected at a heating rate of 5^{o}C/min up to 250^{o}C for both the MRE samples from room temperature. The tensile load is adjusted to 0.1N with a frequency of 0.1 Hz. Two samples from different MREs of 20 mm × 4mm × 0.8 mm are prepared and tested on TMA and CTE are obtained. The variations of CTE with temperature are shown in Fig. 6.12.

From the Fig. 6.12 it has been observed that the CTE is less in case of MRE with carbon black compared to the MRE without carbon black.

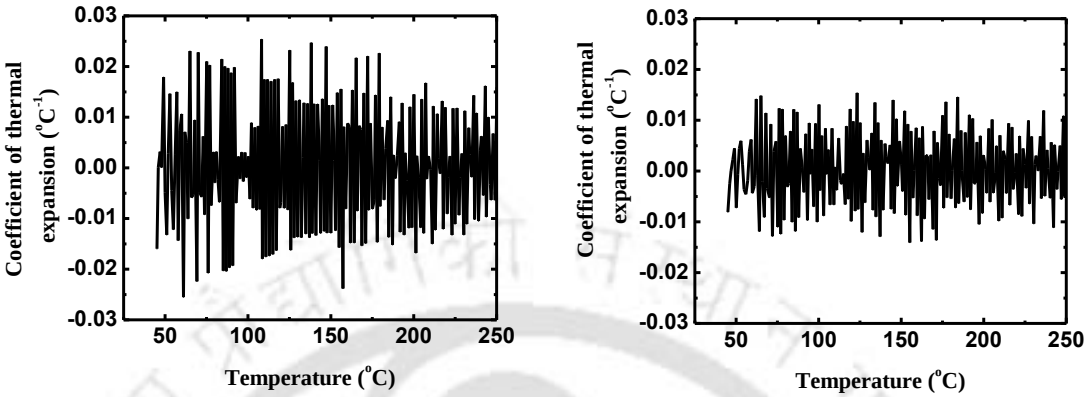

Figure 6.12 Variation of CTE of MRE (a) without carbon black and (b) with carbon black in tensile mode.

Dynamic Mechanical Analysis (DMA)

Dynamic-mechanical analysis is carried out for the MREs with and without carbon black to study the viscoelastic properties. The test is conducted in tensile mode in an EXSTAR TMA/SS 6000, SII Seiko Instrument Inc. using metallic probe as shown in Fig. 6.13. The frequency of the applied load is taken as 0.1 Hz while the heating rate is kept constant at 5 °C.

Figure 6.13 Photograph of DMA/TMA instrument with metallic probe.

Figure 6.14 (a) and (b) demonstrate the change in storage modulus (*E'*), Loss Modulus (*E"*) and loss factor of the MRE without and with carbon black. From both

the graphs it can be seen that initially the storage modulus and loss modulus decreases. The loss factor decreases with increase in temperature. Now comparing both the graphs the amplitude of storage modulus and loss modulus of MRE with carbon black is more than that of the MRE without carbon black as the addition of carbon black increases.

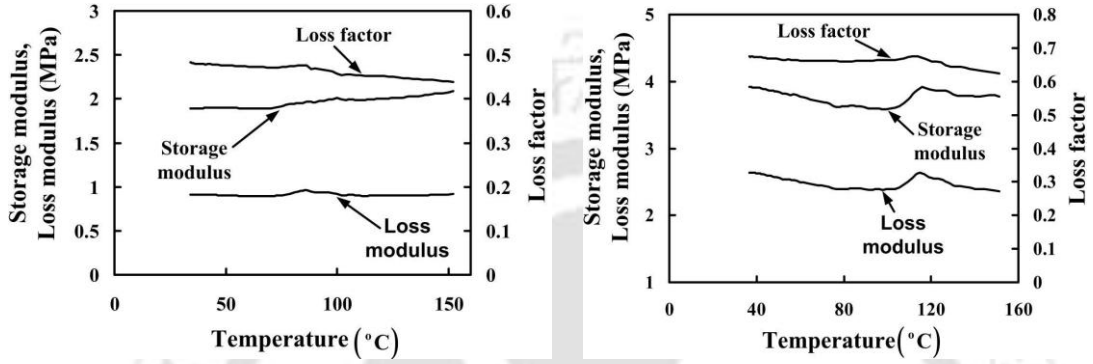

(a) (b)

Figure 6.14 Variation of storage modulus, loss modulus and loss factor of MRE (a) without carbon black and (b) with carbon black.

Viscoelastic Properties in Shear Mode

In this section the viscoelastic properties such as shear storage modulus, loss modulus and loss factor with temperature are found in an experiment done on a parallel-plate rheometer (MCR 101, Anton paar Co., Germany, Serial No. 80794059) as shown in Fig. 6.15. The MRE samples are 25 mm diameter and 0.8 mm thickness. The experiment is done at a constant angular frequency of 5 rad/s.

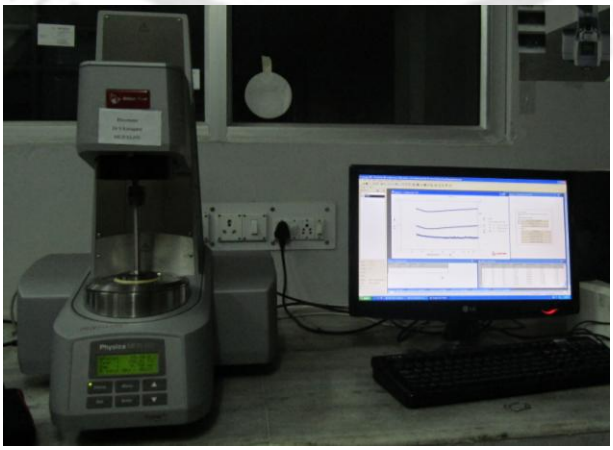

Figure 6.15 Photograph of parallel-plate rheometer.

Figure 6.16 (a) and (b) shows the shear storage modulus, loss modulus and loss factor with variation of temperature of MRE with and without carbon black respectively. From the Fig. 6.16 (a), it is observed that with increase in temperature the shear storage modulus, loss modulus increases and loss factor decreases. But in case of MRE with carbon black (Fig. 6.16 (b)) the shear storage modulus increases and the loss modulus decreases. Also it is observed that the addition of carbon black increases the shear storage modulus. The decrease in loss modulus describes the decrease in energy dissipation during the deformation of MRE.

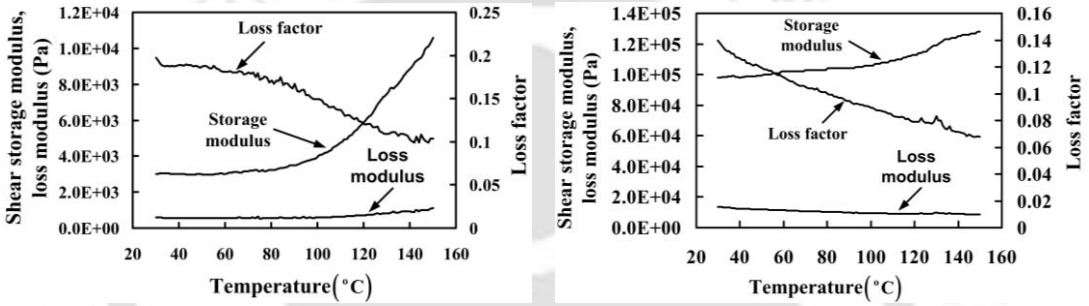

Figure 6.16 Variation of shear storage modulus and loss modulus and loss factor of MRE (a) without carbon black and (b) with carbon black.

6.3.4 Rheological Properties of MRE

In the MRE-based sandwich beam configuration, the MRE deforms due to shear. The viscoelastic properties such as shear storage modulus and loss modulus with variation of magnetic field are found in an experiment done on a parallel-plate rheometer (MCR 301, Anton paar Co., Germany, Serial No. 80833284, CGCRI Kolkata) as shown in Fig. 6.17. The MRE samples are 25 mm diameter and 0.8 mm thickness. The experiment is done at a constant angular frequency 10 rad/s and the relationship between the shear storage modulus and loss modulus are obtained. The magnetic field is applied through a tuning current.

Figures 6.18 and 6.19 show the variation of the storage modulus and loss modulus with strain for MRE without carbon black and with carbon black respectively under different magnetic field. It is observed that the storage modulus and loss modulus increases with magnetic field.

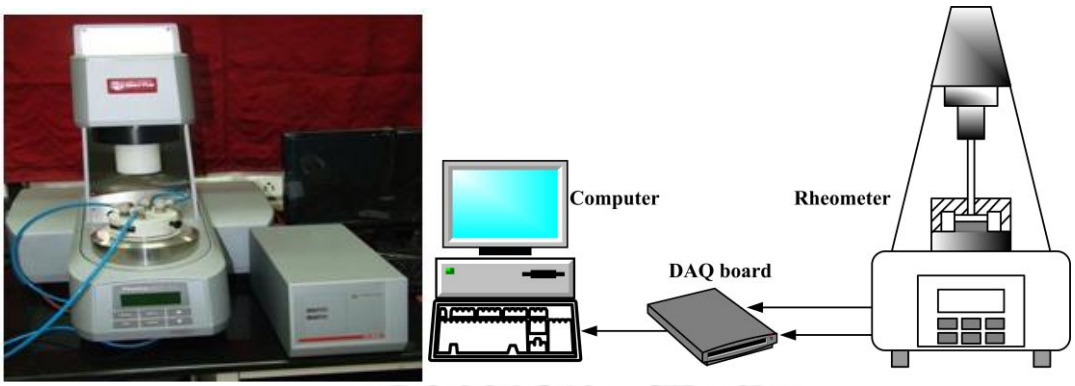

(a) (b)

Figure 6.17 (a) Photograph of parallel-plate rheometer with magneto rheology attachment (Source: CGCRI, Kolkata) (b) Schematic diagram of setup for measurement of rheological properties

Figure 6.20 shows the storage modulus and loss modulus of MREs as a function of the magnetic field. From these figures it is noted that the storage modulus and loss modulus increased as the magnetic field strength increased. It can be seen that the storage modulus and loss modulus of MRE with carbon black are more than the MRE without carbon black for the same magnetic field.

6.3.5 Tensile test

Tensile tests are conducted to investigate the stress-strain behaviour of MREs without and with carbon black using universal testing machine (INSTRON-8801, 100 kN capacity). Figure 6.21 (a) and (b) show the tensile test setup and ASTM standard sample for tensile test. The tensile tests are performed with a 0.5 mm/min test speed. The curve fitted stress-strain graphs for both MREs are shown in Fig. 6.22. The Young's modules of MRE without and with carbon black are found to be 1.077 MPa and 1.738 MPa respectively. From the experimental data it has been observed that with the addition of carbon black proportional limit point occurs at a higher load as compare to the MRE without carbon black.

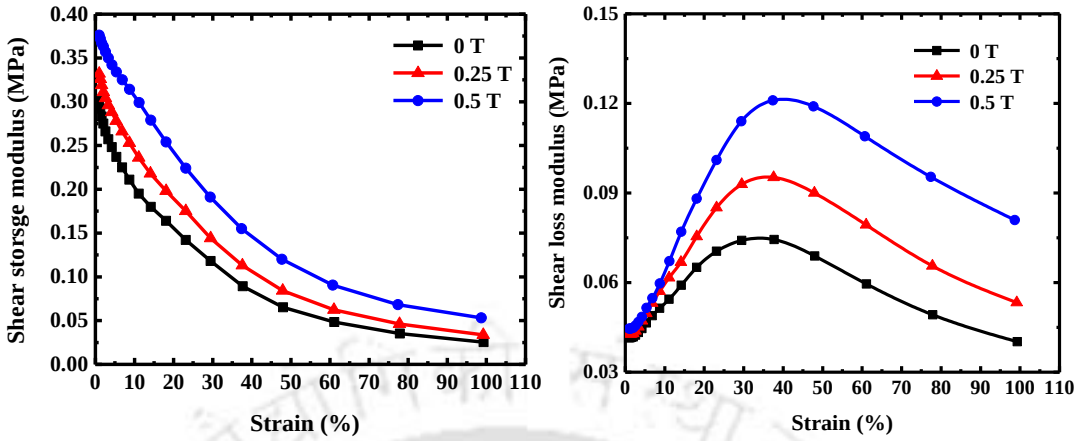

(a) (b)

Figure 6.18 Variation of (a) storage modulus and (b) loss modulus with strain of MRE without carbon black under different magnetic fields.

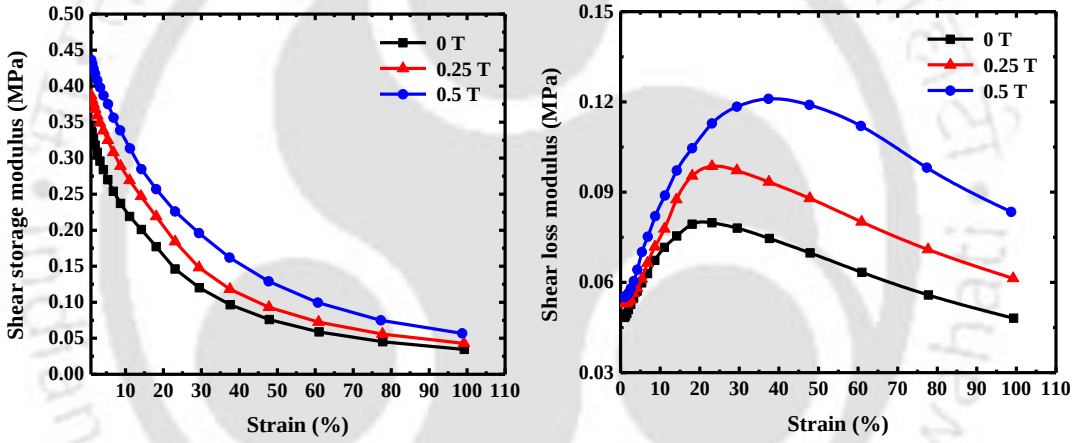

(a) (b)

Figure 6.19 Variation of (a) storage modulus and (b) loss modulus with strain for MRE with carbon black under different magnetic fields.

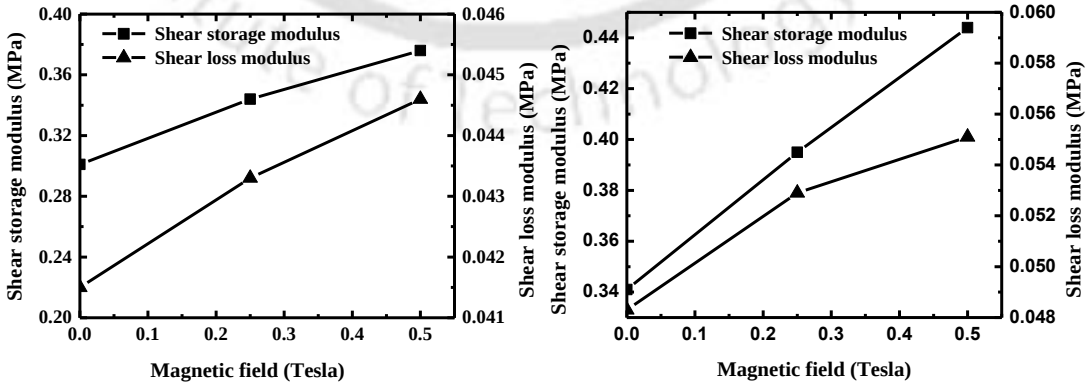

(a) (b)

Figure 6.20 Variation of storage modulus and loss modulus with magnetic field for (a) MRE without carbon black and (b) MRE with carbon black.

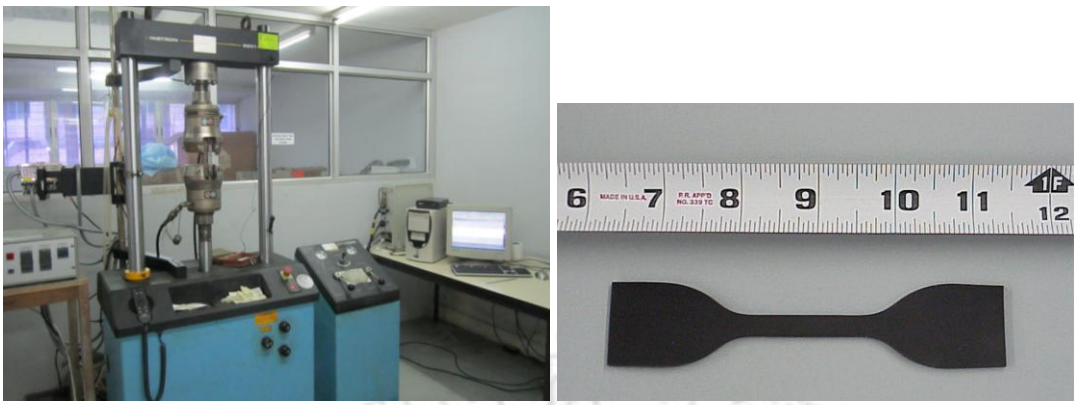

(a) (b)

Figure 6.21 (a) tensile test setup and (b) ASTM standard specimen

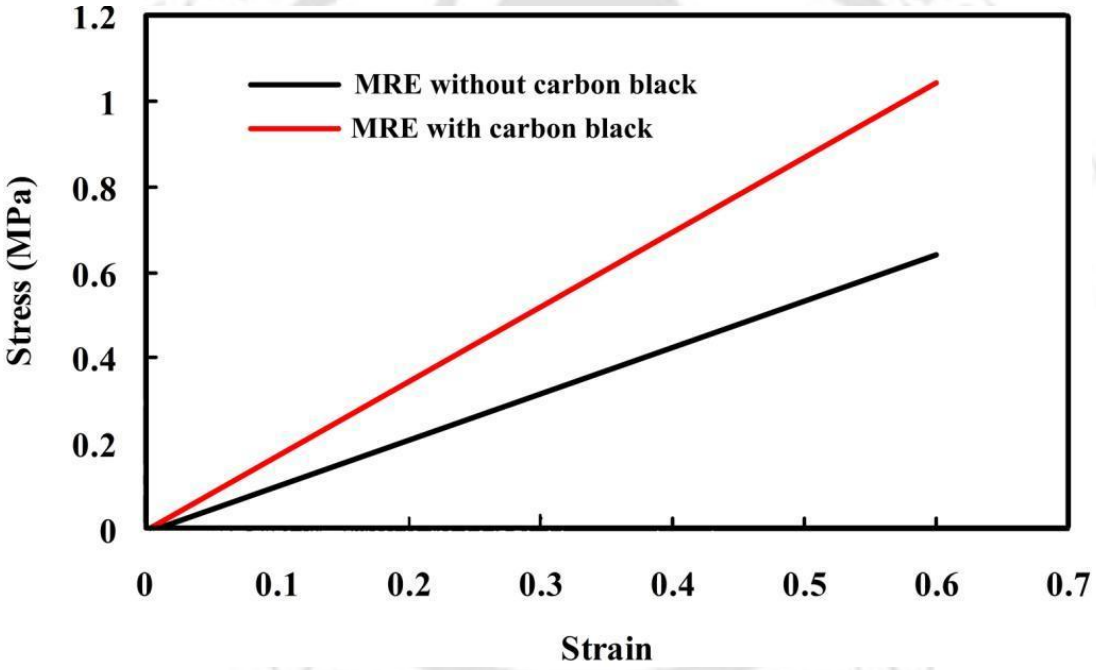

Figure 6.22 Curve fitted stress-strain graphs of MRE with and without carbon black

6.4 Experimenal Investigation of Vibration Characteristics of MRE Cored Sandwich Beams

6.4.1 Test Specimen Preparation and Material Properties

Six sandwich beams with MRE core have been prepared by varying the core thickness, skin thickness and considering MRE with and without carbon black. The thicknesses of fabricated MREs used in the sandwich beam are 1.8 mm and 2.6 mm.

Also the thicknesses of aluminum skins used for the skins are 0.4 mm and 1.28 mm. The aluminums are chosen for the skins due to its low damping properties and relatively high stiffness properties compared to those of MREs. The fabricated MRE core is bonded to two aluminum skins with the aid of epoxy glue. The length and width of the sandwich beams are 245 mm and 20 mm respectively. The density of aluminum plies is 2618.03 kg/m^3. The densities of MRE with and without carbon black are 2455.36 kg/m^3 and 2022.7 kg/m^3 respectively. The Young's modulus of aluminum skin is 69.53 GPa. The Young's modules of MRE without and with carbon black are found to be 1.124 MPa and 1.763 MPa respectively.

6.4.2 Experimental Set-up and Procedure

To know the mechanical properties of the aluminum plies, a tensile test has been conducted using a universal testing machine (INSTRON-8801, 100 kN capacity) as shown in Fig. 6.23. Similarly the Young's modulus of the MREs without and with carbon black has been determined which is explained in the section 6.3.5.

To study free and forced vibration of the sandwich beam with and without magnetic field an experimental test rig is fabricated as shown in Fig. 6.24. In this experimental test, the MRE sandwich beam was clamped to a fixed platform using a cantilever configuration. The experimental set up is integrated with permanent magnets, sensor, shaker, PC driven ACE dynamic signal analyzer and signal analysis equipments. The instruments used in the experiment include Brüel and Kjaer made PULSE Lab Shop, Rotational Laser Vibrometer, shaker and amplifier. A magnetic field is generated by permanent magnets over the test sandwich beam. The magnetic field is applied in the vertical direction i.e. perpendicular to the surface of the skins. In this experiment the maximum field intensity generated by the permanent magnets is 1000 G. The magnetic field is varied by changing the air gap between the sandwich beam and the permanent magnets. The tip of the shaker is connected to the sandwich beam at the actuation location of 80 mm from the fixed end of the beam. The laser point is located at the tip of the sandwich beam.

The shaker (Type 4824, V 22.5, make: Brüel and Kjaer) is driven by the voltage signal from the power amplifier (Type 2732, make: Brüel and Kjaer. This voltage

signal is generated by acquisition system (Type 3560 A-002; make: Brüel and Kjaer) output through PULSE Lab Shop (Version 5.2; make: Brüel and Kjaer). The laser sensor (RLV-5500, Polytech GmbH) is used to measure vibration displacement at a single location, and this sensor could sense the velocity from 0 to 200 *mm*/*s*/V .

Figure 6.23 Photograph of an universal testing machine (INSTRON-8801, 100 kN capacity) for tensile test of aluminum and MRE.

The software, PULSE Lab Shop (type 3560 D; make: Brüel and Kjaer, software version 13.1.0.246) is used to obtain and analyse the acquired analogue signals from the laser sensor through data acquisition system (Type 3560D; make: Brüel and Kjaer). The Tesla gauge provided by Scientific Equipment and Services (DGM-103, S No. 91) is used to measure the amplitude of strength of magnetic field. To excite the sandwich beam, different options were employed such as free vibration, impact hammer and shaker. In each case, even though the applied forces are different and the sandwich beam vibrated at different amplitudes, the beam vibrated at the same natural frequency. To study the free vibration, the MRE cored sandwich beam was released from a specific deflected set position to maintain the excitation force

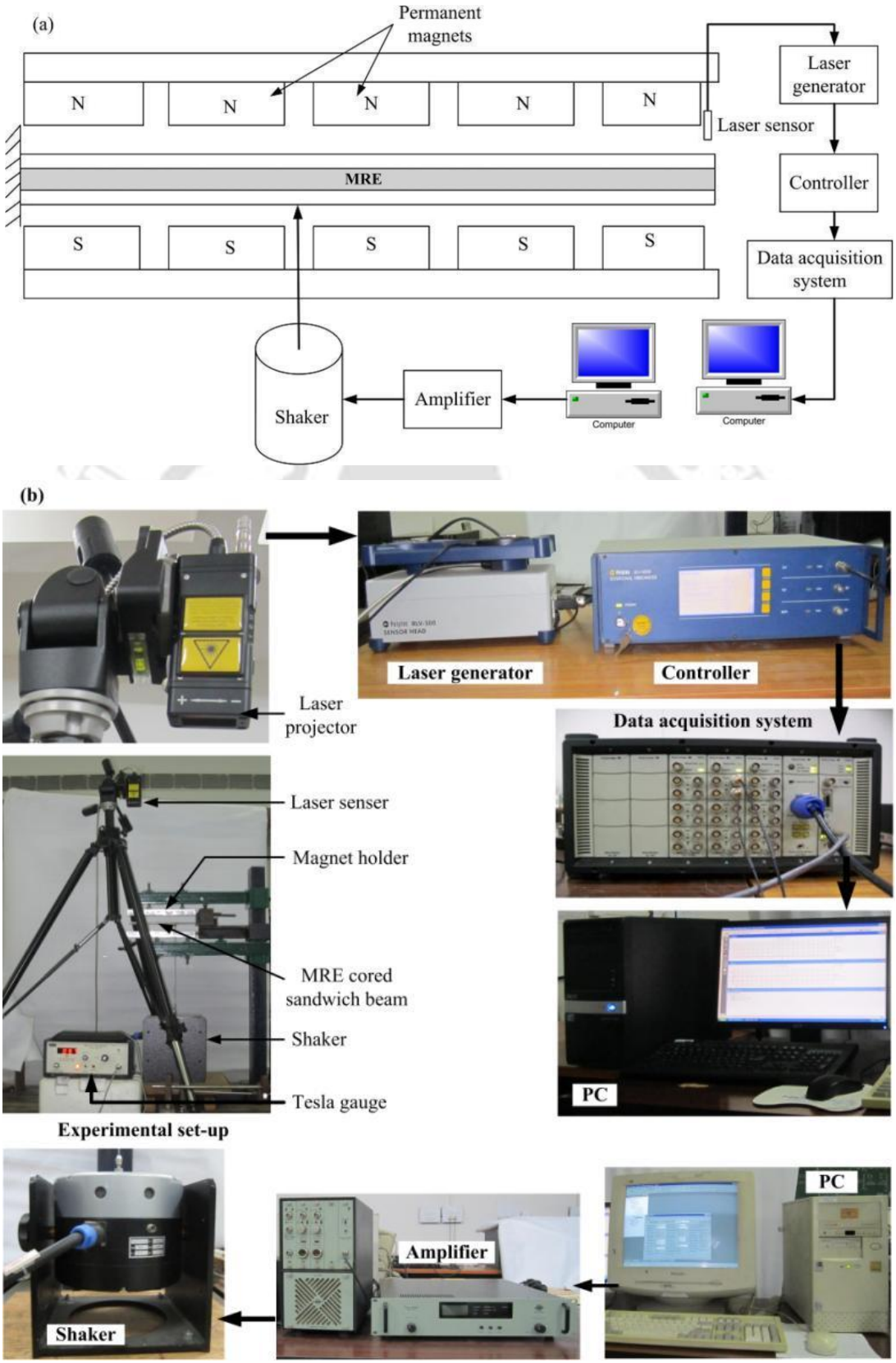

Figure 6.24 (a) Schematic diagram and (b) Photograph of Experimental setup.

constant when comparing the response of the beam with and without a magnetic field. In a modal test the shaker is used to excite the sandwich beam.

The experimental procedure is summarised as follows; first the free vibration of the sandwich beam was studied. Then the forced vibration was studied. The PULSE Lab Shop is set using a swept sine actuation at a range of 0-300 Hz with 1 Hz increment. The voltage amplitude of the excitation signal is set at 200 mV. The signal out put from the computer is send to the shaker through the amplifier. The shaker provides the external vibration over the test sandwich beam. The vibration data of the test sandwich beam are acquired by the laser sensor and sends to the computer through controller and data acquisition system. The PULSE Lab Shop software in the computer processes the input signal. Then the vibration response in the frequency domain, natural frequencies and amplitudes of the vibration are presented in the output of the analysis result.

6.4.3 Results and Discussions

The vibration frequency response of a structure subjected to an external dynamic force depends on the stiffness and mass distribution of the structural elements. Similarly, the magnitude of this vibration is controlled by the damping characteristics of the structure. Therefore, the vibration characteristics of the magnetorheological elastomer embedded sandwich beams were studied by obtaining their resonant natural frequencies under different amplitude of magnetic field.

Figure 6.25 to 6.30 show the vibration response of the sandwich beam with two different MRE cores and variation of skin and core thickness for the first three modes. In the test the distance between the magnetic poles are varied to apply the required magnetic field intensities. The frequencies obtained from the experiment are presented in the Tables 6.1-6.6 for different skin and core thickness and MRE core. It is noted that the modal frequencies of the sandwich beam increased as the magnetic field increased. So this showed the trend of a frequency right shift.

The frequencies of sandwich beam with different MRE cores (MRE without carbon black and MRE with carbon black) and same core and skin thickness are presented in Tables 6.1 and 6.2. It can be observed that the modal frequencies of

sandwich beam with MRE (with carbon black) core are more than the frequencies of the sandwich beam with MRE (without carbon black) core. This is due to the increase in shear modulus of the MRE containing carbon black. Compared with the frequency of sandwich beam with MRE (without carbon black) core under zero magnetic fields, the first natural frequency of the sandwich increased by 15.38%.

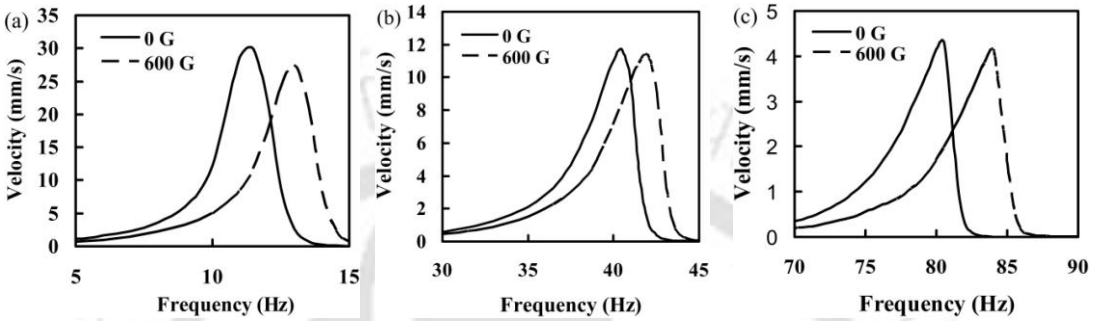

Figure 6.25 Vibration response of the MRE (without carbon black) cored sandwich beam (0.4 mm skin and 1.8 mm core thickness) under different magnetic field. (a) 1st mode, (b) 2nd mode and (c) 3rd mode.

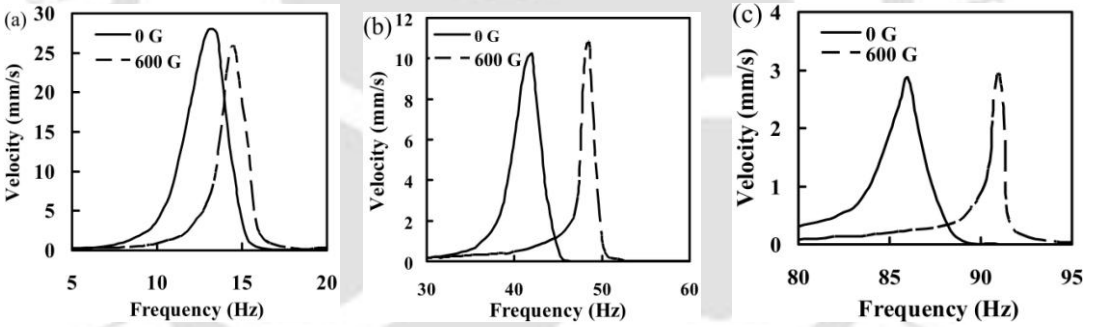

Figure 6.26 Vibration response of the MRE (with carbon black) cored sandwich beam (0.4 mm skin and 1.8 mm core thickness) under different magnetic field. (a) 1st mode, (b) 2nd mode and (c) 3rd mode.

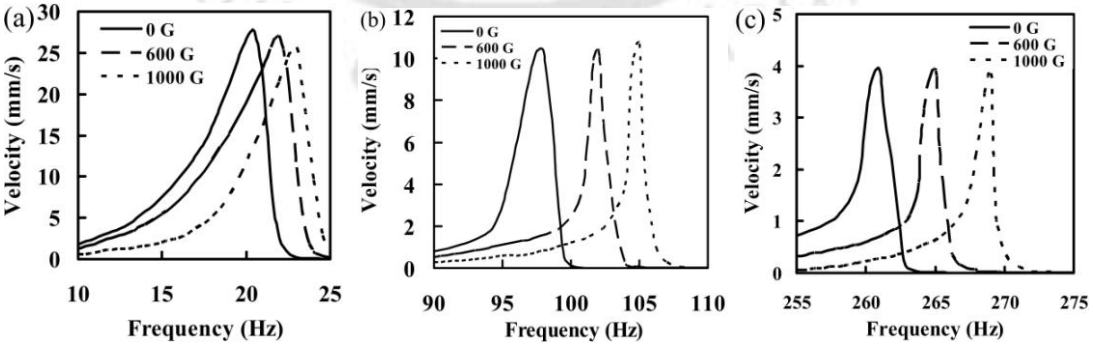

Figure 6.27 Vibration response of the MRE (without carbon black) cored sandwich beam (1.28 mm skin and 1.8 mm core thickness) under different magnetic field. (a) 1st mode, (b) 2nd mode and (c) 3rd mode.

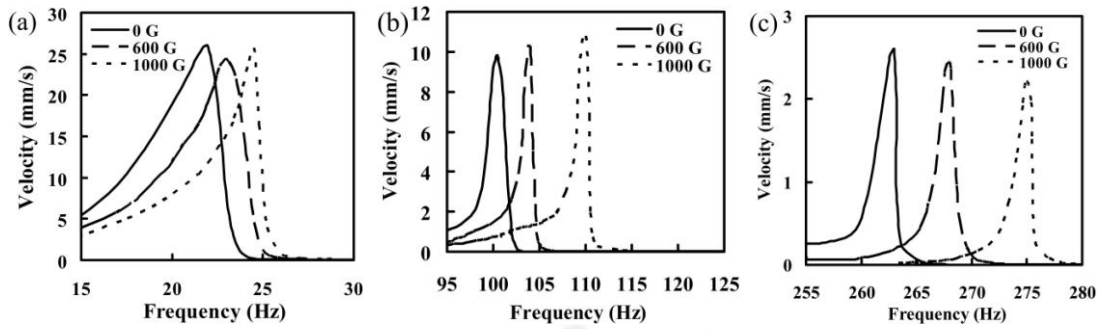

Figure 6.28 Vibration response of the MRE (with carbon black) cored sandwich beam (1.28 mm skin and 1.8 mm core thickness) under different magnetic field. (a) 1st mode, (b) 2nd mode and (c) 3rd mode.

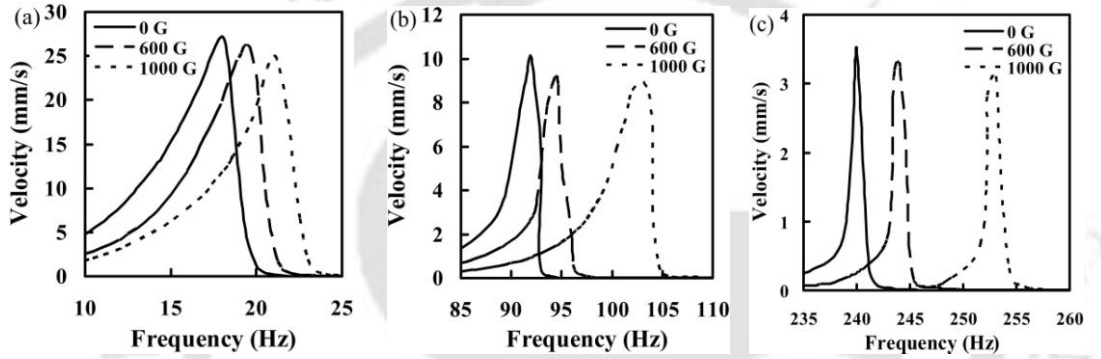

Figure 6.29 Vibration response of the MRE (without carbon black) cored sandwich beam (1.28 mm skin and 2.6 mm core thickness) under different magnetic field. (a) 1st mode, (b) 2nd mode and (c) 3rd mode.

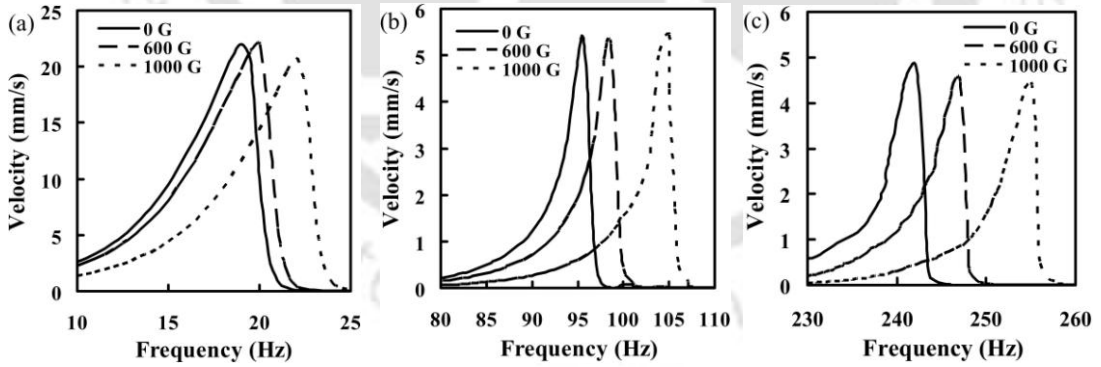

Figure 6.30 Vibration response of the MRE (with carbon black) cored sandwich beam (1.28 mm skin and 2.6 mm core thickness) under different magnetic field. (a) 1st mode, (b) 2nd mode and (c) 3rd mode.

Keeping the core thickness remains same and increasing the skin thickness to 1.28 mm, the modal frequencies of the sandwich beam measured for different MRE core are presented in Tables 6.3 and 6.4. It can be seen that with increase in skin

thickness the modal frequencies increase as the flexural rigidity of the sandwich beam increases with increase in skin thickness. With increase in skin thickness of the sandwich beam from 0.4 mm to 1.28 mm the first natural frequency increased by 43.9 % and 40.9 % for the MRE without carbon black and MRE with carbon black core respectively.

Table 6.1 Modal frequencies obtained from experiment and its comparison with the frequencies obtained from different models for the first three modes of a sandwich beam under different magnetic field. (Beam of 0.4 mm skin and 1.8 mm core and MRE without carbon black).

	0 G			600 G			1000 G		
	1st Mode	2nd Mode	3rd Mode	1st Mode	2nd Mode	3rd Mode	1st Mode	2nd Mode	3rd Mode
Experimental	11.50	40.50	81.00	13.00	42.00	84.00	----	------	----
Analytical method with anti plane core	12.21	41.38	83.22	13.37	43.87	85.05	15.48	46.18	87.57
FEM with anti plane core	12.71	43.6	89.02	13.96	46.58	93.26	15.20	48.69	95.18
FEM with flexible core	12.38	42.06	84.94	13.55	45.56	87.74	15.65	47.88	89.25

Table 6.2 Modal frequencies obtained from experiment and its comparison with the frequencies obtained from different models for the first three modes of a sandwich beam under different magnetic field. (Beam of 0.4 mm skin and 1.8 mm core and MRE with carbon black).

	0 G			600 G			1000 G		
	1st Mode	2nd Mode	3rd Mode	1st Mode	2nd Mode	3rd Mode	1st Mode	2nd Mode	3rd Mode
Experimental	13.00	42.00	86.00	14.50	48.50	91.00	----	----	----
Analytical method with anti plane core	13.51	43.20	84.3	14.68	46.72	87.20	16.79	48.06	89.78
FEM with anti plane core	14.02	45.42	91.03	15.27	48.40	94.29	16.52	50.51	97.17
FEM with flexible core	13.68	43.88	86.92	14.85	47.41	89.80	15.97	48.75	91.36

Table 6.5 and 6.6 presents the modal frequencies of the sandwich beams with increase in core thickness. It can be observed that with increase in core thickness from 1.8 mm to 2.6 mm without increase in skin thickness, the modal frequencies

decrease. With increase in core thickness of the sandwich beam from 1.8 mm to 2.6 mm the first natural frequency decreased by 12.2 % and 13.64 % for the MRE without carbon black and MRE with carbon black core respectively.

Table 6.3 Modal frequencies obtained from experiment and its comparison with the frequencies obtained from different models for the first three modes of a sandwich beam under different magnetic field. (Beam of 1.28 mm skin and 1.8 mm core and MRE without carbon black).

	0 G			600 G			1000 G		
	1st Mode	2nd Mode	3rd Mode	1st Mode	2nd Mode	3rd Mode	1st Mode	2nd Mode	3rd Mode
Experimental	20.50	98.00	261.00	22.00	102.00	265.00	23.00	105.00	269.00
Analytical method with anti plane core	20.76	96.92	252.60	21.95	99.27	255.95	22.07	103.49	257.17
FEM with anti plane core	21.91	101.44	265.74	22.25	104.42	268.92	24.21	107.13	271.51
FEM with flexible core	21.29	100.76	264.20	22.47	103.1	267.53	23.59	105.31	269.74

Table 6.4 Modal frequencies obtained from experiment and its comparison with the frequencies obtained from different models for the first three modes of a sandwich beam under different magnetic field. (Beam of 1.28 mm skin and 1.8 mm core and MRE with carbon black).

	0 G			600 G			1000 G		
	1st Mode	2nd Mode	3rd Mode	1st Mode	2nd Mode	3rd Mode	1st Mode	2nd Mode	3rd Mode
Experimental	22.00	100.50	263.00	23.00	104.00	268.00	24.50	110.00	275.00
Analytical method with anti plane core	22.14	98.93	254.74	23.35	101.32	257.14	24.48	104.57	260.40
FEM with anti plane core	23.30	103.42	267.67	24.86	106.39	271.77	26.59	109.02	273.17
FEM with flexible core	22.66	102.69	266.15	23.86	105.07	270.53	25.99	107.31	272.78

For validation of the models the resonance frequencies obtained from the different models are compared with the frequencies measured by conducting the experiments. The Tables 6.1 to 6.6 shows the comparison of resonance frequencies of the sandwich beams for different MRE core and variation of the skin and core thickness.

It can be seen that there is small variation in the frequencies. This is due to the assumptions taken for the modeling of the system.

Table 6.5 Modal frequencies obtained from experiment and its comparison with the frequencies obtained from different models for the first three modes of a sandwich beam under different magnetic field. (Beam of 1.28 mm skin and 2.6 mm core and MRE without carbon black).

	0 G			600 G			1000 G		
	1st Mode	2nd Mode	3rd Mode	1st Mode	2nd Mode	3rd Mode	1st Mode	2nd Mode	3rd Mode
Experimental	18.00	92.00	240.00	19.50	95.00	244.00	21.00	103.00	253.00
Analytical method with anti plane core	19.74	90.28	233.59	20.93	93.63	236.95	21.05	95.86	240.17
FEM with anti plane core	20.71	95.70	244.2	21.23	98.44	248.69	23.91	102.73	252.08
FEM with flexible core	20.21	93.77	241.23	21.4	95.12	247.57	22.52	100.33	250.78

Table 6.6 Modal frequencies obtained from experiment and its comparison with the frequencies obtained from different models for the first three modes of a sandwich beam under different magnetic field. (Beam of 1.28 mm skin and 2.6 mm core and MRE with carbon black).

	0 G			600 G			1000 G		
	1st Mode	2nd Mode	3rd Mode	1st Mode	2nd Mode	3rd Mode	1st Mode	2nd Mode	3rd Mode
Experimental	19.00	96.00	242.00	20.00	99.00	247.00	22.00	105.00	255.00
Analytical method with anti plane core	20.08	92.15	235.35	21.30	95.55	238.76	22.43	97.81	242.02
FEM with anti plane core	21.06	97.53	247.72	22.59	101.25	251.16	24.26	104.47	254.30
FEM with flexible core	21.55	96.56	245.78	22.75	99.95	249.17	23.89	103.20	253.42

Figure 6.31 and 6.32 show the time responses for free vibration of the MRE cored sandwich beam to an impulse applied at the free end in absence and presences of a magnetic field (600 G). Here the MRE without and with carbon black are taken as the core. The data show that the beams damping increases considerably with the applied magnetic field. The rate of decay of the response in the free vibration plots can be described in terms of the damping ratio ζ in the following form:

$$\delta = \frac{1}{n} \ln \frac{x_1}{x_{n+1}} \tag{6.1}$$

$$\zeta = \frac{\delta}{2\pi} \tag{6.2}$$

where, δ corresponds to the log decrement, x is the vibration amplitude and n is the number of cycles. In case of sandwich beam with MRE without carbon black core, the damping ratio in the absence of magnetic field is 0.0031; it increases to 0.0055 with a magnetic field of 600 G. It results a 43.64% increase in damping ratio. Similarly in case of sandwich beam with MRE with carbon black, the damping ratio in the absence of magnetic field is 0.0035 and it increases to 0.0079 (55% increase) with a magnetic field of 600 G.

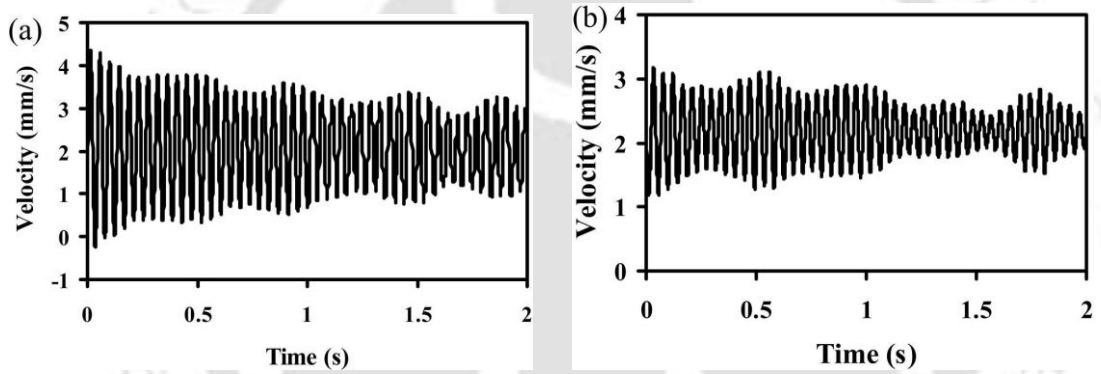

Figure 6.31 Free vibration responses of MRE (without carbon black) cored sandwich beam (0.4 mm skin thickness and 1.8 mm core thickness): (a) without magnetic field; (b) with magnetic field of 600 G.

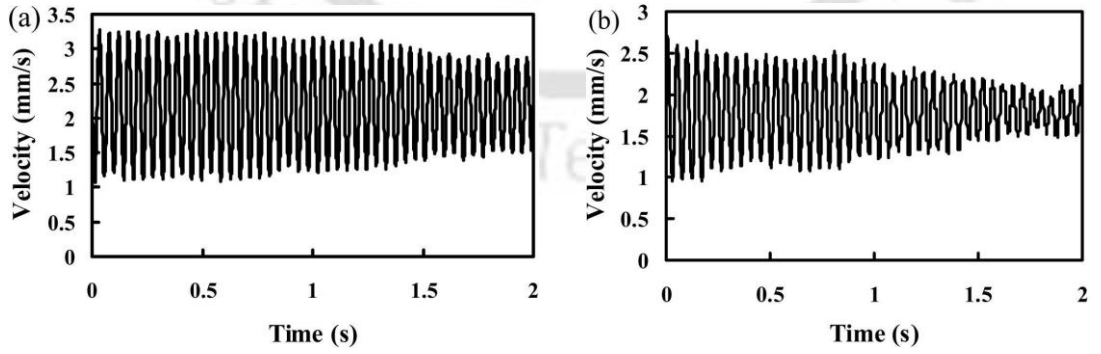

Figure 6.32 Free vibration responses of MRE (with carbon black) cored sandwich beam (0.4 mm skin thickness and 1.8 mm core thickness): (a) without magnetic field; (b) with magnetic field of 600 G.

6.5 Summary

In this chapter, initially the isotropic MREs are fabricated with and without addition of carbon blacks in to the matrix material. Various tests are conducted to characterise these MREs. It has been observed that with the addition of Carbon black the thermal stability increases so that the MRE with carbon black can operate at higher temp compare to MRE without carbon black. The mechanical properties such as young's modulus, shear storage modulus are significantly increases with the addition of carbon black. Then an experimental approach to study the dynamic characteristics of MRE cored sandwich beams was described. Sandwich beams were fabricated with different MRE cores and variation of skin and core thickness. For validation of models the modal frequencies were compared with the frequencies obtained from different models discussed in this thesis. The stiffness and damping characteristics of the MRE cored sandwich beams are investigated under different intensities of the magnetic field. The free and forced vibrations of the beams are studied.

7

Conclusions and Scope for Future Work

7.1 General Conclusions

In the present work, the dynamic characteristics and stability of magnetorheological elastomer based sandwich beam have been carried out. Different skin materials such as metallic skins of conductive and non-conductive type and composite skins of non-conductive type are taken for the analysis. MRE embedded viscoelastic core has been used in the sandwich beam and static and time varying magnetic field is applied to change the shear modulus and stiffness of the core. In case of conductive skins the magnetoelastic loads due to magnetic field has been considered in the skin. The properties of isotropic and anisotropic MREs with and without considering carbon blacks have been taken in this work. Different configurations of the sandwich beam with variation in number, length and location of MRE patch in a non-MRE viscoelastic core have been considered for the study. Different support conditions such as simply supported, guided pinned, clamped free, clamped-pinned and clamped-clamped unrestrained have been taken in this study.

Initially the mathematical modelling of the MRE embedded viscoelastic cored sandwich beam with metallic skins subjected to both static and time varying magnetic field has been carried out using classical sandwich beam theory. Using extended Hamilton's principle along with generalized Galarkin's method the governing temporal equation of motion has been derived. For periodic axial loading the equation of the system reduces to that of parametrically excited system having Mathu-Hill type of equation with complex coefficients. The parametric instability regions have been obtained by using modified Hsu method and method of multiple

scales. The obtained results are verified by a number of published results and conducting experiments.

Also, finite element method has been used to derive the governing equation of motion of the MRE embedded sandwich beam with metallic and composite skins subjected to static magnetic field. Analysis has been made for eight different configurations of the sandwich beam by varying the number, location and length of MRE patch. For metallic skin classical approach is used where the transverse displacement is considered to be same along the cross section of the beam. For composite skins higher order approach is used where the transverse displacement is different in top and bottom skins and in the core it varies linearly. Here, analysis has been carried out for both rotating and non-rotating sandwich beams. Free and forced vibration studies have been carried out for a wide range of system parameters. The parametric instability regions have been obtained by using Harmonic balance method.

Further, two different isotropic MREs are fabricated by using carbonyl iron particles (CIP) with silicone. To increase the strength of this MRE, carbon black has also been added. Various tests such as microscopic and morphological analysis, thermo-gravimetric analysis (TGA), MH measurement, dynamic-mechanical analysis (DMA) tests, thermo-mechanical analysis (TMA) tests, tensile test and magneto-rheological test are conducted to characterize the fabricated MREs.

To validate theoretical formulation for free and forced vibration, four non-MRE (Two stiff rubber core, two flexible foam core) and six different MRE embedded sandwich beams with aluminium skins have been fabricated by varying the skin thickness, core thickness and MRE type (with and without carbon black). Also a set up has been fabricated incorporating permanent magnetic field with provision for varying the air gap between the magnet and specimen so as to change the magnetic field. Only static magnetic field has been applied. Laser vibrometer is used to measure the vibration response of the system.

Finally the frequencies obtained by considering classical sandwich beam theory for stiff core and finite element model for both stiff and flexible cored sandwich

beam have been verified experimentally. Following general conclusions have been drawn from the present work.

- It has been observed that for a MRE embedded sandwich beam with periodic axial load and magnetic field, the system starts buckling even though the applied load is well below the critical Euler buckling load. The critical dynamic load (below which the system will remain in static equilibrium position) is found to depend on the boundary conditions, dimension and material properties of the system, damping and applied magnetic field.
- To have a vibration free sandwich beam, the control parameters viz., amplitude and frequencies of magnetic field and axial load should be in the stable regions of the instability plots. These plots can easily be developed using the expressions developed for transition curves in this work. Hence, these plots can be used in application for passive and active vibration suppression of sandwich beams.
- The amplitude of vibration of the MRE embedded sandwich beam can be considerably reduced passively by using conductive skins and conveniently placing MRE patches in the core and actively reduced by applying magnetic field of suitable amplitude.

  Following are the specific conclusions drawn from the present work.

7.2 Specific Conclusions

7.2.1 MRE Embedded Sanwich Beam wth Static Magnetic Field

- It is observed that the free vibration response of the sandwich beam can be passively or actively suppressed by using MRE patch in the viscoelastic core and by applying magnetic field. It has been shown that up to 30% vibration reduction is possible in a cantilevered MRE embedded sandwich beam in comparison to that of a sandwich beam only with viscoelastic core.
- With increase in magnetic field strength, length of MRE patch and the core thickness, the instability region decreases and shifts towards right and the system becomes unstable for a higher value of amplitude of dynamic loading.

- With increase in percentage of iron particles and carbon black, instability region decreases and also the critical value of the amplitude of dynamic loading increases.
- For stiff MRE cored sandwich beam it is suggested to use the classical theory instead of using higher order theory as it requires less computational time and memory.

7.2.2 MRE Embedded Sanwich Beam with Time Varying Magnetic Field

- When a sandwich beam is subjected to time varying magnetic field and periodic axial load the developed closed form expressions using first and second order method of multiple scales can be conveniently used to obtain the transition curve and the critical dynamic load and magnetic field for active and passive vibration attenuation.
- For the system without periodic axial load, it is shown that the instability region marginally increases with the use of less percentage of iron particles along with carbon black. Hence, one may use this light weight, high strength sandwich beam instead of using sandwich beam with higher percentage of iron particles.
- For the system with periodic axial load, when it is subjected to time varying magnetic field the temporal equation of motion contains two frequency parametric excitation terms and one may observe three different resonance conditions viz., simple resonance, principal parametric resonance and simultaneous simple and principal parametric resonance.
- The instability regions decrease with the application of static magnetic field and increase with increase in static axial load. With the increase in percentage of iron particles in case of MRE patch containing iron particles the instability regions decreases. However with the increase in percentage of carbon black in case of MRE patch containing less percentage of iron particles and carbon blacks, the instability regions increases.

7.2.3 FE Analysis of MRE Embedded Sandwich Beam with Metallic Skins

- It has been observed that for the effective vibration suppression the MRE patches should be placed at a particular location depending on the boundary conditions and the mode of vibration.
- The transverse response amplitude of a MRE embedded viscoelastic cored sandwich beam can be considerably reduced by using conductive skins, more number of MRE patches and with increase in magnetic field.
- It has been demonstrated that the parametric instability regions decreases with increase in MRE patches in the viscoelastic core of a sandwich beam subjected to periodic axial load and magnetic field.
- It is seen that for simply supported sandwich beam the instability regions decreases when the MRE patches are placed at the ends of the sandwich beam in comparison to that of the case when MRE patches are placed away from the ends.
- For MRE embedded rotating sandwich beam the stability of the system can be improved and the fundamental frequency can be increased with increase in magnetic field, rotating speed and hub radius and by decreasing the setting angle and static load of the system.
- As the variation of fundamental frequency and loss factor are not linear with respect to various system parameters it is difficult to predict these values intrusively and hence one can use the developed formulation for finding the fundamental frequency and loss factor for the particular values of system parameters.

7.2.4 MRE Embedded Sanwich Beam with Composite Skins

- With increase in composite skin fiber angle and static load the fundamental frequency decreases as the stiffness and strength of the sandwich beam decreases.
- It is observed that the stability of the system can be improved by increasing the magnetic field or decreasing the fibre angle and static load factor.

- It is shown that with increase in the core loss factor of MRE, the critical value of dynamic load increases and hence the system can operate at any excitation frequency below this critical amplitude of excitation. Thus, the system stability can be improved actively by applying magnetic field with suitable amplitude and passively by changing the composite skins with different fiber angle.

7.2.5 Experimental Analysis of MRE Embedded Sanwich Beam

- It has been observed that the mechanical properties such as Young's modulus, shear storage modulus are significantly increased with the addition of carbon black. While the Young's modulus has increased from 1.077 MPa to1.738 MPa with addition of 7% carbon black (56.8% increase), the storage shear modulus has increased from 0.3 MPa to 0.34 MPa (13% increased at zero magnetic field) and 0.37 MPa to 0.45 MPa (22% increase for magnetic field of 0.5 T). It has been observed that MRE with carbon black has higher thermal stability and can operate at higher temperature than the MRE without carbon black.
- From the experimental vibration study of MRE cored sandwich beams it has been observed that the natural frequency increases with addition of carbon black. Also it increases with increase in skin thickness and decrease in core thickness.
- The damping ratio is found to increase from 0.0031 to 0.0055 for MRE embedded sandwich beam without carbon black. For the same system with carbon black it increases to 0.0035 for 0 T (without magnetic field) and to 0.0079 with magnetic field of 600 G.
- The frequencies obtained from the experiments are compared with the natural frequencies obtained by using analytical and finite element approaches and are found to be in good agreement.

The developed formulations and results can be used for design of MRE embedded sandwich beam for active and passive vibration attenuation.

7.2 Scope for Future Work

The research work reported on the dynamic and stability analyses of sandwich beams with MRE embedded viscoelastic core in this thesis can be extended in several directions. Some of the theoretical and experimental investigations that will need to be addressed are as follows:

- In the present work considering long and slender sandwich beam the skins have been model as Euler Bernoulli beam. One may extend this work by considering thick skin and by using Timoshenko beam theory.
- Here three layered symmetric sandwich beam has been used which can be extended for multilayered symmetric and un-symmetric MRE embedded sandwich beam.
- The number, length and location of the MRE patches in a viscoelastic core can be optimised for further attenuation of vibration of the sandwich beam.
- Multi-frequency axial loading condition can be considered for further study.
- In case of rotating sandwich beam the study can be enhanced by considering the hub and tip mass. In this case the study may be extended by considering skins of composite and functionally graded materials.
- The study can be extended to the sandwich beams with number of laminates in the skins.
- Non-linear analysis of the sandwich beam with MRE core can be carried out.
- One may fabricate different MREs by varying the percentage of iron particles and carbon blacks to study its properties and dynamic analysis of sandwich beams.

References

1. Abbas, B.A.H., (1986), Dynamic stability of a rotating Timoshenko beam with a flexible root, *Journal of Sound and Vibration*, **108**, 25-32.
2. Abramchuk, S., Kramarenko, E., Stepanov , G., Nikitin , L.V., Filipcsei, G., Khokhlov, A. R., Zrnyi, M., (2007), Novel highly elastic magnetic materials for dampers and seals: Part I. Preparation and characterization of the elastic materials, *Polymers for Advanced Technologies*, **18**, 883-890.
3. Ahmed K.M., (1972), Dynamic analysis of sandwich beams, *Journal of Sound and Vibration*, **21**, pp.263-276.
4. Allen, H.G., (1969), *Analysis and design of structural sandwich panels*, Pergamom Press Ltd., Headington Hill, Oxford.
5. Allen, H.G., (1969), *Analysis and Design of Structural Sandwich Panels*, Pergamon Press, Oxford.
6. Allen, H.G., Feng, Z., (1998), Classification of structural sandwich panel behaviour, *Proceedings Euromech 360 Colloquium, Mechanics of sandwich panels, Ecole des Mines de Saint-Étienne*, France, 13-15 May 1997, A. Vautrin (Ed.), Kluwer Academic Publisher, pp. 1-12.
7. Amichi, K., Atalla, N., (2009), A new 3D finite element for sandwich beams with a viscoelastic core, *Journal of Vibration and Acoustics*, **131**, pp. 1-9.
8. Arvin, H., Sadighi, M., Odhadi, A.R., (2010), A numerical study of free and forced vibration of composite sandwich beam with viscoelastic core, *Composite Structures*, **92**, pp. 996-1008.
9. Asnani, N.T., Nakra, B.C., (1970), Vibration analysis of multilayered beams with alternate elastic and viscoelastic layers, *Journal of Institution of Engineers (India)-Mechanical Engineering Division*, **50**, pp. 187-193.
10. Baber, T.T. Maddox, R.A., Orozco, C.E., (1998), A finite element model for Harmonically Excited Viscoelastic sandwich beams, *Computers and Structures*, **66(1)**, pp. 105-113.

11. Banerjee, J.R., (2003), Free vibration of sandwich beams using the dynamic stiffness method, *Computers and Structures*, **81**, pp. 1915-1922.
12. Banerjee, J.R., Cheung, C.W., Morishima, R., Perera M., Njuguna, J., (2007), Free vibration of a three-layered sandwich beam using the dynamic stiffness method and experiment, *Journal of Solids and Structures*, **44**, pp. 7543-7563.
13. Banerjee, J.R., Sobey, A.J., (2005), Dynamic stiffness formulation and free vibration analysis of a three-layered sandwich beam, *Journal of Solids and Structures*, **42**, pp. 2181-2197
14. Barbosa, F.S., Farage, M.C.R., (2008), A finite element model for sandwich viscoelastic beams: Experimental and numerical assessment, *Journal of Sound and Vibration*, **317**, pp. 91-111.
15. Bauld, N.R., (1967), Dynamic stability of sandwich columns under pulsating axial loads, *American Institute of Aeronautics and Astronautics Journal*, **5**, pp. 1514-1516.
16. Bergstrom, J.S., (1999), Large strain time-dependant behavior of elastomeric materials, *PhD. Thesis*, Massachusetts Institute of Technology, Cambridge, US.
17. Bhat, R.B., (1986), Transverse vibrations of a rotating uniform cantilever beam with tip mass as predicted by using beam characteristic orthogonal polynomials in the Rayleigh-Ritz method, *Journal of Sound and Vibration*, **105**, pp. 199-210.
18. Blom, P., Kari, L., (2005), Amplitude and frequency dependence of magneto-snsitive rubber in a wide frequency range. *Polymer Testing*, **24(5)**, pp. 656-662.
19. Bolotin, V.V., (1964), *The Dynamic Stability of Elastic Systems*. Holden Day, San Francisco.
20. Burton, W.S., Noor, A.K., (1995), Assessment of computational models for sandwich panels and shells, *Computer Methods in Applied Mechanics and Engineering*, **124**, pp. 125-151.
21. Carlson, J.D., Jolly, M.R., (2000), MR fluid, foam and elastomer devices, *Mechatronics*, **10(4-5)**, pp. 555-569.

22. Carlson, J.D., Jolly, M.R., (2000), MR fluid, foam and elastomer devices, *Mechatronics*, **10**, 555-569.

23. Cartmell M.P., (1990*), Introduction to Linear, Parametric and Nonlinear Vibrations*, Chapman and Hall, New York.

24. Cetkovic, M., Vuksanovic, D., (2009), Bending, free vibrations and buckling of laminated composite and sandwich plates using a layerwise displacement model. *Composite Structures*, **88**, pp. 219-227.

25. Chalak, H.D, Chakrabarti, A, Iqbal, M.A, A.H., Sheikh, (2011), Vibration of laminated sandwich beams having soft core. *Journal of Vibration and Control*; doi: 10.1177/1077546311421947.

26. Chatterjee, A., Baumgarten, J.R., (1971) An analysis of viscoelastic damping characteristics of a simply supported sandwich beam, *Journal of Engineering for Industry, Trans of ASME,* **93**, pp. 1239-1244.

27. Chen, L., Gong, X.L., Li, W.H., (2008), Effect of carbon black on the mechanical performances of magnetorheological elastomers, *Journal of Polymer Testing*, **27**, 340-345.

28. Chen, L., Gong, Xl., Jiang, Wq., Yao, Jj., Deng, Hx., Li, Wh., (2007), Investigation on magnetorheological elastomers based on natural rubber, *Journal of material science*, **42**, 5483-5489.

29. Choi, W.J., (2009), Dynamic analysis of magnetorheological elastomer configured sandwich structures, *Ph.D. thesis*, School of Engineering Sciences, University of Southampton, Highfield, Southampton SO17 1BJ.

30. Choi, W.J., Xiong, Y.P., Shenoi, R.A., (2010), Vibration characteristics of sandwich beams with steel skins and magnetorheological elastomer cores, *Advances in Structural Engineering*, **13(5)**, pp. 837-844.

31. Chonan, S., (1982a), Vibration and stability of sandwich beams with elastic bonding, *Journal of Sound and Vibration*, **85**, pp. 525-527.

32. Chonan, S., (1982b), Vibration and stability of a two-layered beam with imperfect bonding, *Journal of Acoustical Society of America*, **72(1)**, pp. 208-213.

33. Cook, R.D., Malkus, D.S., Plesha, M.E., Witt, R.J., (2007), *Concepts and applications of finite element analysis*, John Wiley and Sons (Asia).

34. Davis L. C., (1999), Model of magnetorheological elastomers, *Journal of Applied Physics*, **85**, pp. 3348-3351.

35. Degiovanni, M., Gherlone, M., Mattone, M., Sciuva, M.D., (2010), A sub-laminates FEM approach for the analysis of sandwich beams with multilayered composite faces, *Composite Structures*, **92**, pp. 2299-2306.

36. Deng, H., Gong, X., (2008), Application of magnetorheological elastomer to vibration absorber, *Communications in Nonlinear Science and Numerical Simulation*, **13(9)**, pp. 1938-1947.

37. Deng, H., Gong, X., Wang, L., (2006), Development of an adaptive tuned vibration absorber with magnetorheological elastomer, *Smart Materials and Structures*, **15(5)**, N111–N116.

38. Dewa, H., Okada, Y., Nagai, B., (1991), Damping characteristics of flexural vibration for partially covered beams with constrained viscoelastic layers, *JSME International Journal*, *series iii*, **34**, pp. 210-217.

39. Ditaranto, R.A., (1965), Theory of vibratory bending for elastic and viscoelastic layered finite length beams, *Journal of Applied Mechanics*, **32**, pp. 881-886.

40. Dwivedy, S.K., Sahu, K.C., Babu, S.K., (2007), Parametric instability regions of three layered soft core sandwich beam using higher order theory, *Journal of Sound and Vibration*, **304**, pp. 326–344.

41. Dwivedy, S.K., Mahendra, N., Sahu, K.C., (2009), Parametric instability regions of a soft and magnetorheological elastomer cored sandwich beam, *Journal of Sound and Vibration*, **325**, pp. 686–704.

42. Fereidooni, A., Behdinan, K., Fawaz, Z., (2008), Instability analysis of laminated composite beams subjected to parametric axial load, *International Journal of Mechanical, Industrial and Aerospace Engineering*, **2:2**, pp. 119-129.

43. Frostig Y., Baruch, M., (1994), Free vibrations of sandwich beams with a transversely flexible core: A higher order approach, *Journal of Sound and Vibration*, **176(2)**, pp. 195-204.

44. Frostig, Y., and Thomsen, O.T., (2004), High-order free vibration of sandwich panels with a flexible core, *International Journal of Solids and Structures*, **41**, pp. 1697-1724.

45. Frostig, Y., Baruch, M., (1990), Bending of sandwich beams with transversely flexible core, *American Institute of Aeronautics and Astronautics Journal*, **28**, pp. 523-531.

46. Frostig, Y., Baruch, M., (1994), Free vibrations of sandwich beams with a transversely flexible core: A higher order approach, *Journal of Sound and Vibration*, **176(2)**, 195-208.

47. Frostig, Y., Baruch, M., Vilnai, O., Sheinman, I., (1991), Sandwich beams with unsymmetrical skins and a flexible core-bending behavior, *Journal of Engineering Mechanics*, **117(9)**, pp. 1031-1052.

48. Frostig, Y., Baruch, M., Vilnay, O., Sheinmain, I., (1991), Bending of non-symmetric sandwich beams with transversely flexible core. *Journal of Engineering Mechanics*, **117(9)**, pp. 1931-1952.

49. Galucio, A.C., Deü, J-F., Ohayon, R., (2007), Hybrid active-passive damping treatment of sandwich beams in non-linear dynamics, *Journal of Vibration and Control*, **13**, pp. 851-881.

50. Ghinet, S., Atalla, N., (2011), Modeling thick composite laminate and sandwich structures with linear viscoelastic damping, *Computers and Structures*, **89**, pp. 1547-1561.

51. Ginder , J.M., Nichols, M.E., Elie, L.D., Clark, S.M., (2000), Controllable stiffness components based on magnetorheological elastomers, *Proceedings of SPIE 3985, Smart and Materials 2000: Smart Structures and Integrated Systems*, pp. 418-425.

52. Godaninejad, F., Bert, C.W., (1989), A new theory for bending of thick sandwich beams, *International Journal of Mechanical Science*, **31**, pp. 925-934.

53. Goyal, V.K., Kapania, R.K., (2007), A shear deformeable beam element for analysis of laminated composites, *Finite Elements in Analysis and Design*, **43**, pp. 463-477.

54. Gratzer F., Steinwender H., Kusej A., (2008), Magnetorheological AWD clutches, ATZ Autotechnology, FISITA (http://trid.trb.org/view.aspx?id=883264).

55. Gupta, N., (2003), Characterization of syntactic foams and their sandwich composites: modeling and experimental approaches, *PhD Dissertation*, Louisiana State University and Agricultural and Mechanical College, LA.

56. Herbeck, DR.-ING. L., Kleineberg, M, Schöppinger, C. (2003), Foam cores in RTM structures: manufacturing AID or high-performance sandwich, *proc: 23rd SAMPE, Europe International Conference*, Paris.

57. Hoa S.V., (1979), Vibration of a rotating beam with tip mass, *Journal of Sound and Vibration*, **67**, 369-381.

58. Howson, W.P., Zare, A., (2005), Exact dynamic stiffness matrix for flexural vibration of three-layered sandwich beams, *Journal of Sound and Vibration*, **282,** 753-767.

59. Hsu, C.S., (1963), On the parametric excitation of a dynamic system having multiple degrees of freedom, *Journal of Applied Mechanics*, **30**, pp. 367-372.

60. Hu, G., Guo, M., Li, W., Du, H. Alici, G., (2011), Experimental investigation of the vibration characteristics of a magnetorheological elastomer sandwich beam under non-homogeneous small magnetic fields, *Smart Materials and Structures*, **20**, 127001 (7pp).

61. Hwu, C., Chang, W.C., Gai, H.S., (2004), Vibration suppression of composite sandwich beams, *Journal of Sound and Vibration*, **272**, pp. 1-20.

62. Jansson, J.F., Olsson, K.A., Sorelius, S.E., (1979), *Fiber reinforced plastics 1*, Swedish Tech Books, Solna, Sweden.

63. Jolly, M.R., Bender, J.W., Carlson, J.D., (1999), Properties and applications of commercial magnetorheological fluids, *Journal of Intelligent Material Systems and Structures*, **10(1)**, 5-13.

64. Jolly, M.R., Carlson, J.D., Munoz, B.C., (1996b), A model of the behavior of magnetorheological materials, *Smart Materials and Structures*, **5**, pp. 607-614.

65. Jolly, M.R., Carlson, J.D., Munoz, B.C., Bullions, T.A., (1996a), The magnetoviscoelastic response of elastomer composites consisting of ferrous particles embedded in a polymer matrix, *Journal of Intelligent Material and Structures*, **7**, pp. 613-621.

66. Jones. I.W., Salerno, N.L, Savacchiop, A., (1967), An analytical and experimental evaluation of the damping capacity of sandwich beams with viscoelastic cores, *Journal of Engineering for Industry, Trans. of ASME*, **89**,pp. 438-445.

67. Kaleta, J., Krolewicz, M., Lewandowski, D., (2011), Magnetomechanical properties of anisotropic and isotropic magnetorheological composites with thermoplastic elastomer matrices, *Smart Materials and Structures*, **20,** 085006 (12pp).

68. Kallio, M., (2005), The elastic and damping properties of magnetorheological elastomers, *PhD. Thesis*, Tampere University of Technology.

69. Kant, T., Marurb, S.R., Rae, G.S., (1998), Analytical solution to the dynamic analysis of laminated beams using higher order refined theory, *Composite Structures*, **40**, pp. 1-9.

70. Kapania, R.K., Raciti, S., (1989), Advances in analysis of laminated beams and plates, part I: shear effects and buckling, *American Institute of Aeronautics and Astronautics Journal*, **27**, pp. 923-934.

71. Kapur, A.D., Nakra, B.C., Chawla, D.R., (1977), Shock response of viscoelastically damped beams, *Journal of sound and vibration*, **55**, 351-362.

72. Kar, R.C., Sujata, T., (1991), Dynamic stability of a tapered symmetric sandwich beam, *Computers and Structures*, **40**, pp. 1441-1449.

73. Kaw, A.K., (1997), *Mechanics of composite materials*, CRC Press, Boca Raton, New York

74. Kerwin, E.M., (1959), Damping of flexural waves by a constrained viscoelastic layer, *Journal of the Acoustical Society of America*, **31**, pp. 952-962.

75. Kim, H-Y., Hwang, W., (2002), Effect of debonding on natural frequencies and frequency response functions of honeycomb sandwich beams, *Composite Structures*, **55**, pp. 51-62.

76. Krishnamurthy, A.V., Vellaichamy, S., (1987), On the high-order shear deformation theory of laminated composite panels, *Composite Structures*, **8(4)**, 247-270.

77. Lall. A.K., Asnani, N.T. Nakra, B.C., (1988), Damping analysis of partially covered sandwich beams, *Journal of sound and vibration*, **123**, pp. 247-255.

78. Langdon, G.S., von Klemperer, C.J., Rowland, B.K., Nurick, G.N., (2012), The response of sandwich structures with composite face sheets and polymer foam cores to air-blast loading: Preliminary experiments, *Engineering Structures*, **36**, pp. 104-112.

79. Lee, H.P., (1994), Effect of gravity on the stability of a rotating cantilever beam in a vertical plane, *Computers and Structures*, **53**, pp. 351-355.

80. Li, Z., (2006), Vibration and acoustical properties of sandwich composite materials, *PhD Dissertation*, Auburn University, Auburn, Alabama.

81. Liao, G., Gong, XL., Xuan, S., Guo, C., Zong L., (2012), Magnetic-field-induced normal force of magnetorheological elastomer under compression status, *Industrial and Engineering Chemistry Research*, **51**, pp. 3322−3328

82. Lin C-Y, Chen L-W. (2003), Dynamic stability of a rotating beam with a constrained damping layer. *Journal of Sound and Vibration*, **267**, pp. 209-225.

83. Lin C-Y., Chen, L-W., (2002), Dynamic stability of rotating composite beams with a viscoelastic core, *Composite Structures*, **58**, pp. 185-194.

84. Lokander, M., Stenberg, B., (2003), Performance of isotropic magnetorheological rubber materials, *Polymer Testing*, **22(3)**, 245-251.

85. Mallikarjuna, Kant, T., (1993), A critical review and some results of recently developed refined theories of fiber reinforced laminated composites and sandwiches. *Composite Structures*, **23(4)**, pp. 293-312.

86. Manconi, E., Mace, B.R., (2010), Estimation of the loss factor of viscoelastic laminated panels from finite element analysis, *Journal of Sound and Vibration*, **329**, pp. 3928-3939.

87. Mantari, J.L., Oktem, A.S., Soares, C.G., Static and dynamic analysis of laminated composite and sandwich plates and shells by using a new higher-order shear deformation theory. Doi:10.1016/j.compstruct.2011.07.020.

88. Markus, S., (1974), Damping mechanism of beams partially covered by constrained viscoelastic layer, *ACTA Technica CSAV*, **2**, pp. 179-194.

89. Marur, S.R., Kant, T., (1997), On the performance of higher order theories for transient dynamic analysis of sandwich and composite beams. *Computers and Structures*, **65**, pp. 741-759.

90. Matsunaga, H., (2001), Vibration and stability of angle-ply laminated composite plates subjected to in-plane stresses, *International Journal of Mechanical Sciences*, **43**, pp. 1925-1944.

91. Matsunaga, H., (2007), Vibration and stability of cross-ply laminated composite shallow shells subjected to in-plane stresses. *Composite Structures*, **78**, pp. 377-391.

92. Mead D.J., Markus S., (1969), The forced vibration of a three-layer damped sandwich beam with arbitrary boundary conditions, *Journal of Sound and Vibration*, **10(2)**, pp. 163-175.

93. Mead D.J., Markus S., (1970), Loss factors and resonant frequencies of encastre damped sandwich beams, *Journal of Sound and Vibration*, **12 (1)**, pp. 99-112.

94. Mead, D.J., Sivakumaran, S., (1966), The Stodola method applied to sandwich beam vibration, *Proceedings of the Symposium on Numerical Methods for Vibration Problems*, University of Southampton, UK.

95. Meyer-Piening, H.R., Remarks on higher order sandwich stress and deflection analyses, in sandwich construction -1. *Proceedings: First International Conference on Sandwich Construction*, Royal Institute of Technology Stockholm, Sweden, 19-21 June, Eds. K-A. Olssen and R.P. Reichard, pp. 107-127.

96. Murthy, M.V.V.S., Mahapatra, D.R., Badarinarayana, K., Gopalakrishnan, S., (2005), A refined higher order finite element for asymmetric composite beams. *Composite Structures*, **67**, pp. 27-35.

97. Nayak A.K., Shenoi, R.A., Moy, S.S.J., (2004), Transient response of composite sandwich plates, *Composite Structures*, **64**, pp. 249-267.

98. Nayfeh, A.H., Balachandran B., (2004), *Applied Nonlinear Oscillations*, WILEY-VCH Verlag GmbH & Co. KGaA, Weinheim.

99. Nayfeh, A.H., Mook, D.T., (1979), *Nonlinear Oscillations*, Wiley-Interscience, New York.

100. Noor, A.K., Burton, W.S., Bert, C.W., (1996), Computational models for sandwich panels and shells, *Applied Mechanics Reviews*, **49 (3)**, pp. 155-199.

101. Plantema, F.J., (1966), *Sandwich construction-the bending and buckling of sandwich beams, plates and shells*, John Wiley and Sons, New York.

102. Pradeep, V., Ganesan, N., Bhaskar, K., (2007), Vibration and thermal buckling of composite sandwich beams with viscoelastic core, *Composite Structures*, **81**, pp. 60-69.

103. Prieto, V.L., Parkin, R., Jackson, M., Silberschmidt, V., Kesy, Z., (2010), Vibration characteristics of MR cantilever sandwich beams: experimental study, *Smart Materials and Structures*, **19**, 015005 (9pp).

104. Putter, S., Manor, H., (1978), Natural frequencies of radial rotating beams, *Journal of Sound and Vibration*, **56**, pp. 175-185.

105. Qian, C., Demao, Z., (1990), Vibration analysistheory and application to elastic-viscoelastic composite structures, *Computers and structures*, **37**, pp. 585-592.

106. Rajamohan, V., Rakheja, S., Sedaghati, R., **(**2010), Vibration analysis of a partially treated multi-layer beam with magnetorheological fluid, *Journal of Sound and Vibration*, **329**, pp. 3451-3469.

107. Rao D.K., (1978), Frequency and loss factors of sandwich beams under various boundary conditions, *Journal of Mechanical Engineering Science*, **20**, 271-282.

108. Rao, D.K., (1977), Forced vibration of a damped sandwich beam subjected to moving forces, *Journal of sound and vibration*, **54**, 215-227.

109. Rao, S.S., (2005), *The finite element method in engineering*, USA: Elsevier.

110. Ray, K., Kar, R.C., (1995a), Dynamic stability of a pre-twisted, three layered, symmetric sandwich beam, *Journal of Sound and Vibration*, **183(4)**, pp. 591-606.

111. Ray, K., Kar, R.C., (1995b), Parametric instability of a sandwich beam with various boundary conditions, *Computer and Structures*, **55**, pp. 857-870.

112. Ray, K., Kar, R.C., (1996a), The parametric instability of partially covered sandwich beams, *Journal of Sound and vibration*, **197**, pp. 137-152.

113. Ray, K., Kar, R.C., (1996b) Parametric instability of multi-layered sandwich beams, *Journal of Sound and Vibration*, **193(3)**, pp. 631-644.

114. Ray, K., Kar, R.C., (1996c), Parametric instability of a dual-cored sandwich beam, *Computers and Structures*, **61(4)**, pp. 665-671.

115. Ray, K., Kar, R.C., (1996d), Parametric instability of a symmetric sandwich beam with higher order effects, *Computers and Structures*, **60**, pp. 817-824.

116. Reddy, J.N., (1984), A simple higher order theory for laminated composite plates, *Journal of Applied Mechanics*, **51**, pp. 745-752.

117. Reddy, J.N., (1990), A review of refined theories of laminated plates, *The Shock and Vibration Digest*, **22(7),** pp. 3-17.

118. Reissner, E., (1998) Finite deflections of sandwich plates, *Journal of Aerospace Sciences*, **15 (7)**, pp. 435-440.

119. Ribakov, Y., Gluck, J., (2002), Selective controlled base isolation system with magnetorheological dampers, *Earthquake engineering and structural dynamics*, **31**, pp. 1301-1324.

120. Sahasrabudhe, S.S., Nagarajaiah, S., (2005), Semi-active control of sliding isolated bridges using MR dampers: an experimental and numerical study, *Earthquake engineering and structural dynamics*, **34**, pp. 965-983.

121. Saito, H., Otomi, K., (1979), Parametric response of viscoelastically supported beams, *Journal of Sound and Vibration*, **63**, pp. 169-178.

122. Salet, T.A.M, Hamelink, S.A., (1991), Numerical analysis of sandwich beams, *Computers and structures*, **41**, pp. 1231-1239.

123. Sastri, J.B.S., (2012), Dynamic analysis of magneto rheological elastomer cored sandwich beam, *M.Tech. Thesis*, Indian Institute of Technology Guwahati, India.

124. Shiga, M., Hirose, M., Okada, K., (1992), Tokkai. *Japan Patents, Hei4266970*.

125. Shiga, T., Okada, A., Kurauchi, T., (2003), Magnetroviscoelastic behavior of composite gels, *Journal of Applied Polymer Science*, **58 (4)**, 787-792.

126. Srinath, L.S., (2007), *Advanced Mechanics of Solids*, Tata McGraw-Hills, New Delhi.

127. Stamm, K., Witte, H., (1974), *Sandwichkonstruktionene* (in German), Springer-Verlag, Wien, Austria.

128. Stepanov G.V., Abramchuk, S.S., Grishin, D.A., Nikitin, L.V., Kramarenko, A.R., (2007), Effect of a homogeneous magnetic field on the viscoelastic behavior of magnetic elastomers, *polymer Testing*, **48**, pp. 488-495.

129. Stevens, K.K., (1966), On the parametric excitation of a viscoelastic column, *AIAA journal*, **4**, pp. 2111-2115.

130. Stewart, W.M., Ginder , J.M., Elie, L.D., Nichols, M.E., (1998), Method and apparatus for reducing brake shudder, *US Patent* 5816587.

131. Straalen, I.J.V., (2000), Modeling of sandwich structures and adhesive bonded joints, *TNO-Report*, TNO Building and Construction Research, DELFA, The Netherlands.

132. Subramanian, P., (2006), Dynamic analysis of laminated composite beams using higher-order theories and finite elements, *Composite Structures*, **73**, pp. 342-353.

133. Sun, Q., Zhou, J-X., Zhang, L., (2003), An adaptive beam model and dynamic characteristics of magnetorheological materials, *Journal of Sound and Vibration*, **261**, pp. 465- 481.

134. Tagarielli, V.L., Deshpande, V.S., Fleck, N.A., (2007), The dynamic response of composite sandwich beams to transverse impact, *International Journal of Solids and Structures*, **44**, pp. 2442-2457.

135. Thomsen, O.T., (1992), Analysis of local bending effects in sandwich panels subjected to concentrated loads, *Second International conference on Sandwich construction*, University of Florida, Gainesville, U.S.A.

136. Thomsen, O.T., (1995), Theoretical and experimental investigation of local bending effects in sandwich plates, *Composite Structures*, **30**, pp. 85-101.

137. Tsai, S.W., Hahn, H.T., (1980), *Introduction to composite materials*, Technomic Publishing Co., Lancaster, PA, USA.

138. Varga, Z., Filipcsei, G., Zrinyi, M., (2006), Magnetic field sensitive functional elastomers with tuneable elastic modulus, *Polymer*, **47**, 227-233.

139. Vidal, P., Polit, O., (2011), A sine finite element using a zig-zag function for the analysis of laminated composite beams. *Composites: Part B*, **42**, pp. 1671-1682.

140. Vinson, J.R., (1999), *The Behavior of Sandwich Structures of Isotropic and Composite Materials*, Technomic Publishing Co., Lancaster, PA, USA.

141. Vinson, J.R., Chou T.W., (1975), *Composite materials and their use in structures*, John Wiley and Sons, New York-Toronto.

142. Von Lockette P.R., Kadlowec, J., Koo, J.H., (2006), Particle mixtures in magnetorheological elastomers (MREs), Article No. 61700T. *Smart Structures and Materials*, Active Materials: Behavior and Mechanics **6170**: T1700-T1700. doi:10.1117/12.658750.

143. Wang, Y., Hu, Y., Chen, L., Chen, Z., (2006), Effects of rubber/magnetic particle interactions on the performance of magnetorheological elastomers, *Polymer Testing*, **25**, 262-267.

144. Watson J.R., (1997), Method and apparatus for varying the stiffness of a suspension bushing, *US Patent 5609353*.

145. Wei K-X., Meng, G., Zhang, W-M., Zhu, S-S., (2008), Experimental investigation on vibration characteristics of sandwich beams with

magnetorheological elastomers cores, *Journal of Central South University of Technology*, *15, pp. 239-242.*

146. Wei, K., Meng, G., Zhou, S., Liu, J., (2006), Vibration control of variable speed/acceleration rotating beams using smart materials, *Journal of Sound and Vibration*, **298**, pp. 1150-1158.
147. Yabuno, H., Kida K., Yoshizawa, M., Tsujioka, Y., (1989), Characteristics of a magnetically levitated carrying system by using permanent magnets, *Transaction of the Japan Society of Mechanical Engineers*, **55-519C**, pp. 2731-2739.
148. Yabuno, H., Seino, T., Yoshizawa, M., Tsujioka, Y., (1988), Dynamical behavior of a levitated body with magnetic guides (Parametrically excitation of the subharmonic type due to the vertical motion of levitated body), *JSME International Journal*, **32-3**, pp. 428-435.
149. Yalcintas, M., Dai, H., (2004), Vibration suppression capabilities of magnetorheological materials based adaptive structures, *Smart Materials and Structures*, **23**, 1-11.
150. Yeh, J.Y., Chen, L.W., Wang, C.C., **(**2004), Dynamic stability of a sandwich beam with a constrained layer and electrorheological fluid core, *Composite Structures*, **64**, pp. 47-54.
151. Yim J.H., Cho, S.Y., Seo, Y.J., Jang, B.Z., (2003), A study on material damping of 0_ laminated composite sandwich cantilever beams with a viscoelastic layer. *Composite Structures*, **60**, pp. 367-734.
152. Yim, J.H., Cho, S.Y., Seo, Y.J., Jang, B.Z., (2003), A study on material damping of 0^o laminated composite sandwich cantilever beams with a viscoelastic layer, *Composite Structuress*, **60**, pp. 367-374.
153. Ying, Z.G., Ni, Y.Q., (2009), Micro-vibration response of a stochastically excited sandwich beam with a magnetorheological elastomer core and mass, *Smart Materials and Structures*, **18**, 095005 (13pp).
154. Zenkert, D., (1995), *An Introduction to Sandwich Construction*, EMAS Publishing.

155. Zhang, X., Li, W., Gong, X.L., (2008), An effective permeability model to predict field-dependent modulus of magnetorheological elastomers, *Communications in Nonlinear Science and Numerical Simulation*, **13**, pp. 1910-19016.

156. Zhen, W., Chen, W., (2008), An assessment of several displacement-based theories for the vibration and stability analysis of laminated composite and sandwich beams, *Composite Structures*, **84**, pp. 337-349.

157. Zhou, G.Y., Lin, K.C., Wang, Q., (2006), Finite element studies on field-dependent rigidities of sandwich beams with magnetorheological elastomer cores, *Smart Materials and Structures*, **15**, pp. 787-791.

158. Zhou, G.Y., Wang, Q., (2005), Magnetorheological elastomer-based smart sandwich beam with nonconductive skins, *Smart Materials and Structures*, **14**, pp. 1001-1009.

159. Zhou, G.Y., Wang, Q., (2005), Magnetrorhelogical elastomer-based smart sandwich beams with nonconductive skins, *Smart Materials and Structures*, **14**, pp. 1001-1009.

160. Zhou, G.Y., Wang, Q., (2006a), Use of magnetorheological elastomer in an adaptive sandwich beam with conductive skins. Part I: magnetoelastic loads in conductive skins, *International Journal of Solids and Structures*, **43**, pp. 5386-5402.

161. Zhou, G.Y., Wang, Q., (2006b), Use of magnetorheological elastomer in an adaptive sandwich beam with conductive skins. Part II: dynamic property, *International Journal of Solids and Structures*, **43**, pp. 5403-5420.

Appendix

Appendix A

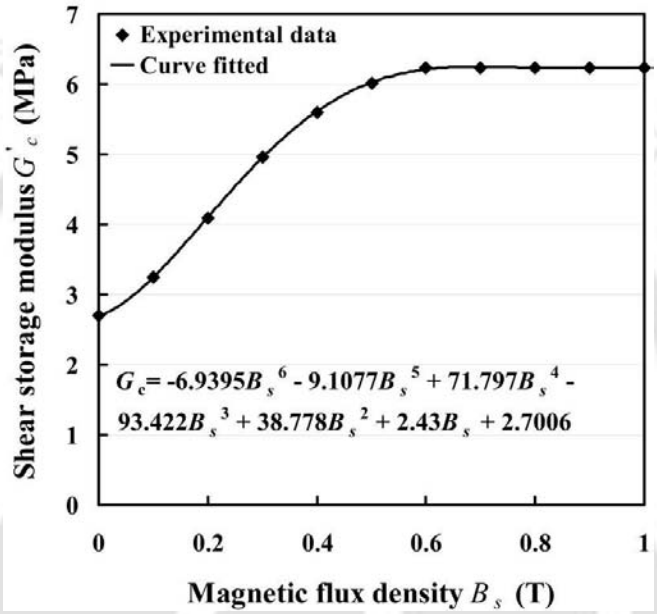

Figure A1 Curve fitting for shear storage modulus data of Chen *et* al., 2007.

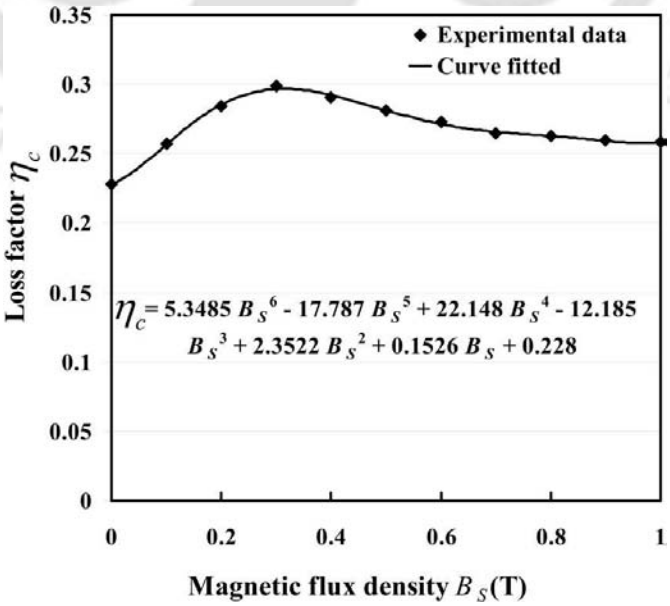

Figure A2 Curve fitting for loss factor data of Chen *et al*., 2007.

Publications from the Present Thesis

International Journals

1. B. Nayak, S. K. Dwivedy, K. S. R. K. Murthy, (2011), Dynamic analysis of magnetorheological elastomer-based sandwich beam with conductive skins under various boundary conditions, *Journal of Sound and Vibration*, 330(9), pp 1837-1859.
2. B. Nayak, S. K. Dwivedy, K. S. R. K. Murthy, (2012), Multi-frequency excitation of magnetorheological elastomer-based sandwich beam with conductive skins, *International Journal of Non-Linear Mechanics*, 47, pp 448-460.
3. B. Nayak, S. K. Dwivedy, K. S. R. K. Murthy, (2012), Vibration analysis of a three-layer MRE embedded sandwich beam with conductive skins using FEM, *Proceedings of the Institution of Mechanical Engineerings, Part C: Journal of Mechanical Engineering Science*, 227(4) 714-729.
4. B. Nayak, S. K. Dwivedy, K. S. R. K. Murthy, Dynamic stability of magnetorheological elastomer based adaptive sandwich beam with conductive skins using FEM and the harmonic balance method, *International Journal of Mechanical Sciences*, (Under Review).
5. B. Nayak, S. K. Dwivedy, K. S. R. K. Murthy, Dynamic stability of a rotating sandwich beam with magnetorheological elastomer core, *European Journal of Mechanics A/Solids*, (Under Review).
6. B. Nayak, S. K. Dwivedy, K. S. R. K. Murthy, Fabrication and characterization of magnetorheological elastomer with carbon black, *Journal of Intelligent Material Systems and Structures*, (Under Review).
7. B. Nayak, S. K. Dwivedy, K. S. R. K. Murthy, Dynamic stability of a flexible Magnetorheological elastomer cored sandwich beam with composite skins, *Mechanics of Advanced Materials and Structures*, (Under Review).

8. B. Nayak, S. K. Dwivedy, K. S. R. K. Murthy, Vibration characteristics of magnetorheological elastomer cored sandwich beams: experimental study, *International Journal of Dynamics and Control*, (Under Review).

Conferences

1. B. Nayak, S. K. Dwivedy, and K. S. R. K. Murthy, 2009, "Parametric instability regions of magnetorheological elastomer (MRE) embedded viscoelastic cored sandwich beam", *National Conference on Computer Aided Modelling and Simulation in Computational Mechanics* (CAMSCM 2009), NERIST, Itanagar, India, 13-14 March 2009, pp 125-134.
2. B. Nayak, S. K. Dwivedy, and K. S. R. K. Murthy, 2010, "Free vibration analysis of MRE embedded viscoelastic cored sandwich beam with time varying magnetic field", *ASME / ASME 2010 10th Biennial Conference on Engineering Systems Design and Analysis* (ESDA2010-24613), Dynamic Systems and Control, Istanbul, Turkey, 12-14 July 2010, 5, pp. 211-220.
3. B. Nayak, M. Srinivas, S. K. Dwivedy, and K. S. R. K. Murthy, 2010, "Free vibration of MRE-based sandwich beam with nonconductive composite skins", *International Conference on Vibration Engineering and Technology of Machinery* (VETOMAC-VI), IIT Delhi, India, 13-15 December 2010, pp 687-693.
4. B. Nayak, K. K. Nagabandi,, S. K. Dwivedy, and K. S. R. K. Murthy, 2010, "Experimental investigation of free and forced vibration of stiff and soft cored sandwich beams", *International Conference on Theoretical, Applied, Computational and Experimental Mechanics* (ICTACEM 2010), IIT Kharagpur, India, 27-29 Dec. 2010, pp 345-347.
5. B. Nayak, J. B. S. Sastri, S. K. Dwivedy, and K. S. R. K. Murthy, 2012, "A Comparative Study of the Classical and Higher Order Theory for Free Vibration Analysis of MRE Cored Sandwich Beam with Composite Skins Using Finite Element Method", IEEE - *International Conference on Advances in Engineering, Science and Management* (ICAESM 2012), EGS Pillay Engineering College, Nagapattinam, India, 30-31, Mar. 2012, pp 172-178.